Ministry of Oceans and Fisheries

KOPRI 극지연구소 Korea Polar Research Institute

Cruise Report 2023

For the Arctic Ocean Expedition 2023 (ARA14B) using IBRV ARAON

August 1 ~ August 31, 2023

Bering Strait, Pacific Central Arctic Ocean (CAO), Chukchi/East Siberian Seas

K-AWARE KOREA ARCTIC OCEAN WARMING & RESPONSE OF ECOSYSTEM

Eun-Jin Yang, Chief Scientist

Korea Polar Research Institute (KOPRI)

Report contributors:

Eun-Jin Yang[1*], Tae-Wook Park[1], Jin Young Jung[1], Jee-Hoon Kim[1], Jaeill Yoo[1], Catherine Lalande[1], Jun-Oh Min[1], Myung Suk Kim[1], Ahra Mo[1], Jong Kuk Moon[1], Chorom Shim[1], Jeong-Hyun Kim[1,14], Hyeju Yoo[1,14], Ju Young Son[1,11], Joo Hong Kim[2], Junghyun Park[2,11], Jeongwon Park[3], Sungjae Lee[3], Hyunggyu Choi[4], Suk Hyun Haam[5], Dong Ha Kang[6], JinSoo Son[7], Jeong Yeob Chae[8], Su Jin Park[8], Hui Chan Kim[9], Jeong Uk Lee[9], Dong Geon Lee[10], I Jin Lim[11], Jiwoo Kim[11], SangHoon Park[12], Seong Young Lee[13], Han Woong Byun[15], Byeong Jun Cho[15],

[1]Division of Ocean Sciences, Korea Polar Research Institute (KOPRI), Republic of Korea (ROK)
[2]Division of Atmosphere Sciences, KOPRI, ROK
[3]Center of Satellite and GIS, KOPRI, ROK
[4]Department of Future Technology Convergence, KOPRI, ROK
[5]Neosea Tech, ROK
[6]Gyeongsang National University, ROK
[7]Hanyang University, ROK
[8]Inha University, ROK
[9]Korea Maritime & Ocean University, ROK
[10]Pohang University of Science and Technology, ROK
[11]Pukyong National University (PKNU), ROK
[12]Pusan National University (PNU), ROK
[13]Sejong University, ROK
[14]University of Science and Technology (UST), ROK
[15]SBS, ROK

***Chief Scientist, Eun-Jin Yang**
E-mail: ejyang@kopri.re.kr
Tel.: +82-32-760-5334
Korea Polar Research Institute
26 Songdomirae-ro, Yeonsu-gu
Incheon 21990, Republic of Korea

Editor's Note: All data and summaries provided herein is subject to revision or correction and should be treated as unpublished data with intellectual property reserved to the scientist contributing to the report. Please contact the individuals listed as having responsibility for each report section for additional information or Dr. Eun-Jin Yang (ejyang@kopri.re.kr), the chief scientist of 2023 ARAON Arctic Ocean Cruise (2nd Leg, ARA14B). Report prepared September 2023, Chukchi/East Siberian seas, the Arctic Ocean.

How to cite this report:
Yang, E.J. and et al. (2023) Cruise Report for the Arctic Ocean Expedition 2023 using IBRV ARAON: The 2nd Leg, Report No. XXXX, Korea Polar Research Institute, pp162.

Contents

IBRV *ARAON* Arctic Cruise ARA14B

August 1 – August 31, 2023

Summary:

The mission of Korea's Arctic Ocean research is to determine how the Arctic Ocean system is changing on time scales of seasons to decades, particularly with respect to the consequences that may result from the influence of sea ice loss on Arctic ecosystems, transpolar sea route (TSR) and severe weather events in Korean Peninsula. Arctic Ocean research priority 1 is to develop sustained Arctic Ocean observing and data management capabilities to improve coupled ocean-sea ice-atmosphere monitoring and modeling efforts in order to advance understanding of climate impacts on weather and ecosystems. Arctic Ocean research priority 2 is to enhance the scientific framework and capabilities forming the foundation for protecting environments and sustainable developments in the Central Arctic Ocean (CAO). The Korea-Arctic Ocean Warming and Responses of Ecosystem (K-AWARE) program using the icebreaking R/V ARAON, funded by the Korean Ministry of Oceans and Fisheries (MOF), has been developed and undertaken by the Korea Polar Research Institute (KOPRI) to establish a monitoring system for analyzing medium-term variation in the Arctic marine environment caused by warming of the Arctic Ocean, including a decline in sea ice coverage, increases in water temperature and riverine discharge, and for analyzing ecosystem reactions, and to project future changes in the Arctic Ocean environment using observational data. The K-AWARE project is to pursue three key foci: 1) physical variability and material cycle between sea ice and ocean, 2) reactions between sea ice and marine ecosystem and fisheries resources, and 3) future outlook for environmental changes in the Arctic Ocean according to human activity scenarios. K-AWARE is seeking out new ideas and methodologies so that Arctic researchers can understand the unrevealed Arctic processes in the ice-covered region which has been rarely visited and poorly studied. The researchers observe physical, ecological, and biogeochemical parameters in rapid transition and how quickly environmental changes affect the ecosystem in the Arctic Ocean. These are critical for the policy makers looking to preserve

thriving Arctic ecosystems as sea ice extent continues to decline. Thus, the cruise outcomes integrated with regional impact studies can help them to develop effective adaptation strategies for the rapidly changing Arctic Ocean.

Recently, it is expected that the Arctic Ocean would experience profound changes under the present warming conditions and highly impact even more on future global changes. To verify this, in this summer, the ARAON Arctic Cruise (ARA14B) was conducted from August 1st to August 31th, 2023. The cruise covered the Bering Sea, the Chukchi Sea, the East Siberian Sea, and central Arctic Ocean including the Chukchi Borderland and the Makarov Basin. With funding provided by the Ministry of Oceans and Fisheries (MOF) of Korea (3rd Year) and by Korea Polar Research Institute (KOPRI), the aim of the cruise was to identify key environmental parameters (physical and biogeochemical) in rapid transition due to the sea-ice decrease in the western Arctic Ocean and predict environmental change patterns. The research effort was also conducted for the K-AWARE Program to observe physical, ecological, and biogeochemical parameters in rapid transition and how quickly environmental changes affect the ecosystem in the Arctic Ocean. Again, the results obtained from the 2023 Arctic cruise will be integrated with regional studies and be used to improve prediction models and to make effective adaptation strategies for the rapidly changing Arctic Ocean.

Acknowledgements:

We thank the IBRV ARAON crew, officers and commanding officer onboard ARAON for well-executed hard work and flexibility under cold and often difficult conditions. We wish to specifically thank the experienced Marine Science Technician team aboard the ship which was invaluable in facilitating the research operations. This research was supported by Korea Institute of Marine Science & Technology Promotion(KIMST) funded by the Ministry of Ocean and Fisheries, Korea (20210605, ‘Korea-Arctic Ocean Warming and Response of Ecosystem ,K-AWARE, KOPRI).

Projects:

K-AWARE (Korea-Arctic Ocean Warming and Response of Ecosystem) Program: Ministry of Oceans and Fisheries (MOF, 20210605), KOPRI Project No. PM23040, PI: Eun Jin Yang, KOPRI

Cruise Participants (research):

1. Eun Jin Yang, KOPRI, Republic of Korea (ejyang@kopri.re.kr)
2. Suk Hyun Haam, Neosea Tech, Republic of Korea (haam6481@gmail.com)
3. Seong Yong Lee, Sejong University, Republic of Korea (leoly01@hanmail.net)
4. Tae-Wook Park, KOPRI, Republic of Korea (twpark @korpri.re.kr)
5. Joo-Hong Kim, KOPRI, Republic of Korea (joo-hong.kim@korpri.re.kr)
6. Catherine Lalande, KOPRI, Republic of Korea (catherine.lalande@kopri.re.kr)
7. Jinyoung Jung, KOPRI, Republic of Korea (jinyoungjung@kopri.re.kr)
8. Jaeill Yoo, KOPRI, Republic of Korea (jiyoo@kopri.re.kr)
9. Jeongwon Park, KOPRI, Republic of Korea (jeong-won.park@kopri.re.kr)
10. Han Woong Byun, SBS, Republic of Korea (bhw82@hotmail.com)
11. Jun-Oh Min, KOPRI, Republic of Korea (jomin@kopri.re.kr)
12. Jee-Hoon Kim, KOPRI, Republic of Korea (jeehoonkim@kopri.re.kr)
13. Myung Suk Kim, KOPRI, Republic of Korea (kmspban@kopri.re.kr)
14. Ahra Mo, KOPRI, Republic of Korea (ahramo@kopri.re.kr)
15. Sungjae Lee, KOPRI, Republic of Korea (sungjae@kopri.re.kr)
16. Hyunggyu Choi, KOPRI, Republic of Korea (langyu7@kopri.re.kr)
17. Jong Kuk Moon, KOPRI, Republic of Korea (jkmoon@kopri.re.kr)
18. Sang Hoon Park, Pusan National Univ., Republic of Korea (mossinp@pusan.ac.kr)
19. Jeong Yeob Chae, Inha Univ., Republic of Korea (jychae92@gmail.com)
20. Chorom Shim, KOPRI, Republic of Korea (chorom@kopri.re.kr)
21. Junghyun Park, KOPRI/PKNU, Republic of Korea (james70712@gmail.com)
22. Jeong-Hyun Kim, KOPRI/UST, ROK (jeonghkim@kopri.re.kr)
23. I Jin Lim, Pukyong National University, ROK (ijinlim@pukyong.ac.kr)
24. Dong Geon Lee, POSTEC, Republic of Korea (dglee9613@gmail.com)

25. Byeong Jun Cho, SBS, Republic of Korea (blujun@sbs.co.kr)

26. Hui Chan Kim, Korea Maritime & Ocean University, ROK (khc1996@g.kmou.ac.kr)

27. Hyeju Yoo, KOPRI/UST, Republic of Korea (hjyoo@kopri.re.kr)

28. Jeong Uk Lee, Korea Maritime & Ocean University, ROK (wjddnr7078@g.kmou.ac.kr)

29. Dong Ha Kang, Gyeongsang National Univ., ROK (rkdehdgk789@naver.com)

30. JinSoo Son, Hanyang Univ., Republic of Korea (tngur1107@hanyang.ac.kr)

31. Ju Young Son, KOPRI/PKNU, Republic of Korea (mh0980@kopri.re.kr)

32. Jiwoo Kim, Pukyong National University, ROK (zoo04154@naver.com)

33. Su Jin Park, Inha Univ., Republic of Korea (qkrtnwls516@naver.com)

2023 ARAON ARCTIC CRUISE
ARA14B (01 – 31 AUGUST)


양은진 (Eun Jin, Yang) 극지연구소


함석현 (Sukhyun, Haam) 네오씨텍


이성용 (Seong Yong, Lee) 세종대학교


박태욱 (Tae Wook, Park) 극지연구소


김주홍 (Joo Hong, Kim) 극지연구소


정진영 (Jin Young, Jung) 극지연구소


박정원 (Jeong Won, Park) 극지연구소


김지훈 (Jee Hoon, Kim) 극지연구소

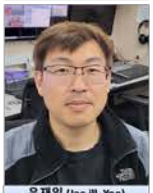
유재일 (Jae Ill, Yoo) 극지연구소


문중국 (Jong Kuk, Moon) 극지연구소


심초롬 (Chorom, Shim) 극지연구소

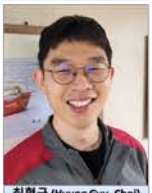
최형규 (Hyung Gyu, Choi) 극지연구소


Catherine Lalande 극지연구소


민준오 (Jun Oh, Min) 극지연구소

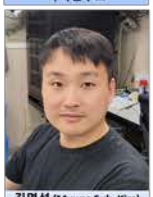
김명석 (Myung Suk, Kim) 극지연구소


모아라 (Ahra, Mo) 극지연구소


이성재 (Sungiae, Lee) 극지연구소


박상훈 (Sang Hoon, Park) 부산대학교


채정엽 (Jeong Yeob, Chae) 인하대학교

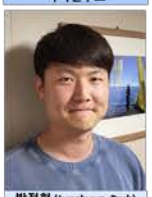
박정현 (Junghyun, Park) 극지연구소


김정현 (Juong Hyun, Kim) 극지연구소, UST

KOPRI 극지연구소 Korea Polar Research Institute

stx Marine Service Co.,Ltd

대한민국해군 REPUBLIC OF KOREA NAVY

NEOSEA TECH 네오씨텍

SBS

UST UNIVERSITY OF SCIENCE & TECHNOLOGY

INHA UNIVERSITY 1954

PUKYONG NATIONAL UNIVERSITY 부경대학교

SEJONG UNIVERSITAS SEJONGENSIS

MOKPO NATIONAL MARITIME UNIVERSITY 1936

HANYANG UNIVERSITY 한양 1939

KOREA MARITIME & OCEAN UNIVERSITY 1945


임이진 (I Jin, Lim) 부경대학교

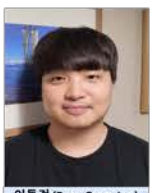
이동건 (Dong Geon, Lee) 포항공과대학교


김희찬 (Hui Chan, Kim) 한국해양대학교


유혜주 (Hye Ju, Yoo) 극지연구소, UST


이정욱 (Jeong Uk, Lee) 한국해양대학교


강동하 (Dong Ha, Kang) 극지연구소


손진수 (Jin Soo, Son) 한양대학교


손주영 (Ju Young, Son) 극지연구소, 부경대학교

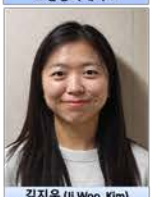
김지우 (Ji Woo, Kim) 부경대학교


박수진 (Su Jiin, Park) 인하대학교


변한웅 (Han Woong, Park) SBS


조병준 (Byeong Jun, Cho) SBS


선병호 (Byung Ho, Sun) 선의 (Doctor)


박은혜 (Eun Hye, Park) 해군


Machacek Todd NANA Management Service


Spinde Martine NANA Management Service


Darvet Michael Maritime Helicopters

Korosov Anton Maritime Helicopters

Stolz Tobin Maritime Helicopters

ARA14B Cruise Track (August 1 ~ August 31, 2023):

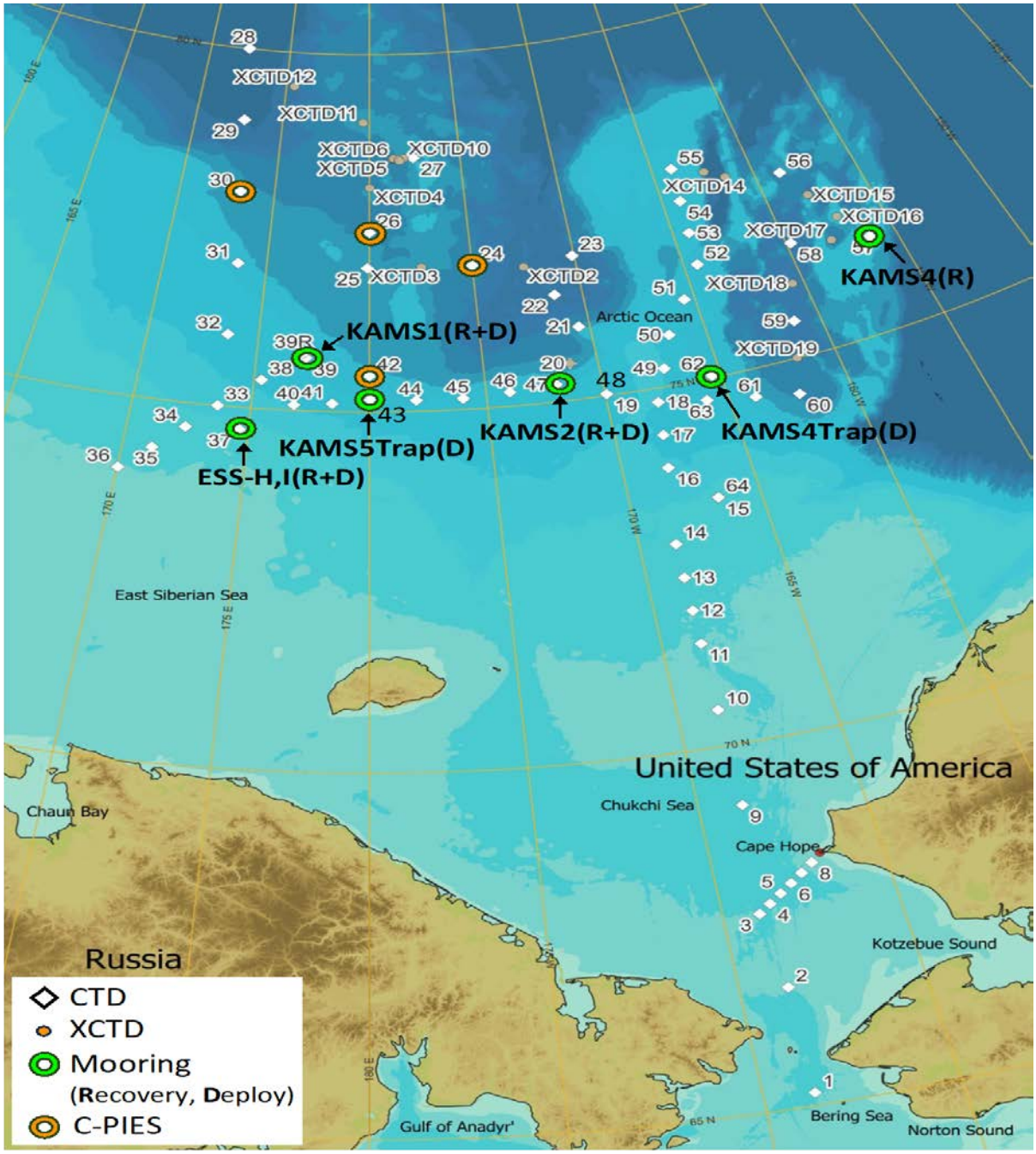

Figure 1. A station map of the 2023 Arctic Summer Expedition (ARA14B): CTD, mooring, and C-PIES mooring stations.

2023 ARAON Arctic Cruise

ARAON Arctic Cruise (ARA14B) departed Dutch Habar, Alaska on August 1st, 2023 and returned to Barrow on August 31th, 2023. With funding provided by the Ministry of Oceans and Fisheries (MOF) and by Korea Polar Research Institute (KOPRI), the aim of the cruise was was the aim of the cruise was to identify key environmental parameters (physical and biogeochemical) in rapid transition due to the sea-ice decrease in the western Arctic Ocean and predict environmental change patterns. The research effort was also conducted for the K-AWARE Program to observe physical, ecological, and biogeochemical parameters in rapid transition and how quickly environmental changes affect the ecosystem in the Arctic Ocean. Again, the results obtained from the 2023 Arctic cruise will be integrated with regional studies and be used to improve prediction models and to make effective adaptation strategies for the rapidly changing Arctic Ocean. For ARA14B, total of 31 scientists and other staffs have participated, representing 12 different organizations that are comprised of 9 universities, 1 research institutes and 2 companies.

The in-situ data were collected on the physical, biological, chemical, and biogeochemical properties of Arctic seawater in the shelf, slope and deep-sea regions of the Bering/Chukchi/East Siberian seas and the Makarov Basin. Profiles of water temperature and salinity were obtained with CTD (Conductivity-Temperature-Depth). Additional sensors on the CTD profiler were collected in-situ data on phytoplankton concentrations (fluorometer), optical clarity (transmissometer), dissolved oxygen (DO) and photosynthetic active radiation (PAR). A rosette sampler was used with the CTD to obtain water samples from discrete depths for a broad suite of biological and geochemical parameters, some for onboard analysis, others to be stored for later analysis in shore-based laboratories. Both bio-acoustic backscatter data and depth-varying current information were collected using an Lowered Acoustic Doppler Current Profiler (LADCP) attached to CTD at most of the science stations. Data were also collected from the ship-mounted transducer along the ship track to evaluate the possibility of using these data for bottom classification purposes. Plankton samples were obtained in vertical hauls by phyto- and bongo-nets lowered to 200 m.

Survey components:

- Water Column components
  - Water mass structure (water temperature, salinity, water velocity)
  - Pelagic ecosystems observations
    (bacteria, phytoplankton, zooplankton, Ichthyoplankton, Fish)
  - Primary Production & Secondary Production
  - Bio-geochemical measurements (nutrient, DOC, DIC, POC, DO, TEP, Macromolecular, Composition, Black carbon, Dissolved Amino Acid)
  - Stable Isotope
  - Seawater dissolved gas (pCO_2)
  - Trace Metal
- Benthic organism
- Biological Acoustic
- Underway collection of meteorological and near-surface seawater
- Meteorological data from ship sensors
- On-shore calibration of instrument compasses
- CTD/rosette casts for hydrography and geochemistry
- LADCP (Lowered ADCP) for vertical profiles of water velocity at the CTD stations
- Ocean mooring systems recovered and re-deployed for measuring year-long water temperature, salinity, and water velocity
- Sea-ice (ICE) observations through regular visual observations from bridge and automated fixed-camera photos.
- Arctic Sea-ice camp operation
  - Sea-ice physic and dynamic
  - Sea-ice biogeochemistry and biota
  - Buoy deployment
  - Helicopter survey
  - Melt pond ecosystem

Chapter 1. Atmospheric Observations

Joo-Hong Kim[1], Jung Hyun Park[1,2], Dong-Geon Lee[3], and Eun-Hye Park[4]

[1]*Korea Polar Research Institute, Incheon, Republic of Korea*

[2]*Pukyong National University, Busan, Republic of Korea*

[3]*Pohang University of Science and Technology, Pohang, Republic of Korea*

[4]*Navy, Republic of Korea*

Email: joo-hong.kim@kopri.re.kr; james70712@kopri.re.kr; donggeon0103@postech.ac.kr; eunhye1@navy.mil.kr

1.1. Introduction

The Arctic Ocean has dramatically opened during the summer melting seasons of recent decades with the unprecedented reduction of sea ice due to global warming, at least over the past thousand years (Kinnard et al., 2011). The reduction of the ice-covered surface should change the energy balance, leading to the warming of the polar lower atmosphere (Serreze et al., 2011) and influencing the atmospheric profile. To understand the rapidly changing climate in the Arctic, it is essential to understand the feedback mechanisms that are specific to the Arctic. All of these facts emphasize the continuous, on-site observations of atmospheric parameters in the Arctic Ocean. However, the polar weather is cold and harsh even during the summer season, so autonomous platforms measuring atmospheric properties (e.g., air temperature, humidity, pressure, wind, etc.) often suffer from malfunction arising from freezing, which means difficulty in maintaining them without regular management by humans. Alternatively, ship-based observations of the Arctic atmosphere can provide invaluable records along the cruise track, though the observations are only able to be done in a limited period.

In 2023 summer, Korean ice-breaking research vessel (IBRV) Araon carried out the 2nd leg of her Arctic research cruise (ARA14B) over the Bering Strait, Chukchi and East Siberian seas from 2 August to 31 August. Various atmospheric properties were observed during the cruise. Basic meteorological parameters (e.g., air temperature, humidity, pressure, and wind) and radiative fluxes (e.g., shortwave and longwave radiations) at the surface were continuously observed by multiple instruments at the radarmast and foremast. The vertical profiles of air temperature, humidity, pressure, and wind were also obtained by regular radiosonde

observations. In addition, cloud-related observations were carried out by Micro Pulse Lidar (MPL) at 04 deck and all-sky camera at compass deck. This report provides the information about instruments and some preliminary results of observation for post-data processing and further analysis.

1.2. Instruments

Figure 1.1 shows the illustrative overview of atmospheric observations on IBRV Araon during the 2023 Arctic cruise, including list of instruments at each observation location.

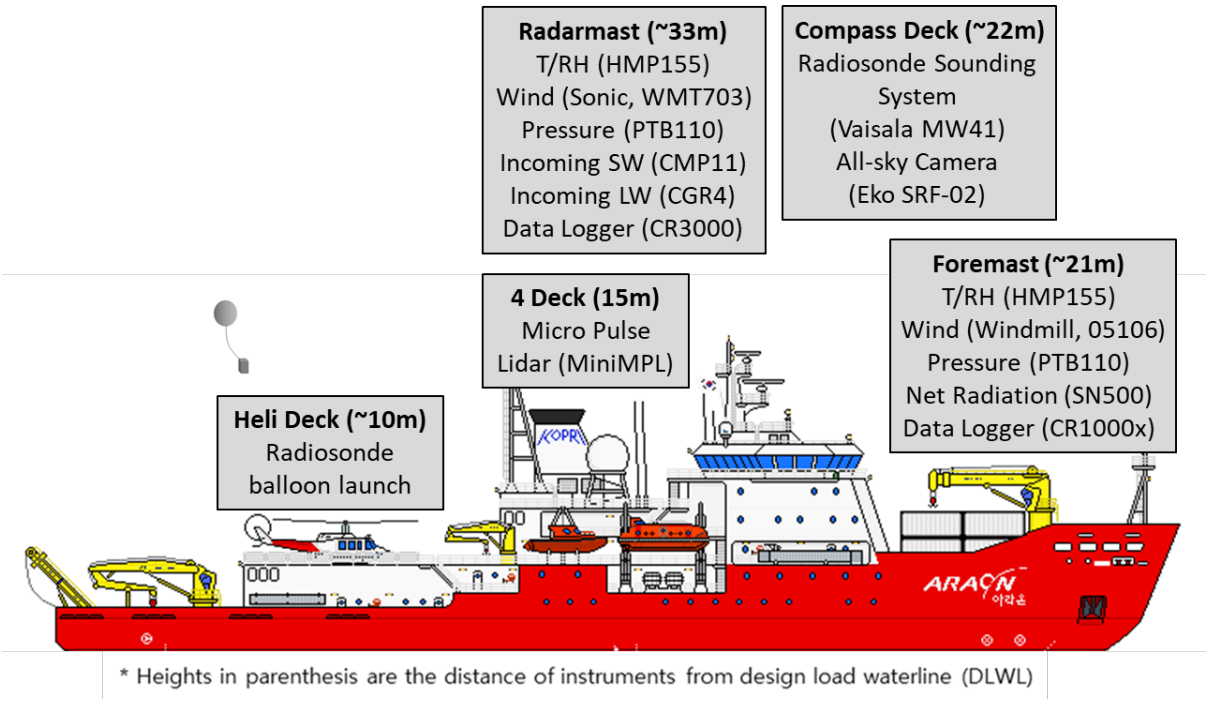

Fig 1.1 Illustrative overview of atmospheric observations on IBRV Araon during the 2023 Arctic cruise (ARA14B)

1.2.1. Radarmast

Figure 1.2a shows a photo taken at compass deck toward radarmast. On its top (~33 meters above the water surface), two sonic anemometers (WMT703, Vaisala, Finland) are running to collect temporal changes in on-site wind speed and direction relative to ship's course and speed, and a temperature-humidity prove (HMP155, Vaisala, Finland) is installed at the guardrail to collect air temperature and relative humidity. A barometer (PTB110, Vaisala, Finland) that is put inside a data logger enclosure collects near-surface pressure. Besides, a couple of radiometers, i.e., a pyranometer (CMP11, Kipp&Zonen, Netherland) and a pyrgeometer (CGR4, Kipp&Zonen, Netherland), measures incoming shortwave (solar) and

longwave (terrestrial) radiative fluxes, installed at the tip of two horizontal arms toward ship's starboard and port sides, respectively. A data logger (CR3000, Campbell Scientific, Inc., USA) collects all of these data, averages for 10 minutes, and saves at 10-minute intervals.

1.2.2. Foremast

Figure 1.2b shows a photo taken at ship's front side toward foremast. Around the foremast, there is also a set of meteorological instruments running continuously. A windmill anemometer (05106, RM Young, USA) collects wind speed and direction.at the top of the mast (~21 meters above the water surface). However, the wind direction data shows several shifts since March 2023, which is very likely due to the rotational movement of fixing point. The same temperature-humidity prove (HMP155, Vaisala, Finland) and barometer (PTB110, Vaisala, Finland) as those at the radarmast are respectively installed at the vertical bar and the inside of a data logger enclosure. Besides, in front of the mast, a net radiometer (SN-500, Apogee, USA) is mounted outside from ship bow which measures 4 components of upward and downward radiative fluxes together (Fig. 1.2c). A data logger (CR1000x, Campbell Scientific, Inc., USA) logged all data every second except for radiations with an interval of five seconds. As in the radarmast, 10-minute averaged data were saved and sent to the computer in the atmospheric sciences lab at 03 Deck.

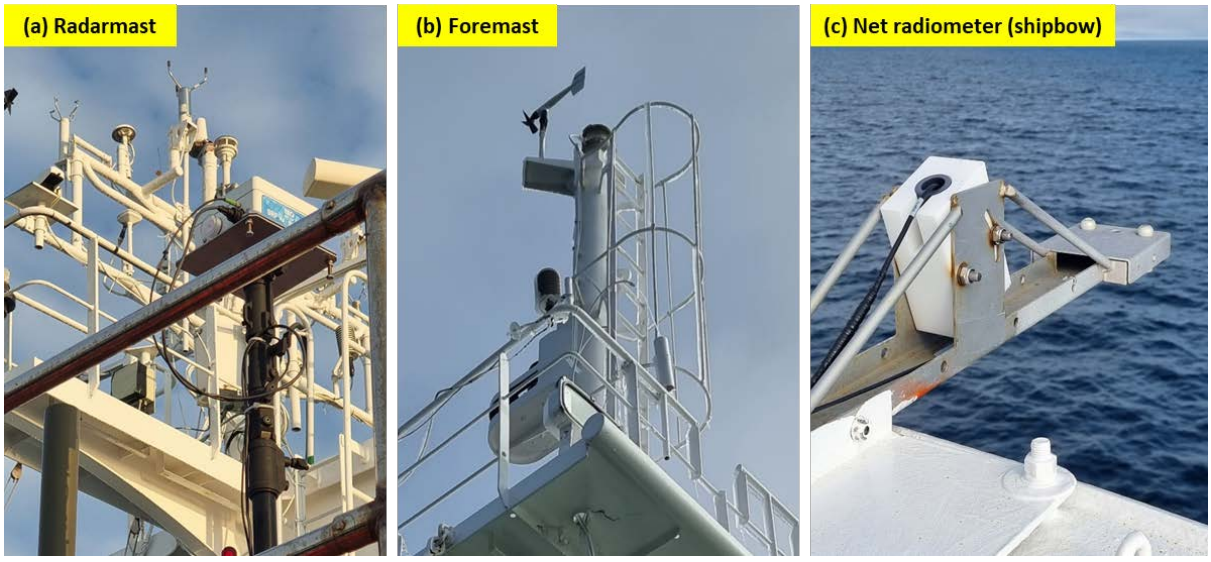

Fig 1.2 Meteorological instruments at radarmast (a) and foremast (b-c)

1.2.3. Compass deck

Radiosonde instruments are installed at the seatainer on compass deck (Fig 1.3a-c), except for the balloon launcher put on helideck (Fig 1.3d). Next to the radiosonde UHF antenna at the seatainer rooftop, all-sky camera (Eko SRF-02, Eko, Japan) regularly takes all-sky photos at 15-min intervals to observe cloud amount (Fig. 1.4a). The radiosonde sounding system (MW41, Vaisala, Finland) consisting of UHF antenna (Fig. 1.3a), receiver and ground checker (Fig. 1.3c) receives the transmitted data from the ascending balloon-tethered radiosonde sensor (RS41-SG, Vaisala, Finland). The radiosonde has been launched mostly every 12 hours (00 and 12 UTC) on helideck where a balloon launcher helps to prepare helium injection into 350g Totex balloons (TA350). Radiosonde data are transmitted to the real-time radiosonde data network of the World Meteorological Organization via the Global Telecommunication System (GTS) twice per launch when the ascending radiosonde reaches 100 hPa and the sounding is finished. For the real-time radiosonde data transmission, an Iridium Certus device (antenna and modem; Fig. 1.3a, b) was used during the cruise. The GTS broadcasting has been successful with the aid of the Korea Meteorological Administration and, in near real-time, can be monitored on the commercial weather information website ‘Windy’ (Fig. 1.5).

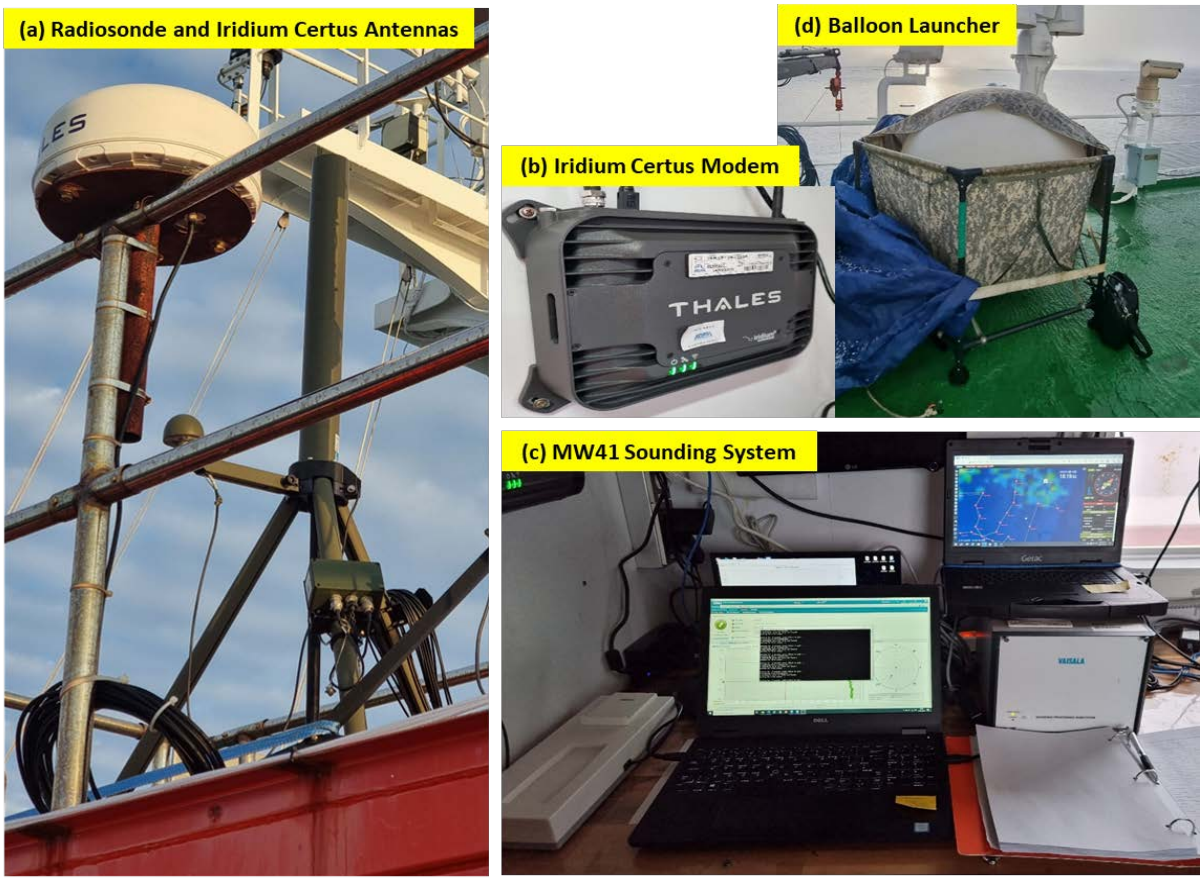

Fig 1.3 Radiosonde instruments at compass deck (a-c) and heli deck (d)

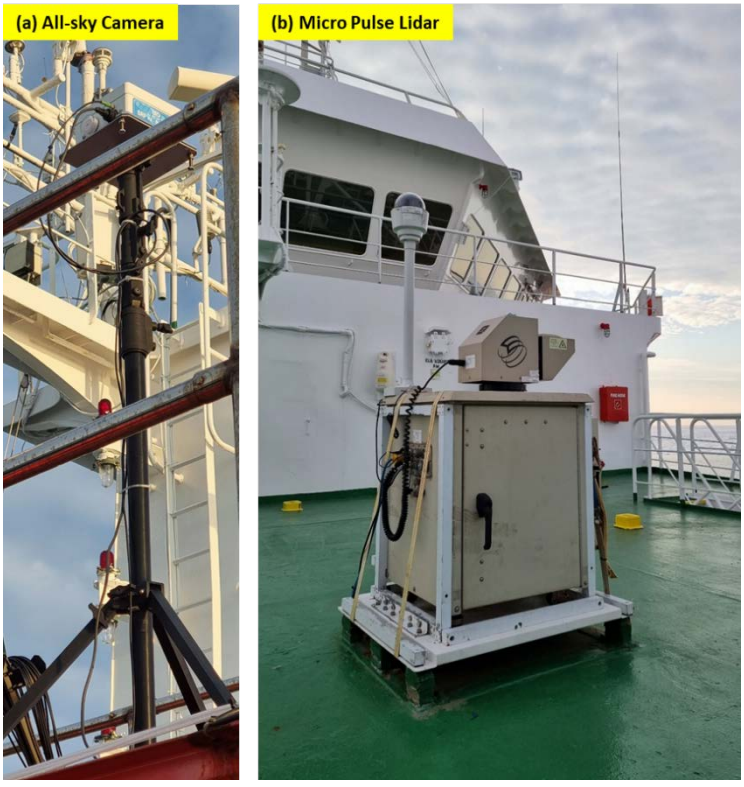

Fig 1.4 All-sky camera at compass deck, (b) Radiosonde antenna, (c) Sounding Process System

(MW41), (d) Iridium Certus Modem at the compass deck

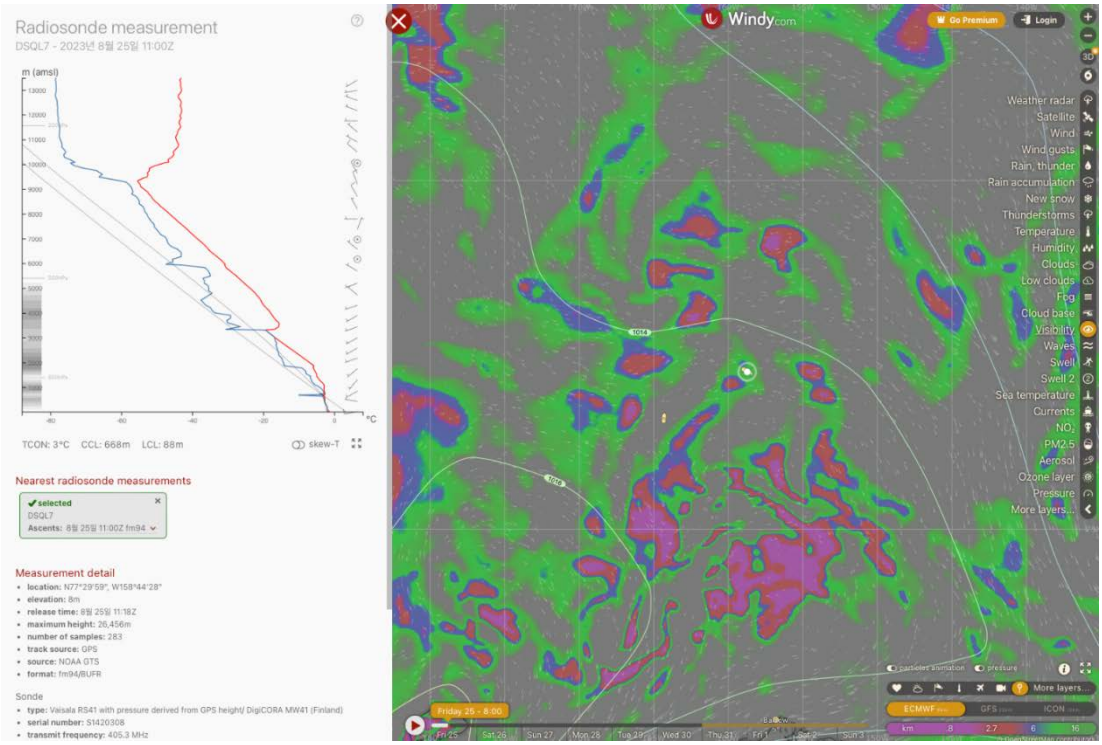

Fig 1.5 Near-real-time monitoring of radiosondes launched on IBRV Araon (call sign: DSQL7) (captured on the web page: https://www.windy.com)

1.2.4. 04 deck

At 04 Deck, a micro pulse lidar (MPL) is redeployed again since it was out of order in 2021 (Fig. 1.4b). The MPL observes the cloud and aerosol particles in vertical direction up to 15 km by actively emit a visible-band laser beam in co- and cross-polarization modes. Variables that can be retrieved includes normalized relative backscatter, depolarization ratio, cloud base height, planetary boundary layer height, and aerosol extinction coefficient. It also has a built-in sky camera and GPS.

1.3. Observed results

1.3.1. Surface meteorological variables

Figure 1.6 presents the air temperature, relative humidity, air pressure taken from foremast, and calculated true wind speed and direction from relative wind speed and direction taken at radarmast. To calculate the true wind speed and direction, the ship's heading (HDG), course

over ground (COG), and speed over ground (SOG) data are retrieved from GPS and Gyro Compass of the DaDis dataset.

Along the cruise track, the air temperature ranged from about 14.1°C (between St.7 and St.8 around 68°N) to about -3.2°C (between St. 21 and St.22 around 76°N). The temperature records indicate that the transition from the midlatitude atmosphere to the Arctic atmosphere (i.e., the rapid drop of the air temperature below freezing) occurred on 5-6 August when the ship moved northward across 72-74°N. In the Arctic regime (6 August and onward), the temperature varied between -3 and 2°C. While, in the early and late period of the cruise, the ship was in the high pressure regime and met a thick fog zone frequently with relative humidity over 95%, the ship encountered an arctic cyclone in the mid-period of the cruise (from 14 August to 22 August) during which the pressure dropped below 1000 hPa and the relative humidity varied between 75-95% depending on the ship's position relative to the cyclone's frontal zones. Wet snowfall was frequent when the frontal zone passed the ship. The pressure dropped down to 988 hPa and maximum wind speed reached 18 m/s when winds blew from west-northwest on 16 August.

Figure 1.7 shows the wind rose plot to identify prevailing wind speed and direction. The prevailing winds were the southwesterly and westerly. While the winds from the west (NW-W-SW) were strong, the mild winds mainly blew in the directions from the east (NE-E-SW).

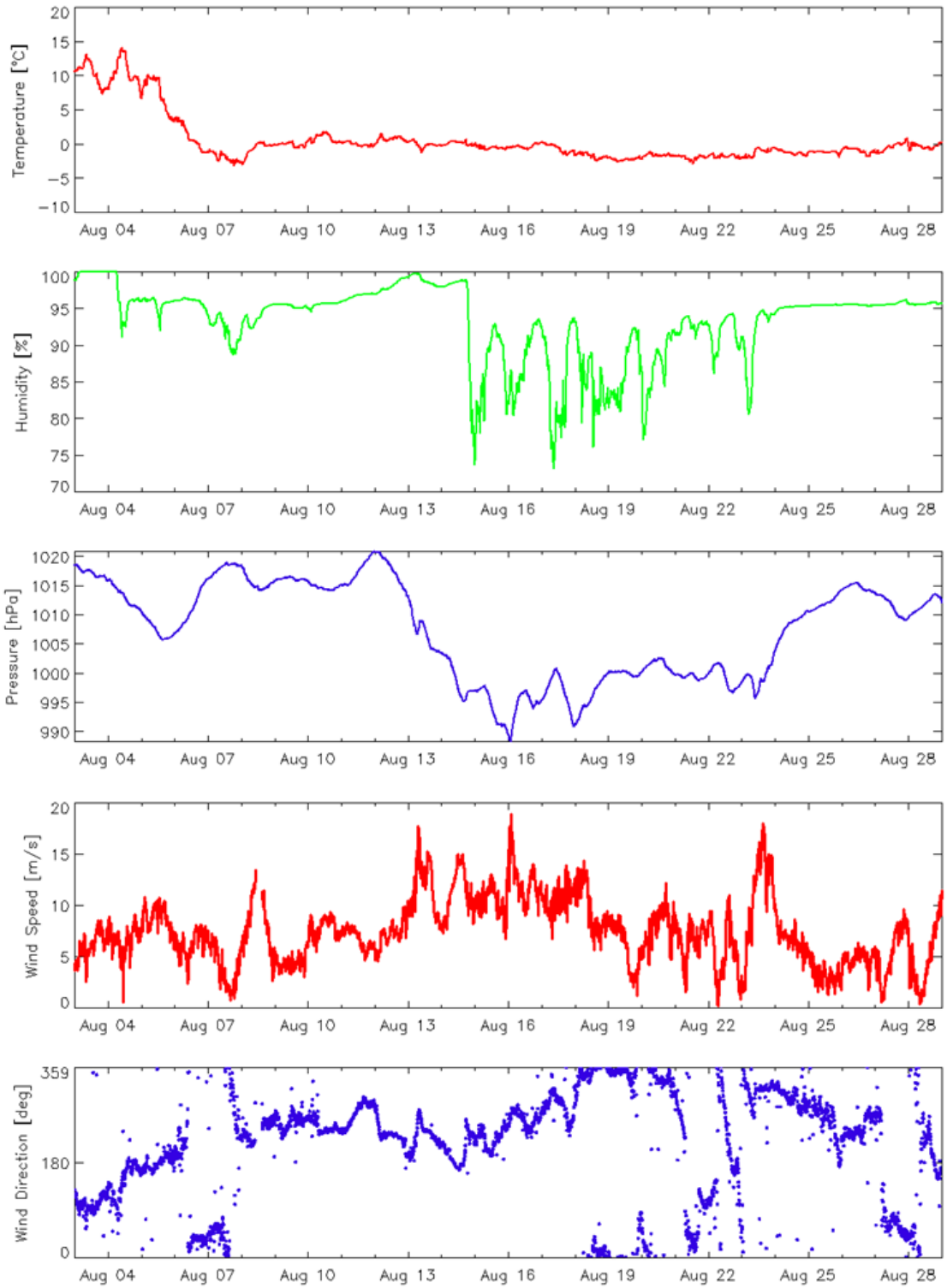

Fig 1.6 (From top to bottom) Time series of air temperature (° C) and relative humidity (%) from HMP155, air pressure (hPa) from PTB110, and true wind speed (m/s) and direction (deg) from WMT703 during ARA14B

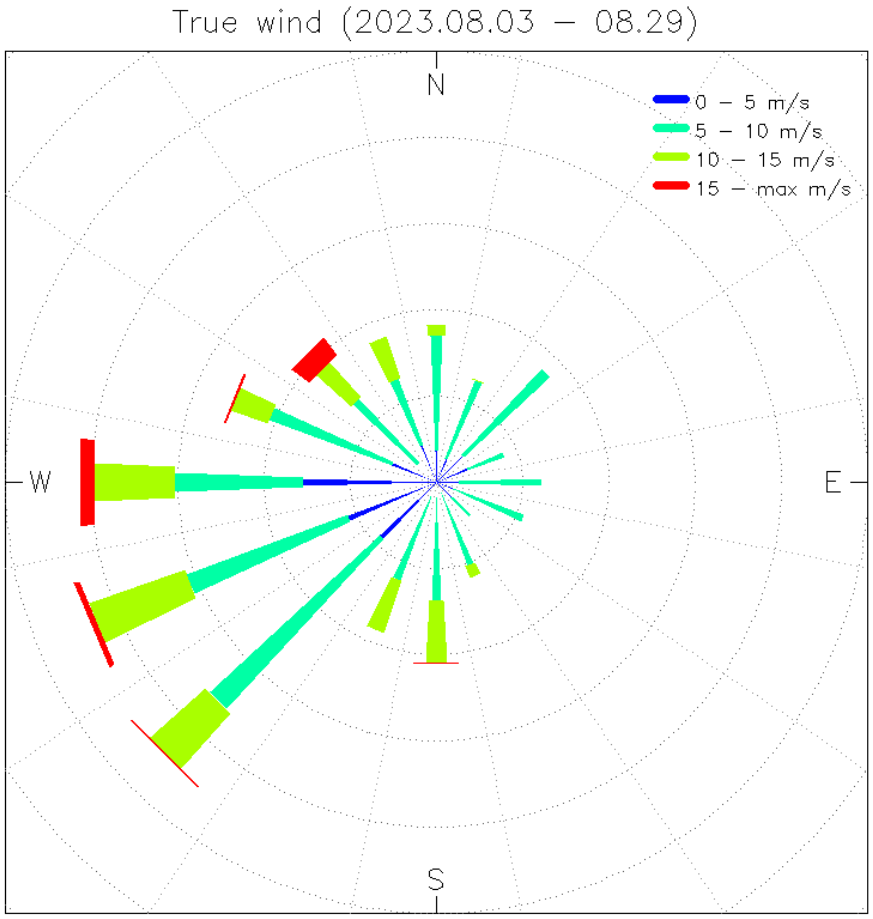

Fig 1.7 Wind rose to show the statistics of wind speed and direction during ARA14B

1.3.2. Radiosonde profile

During this 2nd leg, a total of 65 radiosonde balloons was launched and got the atmospheric vertical profiles in the Arctic. The launched locations are displayed in Fig. 1.8. The highest latitude was for the 23rd one near the St.28 (80°N, 172.4°E) at 00 UTC 14 August. Most of the balloons were launched twice daily (00, 12 UTC) in the early-middle period, but four times daily (00, 06, 12, 18 UTC) at the later period (24-29 August). Table 1.1 summarizes the log of all radiosonde observations. These data are crucial for understanding the thermodynamic properties in the Arctic summer atmosphere over the sea where no permanent in-situ observation is possible. Most of the profiles cover the tropospheric levels, with many of them reached the stratospheric levels (20 to 30 km altitude). The average flying time and altitude of all balloons was 4629 s and 24861 m (46.18 hPa). The highest altitude reached was 29798 m (13.5 hPa) for the launch done at 12 UTC 4 August. Considering that the average height of the good quality TA350 balloon is 25 km, the average altitude is close to the target level. As

these data were all transmitted to the world real-time radiosonde data network via the GTS, they are used not only for the operational weather forecast, but also for the production of atmospheric reanalysis.

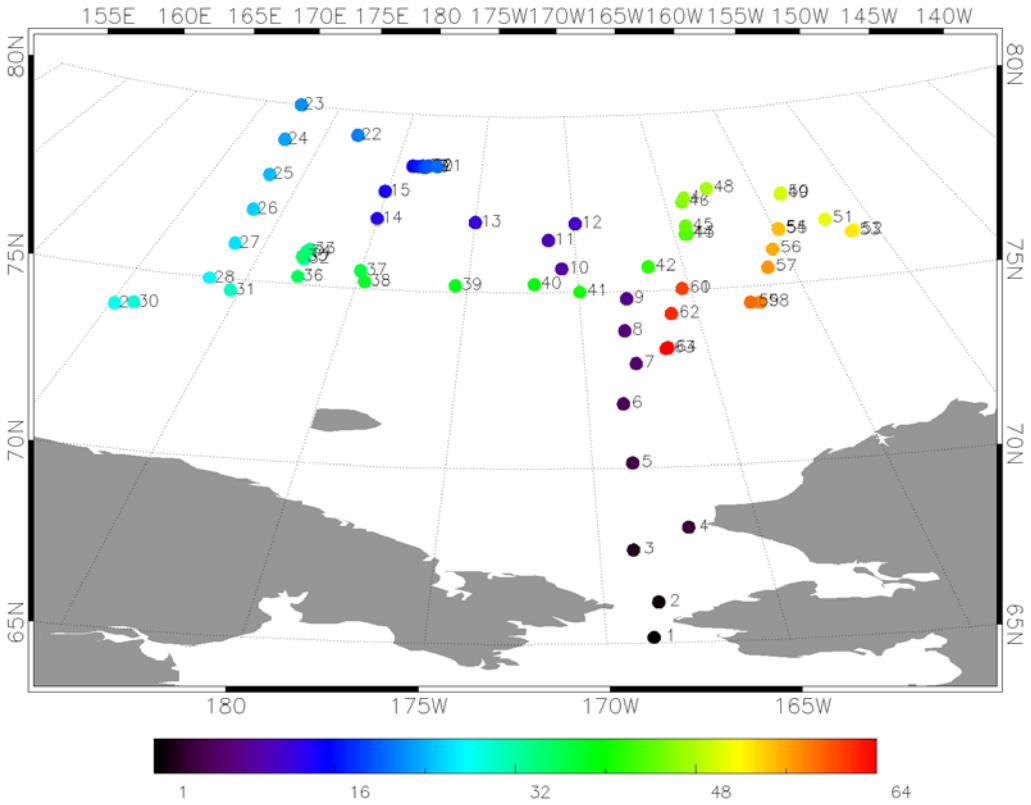

Fig 1.8 The locations of radiosonde balloon release during ARA14B

Table 1.1. Log of radiosonde observations during ARA14B

No	Date	Time (UTC)	Start Time	Duration (sec)	Height (m)	Pressure (hPa)	weather	Remarks
1	2023-08-03	0	00:27	5172	28049	17.36	cloudy	Launched during St.1
2	2023-08-03	12	11:32	5302	27212	19.69	cloudy	
3	2023-08-04	0	23:25	4440	25759	24.53	cloudy	Launched during St.3
4	2023-08-04	12	11:26	6648	29798	13.5	cloudy	
5	2023-08-05	0	23:23	4777	26682	21.43	cloudy	
6	2023-08-05	12	11:23	5098	27161	20.01	cloudy	Launched during St.12
7	2023-08-06	0	23:34	6224	28697	15.97	foggy & cloudy	
8	2023-08-06	12	11:20	5203	27686	18.48	Rainy	Launched during St.16
9	2023-08-07	0	23:24	4761	26547	21.92	cloudy	Launched during St.18

10	2023-08-07	12	11:19	4834	26938	20.83	clear	
11	2023-08-08	0	23:27	4800	26079	23.66	cloudy	Launched during St.22
12	2023-08-08	12	11:16	4557	22529	40.34	cloudy	Launched near St.23
13	2023-08-09	0	23:23	4511	25622	25.31	foggy & cloudy	Launched during St.24
14	2023-08-09	12	11:23	1641	9016	314.72	clear	Launched during St.25 Temperature sensor failure
15	2023-08-10	0	23:20	4848	26031	23.79	clear	
16	2023-08-10	12	11:23	4826	26585	21.90	rainy	Launched during 1st ice camp station
17	2023-08-11	0	23:11	4838	23957	32.52	cloudy	Launched during 1st ice camp station
18	2023-08-11	12	11:20	4505	25522	25.72	foggy	Launched during 1st ice camp station
19	2023-08-12	0	23:41	4523	26150	23.41	foggy & cloudy	Launched during 1st ice camp. station
20	2023-08-12	12	11:30	5466	28012	17.73	cloudy	Launched during 1st ice camp station
21	2023-08-13	0	23:25	5310	28098	17.48	foggy & cloudy	Launched near St.27
22	2023-08-13	12	11:23	4374	25483	25.81	cloudy	
23	2023-08-14	0	23:23	1050	5801	472.82	cloudy	Launched during St.28 Excessive missing GPS height
24	2023-08-14	12	11:25	2157	11276	211.65	cloudy	Launched during St.29 Excessive missing GPS height
25	2023-08-15	0	23:22	5390	26995	20.49	cloudy	Launched during St.30
26	2023-08-15	12	11:17	4860	25857	24.17	snowy & cloudy	Launched right after departed from St.31 to St.32
27	2023-08-16	0	23:19	5119	27234	19.66	clear	Launched during St.32
28	2023-08-16	12	11:25	3824	15228	117.69	cloudy	Excessive missing GPS height
29	2023-08-17	0	23:27	1331	7507	365.25	cloudy	Launched during St.36 Excessive missing GPS height
30	2023-08-17	12	11:22	5480	27164	19.76	cloudy	
31	2023-08-18	0	23:46	5714	28070	17.21	snowy	Launched during St.37-H Failed 1st trial
32	2023-08-18	12	11:22	5251	26029	23.35	cloudy	Launched near St.39
33	2023-08-19	0	23:44	4510	25893	23.77	cloudy	Launched during 2nd ice camp station
34	2023-08-19	12	11:24	4363	24133	30.98	cloudy	Launched during 2nd ice camp station
35	2023-08-20	0	23:22	5105	26811	20.65	cloudy	Launched during St.39
36	2023-08-20	12	11:09	5470	25664	24.48	cloudy	
37	2023-08-21	0	23:26	5065	27154	19.58	snowy & cloudy	Launched during St.42
38	2023-08-21	12	11:23	4543	25211	26.12	snowy	

39	2023-08-22	0	23:19	4028	23609	33.24	snowy & cloudy	
40	2023-08-22	12	11:18	6054	28833	15.17	snowy & cloudy	Launched during St.47
41	2023-08-23	0	23:16	5274	26113	22.81	snowy & cloudy	
42	2023-08-23	12	11:23	5349	27275	19.16	snowy & cloudy	Launched during St.50
43	2023-08-24	0	23:18	4472	25444	25.19	cloudy	Launched during St.52
44	2023-08-24	6	05:12	4530	25676	24.32	cloudy	Launched near St.52
45	2023-08-24	12	11:20	4774	26709	20.78	cloudy	
46	2023-08-24	18	17:32	4734	25509	24.8	foggy	Launched during St.54 Drifted south-eastward
47	2023-08-25	0	23:23	4076	24977	26.92	cloudy	
48	2023-08-25	6	05:16	4707	26324	21.98	cloudy	
49	2023-08-25	12	11:18	4754	26445	21.57	cloudy	
50	2023-08-25	18	18:04	4971	27151	19.36	foggy, cloudy & calm	Failed 1st trial
51	2023-08-26	0	23:20	4734	25500	24.84	snowy & cloudy	
52	2023-08-26	6	05:22	5153	26945	19.97	cloudy & foggy	Launched during St.57
53	2023-08-26	12	11:14	5856	27377	18.68	cloudy & snowy	
54	2023-08-26	18	17:24	4802	27142	19.35	snowy & foggy → partly cloudy	Launched during St.58
55	2023-08-27	0	23:22	4952	26548	21.15	foggy & cloudy	Launched during St.58
56	2023-08-27	6	05:17	1866	12044	186.89	cloudy & calm (No wind)	Terminated by Excessive missing GPS height
57	2023-08-27	12	11:19	4244	24696	27.95	cloudy	Launched during St.59 Excessive missing GPS height
58	2023-08-27	18	17:28	4916	26745	20.47	foggy & cloudy	Launched during St.60
59	2023-08-28	0	23:21	4773	26278	22.00	cloudy & calm	
60	2023-08-28	6	05:35	4045	25319	25.44	cloudy & partly clear	
61	2023-08-28	12	11:22	4023	25032	26.50	clear & partly cloudy	
62	2023-08-28	18	17:25	4158	25522	24.57	cloudy	
63	2023-08-29	0	23:23	4678	26639	20.81	snowy & cloudy	Launched during St.65
64	2023-08-29	6	05:21	4603	26454	21.38	cloudy & partly clear	
65	2023-08-29	12	11:23	4468	26041	22.72	foggy & cloudy	

The skew T-log P plots are presented for three representative times, i.e., the early period high pressure regime (P1), mid-period low pressure regime (P2), and later period high pressure regime (P3), with the sky image taken by the all-sky camera. In P1, a strong surface

inversion occurred above which clear lower tropospheric and cloud mid-tropospheric layers existed. Sunlight in the image indicates the cloud amount was not much large. The middle-to-upper tropospheric was humid, so that the boundary between troposphere and stratosphere was clearly seen near 250 hPa. In another high pressure regime P3, the surface inversion was not presented and low stratus cloud covered the sky below 700 hPa which made snowfall at this time. The middle-to-upper troposphere was relatively drier, compared to P1. Nevertheless, the boundary between troposphere and stratosphere was clear around 300 hPa, slightly lower than that at P1. By contrast, P2 shows a distinctive atmospheric profile with a steeper temperature decrease with height up to 650 hPa. Below this level, some patches of clouds formed under active mixing by strong winds. Above this level, the very dry layer akin to stratospheric air existed with a weak temperature decrease with height, indicating that a deep mixing with stratospheric air. Very dry air between 650-100 hPa made the sky clear. Deep mixed stratosphere-troposphere air moved the stratospheric layer up above 100 hPa.

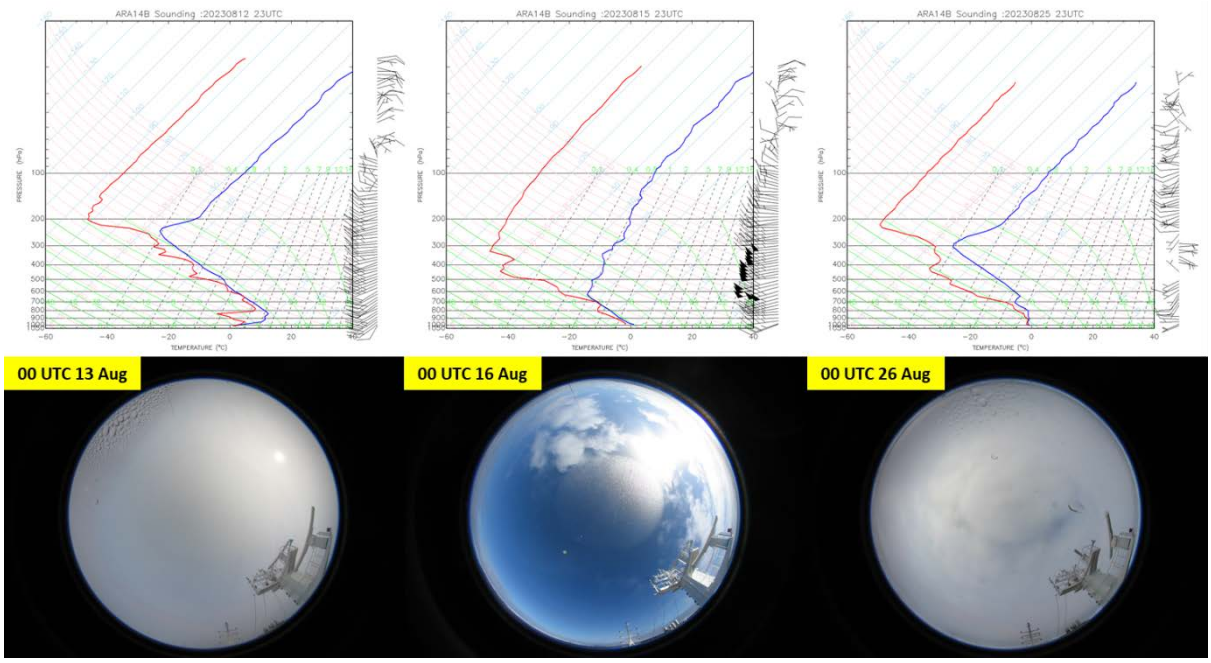

Fig 1.9 Skew T-log P diagrams (blue: temperature, red: dew-point temperature) from radiosonde sounding data for three cases: (left) 00 UTC 13 August, (middle) 00 UTC 16 August, and (right) 00 UTC 26 August. All-sky camera images taken for the three cases are shown at the bottom of each profile diagram

1.3.3. MPL profile

The active laser beam sounding of atmospheric cloud and aerosol particles by the MPL produced the profiles of backscattered co-polarized and cross-polarized signal strength (Fig. 1.10). With the aid of the surface and upper-air meteorological observations (1.3.1 and 1.3.2), temporal changes of the signal could be understood. During this cruise, frequent foggy and snowy days caused strong attenuation of backscatter signals at lower altitudes. During 10-14 August, frequent thick fog made the signal attenuate completely near the surface. The cloud base height was yielded by applying a wavelet method to the normalized relative backscatter. After the cruise, the MPL data collected this year with those collected during 2018-2020 are analyzed together to study the cloud's radiative role in surface temperature variations.

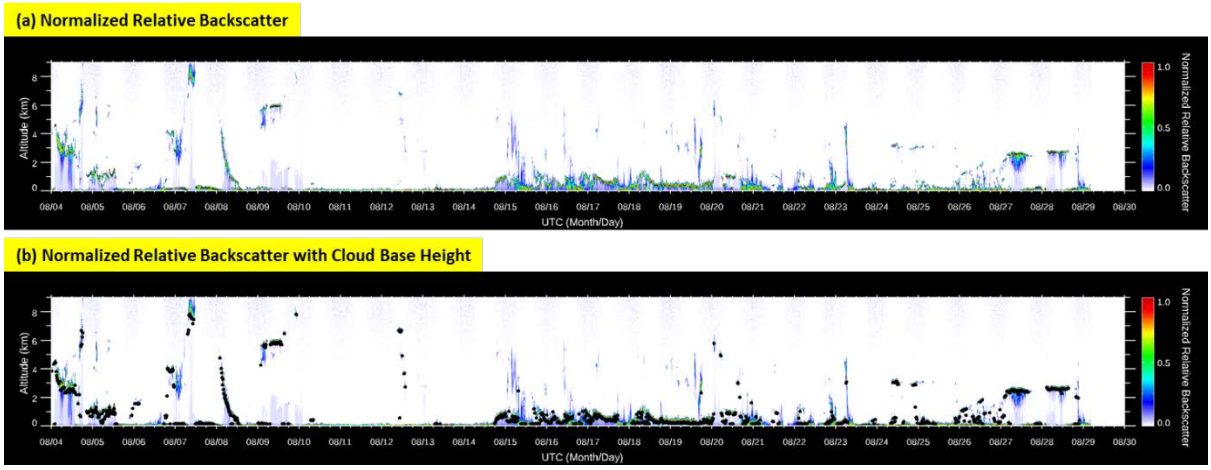

Fig 1.10 Normalized relative backscatter (a) and that with cloud based height calculated from the MPL raw data

1.4. Summary

During the ARA14B cruise, weather conditions in the Arctic were generally unfavorable. In regions north of the high pressure, characterized by relatively colder temperatures, instances of surface inversion layers led to frequent dense fog. When a low pressure trough was intruded, wet snowfall occurred along its frontal boundaries. This phenomenon can be attributed to the cooling of air masses as they traversed over the low sea surface temperatures, accompanied by a substantial moisture content within the atmosphere.

In this year, the Pacific Arctic region extending over the southern reaches of the Chukchi Sea (the latitude range of 73-75°N) exhibited a broadening belt of diminishing multi-year ice floes, where AMSR2 sea ice concentration data was almost zero. The presence of this diminishing sea ice zone over the low ice concentration sea indicates that an ongoing process of thawing inhibits the rise of sea surface temperatures. It is postulated to have facilitated the saturation of the atmosphere with higher levels of moisture over the colder sea surface. However, a thorough post-analysis is deemed necessary to validate these suppositions.

References

Kinnard, C., C. M. Zdanowicz, D. A. Fisher, E. Isaksson, A. de Vernal, and L. G. Thompson (2011), Reconstructed changes in Arctic sea ice over the past 1,450 years, Nature, 479(7374), 509–512.

Serreze, M. C., A. P. Barrett, and J. J. Cassano (2011), Circulation and surface controls on the lower tropospheric air temperature field of the Arctic. J. Geophys. Res., 116, D07104, doi:10.1029/2010JD015127.

Chapter 2. Physical Oceanography

Taewook Park, Jaeill Yoo, Myung-Seok Kim

Korea Polar Research Institute, Incheon, Republic of Korea

E-mail: twpark@kopri.re.kr; jiyoo@kopri.re.kr; kmspban@kopri.re.kr

Suk Hyun Haam

Neosea Tech, Ansan, Republic of Korea

E-mail: haam6481@gmail.com

Jeong-Yeob Chae, Su Jin Park

Inha University, Incheon, Republic of Korea

E-mail: jychae92@gmail.com;qkrtnwls516@gmail.com

Dong Ha Kang

Gyeongsang National University, Republic of Korea

E-mail: rkdehdgk789@naver.com

2.1. Hydrographic Survey

2.1.1 Motivation and Objective

Since 2010, KOPRI has conducted hydrographic surveys in the Arctic Ocean's Pacific sector every summer to explore temporal and geographical variations in water mass characteristics caused by recent rapid sea ice retreat and Arctic warming. During the summer, the majority of oceanic warming in the Pacific sector, which includes the Beaufort, Chukchi, and East Siberian Seas, as well as the central Arctic Ocean, originates from ocean surface heat flux and lateral heat flux convergence (Serreze et al., 2007; Steele et al., 2010). There are various types of Pacific-derived halocline waters that intrude through the Bering Strait and reach the Chukchi Sea (Shimada et al., 2001; Shimada et al., 2006; Steele et al., 2004; Woodgate et al., 2010). The Pacific summer water (PSW), which includes summer Bering Sea Water and Alaskan Coastal Water, is distributed to the northern Chukchi Sea through the shelf and to the Beaufort Sea along the Alaskan coast, and then redistributed to the Chukchi Borderland and

Mendeleev Ridge (CBLMR) (Shimada et al., 2005; Gong and Pickart, 2015 and 2016; Corlett and Pickart, 2017; Pickart et al. One of the cold halocline waters found in the study area is Pacific Winter Water (Zhong et al., 2019). PWW is classified into two types: remnant winter water flowing along the Alaskan coastal pathway and newly ventilated winter water flowing along the two interior Chukchi Sea pathways (Shroyer and Pickart, 2019). Variations in the paths and timing of inflowing Pacific-derived water masses may be important in understanding not just temporal and spatial changes in the halocline structure in CBLMR, but also biological responses to halocline layer changes in the Pacific sector of the Arctic Ocean. To better understand these changes, we performed a 27-day expedition (ARA14B) in the summer of 2023, using the ice-breaking R/V Araon.

2.1.2 CTD Casting

An oceanographic survey was conducted at 63 CTD stations from the north of the East Siberian Sea to the Chukchi Borderland during the period of August 2 to August 29, 2023 (Fig. 2.1.1). Along the transects of hydrographic stations (Table 2.1.1 and Appendix I), vertical profiles of temperature, conductivity, fluorescence, turbidity, transmissivity, and dissolved oxygen and water samples were obtained from the hydro-casts of a SBE32 carousel water sampler equipped with a SBE9plus CTD profiler, PAR, fluorometer, scattering sensor, altimeter and SBE43 dissolved oxygen sensor, and 24 position rosette with 10-liter Nisken bottles. During the CTD upcasting, water samples were collected at several depths for biochemical analyses. For the precise reading, the salinities of collected water samples were further analyzed by an Autosal salinometer (Guildline, 8400B). The measurement was performed when the temperature of water samples was stabilized to a laboratory temperature, usually within 24-48 h after the collection.

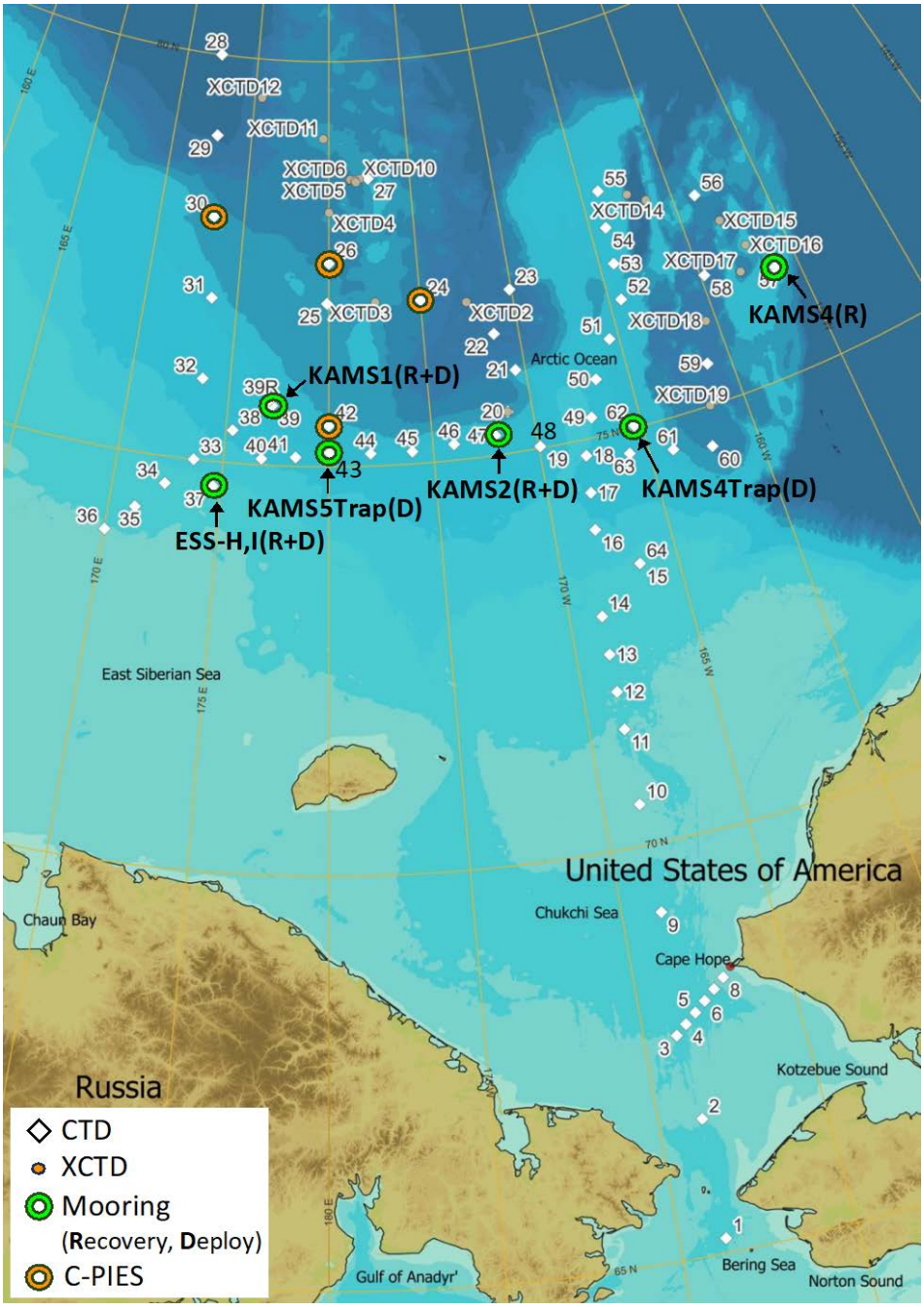

Figure 2.1.1. A station map of the ARA14B Arctic summer expedition with color-shaded bathymetry : CTD, mooring, and C-PIES mooring stations.

Table 2.1.1. Hydrographic CTD stations for Arctic Ocean expedition in 2023 (ARA14B).

CTD Station	Longitude (Deg/Min)	Latitude (Deg/Min)
ARA13B001	168° 41.44639' W	65° 10.40870' N
ARA13B002	168° 41.25130' W	66° 37.79659' N
ARA13B003	168° 57.59916' W	67° 40.20005' N
ARA13B004	168° 36.13271' W	67° 46.97993' N
ARA13B005	168° 14.09820' W	67° 53.87564' N
ARA13B006	167° 52.01998' W	68° 00.78092' N
ARA13B007	167° 29.70194' W	68° 07.68178' N
ARA13B008	167° 07.32392' W	68° 14.51859' N
ARA13B009	168° 40.00182' W	69° 10.01086' N
ARA13B010	168° 39.99353' W	70° 29.99280' N
ARA13B011	168° 40.00512' W	71° 25.80133' N
ARA13B012	168° 40.00715' W	71° 53.69953' N
ARA13B013	168° 39.74209' W	72° 21.55072' N
ARA13B014	168° 39.21821' W	72° 50.02826' N
ARA13B015	166° 37.75121' W	73° 22.07199' N
ARA13B016	168° 11.97683' W	73° 53.33832' N
ARA13B017	168° 03.00266' W	74° 20.69186' N
ARA13B018	167° 53.92643' W	74° 48.03374' N
ARA13B019	169° 56.19456' W	75° 01.23366' N
ARA13B020	171° 12.85547' W	75° 30.43043' N
ARA13B021	170° 29.99745' W	75° 59.99723' N
ARA13B022	171° 18.36300' W	76° 28.87204' N
ARA13B023	170° 05.76087' W	76° 59.41772' N
ARA13B024	174° 59.19580' W	76° 59.92268' N
ARA13B025	179° 54.25802' E	77° 00.28331' N
ARA13B026	179° 59.87909' W	77° 30.04519' N
ARA13B027	177° 35.15482' W	78° 32.44974' N
ARA13B028	172° 24.04193' E	80° 00.00647' N
ARA13B029	172° 47.98697' E	79° 00.00047' N
ARA13B030	173° 11.84474' E	78° 00.00376' N
ARA13B031	173° 35.99037' E	77° 00.00259' N
ARA13B032	173° 36.02559' E	75° 59.99561' N
ARA13B033	173° 36.02484' E	75° 00.00334' N
ARA13B034	172° 23.99308' E	74° 40.00318' N
ARA13B035	171° 11.99902' E	74° 19.99893' N
ARA13B036	170° 01.42409' E	74° 00.15024' N
ARA13B037	174° 37.44186' E	74° 41.62350' N
ARA13B038	175° 19.69794' E	75° 24.01665' N
ARA13B039	177° 11.39302' E	75° 44.05441' N
ARA13B040	176° 48.00367' E	75° 04.49581' N
ARA13B041	178° 25.20354' E	75° 06.47664' N
ARA13B042	179° 59.99260' E	75° 30.04253' N
ARA13B043	179° 57.94807' W	75° 10.21016' N
ARA13B044	177° 59.88517' W	75° 09.03457' N
ARA13B045	176° 00.00921' W	75° 09.00292' N
ARA13B046	173° 59.23691' W	75° 11.71825' N
ARA13B047	171° 58.34980' W	75° 14.42806' N
ARA13B048	169° 56.17203' W	75° 01.23671' N
ARA13B049	167° 16.08259' W	75° 14.75331' N
ARA13B050	166° 38.27664' W	75° 41.46791' N
ARA13B051	165° 29.11826' W	76° 07.95582' N
ARA13B052	164° 21.68823' W	76° 34.04565' N
ARA13B053	164° 13.39872' W	77° 00.90013' N
ARA13B054	164° 06.08906' W	77° 28.06606' N
ARA13B055	163° 58.03662' W	77° 55.66502' N
ARA13B056	158° 44.47557' W	77° 29.98794' N
ARA13B057	156° 13.26424' W	76° 18.23406' N
ARA13B058	159° 47.51447' W	76° 32.13080' N
ARA13B059	161° 08.82661' W	75° 29.90883' N
ARA13B060	162° 09.11692' W	74° 30.98136' N

ARA13B061	163° 55.01843' W	74° 36.91356' N
ARA13B062	165° 22.90469' W	75° 01.54665' N
ARA13B063	165° 54.45331' W	74° 42.48257' N

Table 2.1.2. Expendable CTD (XCTD) stations for Arctic Ocean expedition in 2023 (ARA14B).

XCTD Station	Longitude (Deg/Min)	Latitude (Deg/Min)
ARA13BX01	171° 12.85232' W	75° 30.43043' N
ARA13BX02	172° 30.89829' W	76° 54.96356' N
ARA13BX03	177° 27.65449' W	77° 00.69413' N
ARA13BX04	179° 59.08672' W	78° 07.72016' N
ARA13BX05	178° 44.24979' W	78° 31.78150' N
ARA13BX06	178° 40.10154' W	78° 31.82998' N
ARA13BX07	178° 39.39574' W	78° 32.11726' N
ARA13BX08	178° 23.50306' W	78° 31.45009' N
ARA13BX09	178° 19.90182' W	78° 30.11653' N
ARA13BX10	178° 06.77926' W	78° 32.34309' N
ARA13BX11	179° 38.612007' E	79° 02.45122' N
ARA13BX12	175° 28.825204' E	79° 31.16635' N
ARA13BX13	162° 23.68703' W	77° 47.16688' N
ARA13BX14	161° 27.46390' W	77° 38.92790' N
ARA13BX15	157° 57.80490' W	77° 05.88970' N
ARA13BX16	157° 10.77830' W	76° 43.29420' N
ARA13BX17	158° 00.71737' W	76° 25.09539' N
ARA13BX18	160° 31.24550' W	75° 59.90230' N
ARA13BX19	161° 39.93798' W	74° 59.96606' N

θ-S Diagram

During the expedition, we carried out CTD deep casts at 63 stations. Using the CTD deep downcasting, we plotted the potential temperature (θ)–salinity (S) diagram (Fig. 2.1.2). It shows that the study area is occupied by several distinct water masses: Surface mixed layer water (SMLW), Pacific summer water (PSW), Pacific winter water (PWW), Atlantic water (AW), and some halocline waters. SMLW has the lowest salinity (down to about 27 psu) due to sea ice melting and fresh water input. SMLW includes the early season melting water, riverine water, and seasonal mixed layers. PSW is composed of three types of water masses: The first is the Alaska Coastal Water (ACW) which is the warmest, freshest water mass presenting temperature maximum layer at surface. The second is the Bering Summer Water (BSW) which is relatively colder and saltier than ACW. The last is the remnant summer water (rSW) which has a temperature maximum at 30~60 m depths. Its salinity is in the range of 30.0-32.5 psu, and temperature is around -0.7~3.0°C. PWW, a layer of relatively fresh (i.e., buoyant), cold

water, lies immediately above the warm AW that is the water mass with the highest temperature and highest salinity. PWW plays a role in shielding the exchange of heat flux between overlying rSW and underlying AW. PWW is composed of two types of water masses: Newly ventilated winter water (WW) and remnant winter water (RWW) (Pickart et al., 2016). There is another cold halocline water derived from the eastern Arctic Ocean, which is located between PWW and AW, so-called the Atlantic-derived lower halocline water (AHW).

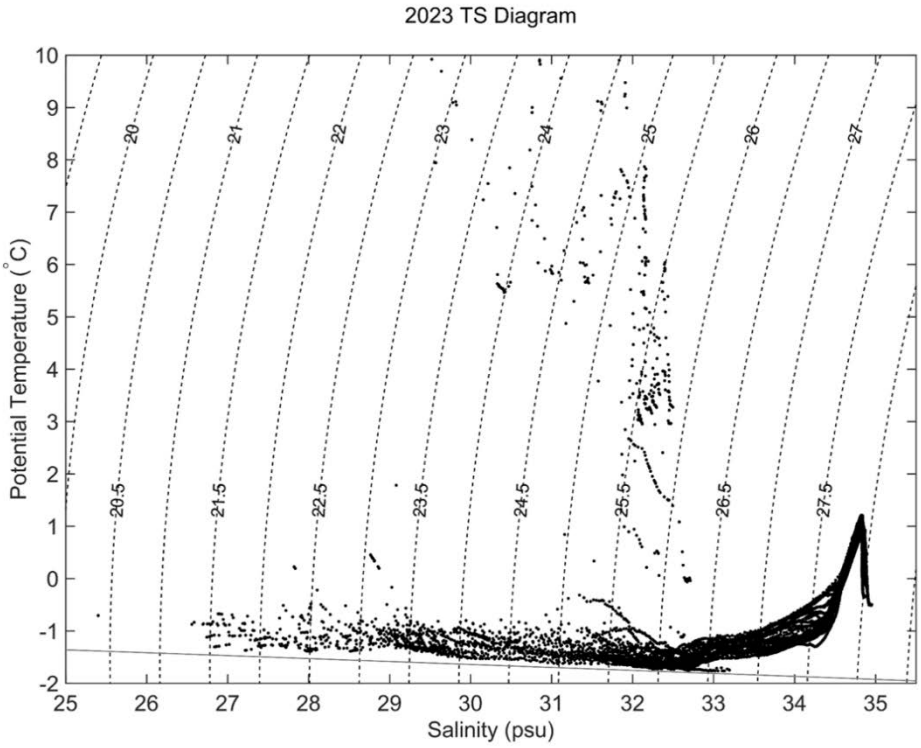

Figure 2.1.2. Potential temperature (θ)−salinity (S) diagram from ship-based CTD stations

Vertical Structure of Water Masses

We plotted the distributions of potential temperature and salinity in the water column along two transects: the west-east line (TR1) and the north-south line (TR2) in Fig. 2.1.3. Along TR1, the warm water was distributed on top of cold water near the Chukchi shelf. Along TR2, there were warm (> 5oC) water layers from St.01 to St.12 due to an inflow of the Alaska Coastal Water (ACW) through the surface layer during the absence of sea ice.

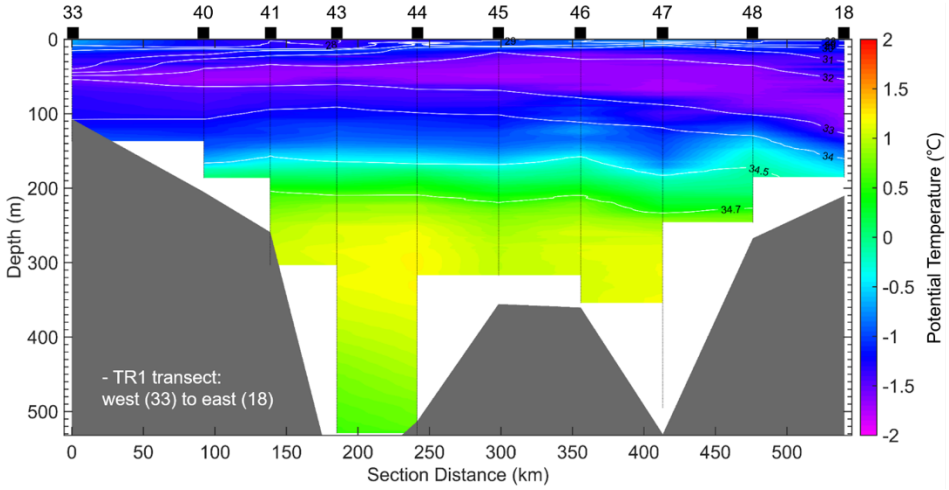

Figure 2.1.3. Vertical structures of potential temperature (color-shaded) and salinity (white contour lines) along the TR1 transect from St.33 (west) to St.18 (east).

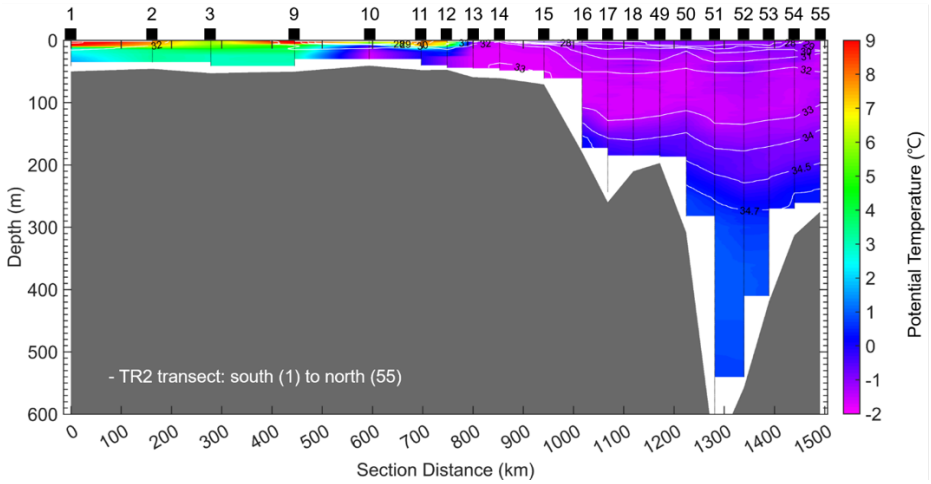

Figure 2.1.4. Same as Fig.2.1.3 but at the TR2 transect from St.01 (south) to St.55 (north).

2.2 Ocean Mooring Systems

2.2.1 KOPRI Arctic Mooring Systems (KAMS)

We recovered three mooring systems which had been deployed at the KAMS1-21 in the East Siberian Sea, KAMS2-22, and KAMS4-21 in the Northwind Ridge area. Unfortunately, KAMS5-22 was unable to be recovered owing to severe sea ice. We did, however, check that the mooring was still present. It will be recovered the next year. Instead, KAMS5Trap-23's mooring system was deployed. KAMS4Trap-23's mooring point has been moved southward near the Chukchi Sea continental shelf, which differs from the last deployment in 2021. The 4

deploymen sites of KAMS1-23, KAMS2-23, KAMS4Trap-23, KAMS5Trap-23 are St. 39, 47, 62, and 43, respectively.

KAMS1-23 is comprised of one upward looking ADCP (Work Horse Sentinel 150 kHz, Teledyne RDI), 6 MicroCAT CTD sensors (SBE37SM), 8 temperature loggers (SBE56), two sediment traps (Parflux Mark 78H-21, McLane), one Satlantic submergible Ultraviolet Nitrate Analyzer (SUNA V2), 4 RBRduo FI.PAR (RBR Ltd), one acoustic zooplankton and fish profiler (AZFP) and dual acoustic releasers (Fig. 2.2.1a). KAMS2-23 is comprised of one upward looking ADCP (WHS 150 kHz), 5 MicroCAT CTD sensors, 8 T-loggers, two sediment trap (PM 78H-21, SMD26S-6000), 1 RBRduo FI.PAR, and dual acoustic releasers (Fig. 2.2.1b). Theses two mooring systems were deployed at around 500 m depth and the CTD sensors and temperature loggers were distributed from the upper halocline layer to Atlantic water layer to investigate the shelf-basin interaction and variations of boundary current and water masses. KAMS4Trap-23 is 540-m long and comprised of one upward looking ADCP (WHS 150 kHz), 3 microCATs, 9 T-loggers, one sediment trap (SMD26S-6000, NiGK OCEAN), 2 RBRduo FI.PAR, and dual acoustic releasers. KAMS5Trap-23 is composed of one UVP3, HydroC, sediment trap, 2 MicroCAT CTD sensors, and dual acoustic releasers (Fig. 2.2.1d).

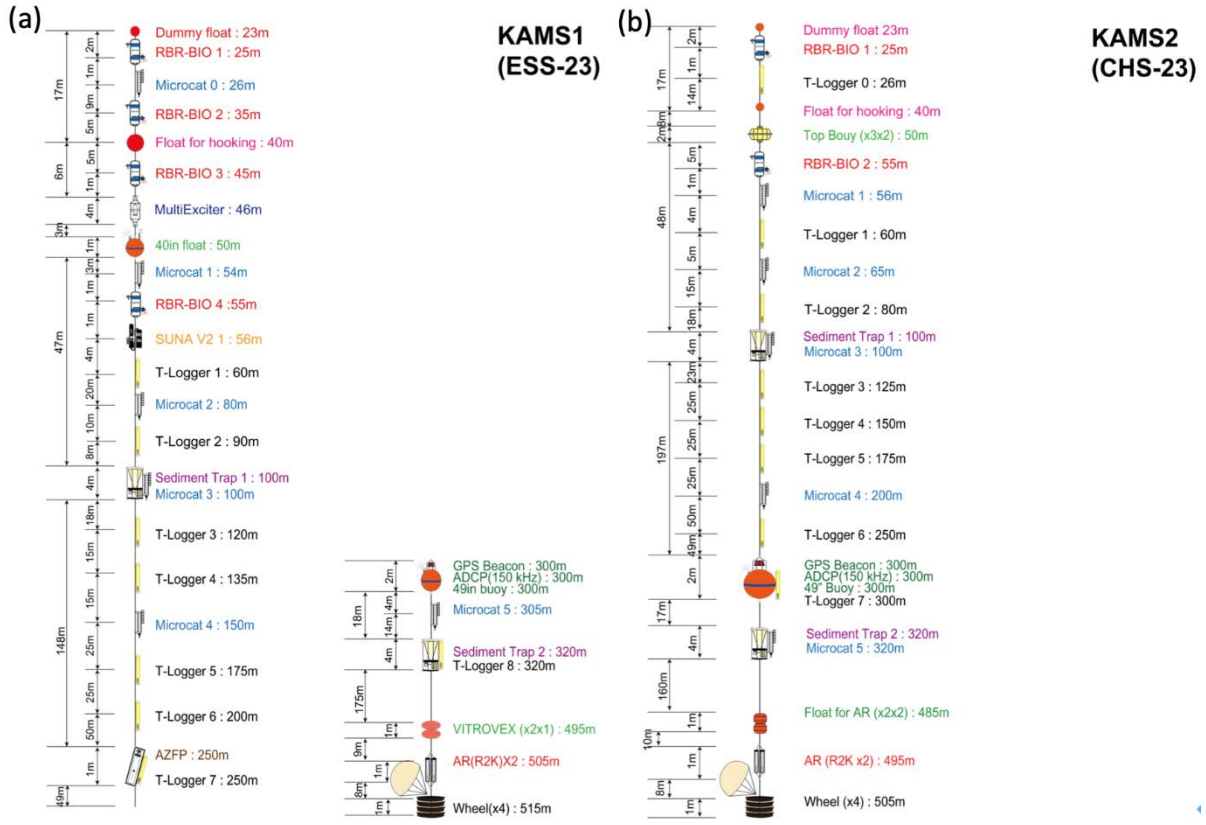

Figure 2.2.1. KOPRI mooring systems deployed in the western Arctic Ocean: (a) KAMS1-23, (b) KAMS2-23, (c) KAMS4Trap-23, (d) KAMS5Trap-23.

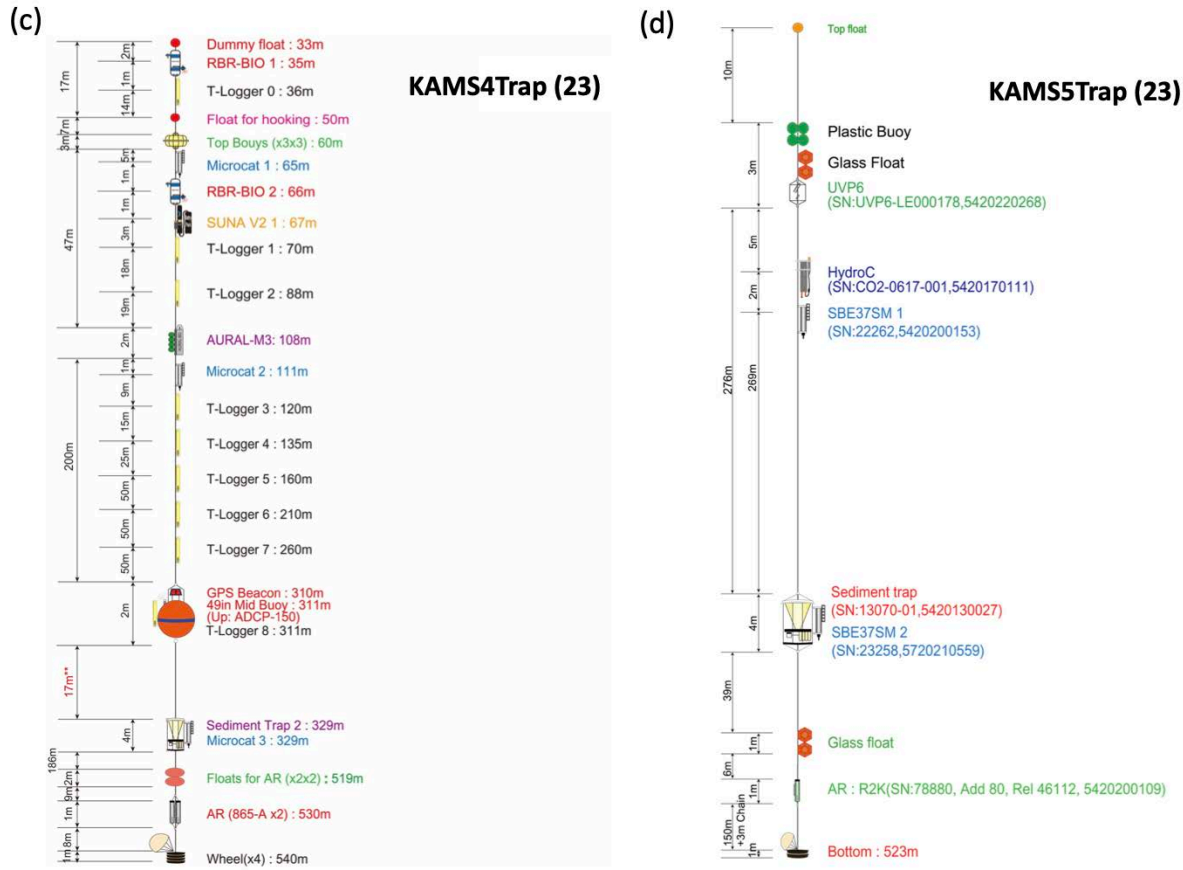

Figure 2.2.1. Continued.

2.2.2 KOPRI East Siberian Sea Mooring Systems (KESS)

A mooring system was recovered (ESS_I2022), and then it was deployed (ESS_I2023) on the similar location to monitor the dynamics of sea ice in the East Siberian Shelf after finishing data download and maintenance (Table 2.2.1. and 2.2.2). The recovery mooring (ESS_I2022) was equipped with an ice profiler sonar (ASL Environmental Sciences Inc., IPS5) measuring the sea ice draft, a MicroCats measuring conductivity, temperature, and pressure (Seabird, SBE-37) near IPS5, and a 614-kHz acoustic Doppler current profiler (RDI, Workhorse Sentinel) to measure current and sea ice velocity (Figure 2.2.2).

Table 2.2.1. Recovery and deployment information of ESS_I. Recovery date represent the time when the acoustic release was on the deck after the anchor was r released. Deployment date and location represent the anchor drop time and position.

	Date and time (UTC)	Longitude (DM)	Latitude (DM)	Depth (m)	Equipment
Recovery	2023.08.17 17:31	174° 30.905’E	74° 41.945’N	71	- IPS5 (SN: 55163) - RBR duet TD (SN:083009) - SBE 37 SM (SN: 23895, 23896, 23897,24236)
Deployment	2023.08.18 01:35	174° 31.162’E	74° 42.031’N	70	- IPS5 (SN: 55163) - RBR duet TD (SN:083009) - SBE 37 SM (SN: 23895, 23896,24236)

High resolution of ice thickness and ice velocities can be obtained using the IPS5 and ADCP over the mooring location. The accuracy of the MicroCats is 0.00003 Sm-1 for conductivity, 0.002oC for temperature, and 0.1% of the full depth of range for pressure. MicroCats are recorded at 5-min intervals in order to measure hydrographic variation near IPS5. Ice draft are recorded at 3-sec interval with IPS5, which provides high precision of approximately +-0.05 m vertical of the underside of the sea ice. ADCP are recorded at 15-min intervals to estimate ice velocity (Table 2.2.3).

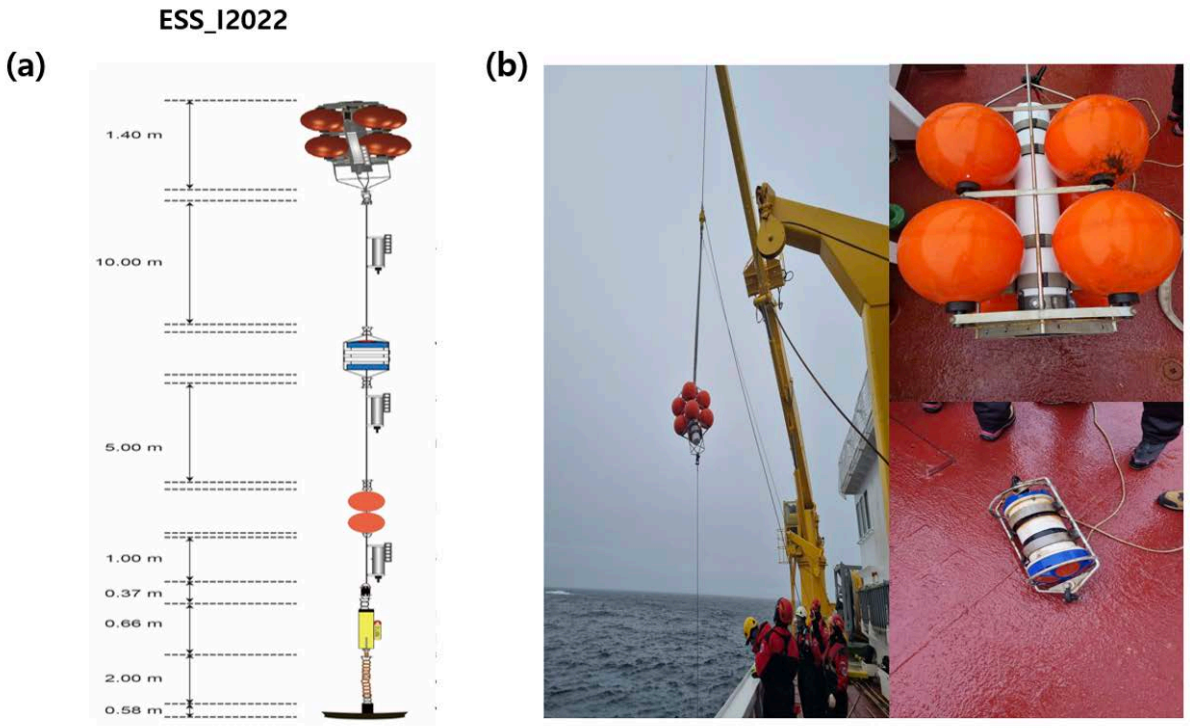

Figure 2.2.2. Mooring design and the recovery picture of ESS_I2022 mooring

After changed the battery and downloaded data from ESS_I2022 mooring, the IPS5 and ADCP were moored with four MicroCats, and one RBR duet TD logger in an upward-looking configuration at a depth of 40-m and 50-m, respectively (Table 2.2.1). Data will be collected between August 2022 and August 2023 for about 1 year (Table 2.2.3).

Table 2.2.2. Recording date and time from Aug. 2022 to Aug. 2023

Instruments	Data recording time (Start – Stop, UTC)	Recording interval
IPS5	2022.08.09 00:00 – 2023.08.17 21:12	3 sec.
SBE 37 SM(sn23895)	2022.08.08 18:00 – 2023.08.16 19:50	5 min.
SBE 37 SM(sn23896)	2022.08.08 18:00–2023.08.16 18:25	5 min.
SBE 37 SM(sn24236)	2022.08.08 18:00–2023.08.16 19:10	5 min.

Table 2.2.3. Deployment schedule of instruments for ESS_I2023 mooring

Instruments	Start date and time (UTC)	Recording interval	Observation interval	Ensemble ping number
IPS5	2023.08.17 14:02	3 sec.	3 sec	-
RBR duet TD(sn083009)	2023.08.18 00:00	3 sec.	3 sec.	-
SBE 37 SM(sn23896)	2023.08.18 00:00	5 min.	5 min.	-
SBE 37 SM(sn24236)	2023.08.18 00:00	5 min	5 min.	

2.2.3 Stablemoor Multi-sensor System (SMS)

In ARA13B, in order to investigate the heat transfer from warm summer water to the mixed layer through a thermocline, we deployed it at ARA13B St.58 (73° 22.129 'N, 166° 37.747 'W) for a year-long record. It is composed of one ADCP (Signature500, Nortek), 2 thermoster chains (25-m long, 1-m interval), 4 microCATs, one T-logger, and dual acoustic releasers (Fig. 2.2.3). We planned to recover and re-deploy the SMS at St.64. At the station, we tried to wake up and release the SMS, but could not receive returned signal. We completed a 10-hour survey using a hydrophone and an EK80, however we were unable to recover the SMS.

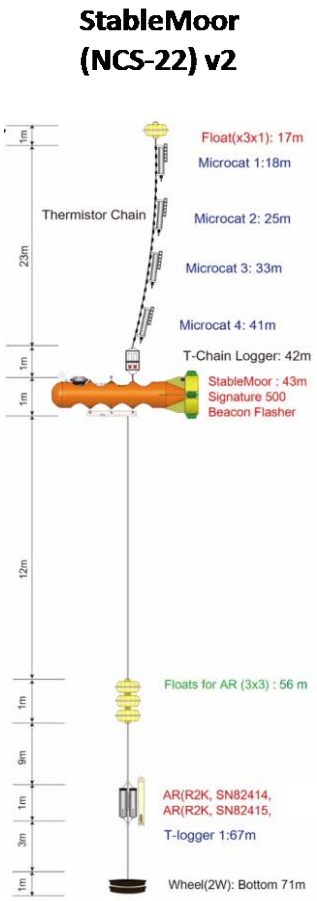

Figure 2.2.3. A stablemoor multi-sensor system (SMS) deployed in ARA13B.

2.3 PDS-CPIES

2.3.1 Introduction

The Arctic Ocean was known as one of the most quiescent oceans due to the ice cover, but it has undergone significant warming and retreat of sea-ice due to increased solar heating and heat transports from inflowing Atlantic and Pacific waters. In the western Arctic Ocean, the inflowing Atlantic Water which is the largest source of the heat input is warmer and saltier than Pacific Water, and thus, lighter Pacific water lies on denser Atlantic water in the western Arctic Ocean. Recent observations have reported 'Atlantification' which indicates an increase in Atlantic Water influence to the Arctic, resulting in weakening of the halocline and shoaling of the Atlantic Water (Polyakov et al., 2017); and hence, the possible warming of the water column by the Atlantic Water. Also, warming of Beaufort Gyre halocline water (shallower than 250 m) which would be linked to solar heating and sea ice retreat in the northern Chukchi Sea (Timmermans, 2018) is the other important source for the western Arctic Ocean warming.

The Arctic Ocean has been revealed that the near-inertial wave (NIW) activity in the upper ocean can be enhanced by increase of sea-ice melting, which may result in a significant change of dynamical environment (e.g., Rainville and Woodgate, 2009). Vertical mixing driven by the enhancement of NIW would have ability to significantly enhanced upward heat flux from warm and salty Atlantic water to overlying cooler Pacific summer and winter waters. A modeling study of Zhang and Steele (2007) found that a small mixing coefficient (10-6 m2 s-1) due to sea-ice coverage produces a shallow halocline and more cyclonic circulation of Atlantic Water in the Arctic Ocean, which matches with observations. A recent numerical simulation using a global Ocean General Circulation Model (OGCM) demonstrated that the small mixing coefficient of 10-6 m2 s-1 even can increase the Atlantic meridional overturning circulation about 14 % (Kim et al., 2015).

Complexity of the Arctic Ocean stratifications can make the passage of wind-induced NIWs through the water column as a nontrivial process. For example, the results of a recent analysis (Ghaemsaidi et al., 2016) show substantial reflection and scattering of the internal wave field in the upper Arctic Ocean and selective deep-ocean transmission of energy flux at particular combinations of near-inertial frequency and wavenumber. While there have been some studies of NIWs in the upper Arctic Ocean, little data are available to investigate deep NIW

energetics in the Arctic Ocean.

Coastal-trapped waves, which have potential to enhance diapycnal ocean mixing, including bottom-trapped waves drive water exchanges between the shallow continental shelf and deep basin (Nilsen et al., 2006; Zhao & Timmermans, 2018). Complexity of the Arctic Ocean stratifications can make bottom-trapped waves propagate in cross-shelf direction which affect onshore momentum flux and mixing (Garrett, 1978). Some of bottom-trapped waves were found to be triggered by wind forcing, suggesting that the surface ice cover in the Arctic Ocean prevents a more frequent occurrence of those waves (Ku et al., 2020).

For better understanding of warming of the water column, deep NIW, and wind-induced bottom-trapped wave activities associated with sea-ice cover and environmental changes, we deployed an array of five Pop-up Data Shuttle Current and Pressure recording Inverted Echo Sounders (PDS-CPIES) to make simultaneous measurements of several different physical quantities for 4 years from August 2021 through August 2025. We are expected to exploit a coherent picture relating warming of water column, deep-ocean NIW, bottom-trapped waves and surface-ice cover in the Arctic Ocean.

2.3.2 Equipment: PDS-CPIES

1) IES: An Inverted Echo Sounders (IES) measure acoustic echo time (τ) from the sea floor to the sea surface. Because the speed of sound is approximately a linear function of temperature, an upward displacement of the main thermocline or an intrusion of warm or cold water leads to proportional change of τ measurements. The operating depth is in the range of 500 to 6700 m and a custom acoustic transducer with conical radiation beam (±45°) is used. An IES is deployed on a stand with weights and has an acoustic release that disconnects the weights to allow the IES to float to the surface and be recovered. The IES is relatively small and easy to handle and can be launched using the A-frame or any lifting devices that lifts the entire set including the stand and weights. There is an operational lifetime of 2–5 years depending on the measurement schedule. For the three PDS-CPIES we configured for an operational lifetime of 3 years. IESs are a well-established and highly reliable tool for the long-term monitoring of large-scale ocean flows, and have been successfully used in this manner in many parts of the world's oceans, including the Southern Ocean (e.g. Sun & Watts, 2001; Watts et al., 2001; Book et al., 2002, Zhu et al., 2003; Park et al., 2005; Andres et al.

2008; Donohue et al., 2010).

2) PIES: A PIES is an IES with added sensors to measure bottom pressure (pb). The pressure sensor is a Parascientific Digiquarts model 410K with a range of 10,000 psi (6000 dbar) and a resolution on the order of 0.001 dbar. A PIES also records near-bottom temperature, but the purpose of this is principally to correct for the temperature sensitivity of the pressure sensor. A typical PIES measures pb and near-bottom temperature once every 10 minutes. For the three PDS-CPIES deployed, we extended time intervals to 30 minutes to facilitate reduced power requirements for 3-year deployment.

3) CPIES: A CPIES adds current measurements at about 50 m above the bottom to a PIES using a Anderaa Data Instruments Doppler current sensor, which is a true vectoring averaging sensor for measuring current speed and direction. The speed range is 0 to 300 cm/s and the sensor has a built in compass and tilt sensor, and also output sea temperature at 50 m above the bottom.

4) PDS-CPIES: Four expendable PDS modules can be deployed with each PDS-CPIES. PDS concept is shown in Figure 2.3.1 On an individually programmed schedule, each PDS self-released and floated to the surface from September 2024 until September 2026. The hourly interval data in the PDS memory is transmitted via the Iridium gateway to email server ashore. The PDS module provides a reliable and cost-effective tool to retrieve data from a deployed CPIES measurement system without sending a ship.

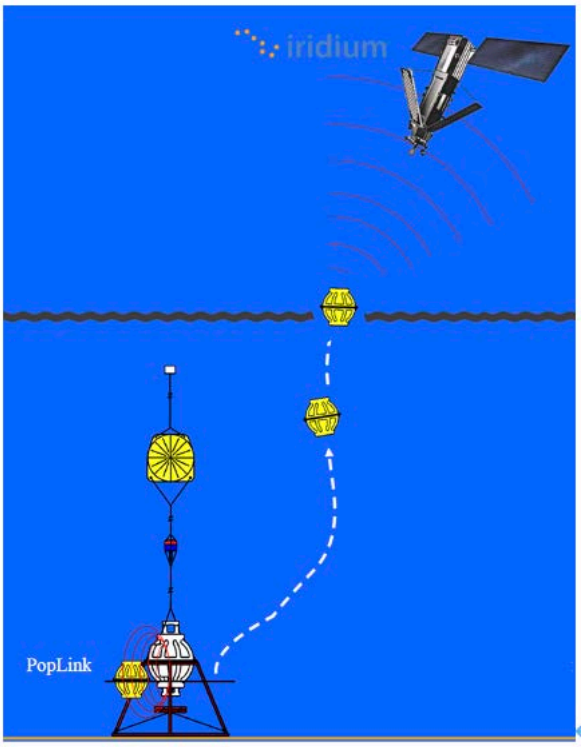

Figure 2.3.1. A schematic of the PopLink PDS system for transmission of data from a CPIES via Iridium satellite.

2.3.3. PDS-CPIES deployment

The four PDS-CPIESs were deployed during the IBRV ARAON's Arctic cruise in 2023 (ARA14B). The 4 CPIESs and 11 PDSs were deployed in CS01-04 and those locations of deployment are shown in Figure 2.3.2 with serial numbers of CPIESs and PDSs. The CPIESs set to measure acoustic echo round-travel time (τ) with 16 pings per 10 minutes (fast ping mode) and bottom pressure with 30-minute interval. The current meter, connected to PIES with 50-m length cable, was configured to record near-bottom current every 30 minutes. The PDSs were configured to receive the recorded measurements of bottom pressure, and hourly averaged τ, near-bottom current and temeperature from CPIESs, every hour.

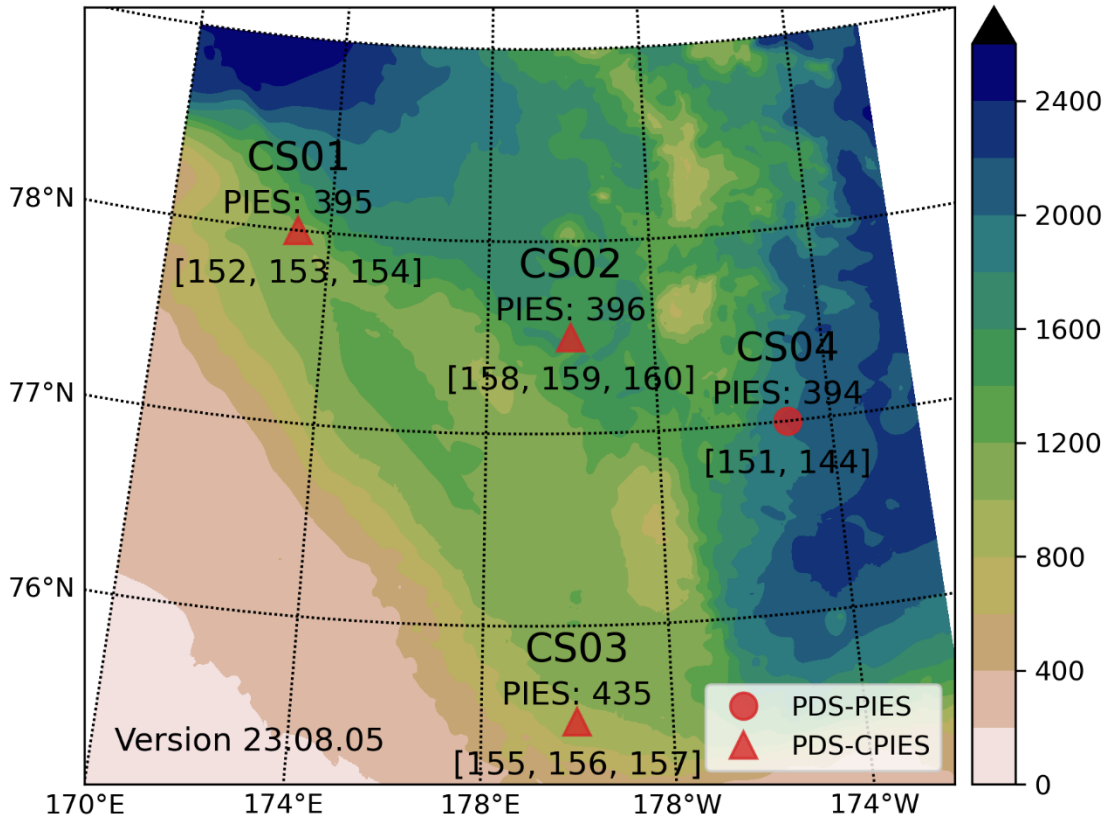

Figure 2.3.2. Location of deployed PDS-PIES/CPIES in 2023. The number reveals the serial number of the CPIES/PIES and PDS

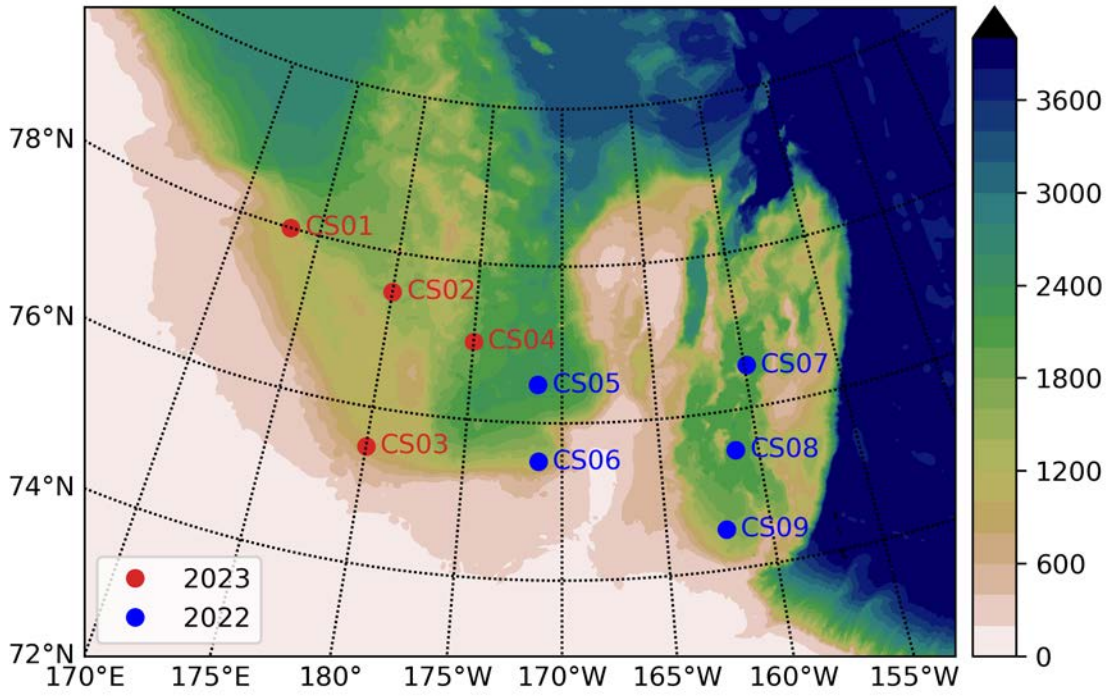

Figure 2.3.3. Location of deployed PDS-PIES/CPIES from 2022 (blue dots) to 2023 (red dots).

Figure 2.3.4. The all-equipped PDS-CPIES which is ready to deploy.

The four PDS-CPIES/PIES (CS 01–04) and five PDS-CPIES (CS05–CS09) were deployed during IBRV 2023 Araon's Arctic cruise (ARA14B) and IBRV 2022 Araon's Arctic cruise (ARA13B). Related information is summariazed in the following tables.

Table 2.3.1. Summary of PDS-CPIES deployment in 2023.

CPIES S/N	Deploy time (UTC)	Depth [m]	Longitude (°E)	Latitude (°N)	Station (Araon2023)
395	2023/08/14	1132	173°11.85549'E	78°0.00496'N	CS01 (St. 30)
396	2023/08/09	1463	179°59.91555'E	77°29.97524'N	CS02 (St. 26)
435	2023/08/20	937	179°59.90920'E	75°30.06178'N	CS03 (St. 42)
394	2023/08/08	2010	174°59.80535'W	76°59.96711'N	CS04 (St. 24)

Table 2.3.2. Summary of PDS-CPIES deployment in 2022.

CPIES S/N	Deploy time (UTC)	Depth [m]	Longitude (°E)	Latitude (°N)	Station (Araon2022)
397	2022/08/13	2241	171° 09.044´W	76° 29.100´N	CS05 (St.45)
398	2022/08/12	1302	171° 12.847´W	75° 30.432´N	CS06 (St.43)
399	2022/08/15	2139	159° 53.435´W	75° 32.336´N	CS07 (St.53)
434	2022/08/17	2117	161° 08.797´W	75° 29.903´N	CS08 (St.55)
436	2022/08/18	1614	162° 09.093´W	74° 30.980´N	CS09 (St.56)

Table 2.3.3. Summary of PDS Information and configuration in 2023.

PDS S/N	with CPIES	Planned release date (UTC)	IMEI 30053406+
152	395	2024.09.20 00:00	2595410
153	395	2025.09.20 00:00	2596410
154	395	2026.09.20 00:00	2694570
158	396	2024.09.20 00:00	2794360
159	396	2025.09.20 00:00	2795350
160	396	2026.09.20 00:00	2797370
155	435	2024.09.20 00:00	2697540
156	435	2025.09.20 00:00	2697670
157	435	2026.09.20 00:00	2792360
144	394	2024.09.20 00:00	1484880
151	394	2025.09.20 00:00	2592430

Table 2.3.4. Summary of PDS Information and configuration in 2022.

PDS S/N	with CPIES	Planned release date (UTC)	IMEI 300534061+
141	397	2023.08.28 00:00	449590
142	398	2023.08.28 00:00	481960
143	399	2023.08.28 00:00	482880

145	399	2024.08.28 00:00	484890
146	434	2023.08.28 00:00	488860
147	434	2024.08.28 00:00	580320
148	436	2023.08.28 00:00	582270
149	436	2024.08.28 00:00	586320

Table 2.3.5. Summary of PDS-CPIES command codes and configurations.

Deployment PDS_CPIES (ARAON 2023)				
PIES (+CM)	395 (+189)	396 (+192)	435 (+241)	394 (+)
PDS	152 153 154	158 159 160	155 156 157	144 151
Site name (CTD site)	CS01 (ARA14B30)	CS02 (ARA14B26)	CS03 (ARA14B42)	CS04 (ARA14B24)
Location	173°11.85549'E 78°0.00496'N	179°59.91555'E 77°29.97524'N	179°59.90920'E 75°30.06178'N	174°59.80535'W 76°59.96711'N
Depth (GEBCO)	1131	1545	936	2021
Depth (CTD)	1132	1463	937	2010
Set depth	1030	1450	830	1900
Clear	76	76	76	76
XPND	70	71	71	69
Beacon	74	75	75	73
Telemetry	66	67	67	65
Release	11	12	51	10
Auto release	2027/08/21 12:00	2027/08/21 00:00	2027/08/20 12:00	2027/08/20 00:00

2.4 Summary

In this year, we newly deployed 4 CPIESs to investigate the properties of internal waves, currents, ocean heat contents, and bottom temperature. For the future work, the mooring data will be analyzed to understand temporal variations of water masses and current fields on study area. Furthermore, the heat and freshwater contents will be calculated to understand thermodynamic processes related with sea ice melting in the vicinity of the Chukchi Borderland.

References

Andres, M., Wimbush, M., Park, J.-H., Chang, K.-I., Lim, B.-H., Watts, D. R., Ichikawa, H. and Teague, W. J. Observations of Kuroshio flow variations in the East China Sea. J. Geophys. Res., 113, C05013 (2008).

Book, J., Wimbush, M., Imawaki, S., Ichikawa, H., Uchida, H. and Kinoshita, H. Kuroshio temporal and spatial variations south of Japan, determined from inverted-echo-sounder measurements, J. Geophys. Res. 107 (2002).

Donohue, K.A., Watts, D.R., Tracey, K.L., Greene, A.D. and Kennelly, M. Mapping circulation in the Kuroshio extension with an array of current and pressure recording inverted echo sounders, Journal of Atmospheric and Oceanic Technology, 27 (3), 507–527 (2010).

Garrett, C. Topographic Rossby waves off east Australia: Identification and role in shelf circulation, J. Phys. Oceanogr., 9, 244–253. (1978)

Ghaemsaidi, S.J., Dosser, H., Rainville, L. and Peacock, T. The impact of layering on internal wave transmission, J. Fluid Mech. (2016).

Kim, S.Y., Lee, H.J., Park, J.-H., and Kim, Y.H. Effects of reduced vertical mixing under sea ice on Atlantic meridional overturning circulation (AMOC) in a global ice ocean model. Ocean Sci. J., 50, 155–161 (2015).

Kwok, R., Spreen, G., & Pang, S. (2013). Arctic sea ice circulation and drift speed: Decadal trends and ocean currents. Journal of Geophysical Research: Oceans, 118, 2408–2425. https://doi.org/10.1002/jgrc.20191

Ku, A., Seung, Y.H., Jeon, C., Choi, Y., Yoshizawa, E., Shimada, K., Cho, K. and Park, J. Observation of Bottom-Trapped Topographic Rossby Waves on the Shelf Break of the Chukchi Sea, J. Geophys. Res., 125(7) C015436 (2020).

Nilsen, F. Gjevik, B. and Schauer, U. Cooling of the West Spitsbergen Current: Isopycnal diffusion by topographic vorticity waves, J. Geophys. Res., 111, C08012 (2006).

Park, J.-H. and Watts, D. R. Near-inertial oscillations interacting with mesoscale circulation in the southwestern Japan/East Sea, Geophys. Res. Lett., 32, L10611 (2005).

Pickart, R.S., Moore, G.W.K., Mao, C., Bahr, F., Nobre, C., and Weingartner, T.J. Circulation of winter water on the Chukchi shelf in early summer. Deep-Sea Research II, 130, 56-75 (2016).

Polyakov, I. V., Pnyushkov, A. V., Alkire, M. B., Ashik, I. M., Baumann, T. M., Carmack, E. C., et

al. (2017). Greater role for Atlantic inflows on sea-ice loss in the Eurasian Basin of the Arctic Ocean. Science, 356, 285–291. https://doi.org/10.1126/science.aai8204

Rainville, L. and Woodgate, R.A. Observations of internal wave generation in the seasonally ice-free Arctic. Geophys. Res. Lett. 36, L23604 (2009).

Rippeth, T. P., Lincoln, B. J., Lenn, Y. D., Green, J. A. M., Sundfjord, A., & Bacon, S. (2015). Tide-mediated warming of Arctic halocline by Atlantic heat fluxes over rough topography. Nature Geoscience, 8(3), 191–194. https://doi.org/10.1038/ngeo2350

Shimada, K., Carmack, E.C., Hatakeyama, K., and Takizawa, T. Varieties of shallow temperature maximum waters in the western Canadian Basin of the Arctic Ocean. Geophysical Research Letters, 28(18), 3441-3444 (2001).

Steele, M., Morison, J., Ermold, W., Rigor, I., Ortmeyer, M., and Shimada, K. Circulation of summer Pacific halocline water in the Arctic Ocean. Journal of Geophysical Research, 109, C02027, doi:10.1029/2003JC002009 (2004).

Steele, M., Zhang, J., and Ermold, W. Mechanisms of summertime upper Arctic Ocean warming and the effect on sea ice melt. Journal of Geophysical Research, 115, C11004, doi:10.1029/2009JC005849 (2010).

Sun, C. and Watts, D.R. A circumpolar gravest empirical mode for the Southern Ocean hydrography. J. Geophys. Res., 106, 2833–2855 (2001).

Watts, D.R., Sun, C. and Rintoul, S. A two-dimensional gravest empirical mode determined from hydrographic observations in the subantarctic front. J. Phys. Oceanogr., 31, 2186–2209 (2001).

Zhang, J. and Steele, M. Effect of vertical mixing on the Atlantic Water layer circulation in the Arctic Ocean, J. Geophys. Res., 112, C04S04 (2007).

Zhao, B. and Timmermans, M. Topographic Rossby Waves in the Arctic Ocean's Beaufort Gyre, J. Geophys. Res., 123(9), 6521–6530 (2018).

Zhu, X.-H., Han, I.-S., Park, J.-H., Ichikawa, H., Murakami, K. Kaneko, A. and Ostrovskii, A. The northeastward current southeast of Okinawa Island observed during November 2000 to August 2001. Geophys. Res. Lett., 30, 1071 (2003).

Appendix I. Daily Log Sheets

Scientific Cruise Daily Log

Ship: R/V Araon **Cruise:** ARA14 . B **2023.08.02 ~ 2023.08.29**

STN No.	Gear	Cast No.	Date	Cast start	Cast end	Latitude	Longitude	Water depth	Cast depth	Wind speed	Wind direction	Ship speed	Heading	Remarks	Device Driver
			Local time	Local time	Local time			(m)	(m)	m/s	(°)	knot	(°)		
CTD: CTD, TMC: Trace Metal CTD, PHY: Phyto Net, BON: Bongo Net, 150NET: 150 Net, TRIOS: TriOS, MOCNESS: MOCNESS, C-PIES CHECK: C-PIES Check, XCTD: xCTD, FTN: Frame Trawl Net, C-PIES DEPLOY: C-PIES Deploy															
WAVEBUOY: Wave Buoy Deploy, DSC: Deep Sea Camera, FISHING: Fishing, DRG: Dredge, FISHPOT: Fish Pot, MR: Mooring Recovery, MD: Mooring Deploy, IC: Ice Camp															
1	CTD	1	2023-08-02	19:09	19:24	65°10.409' N	168°41.446' W	50	41	6.06	91	0.07	140.2	CTD	JYoo
	TMC	1		19:47	19:59	65°10.409' N	168°41.446' W	50	43			0.11	140	Trace Metal CTD	PKU
	PHY	1		20:23	20:32	65°10.408' N	168°41.444' W	50	45			0.06	140.1	Phyto Net	JH
	BON	1		20:39	20:44	65°10.408' N	168°41.444' W	50	45			0.04	140.1	Bongo Net	JH
	150NET	1		20:53	20:57	65°10.408' N	168°41.444' W	50	45			0.10	140	150 Net	JH
	TRIOS	1		21:04	21:11	65°10.408' N	168°41.444' W	50	30			0.09	139.8	TriOS	JWPark
	CTD	2		21:23	21:35	65°10.408' N	168°41.445' W	50	41	6.12	99	0.08	140	CTD	MSKim
	MOCNESS	1		21:49	21:58	65°10.408' N	168°41.448' W	50				0.01	150	MOCNESS	JH
2	CTD	1	2023-08-03	05:33	05:47	66°37.797' N	168°41.249' W	44	35	6.45	101	0.05	120.2	CTD	JYoo
	TMC	1		06:05	06:10	66°37.795' N	168°41.250' W	44	37			0.15	140	Trace Metal CTD	PKU
	PHY	1		06:26	06:30	66°37.797' N	168°41.252' W	44	35			0.07	140.1	Phyto Net	JH
	BON	1		06:37	06:41	66°37.797' N	168°41.253' W	44	35			0.03	160	Bongo Net	JH
	150NET	1		06:52	06:55	66°37.797' N	168°41.251' W	44	20			0.04	159.8	150 Net	JH
	TRIOS	1		07:01	07:08	66°37.796' N	168°41.251' W	44	35			0.02	159.9	TriOS	JWPark
	CTD	2		07:22	07:40	66°37.797' N	168°41.251' W	44	36	7.77	98	0.04	159.8	CTD	PSJ
3	CTD	1	2023-08-03	13:04	13:19	67°40.200' N	168°57.599' W	49	40	5.88	127	0.05	137	CTD	MSKim
	TMC	1		13:37	13:43	67°40.200' N	168°57.599' W	49	42			0.02	136.8	Trace Metal CTD	PKU
	CTD	2		14:06	14:21	67°40.198' N	168°57.601' W	50	40.1	7.49	120	0.05	146.8	CTD	MSKim
	PHY	1		14:36	14:40	67°40.200' N	168°57.597' W	50	45			0.03	125.6	Phyto Net	JH
	BON	1		14:47	14:52	67°40.200' N	168°57.597' W	50	45			0.04	125.1	Bongo Net	JH
	150NET	1		15:00	15:05	67°40.200' N	168°57.597' W	50	45			0.16	125	150 Net	JH
	TRIOS	1		15:12	15:20	67°40.200' N	168°57.596' W	50	40			0.06	125	TriOS	JWPark
	MOCNESS	1		15:31	15:38	67°40.208' N	168°57.600' W	50	50			0.03	50.4	MOCNESS	JH
4	CTD	1	2023-08-03	16:49	17:03	67°46.980' N	168°36.133' W	50	40	8.28	141	0.12	150.1	CTD	MSKim
	BON	1		17:14	17:18	67°46.980' N	168°36.132' W	50	45			0.02	150.1	Bongo Net	JH
	150NET	1		17:23	17:27	67°46.981' N	168°36.133' W	50	45			0.05	150	150 Net	JH
5	CTD	1	2023-08-03	18:40	18:55	67°53.876' N	168°14.098' W	58	48	6.09	121	0.08	148.5	CTD	MSKim
	BON	1		19:06	19:10	67°53.880' N	168°14.098' W	58	50			0.14	149.5	Bongo Net	JH
	150NET	1		19:14	19:19	67°53.880' N	168°14.100' W	58	50			0.08	148.8	150 Net	JH
6	CTD	1	2023-08-03	20:40	20:58	68°00.781' N	167°52.020' W	52	42	7.33	112	0.06	144.9	CTD	MSKim
	TMC	1		21:15	21:22	68°00.781' N	167°52.021' W					0.03	145.2	Trace Metal CTD	PKU
	BON	1		21:39	21:43	68°00.780' N	167°52.083' W	52	45			0.03	143.6	Bongo Net	JH
	150NET	1		21:50	21:56	68°00.780' N	167°52.020' W	52	45			0.07	140.4	150 Net	JH
	TRIOS	1		22:02	22:08	68°00.781' N	167°52.020' W	52	30			0.04	140.4	TriOS	JWPark
7	CTD	1	2023-08-03	23:23	23:36	68°07.682' N	167°29.702' W	49	39	6.62	74	0.05	91	CTD	MSKim
	BON	1		23:51	23:56	68°07.682' N	167°29.701' W	49	40			0.07	90.5	Bongo Net	JH
	150NET	1	2023-08-04	00:04	00:09	68°07.683' N	167°29.701' W	49	40			0.01	90.2	150 Net	JH
8	CTD	1	2023-08-04	01:22	01:34	68°14.519' N	167°07.324' W	43	38	4.61	125	0.21	148.9	CTD	JYoo
	TMC	1		01:50	01:54	68°14.520' N	167°07.318' W	43	30			0.02	130.5	Trace Metal CTD	PKU
	PHY	1		02:18	02:22	68°14.520' N	167°07.321' W	43	38			0.08	133.2	Phyto Net	Catherine

Scientific Cruise Daily Log

Ship: R/V Araon **Cruise:** ARA14 . B **2023.08.02 ~ 2023.08.29**

STN No.	Gear	Cast No.	Date	Cast start	Cast end	Latitude	Longitude	Water depth	Cast depth	Wind speed	Wind direction	Ship speed	Heading	Remarks	Device Driver
			Local time	Local time	Local time			(m)	(m)	m/s	(°)	knot	(°)		
	BON	1		02:29	02:33	68°14.520' N	167°07.320' W	43	38			0.06	133.1	Bongo Net	JH
	150NET	1		02:39	02:44	68°14.520' N	167°07.320' W	43	38			0.12	133.2	150 Net	JH
9	CTD	1	2023-08-04	07:58	08:13	69°10.011' N	168°40.002' W	50	40	6.78	177	0.11	199.7	CTD	PSJ
	TMC	1		08:31	08:36	69°10.013' N	168°39.999' W	51	44	6.89	166	0.05	200.1	Trace Metal CTD	PKU
	CTD	2		08:55	09:10	69°10.004' N	168°39.995' W	51	43	8.22	171	0.04	200.2	CTD	JYoo
	TRIOS	1		09:18	09:26	69°10.004' N	168°39.987' W	51	40	7.99	171	0.01	170.2	TriOS	JWPark
	PHY	1		09:32	09:36	69°10.004' N	168°39.987' W	51	43			0.07	170.1	Phyto Net	Catherine
	BON	1		09:43	09:47	69°10.004' N	168°39.987' W	51	45	8.23	174	0.02	170	Bongo Net	JH
	150NET	1		09:53	09:58	69°10.004' N	168°39.988' W	51	45			0.04	175	150 Net	JH
	MOCNESS	1		10:10	10:15	69°10.049' N	168°39.991' W	51	50			2.20	0.3	MOCNESS	JH
10	CTD	1	2023-08-04	17:00	17:15	70°29.993' N	168°39.994' W	39	30	9.32	170	0.28	168.4	CTD	MSKim
	TMC	1		17:29	17:34	70°30.001' N	168°40.014' W	39	33	9.71	169	0.01	185.7	Trace Metal CTD	PKU
	CTD	2		17:54	18:09	70°30.000' N	168°39.999' W	39	30	11.27	180	0.05	186.1	CTD	JYChae
	TRIOS	1		18:18	18:25	70°30.000' N	168°40.000' W	39	30	180.00	10.85	0.02	185.6	TriOS	JWPark
	PHY	1		18:29	18:33	70°30.000' N	168°40.000' W	39	35	182.00	10.76	0.08	186	Phyto Net	Catherine
	BON	1		18:39	18:43	70°30.000' N	168°40.001' W	39	30			0.02	185.6	Bongo Net	JH
	150NET	1		18:48	18:51	70°30.000' N	168°40.002' W	39	30			0.03	185.9	150 Net	JH
	MOCNESS	1		18:59	19:06	70°30.001' N	168°39.996' W	39	30			0.03	163.9	MOCNESS	JH
11	CTD	1	2023-08-04	23:56	00:06(+1)	71°25.801' N	168°40.005' W	47	40.3	10.40	163	0.07	185.5	CTD	MSKim
	PHY	1	2023-08-05	00:15	00:18	71°25.801' N	168°40.006' W	48	40			0.07	174.8	Phyto Net	Catherine
	BON	1		00:24	00:28	71°25.801' N	168°40.008' W	48	40			0.04	178.9	Bongo Net	JH
	150NET	1		00:33	00:38	71°25.801' N	168°40.009' W	48	40			0.03	178.7	150 Net	JH
	CTD	2		00:52	01:06	71°25.801' N	168°40.012' W	48	40	10.60	169	0.05	188.7	CTD	PSJ
12	CTD	1	2023-08-05	03:35	03:42	71°53.700' N	168°40.007' W	50	44	11.62	174	0.18	196.4	CTD	JYoo
13	CTD	1	2023-08-05	06:30	06:46	72°21.551' N	168°39.742' W	55	45	10.52	184	0.02	202	CTD	JYoo
	TMC	1		07:02	07:09	72°21.547' N	168°39.729' W	55	50			0.02	201.1	Trace Metal CTD	PKU
	CTD	2		07:26	07:41	72°21.569' N	168°39.709' W	55	45	11.71	190	0.03	219.5	CTD	PSJ
	TRIOS	1		07:47	07:53	72°21.569' N	168°39.706' W	55	30			0.06	206.4	TriOS	JWPark
	PHY	1		07:57	08:02	72°21.569' N	168°39.705' W	55	50			0.01	205.6	Phyto Net	Catherine
	BON	1		08:09	08:14	72°21.569' N	168°39.705' W	55	50			0.05	206.1	Bongo Net	JH
	150NET	1		08:20	08:25	72°21.569' N	168°39.705' W	54	50			0.04	205.9	150 Net	JH
	MOCNESS	1		08:39	08:42	72°21.696' N	168°39.543' W	54	50			2.27	24.6	MOCNESS	JH
14	CTD	1	2023-08-05	12:31	12:39	72°50.028' N	168°39.218' W	57	48	7.33	191	0.06	271.9	CTD	JYChae
15	CTD	1	2023-08-05	21:20	21:29	73°22.072' N	166°37.751' W	60	70	6.18	198	0.05	257.6	CTD	JYChae
16	CTD	1	2023-08-06	02:32	03:01	73°53.338' N	168°11.977' W	181	172	6.55	15	0.23	79.8	CTD	PSJ
	TMC	1		03:26	03:38	73°53.304' N	168°11.962' W	181	160			0.96	133.5	Trace Metal CTD	PKU
	CTD	2		03:59	04:16	73°53.177' N	168°11.262' W	181	100	6.91	25	0.04	37.3	CTD	JYoo
	TRIOS	1		04:25	04:29	73°53.143' N	168°11.642' W	181	20			0.12	352.4	TriOS	JWPArk
	PHY	1		04:35	04:42	73°53.137' N	168°11.638' W	181	100			0.08	21.7	Phyto Net	JMOON
	BON	1		04:47	04:56	73°53.094' N	168°11.692' W	181	165			0.07	22.1	Bongo Net	JH
	150NET	1		05:02	05:13	73°52.988' N	168°11.843' W	181	165			0.10	19.8	150 Net	JH
17	CTD	1	2023-08-06	08:27	08:45	74°20.692' N	168°03.003' W	253	243	7.04	32	0.01	125.5	CTD	JYoo

Scientific Cruise Daily Log

Ship: R/V Araon | Cruise: ARA14 . B | 2023.08.02 ~ 2023.08.29

STN No.	Gear	Cast No.	Date	Cast start	Cast end	Latitude	Longitude	Water depth	Cast depth	Wind speed	Wind direction	Ship speed	Heading	Remarks	Device Driver
			Local time	Local time	Local time			(m)	(m)	m/s	(°)	knot	(°)		
18	CTD	1	2023-08-06	11:50	12:17	74°48.034' N	167°53.926' W	194	184	8.39	44	0.04	168	CTD	PSJ
	TMC	1		12:38	12:52	74°48.039' N	167°53.895' W					0.20	100.3	Trace Metal CTD	PKU
	CTD	2		13:11	13:31	74°48.032' N	167°53.886' W	193	100	5.90	33	0.19	119.4	CTD	MSKim
	TRIOS	1		13:41	13:53	74°48.071' N	167°53.996' W	194	70			0.04	80	TriOS	JWPark
	PHY	1		13:59	14:06	74°48.071' N	167°53.995' W		100			0.03	80.1	Phyto Net	JMOON
	BON	1		14:18	14:30	74°48.075' N	167°53.962' W	193	185			0.25	72.8	Bongo Net	JH
	150NET	1		14:38	14:53	74°48.087' N	167°53.880' W	193	185			0.04	76.7	150 Net	JH
	MOCNESS	1		15:05	15:17	74°48.089' N	167°53.969' W	193	230			0.03	266.8	MOCNESS	JH
	DRG	1	2023-08-06	16:53	17:35	74°51.945' N	168°33.157' W	173	168	6.93	62	3.46	210.1	Dredge	JH
19	CTD	1	2023-08-06	20:29	20:46	75°01.234' N	169°56.195' W	255	246	5.05	160.1	0.03	159.3	CTD	JYChae
20	C-PIES CHECK	1	2023-08-07	00:25	01:42	75°30.430' N	171°12.855' W					0.04	219.6	C-PIES Check	IU
	CTD	1		00:25	01:32	75°30.430' N	171°12.855' W	1285	1275	36.00	2.31	0.04	219.6	CTD	MSKim
	XCTD	1		00:25	00:32	75°30.430' N	171°12.852' W	1285	1100			0.04	219.7	xCTD	JYoo
21	CTD	1	2023-08-07	04:57	06:04	75°59.997' N	170°29.997' W	1313	1304	2.68	11	0.13	171	CTD	PSJ
	TMC	1		06:21	07:07	75°59.939' N	170°29.818' W	1296	1210			0.02	3.6	Trace Metal CTD	PKU
	CTD	2		07:33	07:47	76°00.063' N	170°29.843' W	1313	100	1.27	44	0.25	161.7	CTD	JYoo
	TRIOS	1		08:04	08:10	76°00.078' N	170°29.626' W	1313	30			0.12	13.4	TriOS	JWPark
	PHY	1		08:18	08:25	76°00.157' N	170°29.614' W	1313	100			0.10	13.1	Phyto Net	JMOON
	BON	1		08:31	08:43	76°00.158' N	170°29.612' W	1313	200			0.03	19.4	Bongo Net	JH
	150NET	1		08:49	09:01	76°00.156' N	170°29.602' W	1313	200			0.02	45.3	150 Net	JH
22	CTD	1	2023-08-07	12:59	13:31	76°28.872' N	171°18.363' W	2178	1060			0.22	262.7	CTD	MSKim
	C-PIES CHECK	1		14:47	15:22	76°29.410' N	171°16.171' W					0.07	280.8	C-PIES Check	IU
	CTD	2		14:47	16:24	76°29.410' N	171°16.171' W	2213	2200	6.18	225	0.07	280.8	CTD	MSKim
23	CTD	1	2023-08-07	20:37	22:13	76°59.418' N	170°05.761' W	2212	2203	9.10	224	0.48	310.6	CTD	MSKim
	TMC	1		22:35	00:10(+1)	76°59.030' N	170°03.368' W	2212	2170			0.36	251.5	Trace Metal CTD	PKU
	CTD	2	2023-08-08	00:30	00:46	76°59.694' N	170°00.711' W	2212	101.2	12.75	222	0.08	244.8	CTD	PSJ
	TRIOS	1		00:56	01:05	76°59.775' N	169°59.761' W	2212	50			0.03	233.3	TriOS	JWPark
	PHY	1		01:10	01:16	76°59.763' N	169°59.716' W	2212	100			0.03	250	Phyto Net	JMOON
	BON	1		01:22	01:36	76°59.777' N	169°59.399' W	2212	200			0.71	259.5	Bongo Net	JH
	150NET	1		01:43	01:55	76°59.793' N	169°58.917' W	2212	200			0.03	259.6	150 Net	JH
	FTN	1		02:56	03:09	76°57.756' N	169°52.301' W	2212	200			0.52	261.9	Frame Trawl Net	JH
XCTD2	XCTD	1	2023-08-08	07:29	07:33	76°54.964' N	172°30.898' W		630			5.56	319.8	xCTD	JYoo
24	C-PIES DEPLOY	1	2023-08-08	11:54	11:59	76°59.963' N	174°59.825' W					0.51	322.2	C-PIES Deploy	IU
	CTD	1		12:21	13:54	76°59.923' N	174°59.196' W	2010	2002	5.80	259	0.03	0.4	CTD	MSKim
	PHY	1		14:05	14:11	76°59.864' N	174°59.310' W		100			0.04	15.4	Phyto Net	JMOON
	150NET	1		14:18	14:30	76°59.828' N	174°59.347' W		200			0.04	15	150 Net	JH
	BON	1		14:33	14:47	76°59.758' N	174°59.501' W		200			0.06	29.6	Bongo Net	JH
	TRIOS	1		14:53	15:05	76°59.693' N	174°59.665' W		70			0.05	28.9	TriOS	JWPark
	CTD	2		15:19	15:37	76°59.545' N	175°00.210' W	2010	100	5.37	282	0.03	40.1	CTD	MSKim
XCTD3	XCTD	1	2023-08-08	19:14	19:21	77°00.694' N	177°27.654' W		1100			3.78	313.7	xCTD	MSKim
25	CTD	1	2023-08-08	23:37	00:38(+1)	77°00.283' N	179°54.258' E	1079	1069	4.10	230	0.03	330.2	CTD	JYChae
	TMC	1	2023-08-09	00:59	01:46	77°00.116' N	179°55.824' E	1079	1020			0.39	316.1	Trace Metal CTD	PKU

Scientific Cruise Daily Log

Ship: R/V Araon | Cruise: ARA14 . B | 2023.08.02 ~ 2023.08.29

STN No.	Gear	Cast No.	Date	Cast start	Cast end	Latitude	Longitude	Water depth	Cast depth	Wind speed	Wind direction	Ship speed	Heading	Remarks	Device Driver
			Local time	Local time	Local time			(m)	(m)	m/s	(°)	knot	(°)		
	CTD	2		02:04	02:21	76°59.880' N	179°56.542' E	1079	101	4.32	255	0.02	342.8	CTD	PSJ
	TRIOS	1		02:33	02:39	76°59.721' N	179°56.902' E	1079	40			0.03	335	TriOS	JWPark
	PHY	1		02:43	02:50	76°59.720' N	179°56.904' E	1079	100			0.07	335.8	Phyto Net	JMOON
	PHY	2		02:54	03:01	76°59.730' N	179°56.794' E	1979	100			0.18	337.6	Phyto Net	JMOON
	150NET	1		03:05	03:17	76°59.739' N	179°56.672' E	1979	200			0.05	337.4	150 Net	JH
	BON	1		03:22	03:36	76°59.722' N	179°56.371' E	1079	200			1.44	349.2	Bongo Net	JH
	MOCNESS	1		03:47	04:00	77°00.193' N	179°55.213' E	1979	200			0.49	349.5	MOCNESS	JH
26	C-PIES DEPLOY	1	2023-08-09	07:04	07:16	77°30.009' N	179°59.953' W					0.10	256.1	C-PIES Deploy	IU
	CTD	1		07:29	08:41	77°30.045' N	179°59.879' W	1463	1453	4.52	257	0.04	249.9	CTD	JYoo
	WAVEBUOY	1		09:15	09:25	77°31.150' N	179°56.386' E					0.35	355.8	Wave Buoy Deploy	JWPark
IC1	IC	1	2023-08-09	23:38	13:29(+2)	78°31.318' N	179°01.367' W							Ice Camp	
XCTD4	XCTD	1	2023-08-09	16:59	17:06	78°07.720' N	179°59.087' W		1100			5.35	354.4	xCTD	MSKim
XCTD5	XCTD	1	2023-08-10	10:00	10:06	78°31.781' N	178°44.250' W	1625	1100			0.40	159.2	xCTD	MSKim
XCTD6	XCTD	1	2023-08-10	16:02	16:07	78°31.830' N	178°40.102' W	1617	151			0.40	159.8	xCTD	MSKim
XCTD7	XCTD	1	2023-08-10	16:44	16:50	78°32.117' N	178°39.396' W	1614	1100			0.49	155.4	xCTD	MSKim
XCTD8	XCTD	1	2023-08-11	04:03	04:10	78°31.450' N	178°23.503' W	1620	1200			0.12	177.3	xCTD	JYoo
XCTD9	XCTD	1	2023-08-11	16:00	16:09	78°30.117' N	178°19.902' W	1620	1200			0.31	234.2	xCTD	MSKim
XCTD10	XCTD	1	2023-08-12	03:59	04:05	78°32.343' N	178°06.779' W	1540	1100			0.46	340.3	xCTD	JYoo
27	CTD	1	2023-08-12	14:42	15:45	78°32.450' N	177°35.155' W	1008	998	9.45	193	0.02	250	CTD	JYChae
	TMC	1		16:00	16:43	78°32.450' N	177°35.153' W	1008	970			0.15	251.1	Trace Metal CTD	PKU
	CTD	2		16:58	17:14	78°32.465' N	177°35.176' W	1008	100	11.27	196	0.07	230.2	CTD	JYChae
	TRIOS	1		17:21	17:29	78°32.542' N	177°34.938' W	1008	40			0.05	210.6	TriOS	JWPark
	PHY	1		17:33	17:39	78°32.542' N	177°34.935' W	1008	100			12.50	299.9	Phyto Net	JeongHyun
	BON	1		17:50	18:02	78°32.719' N	177°34.280' W	1008	200			0.07	211.2	Bongo Net	JH
27-28	WAVEBUOY	1	2023-08-12	20:52	20:57	78°48.835' N	178°48.856' W	1143				0.32	319.5	Wave Buoy Deploy	JWPark
XCTD11	XCTD	1	2023-08-12	23:37	23:43	79°02.451' N	179°38.612' E	1400	1100			4.11	326.9	xCTD	MSKim
XCTD12	XCTD	1	2023-08-13	05:03	05:09	79°31.166' N	175°28.825' E	2204	1100			4.95	332.5	xCTD	JYoo
28	CTD	1	2023-08-13	09:05	10:55	80°00.006' N	172°24.042' E	2700	2692	12.71	235	0.35	250.4	CTD	JYoo
	TMC	1		11:12	13:01	80°00.005' N	172°24.036' E	2700	2600			0.27	249.6	Trace Metal CTD	PKU
	CTD	2		13:18	13:37	80°00.010' N	172°24.136' E	2700	100	10.83	213	0.14	247.7	CTD	JYChae
	TRIOS	1		13:44	13:53	80°00.009' N	172°24.147' E	2700	40			0.29	220.4	TriOS	JWPark
	PHY	1		13:58	14:06	80°00.011' N	172°24.140' E	2700	100			0.32	225.2	Phyto Net	JeongHyun
	150NET	1		14:11	14:24	80°00.010' N	172°24.142' E	2700	200			0.36	225.3	150 Net	JH
	BON	1		14:30	14:42	80°00.010' N	172°24.144' E	2700	200			0.32	224.8	Bongo Net	JH
	CTD	3		14:55	16:01	80°00.010' N	172°24.139' E	2700	1500	8.96	211	0.09	239.8	CTD	MSKim
	MOCNESS	1		16:17	16:57	79°59.937' N	172°24.005' E	2700	1000			2.24	202.1	MOCNESS	JH
29	CTD	1	2023-08-13	22:18	00:06(+1)	79°00.000' N	172°47.987' E	2560	2551	13.58	192	0.21	240.8	CTD	JYChae
	TMC	1	2023-08-14	00:28	02:01	79°00.001' N	172°47.987' E	2560	2540			0.14	237.6	Trace Metal CTD	PKU
	TRIOS	1		02:15	02:23	79°00.002' N	172°48.009' E	2560	40			0.29	236.2	TriOS	JWPark
	PHY	1		02:31	02:38	78°59.996' N	172°47.989' E	2560	100			0.09	229.3	Phyto Net	JeongHyun
	150NET	1		02:41	02:55	78°59.999' N	172°48.014' E	2560	150			0.14	226.8	150 Net	JH
	BON	1		03:00	03:13	79°00.002' N	172°48.008' E	2560	200			0.11	227	Bongo Net	JH

Scientific Cruise Daily Log

Ship: R/V Araon | Cruise: ARA14 . B | 2023.08.02 ~ 2023.08.29

STN No.	Gear	Cast No.	Date	Cast start	Cast end	Latitude	Longitude	Water depth	Cast depth	Wind speed	Wind direction	Ship speed	Heading	Remarks	Device Driver
			Local time	Local time	Local time			(m)	(m)	m/s	(°)	knot	(°)		
	CTD	2		03:24	05:12	78°60.000' N	172°48.011' E	2560	1520	15.28	176	0.26	237.3	CTD	PSJ
30	C-PIES DEPLOY	1	2023-08-14	10:56	11:04	78°00.001' N	173°12.115' E					1.06	269.6	C-PIES Deploy	IU
	CTD	1		11:18	12:18	78°00.004' N	173°11.845' E	1132	1122			0.39	263.7	CTD	MSKim
	TMC	1		12:32	13:29	78°00.001' N	173°11.867' E	1132	1020			0.79	249.1	Trace Metal CTD	PKU
	CTD	2		13:47	14:04	78°00.003' N	173°11.975' E	1132	100	12.28	237	0.50	254.6	CTD	JYChae
	TRIOS	1		14:11	14:22	78°00.001' N	173°11.979' E	1132	40			0.51	244.5	TriOS	JWPark
	PHY	1		14:24	14:33	78°00.001' N	173°11.976' E	1132	100			0.66	245.4	Phyto Net	JeongHyun
	150NET	1		14:38	14:51	78°00.000' N	173°11.976' E	1132	200			0.71	245.9	150 Net	JH
	BON	1		14:58	15:11	78°00.001' N	173°11.975' E	1132	200			0.18	245.2	Bongo Net	JH
	CTD	3		15:22	16:18	78°00.003' N	173°11.978' E	1132	1122	11.30	222	0.22	259.7	CTD	MSKim
	MOCNESS	1		16:29	17:22	77°59.940' N	173°11.831' E	1132	1300			3.19	210.7	MOCNESS	JH
31	CTD	1	2023-08-14	22:33	23:21	77°00.003' N	173°35.990' E	737	727	11.10	227	0.21	270.3	CTD	JYChae
	TMC	1		23:38	00:14(+1)	76°60.000' N	173°35.965' E	737	670			0.48	253.6	Trace Metal CTD	PKU
	CTD	2	2023-08-15	00:29	00:47	76°59.993' N	173°35.957' E	737	100.5	12.00	208	0.09	270.8	CTD	PSJ
	TRIOS	1		00:56	01:04	76°59.991' N	173°35.956' E	737	40			0.25	250.4	TriOS	JWPark
	PHY	1		01:08	01:15	76°59.989' N	173°35.967' E	737	100			0.71	223.8	Phyto Net	JeongHyun
	PHY	2		01:18	01:26	76°59.990' N	173°35.967' E	737	100			0.02	232.4	Phyto Net	JeongHyun
	150NET	1		01:30	01:45	76°59.990' N	173°35.965' E	737	150			0.76	240.3	150 Net	JH
	BON	1		01:49	02:03	76°59.991' N	173°35.964' E	737	200			0.98	238.6	Bongo Net	JH
	FTN	1		02:12	03:44	76°59.991' N	173°35.963' E	737	650			0.34	240.2	Frame Trawl Net	JH
	DSC	1		04:36	07:15	76°57.923' N	173°23.284' E	607	607			0.69	219.8	Deep Sea Camera	JH
32	CTD	1	2023-08-15	12:55	13:27	75°59.996' N	173°36.026' E	264	255	11.45	271	0.05	29.1	CTD	MSKim
	TMC	1		13:57	14:14	75°59.949' N	173°36.421' E	264	240			0.26	9.5	Trace Metal CTD	PKU
	TRIOS	1		14:03	15:14	75°59.954' N	173°36.526' E	264	60			0.44	30.3	TriOS	JWPark
	CTD	2		14:30	14:47	75°59.956' N	173°36.526' E	264	100	10.42	259	0.02	29.6	CTD	JYChae
	PHY	1		15:21	15:29	75°59.870' N	173°36.638' E	264	100			0.03	178.2	Phyto Net	JeongHyun
	150NET	1		15:34	15:47	75°59.869' N	173°36.638' E	264	200			0.05	189.9	150 Net	JH
	BON	1		15:51	16:03	75°59.870' N	173°36.630' E	264	200			0.09	200.3	Bongo Net	JH
	WAVEBUOY	1		16:22	16:32	76°00.534' N	173°38.126' E	264				1.03	15.9	Wave Buoy Deploy	JWPark
	FISHING	1		16:42	18:00	76°01.188' N	173°40.211' E					2.80	337.2	Fishing	JH
	CTD	3		23:27	08:00(+1)	75°00.000' N	173°35.988' E	146	137	13.44	285	0.04	326.8	CTD	MSKim
33	CTD	1	2023-08-15	23:50	00:30(+1)	74°60.000' N	173°35.991' E					0.03	325.7	CTD	MSKim
	TMC	1	2023-08-16	00:03	00:16	74°60.000' N	173°35.987' E	146	135			0.03	325.9	Trace Metal CTD	PKU
	CTD	2		00:47	08:00(+1)	75°00.003' N	173°36.024' E					0.02	320.4	CTD	PSJ
	TRIOS	1		00:54	01:01	75°00.004' N	173°36.024' E	146	30			0.06	320.1	TriOS	JWPark
	PHY	1		01:06	01:13	75°00.003' N	173°36.022' E	146	100			0.08	320.5	Phyto Net	JeongHyun
	150NET	1		01:16	01:28	75°00.003' N	173°36.022' E	146	140			0.06	319.7	150 Net	JH
	BON	1		01:31	01:42	75°00.003' N	173°36.020' E	146	140			0.02	320.3	Bongo Net	JH
	MOCNESS	1		01:53	02:32	75°00.008' N	173°36.009' E	146	130			0.63	320	MOCNESS	JH
34	CTD	1	2023-08-16	05:17	05:25	74°40.003' N	172°23.993' E	63.6	55.1	13.00	244	0.09	269.9	CTD	JYoo
	WAVEBUOY	1		05:40	05:42	74°40.349' N	172°22.470' E	63.6				0.25	236.5	Wave Buoy Deploy	JWPark
35	CTD	1	2023-08-16	08:57	09:06	74°19.999' N	171°11.999' E	54.6	49	15.66	241	0.09	264.7	CTD	JYoo

Scientific Cruise Daily Log

Ship: R/V Araon | Cruise: ARA14 . B | 2023.08.02 ~ 2023.08.29

STN No.	Gear	Cast No.	Date	Cast start	Cast end	Latitude	Longitude	Water depth	Cast depth	Wind speed	Wind direction	Ship speed	Heading	Remarks	Device Driver
			Local time	Local time	Local time			(m)	(m)	m/s	(°)	knot	(°)		
	WAVEBUOY	1		09:32	09:37	74°20.483' N	171°08.730' E					1.06	178.6	Wave Buoy Deploy	JWPark
36	CTD	1	2023-08-16	12:22	12:35	74°00.150' N	170°01.424' E	47	42.5	11.63	265	0.05	308.8	CTD	MSKim
	CTD	2		12:50	13:02	73°59.611' N	170°03.428' E	46	40.8	13.51	268	0.15	326.2	CTD	MSKim
	TMC	1		13:37	13:43	74°00.147' N	170°09.822' E	47	35			0.03	310.3	Trace Metal CTD	PKU
	CTD	3		13:59	14:12	74°00.149' N	170°09.824' E	47	40	11.63	259	0.06	327.2	CTD	JYChae
	TRIOS	1		14:22	14:29	74°00.148' N	170°09.819' E	47	40			0.07	311	TriOS	JWPark
	PHY	1		14:33	14:37	74°00.148' N	170°09.820' E	47	40			0.03	310.2	Phyto Net	JeongHyun
	150NET	1		14:41	14:46	74°00.148' N	170°09.820' E	47	40			0.02	310.3	150 Net	JH
	BON	1		14:51	14:54	74°00.148' N	170°09.820' E	47	40			0.05	310.3	Bongo Net	JH
	MOCNESS	1		15:14	15:25	73°59.559' N	170°12.174' E	47	47			0.17	301.3	MOCNESS	JH
	DRG	1		16:20	16:42	73°59.457' N	170°12.591' E	47	42			0.80	278.9	Dredge	JH
	DSC	1		18:09	19:59	74°00.228' N	170°09.786' E	47	47			0.06	349.1	Deep Sea Camera	JH
	FISHPOT	1		20:40	22:56	74°00.240' N	170°09.832' E	47	47			0.10	311.3	Fish Pot	JH
	WAVEBUOY	1		23:36	23:42	73°59.133' N	170°20.696' E					1.03	9.6	Wave Buoy Deploy	JWPark
	FISHING	1		23:47	01:50(+1)	73°59.145' N	170°21.133' E					0.91	17.1	Fishing	JH
37	MR	1	2023-08-17	08:55	09:35	74°41.961' N	174°30.841' E					0.02	310.8	Mooring Recovery(ESS-I)	
	MR	1		10:04	10:16	74°41.674' N	174°36.421' E					2.00	14.8	Mooring Recovery(ESS-H)	
	CTD	1		10:28	10:44	74°41.624' N	174°37.442' E	70	62	9.83	247	0.05	319.5	CTD	JYChae
	PHY	1		10:54	10:58	74°41.624' N	174°37.443' E	70	60			0.06	319.9	Phyto Net	JeongHyun
	150NET	1		11:04	11:09	74°41.623' N	174°37.442' E	70	60			0.04	320.1	150 Net	JH
	BON	1		11:15	11:21	74°41.622' N	174°37.437' E	70	60			0.18	311.3	Bongo Net	JH
	TRIOS	1		11:25	11:33	74°41.621' N	174°37.435' E	70	40			0.13	285.3	TriOS	JWPark
	CTD	2		11:45	12:02	74°41.622' N	174°37.440' E	71	62.2	9.56	237	0.04	303.4	CTD	PSJ
	DRG	1		12:27	12:50	74°41.604' N	174°36.929' E	70	70			0.04	118.4	Dredge	JH
	FISHPOT	1		13:44	15:52	74°41.511' N	174°37.457' E	70	70			0.01	322.9	Fish Pot	JH
	MD	1		16:36	16:41	74°41.663' N	174°36.237' E					0.30	13.6	Mooring Deploy(ESS-H)	
	MD	1		17:30	17:35	74°42.004' N	174°31.159' E					0.27	4.9	Mooring Deploy(ESS-I)	
38	CTD	1	2023-08-17	21:47	22:02	75°24.017' N	175°19.698' E	230	220	15.50	342	0.10	10.2	CTD	JYChae
39	CTD	1	2023-08-18	02:16	02:55	75°44.054' N	177°11.393' E	499.5	490.3	12.42	333	0.09	14.9	CTD	PSJ
	PHY	1		03:05	03:13	75°43.836' N	177°10.893' E	499.5	100			0.14	26.8	Phyto Net	JeongHyun
	150NET	1		03:18	03:30	75°43.835' N	177°10.891' E	499.5	200			0.02	23.4	150 Net	JH
	BON	1		03:36	03:49	75°43.718' N	177°10.574' E	499.5	200			2.70	30.7	Bongo Net	JH
	TRIOS	1		03:52	03:56	75°43.703' N	177°10.517' E	499.5	40			0.03	30.1	TriOS	JWPark
	CTD	2		04:07	04:24	75°43.601' N	177°10.282' E	483	100	8.88	352	0.01	42.8	CTD	JYoo
IC2	IC	1	2023-08-19	07:00	08:37	75°56.070' N	176°58.372' E					0.31	306.2	Ice Camp	
	TMC	1		09:32	09:36	75°56.351' N	176°57.257' E	551	35	3.44	334	0.03	318.8	Trace Metal CTD	PKU
39R	MR	1	2023-08-19	10:57	12:11	75°48.075' N	177°03.103' E					0.73	305.7	Mooring Recovery(KAMS1)	
	CTD	1		13:06	13:32	75°48.106' N	177°03.289' E	518.4	506.5	3.83	11	0.01	340.8	CTD	JYChae
	DSC	1		14:19	16:47	75°48.106' N	177°03.296' E	518	518			0.04	0.6	Deep Sea Camera	JH
	BON	1		17:20	17:23	75°48.104' N	177°03.317' E	520	25			0.01	60.1	Bongo Net	JH
	FISHPOT	1		17:36	19:57	75°48.197' N	177°03.967' E	520	520			0.07	60.4	Fish Pot	JH
	MD	1		21:42	22:21	75°48.363' N	177°04.514' E					0.50	227.9	Mooring Deploy(KAMS1)	

Scientific Cruise Daily Log

Ship: R/V Araon **Cruise:** ARA14 . B **2023.08.02 ~ 2023.08.29**

STN No.	Gear	Cast No.	Date	Cast start	Cast end	Latitude	Longitude	Water depth	Cast depth	Wind speed	Wind direction	Ship speed	Heading	Remarks	Device Driver
			Local time	Local time	Local time			(m)	(m)	m/s	(°)	knot	(°)		
	WAVEBUOY	1	2023-08-20	01:02	01:05	75°29.653' N	176°41.760' E					0.75	249.8	Wave Buoy Deploy	JWPark
40	CTD	1	2023-08-20	04:10	04:38	75°04.496' N	176°48.004' E	194.6	185.8	10.19	337	0.04	13.9	CTD	PSJ
	TMC	1		04:51	05:07	75°04.500' N	176°47.999' E	194.6	185			0.08	18.4	Trace Metal CTD	PKU
	CTD	2		05:21	05:42	75°04.498' N	176°48.003' E	194.6	101.1	9.92	345	0.06	17.7	CTD	PSJ
	PHY	1		05:49	05:57	75°04.498' N	176°48.006' E	194.6				0.01	17.4	Phyto Net	JeongHyun
	PHY	2		05:59	06:05	75°04.498' N	176°48.005' E	194.6	100			0.02	17.8	Phyto Net	JeongHyun
	150NET	1		06:08	06:21	75°04.498' N	176°48.006' E	194.6	185			0.07	18.1	150 Net	JH
	BON	1		06:25	06:36	75°04.422' N	176°47.865' E	194.6	185			0.23	19.5	Bongo Net	JH
	DRG	1		06:54	07:37	75°03.694' N	176°45.177' E	186.5	187			0.07	208.9	Dredge	JH
41	CTD	1	2023-08-20	10:33	10:53	75°06.477' N	178°25.204' E	311.1	303.2	8.34	330	0.14	53.3	CTD	PSJ
42	C-PIES DEPLOY	1	2023-08-20	14:55	15:11	75°30.041' N	179°59.616' E					1.02	316.8	C-PIES Deploy	IU
	CTD	1		15:24	16:06	75°30.043' N	179°59.993' E	937	928.5	10.23	311	0.02	335.2	CTD	MSKim
43	CTD	1	2023-08-20	18:16	18:56	75°10.210' N	179°57.948' W	538	529	8.99	291	0.02	310.1	CTD	JYChae
	TMC	1		19:10	19:41	75°10.080' N	179°57.770' W	538	515			0.27	312.9	Trace Metal CTD	PKU
	CTD	2		20:02	20:21	75°09.911' N	179°58.086' W	538	100	8.04	270	0.10	319.8	CTD	JYChae
	TRIOS	1		20:30	20:39	75°09.911' N	179°58.087' W	538	50			0.03	320.1	TriOS	JWPark
	PHY	1		20:43	20:51	75°09.878' N	179°58.115' W	538	100			0.03	327.9	Phyto Net	JeongHyun
	150NET	1		20:56	21:08	75°09.878' N	179°58.116' W	538	200			0.05	326.1	150 Net	JH
	BON	1		21:14	21:26	75°09.878' N	179°58.115' W	538	200			0.04	328.9	Bongo Net	JH
	MOCNESS	1		21:38	22:52	75°09.851' N	179°58.051' W	538	600			1.13	145.2	MOCNESS	JH
	MD	1	2023-08-21	00:20	01:14	75°07.866' N	179°53.643' W					13.25	312.8	Mooring Deploy(KAMS5Trap)	
	WAVEBUOY	1	2023-08-21	03:56	03:58	75°11.199' N	179°12.116' W	563				0.31	111	Wave Buoy Deploy	JWPark
44	CTD	1	2023-08-21	06:23	07:10	75°09.035' N	177°59.885' W	540.8	531.7	0.07	42.9	0.06	51.1	CTD	PSJ
45	CTD	1	2023-08-21	10:02	10:44	75°09.003' N	176°00.009' W	326.3	316.9	118.00	7.36	0.07	163.8	CTD	PSJ
	TMC	1		10:58	11:18	75°09.004' N	175°59.997' W		310			0.04	140	Trace Metal CTD	PKU
	CTD	2		11:34	11:56	75°08.997' N	176°00.015' W	326.3	100.5	7.34	113	0.11	183.9	CTD	PSJ
	TRIOS	1		12:07	12:14	75°08.997' N	175°59.996' W	323.6	40			0.06	146.7	TriOS	JWPark
	PHY	1		12:17	12:25	75°08.997' N	175°59.997' W	326.3	100			0.01	139.6	Phyto Net	JeongHyun
	150NET	1		12:31	12:43	75°08.997' N	175°59.999' W	326.3	200			0.03	149.8	150 Net	JH
	BON	1		12:49	13:02	75°08.998' N	175°59.999' W	323.6	200			0.03	149.9	Bongo Net	JH
	MOCNESS	1		13:22	14:06	75°08.999' N	175°60.000' W	323.6	350			0.02	149.9	MOCNESS	JH
46	CTD	1	2023-08-21	17:12	17:55	75°11.718' N	173°59.237' W	363	353	6.99	103	0.01	183.7	CTD	JYChae
47	MR	1	2023-08-21	20:56	22:04	75°14.379' N	171°58.074' W					1.21	230.1	Mooring Recovery(KAMS2)	
	CTD	1		22:34	23:13	75°14.428' N	171°58.350' W	505	495	0.18	353	0.03	309.9	CTD	JYChae
	TMC	1		23:28	23:56	75°14.428' N	171°58.352' W	505	490			0.01	311.8	Trace Metal CTD	PKU
	CTD	2	2023-08-22	00:12	00:34	75°14.429' N	171°58.348' W	505	100.6	4.51	293	0.05	342.7	CTD	PSJ
	TRIOS	1		00:42	00:48	75°14.429' N	171°58.339' W	505	20			0.01	5	TriOS	JWPark
	PHY	1		00:51	00:59	75°14.429' N	171°58.336' W	505	100			0.01	16	Phyto Net	JeongHyun
	150NET	1		01:03	01:17	75°14.428' N	171°58.335' W	505	200			0.02	22.7	150 Net	JH
	BON	1		01:20	01:34	75°14.428' N	171°58.334' W	505	200			0.02	27.7	Bongo Net	JH
	DSC	1		02:06	04:30	75°14.453' N	171°58.257' W	505	505			0.01	40	Deep Sea Camera	JH
	MD	1		05:42	06:13	75°14.314' N	172°00.080' W					0.49	266	Mooring Deploy(KAMS2)	

Scientific Cruise Daily Log

Ship: R/V Araon **Cruise:** ARA14 . B **2023.08.02 ~ 2023.08.29**

STN No.	Gear	Cast No.	Date	Cast start	Cast end	Latitude	Longitude	Water depth	Cast depth	Wind speed	Wind direction	Ship speed	Heading	Remarks	Device Driver
			Local time	Local time	Local time			(m)	(m)	m/s	(°)	knot	(°)		
	FISHPOT	1		07:29	09:58	75°14.100' N	172°00.509' W	493	493			0.04	238.5	Fish Pot	JH
48	CTD	1	2023-08-22	13:17	13:48	75°01.237' N	169°56.172' W	256	246	3.27	175	0.01	9.4	CTD	JYChae
	150NET	1		14:04	14:15	75°01.282' N	169°56.142' W	256	200			0.05	350.8	150 Net	JH
	BON	1		14:21	14:33	75°01.283' N	169°56.142' W	256	200			0.03	350.3	Bongo Net	JH
	CTD	2		14:45	15:04	75°01.236' N	169°56.167' W	256	100	1.40	62	0.02	30.3	CTD	JYChae
	MOCNESS	1		15:46	16:27	75°00.341' N	169°45.432' W	243	300			0.77	212.1	MOCNESS	JH
	FISHPOT	1		16:46	19:08	74°58.788' N	169°49.507' W	242	242			0.09	34.2	Fish Pot	JH
49	CTD	1	2023-08-22	22:52	23:16	75°14.753' N	167°16.083' W	195	186	8.92	274	0.08	331.2	CTD	JYChae
50	CTD	1	2023-08-23	01:53	02:28	75°41.468' N	166°38.277' W	291.8	282.3	14.22	311	0.03	350.4	CTD	PSJ
	TMC	1		02:46	03:04	75°41.470' N	166°38.275' W	291	280			0.16	345.7	Trace Metal CTD	PKU
	PHY	1		03:18	03:27	75°41.469' N	166°38.283' W	291	100			0.03	0.3	Phyto Net	JeongHyun
	150NET	1		03:30	03:44	75°41.469' N	166°38.283' W	291	200			0.05	5.8	150 Net	JH
	BON	1		03:46	04:00	75°41.469' N	166°38.280' W	291	200			0.08	11.8	Bongo Net	JH
	CTD	2		04:11	04:43	75°41.469' N	166°38.281' W	292	282.4	18.83	318	0.10	7.2	CTD	PSJ
	MOCNESS	1		05:02	05:38	75°39.883' N	166°39.198' W	282	270			0.13	327	MOCNESS	JH
51	CTD	1	2023-08-23	08:58	09:47	76°07.956' N	165°29.118' W	709	700	15.55	322	0.05	63.2	CTD	JYoo
	CTD	2		10:23	11:06	76°06.939' N	165°28.635' W	709.3	700	14.71	312	0.07	130.2	CTD	PSJ
52	CTD	1	2023-08-23	14:10	14:50	76°34.046' N	164°21.688' W	549	539	14.45	330	0.02	9.9	CTD	JYChae
	TMC	1		15:10	15:41	76°34.050' N	164°21.687' W	549	535			0.13	2.7	Trace Metal CTD	PKU
	CTD	2		15:57	16:16	76°34.044' N	164°21.730' W	549	100	7.73	325	0.04	35.3	CTD	JYChae
	TRIOS	1		16:24	16:34	76°34.044' N	164°21.730' W	549	60			0.02	29.7	TriOS	JWPark
	PHY	1		16:37	16:45	76°34.044' N	164°21.730' W	549	100			0.02	29.9	Phyto Net	JeongHyun
	150NET	1		16:51	17:03	76°34.045' N	164°21.730' W	549	200			0.01	30.2	150 Net	JH
	BON	1		17:07	17:23	76°34.045' N	164°21.731' W		200			0.01	30.2	Bongo Net	JH
	DSC	1		20:03	22:36	76°34.226' N	164°26.768' W	553	553			0.11	166	Deep Sea Camera	JH
	FISHPOT	1		22:49	01:16(+1)	76°34.268' N	164°26.967' W	553	553			0.11	279.1	Fish Pot	JH
53	CTD	1	2023-08-24	04:22	04:57	77°00.900' N	164°13.399' W	418	409	6.60	291	0.03	302.8	CTD	JYoo
54	CTD	1	2023-08-24	08:25	09:00	77°28.066' N	164°06.089' W	279.3	269.8	6.93	295	0.05	328.7	CTD	PSJ
	TMC	1		09:16	09:33	77°28.049' N	164°05.683' W	279	265			0.02	309.8	Trace Metal CTD	PKU
	CTD	2		09:51	10:13	77°28.046' N	164°05.732' W	279	100.6	7.10	290	0.24	338.4	CTD	PSJ
	TRIOS	1		10:22	10:32	77°28.042' N	164°05.778' W	279	40			0.04	325.8	TriOS	JWPark
	PHY	1		10:35	10:42	77°28.042' N	164°05.779' W	279	100			0.09	326.5	Phyto Net	JeongHyun
	150NET	1		10:45	10:59	77°28.042' N	164°05.773' W	279	200			0.08	335.2	150 Net	JH
	BON	1		11:05	11:20	77°28.042' N	164°05.771' W	279	200			0.01	335.3	Bongo Net	JH
	WAVEBUOY	1		11:48	11:50	77°27.172' N	164°02.978' W					0.27	258.7	Wave Buoy Deploy	JWPark
	FISHING	1		12:06	12:06	77°27.814' N	164°00.780' W					2.44	80.4	Fishing	JH
	FISHING	2		14:14	08:00(+1)	77°25.428' N	163°58.442' W					2.87	343.8	Fishing	JH
55	CTD	1	2023-08-24	17:27	17:57	77°55.665' N	163°58.037' W	270	260	3.99	275	0.02	339.3	CTD	JYChae
	150NET	1		18:08	18:20	77°55.665' N	163°58.042' W	270	200			0.01	325	150 Net	JH
	BON	1		18:29	18:40	77°55.665' N	163°58.042' W	270	200			0.03	324.9	Bongo Net	JH
	WAVEBUOY	1		19:07	19:12	77°55.700' N	163°53.068' W					0.14	234	Wave Buoy Deploy	JWPark
XCTD13	XCTD	1	2023-08-24	21:18	21:24	77°47.167' N	162°23.687' W		1100			11.62	117.9	xCTD	MSKim

Scientific Cruise Daily Log

Ship: R/V Araon | Cruise: ARA14 . B | 2023.08.02 ~ 2023.08.29

STN No.	Gear	Cast No.	Date	Cast start	Cast end	Latitude	Longitude	Water depth	Cast depth	Wind speed	Wind direction	Ship speed	Heading	Remarks	Device Driver
			Local time	Local time	Local time			(m)	(m)	m/s	(°)	knot	(°)		
XCTD14	XCTD	1	2023-08-24	22:44	22:50	77°38.928' N	161°27.464' W	2600	1100			10.53	132.7	xCTD	MSKim
56	CTD	1	2023-08-25	02:35	03:42	77°29.988' N	158°44.476' W	1323	1313	4.66	258	0.04	319.7	CTD	JYoo
	PHY	1		03:53	04:01	77°29.466' N	158°43.930' W	1323	100			0.09	340.7	Phyto Net	JeongHyun
	150NET	1		04:05	04:17	77°29.409' N	158°43.921' W	1323	200			0.49	341.9	150 Net	JeongHyun
	BON	1		04:21	04:34	77°29.363' N	158°43.949' W	1323	200			1.08	348.6	Bongo Net	JeongHyun
	TRIOS	1		04:37	04:44	77°29.335' N	158°43.957' W	1323	40			1.09	350.8	TriOS	JWPark
	CTD	2		04:55	05:15	77°28.924' N	158°44.051' W	1262	100	2.97	263	0.07	2.4	CTD	PSJ
	CTD	3		05:40	06:35	77°28.627' N	158°44.822' W	1295	1286	2.70	283	0.03	35.5	CTD	PSJ
	MOCNESS	1		06:54	07:25	77°28.434' N	158°45.502' W	1311	500			0.12	355.4	MOCNESS	JH
	WAVEBUOY	1		08:01	08:10	77°29.999' N	158°51.128' W					0.49	121	Wave Buoy Deploy	JWPark
	FISHING	1		08:18	09:42	77°29.985' N	158°50.883' W					1.21	325.6	Fishing	JH
XCTD15	XCTD	1	2023-08-25	12:35	12:41	77°05.890' N	157°57.805' W	1439	1100			8.85	143.9	xCTD	MSKim
XCTD16	XCTD	1	2023-08-25	14:55	14:56	76°41.933' N	157°10.319' W		1100			8.94	214.5	xCTD	MSKim
57	MR	1	2023-08-25	18:08	19:17	76°18.253' N	156°13.455' W					1.28	202.2	Mooring Recovery(KAMS4)	
	CTD	1		19:53	20:39	76°18.234' N	156°13.264' W	725	715	5.65	244	0.04	248.5	CTD	JYChae
	PHY	1		20:46	20:54	76°18.233' N	156°13.265' W	725	100			0.05	239.9	Phyto Net	JeongHyun
	PHY	2		20:59	21:06	76°18.233' N	156°13.267' W	725	100			0.08	239.9	Phyto Net	JeongHyun
	150NET	1		21:10	21:22	76°18.234' N	156°13.267' W	725	200			0.07	240	150 Net	JH
	BON	1		21:27	21:39	76°18.234' N	156°13.268' W	725	200			0.09	240.1	Bongo Net	JH
	TRIOS	1		21:43	21:54	76°18.234' N	156°13.266' W	725	70			0.10	240	TriOS	JWPark
	CTD	2		22:05	22:22	76°18.234' N	156°13.267' W	725	100	4.21	233	0.02	240	CTD	JYChae
	FTN	1		22:54	23:51	76°18.189' N	156°13.438' W	717	625			2.10	221.9	Frame Trawl Net	JH
	DSC	1	2023-08-26	00:16	02:48	76°15.935' N	156°21.427' W	695	695			0.02	209.9	Deep Sea Camera	JH
XCTD17	XCTD	1	2023-08-26	05:14	05:20	76°25.011' N	157°56.806' W	1670	1100			10.66	300.1	xCTD	JYoo
58	CTD	1	2023-08-26	08:26	10:15	76°32.131' N	159°47.514' W	2112	2102	5.22	253	0.07	341.5	CTD	JYoo
	TMC	1		10:46	12:36	76°31.058' N	159°47.022' W	2077	2020			0.61	10.3	Trace Metal CTD	PKU
	CTD	2		12:53	13:09	76°31.115' N	159°47.355' W	2076	100	5.26	264	0.09	101.1	CTD	JYChae
	TRIOS	1		13:20	13:31	76°31.216' N	159°46.662' W	2076	70			0.03	107.5	TriOS	JWPark
	PHY	1		13:34	13:42	76°31.222' N	159°46.645' W	2076	100			0.11	139.1	Phyto Net	JeongHyun
	150NET	1		13:46	13:58	76°31.253' N	159°46.467' W	2076	200			0.06	151.3	150 Net	JH
	BON	1		14:02	14:15	76°31.263' N	159°46.263' W	2076	200			0.04	163	Bongo Net	JH
	CTD	3		14:27	16:01	76°31.258' N	159°46.153' W	2111	2101	5.15	279	0.03	190.5	CTD	JYChae
	C-PIES CHECK	1		16:24	16:41	76°31.957' N	159°53.874' W					0.12	266.9	C-PIES Check	IU
	MOCNESS	1		17:26	18:01	76°29.646' N	159°51.531' W	2070	800			0.92	89.5	MOCNESS	JH
XCTD18	XCTD	1	2023-08-26	20:54	21:00	75°59.902' N	160°31.246' W	2045	1100			8.07	186.2	xCTD	MSKim
59	CTD	1	2023-08-26	23:44	01:22(+1)	75°29.909' N	161°08.827' W	2097	2088	3.25	69	0.04	271.3	CTD	MSKim
	C-PIES CHECK	1		23:50	00:10(+1)	75°29.909' N	161°08.827' W					0.04	271.3	C-PIES Check	IU
	PHY	1	2023-08-27	01:30	01:37	75°29.908' N	161°08.829' W	2097	100			0.07	252.8	Phyto Net	JeongHyun
	150NET	1		01:41	01:54	75°29.908' N	161°08.829' W	2097	200			0.10	252.9	150 Net	JeongHyun
	BON	1		01:58	02:12	75°29.907' N	161°08.829' W		200			0.08	252.9	Bongo Net	JH
	CTD	2		02:22	02:41	75°29.906' N	161°08.828' W	2097	100	4.31	60	0.10	253	CTD	PSJ
	FTN	1		02:58	03:41	75°29.391' N	161°08.263' W	2063				2.49	146	Frame Trawl Net	JH

Scientific Cruise Daily Log

Ship: R/V Araon | Cruise: ARA14 . B | 2023.08.02 ~ 2023.08.29

STN No.	Gear	Cast No.	Date	Cast start	Cast end	Latitude	Longitude	Water depth	Cast depth	Wind speed	Wind direction	Ship speed	Heading	Remarks	Device Driver
			Local time	Local time	Local time			(m)	(m)	m/s	(°)	knot	(°)		
XCTD19	XCTD	1	2023-08-27	06:09	06:14	74°59.966' N	161°39.938' W	1969	1100			9.82	190.6	xCTD	JYoo
60	C-PIES CHECK	1	2023-08-27	08:35	08:45	74°30.949' N	162°09.206' W					0.40	69.1	C-PIES Check	IU
	CTD	1		08:46	10:03	74°30.981' N	162°09.117' W	1595	1585	6.53	77	0.27	78.5	CTD	JYoo
	PHY	1		10:12	10:19	74°30.981' N	162°09.118' W	1595	100			0.18	65.5	Phyto Net	JeongHyun
	150NET	1		10:21	10:35	74°30.982' N	162°09.117' W	1595	200			0.36	65.4	150 Net	JeongHyun
	BON	1		10:40	10:53	74°30.982' N	162°09.117' W	1595	200			0.64	65.2	Bongo Net	JeongHyun
	TRIOS	1		10:56	11:08	74°30.979' N	162°09.115' W	1595	40			0.20	83.6	TriOS	JWPark
	CTD	2		11:24	11:44	74°30.980' N	162°09.112' W	1595	100	8.45	40	0.47	84.4	CTD	PSJ
	CTD	3		12:15	13:22	74°30.979' N	162°09.114' W	1595	1585	11.71	39	0.08	84.1	CTD	JYChae
	MOCNESS	1		13:40	14:22	74°30.989' N	162°09.393' W	1595	1000			1.93	281.3	MOCNESS	JH
61	CTD	1	2023-08-27	16:53	17:40	74°36.914' N	163°55.018' W	833	826	2.67	41	0.21	119.4	CTD	MSKim
62	CTD	1	2023-08-27	21:52	22:10	75°01.547' N	165°22.905' W	544	529	1.91	345	0.12	232.1	CTD	JYChae
	MD	1		22:39	23:40	75°01.426' N	165°21.974' W					0.13	266.1	Mooring Deploy(KAMS4Trap)	PO
	CTD	2	2023-08-28	02:01	02:46	75°01.519' N	165°21.169' W	543	534	1.22	250	0.21	269.7	CTD	PSJ
	150NET	1		02:56	03:08	75°01.519' N	165°21.170' W	543	200			0.17	269.9	150 Net	JeongHyun
	BON	1		03:13	03:26	75°01.518' N	165°21.168' W	543	200			0.27	269.8	Bongo Net	JeongHyun
63	CTD	1	2023-08-28	05:37	06:20	74°42.483' N	165°54.453' W	406	400	5.14	239	0.97	260.9	CTD	PSJ
	150NET	1		06:29	06:45	74°42.479' N	165°54.442' W	406	200			0.53	225.8	150 Net	JeongHyun
	BON	1		06:47	07:01	74°42.477' N	165°54.417' W	406	200			0.08	164.6	Bongo Net	JeongHyun
64	MR	1	2023-08-28	14:00	00:10(+1)	73°21.294' N	166°43.862' W							Mooring Recovery(SM) / Mooring Lost	
	FISHPOT	1	2023-08-29	01:59	10:05	73°24.453' N	166°29.736' W	70	70			0.03	272.8	Fish Pot	JH

Appendix II. XCTD information

(1) Instrument

XCTD-1 probe, Tsurumi-Seiki Co.

XBT/XCTD digital converter model MK-150, Tsurumi-Seiki Co.

XBT/XCTD auto launcher, Tsurumi-Seiki Co.

(2) Data

According to the manufacturer's nominal specifications, the range and accuracy of parameters measured by the XCTD (eXpendable Conductivity, Temperature & Depth profiler) are as follows;

Parameter	Range	Accuracy
Conductivity	0 ~ 60 [mS/cm]	+/- 0.03 [mS/cm]
Temperature	-2 ~ 35 [deg-C]	+/- 0.02 [deg-C]
Depth	0 ~ 1100 [m]	5 [m] or 2 [%] (either of them is major)

However the actual data contain bias in salinity (conductivity) dependent on serial number of XCTD probes. In most cases, the bias is positive about 0.01psu. After the cruise, calibration of XCTD data is planned, using CTD data calibrated by bottle salinity data.

Chapter 3. Chemical Oceanography

3.1. Inorganic carbon system and gas measurements

Ahra Mo

Korea Polar Research Institute, Incheon, Republic of Korea

E-mail: ahramo@kopri.re.kr

3.1.1. Introduction

A significant portion of atmospheric carbon dioxide (CO2) has been absorbed into the Arctic Ocean, constituting around 12% of the total CO2 absorption by the world's oceans (Takahashi et al., 2009). The Arctic Ocean has undergone notable environmental changes, including diminishing sea ice coverage and increased inflowing of Pacific-origin seawater and river water. These changes have led to increased availability of light and nutrients, resulting in heightened primary production and reduced sea surface partial pressure of CO2 (pCO2) of the Arctic Ocean. Additionally, the formation and dissolution of sea ice play a direct role in influencing surface pCO2. Due to its high biological production and low temperature, the Arctic Ocean has significant potential for absorbing atmospheric CO2. However, our understanding of the distribution of CO2, air–sea CO2 fluxes, and the carbon cycle in the Arctic Ocean is uncertain due to relatively few observations and rapid climate changes.

Four variables in the ocean carbonate chemistry system variables (pCO2, dissolved inorganic carbon; DIC, total alkalinity; TA, and pH) can be accurately determined using stoichiometric equations. In other words, if any two of these variables are determined, it is possible to calculate the other two. Generally, absorbed CO2 converts to ionic forms: carbonate (CO32–), bicarbonate (HCO3–), hydrogen ion (H+), carbonic acid (H2CO3), and dissolved CO2. However, these species cannot be directly analyzed using analytical instruments except CO2 and H+. Thus, to determine the carbonate system in the water column, we sampled DIC and TA, from which one can derive ionic and neutral forms of the carbonate system. DIC and TA are defined as follows:

$$DIC = [HCO_3^-] + [CO_3^{2-}] + [CO_2] + [H_2CO_3]$$

$$TA = [HCO_3^-] + 2[CO_3^{2-}] + S[anions] - S[cations]$$

A stable isotope of inorganic dissolved carbon (δ13C-DIC) can serve as an indicator to assess the impact of anthropogenic CO2 on seawater. Mean δ13CO2 values for the atmosphere, surface seawater, and fossil fuels are reported as –7.55‰, 1.8‰, and –28.1‰, respectively. Recently, the atmospheric δ13CO2 has shown a consistent decrease due to depleted 13CO2 in fossil fuels, leading to a reduction in δ13C-DIC in seawater as a result of the ocean's absorption of atmospheric CO2. This phenomenon, known as the 13C Suess effect, perturbs the ratio of heavy carbon isotopes due to the introduction of CO2 from fossil fuel sources. Estimating the variation of anthropogenic CO2 in the ocean is significant for enhancing our understanding of the global carbon cycle.

During this cruise, we aimed to enhance our comprehension of the carbon biogeochemical cycles within the Arctic Ocean. To achieve this, we gathered water samples to measure DIC, TA, and δ13C-DIC. Additionally, we monitored underway pCO2 using the Contros HydroC pCO2 sensor. The data acquired from this cruise will play a crucial role in estimating the fluctuations of anthropogenic CO2 in the Arctic Ocean. Furthermore, it will serve as the foundation for constructing a comprehensive database for carbon cycle modeling in the future.

3.1.2. Materials and methods

A total of 49 samplings for DIC and TA measurements and 10 for δ13C-DIC measurements were successfully conducted at the water column station between August 3 and August 28, 2023, during the ARA14B expedition aboard the R/V Araon, operated by the Korea Polar Research Institute (Fig. 3.1.2.1). To obtain the vertical profiles of DIC, TA and δ13C-DIC, seawater were sampled from the Niskin bottles attached in CTD/Rosette. The sample bottles were flushed 3 times before starting collection in 500 mL (or 250 mL) borosilicate glass bottles. Making small headspace and injecting 200 µL (or 100 µL) of saturated HgCl2 solution to prevent biological activities. Further, the vacuum grease was used to prevent contaminations and gas exchange between the sample and the atmosphere. After sampling, the bottles were tightened with rubber bands and stored in a dark place before analysis. After this cruise, the samples for DIC and TA will be analyzed using the VINDTA system in KIOST, and the samples for δ13C-DIC will be analyzed using an Apollo DIC analyzer coupled to a carbon dioxide Picarro

cavity ring-down spectrometer (CRDS) in KOPRI.

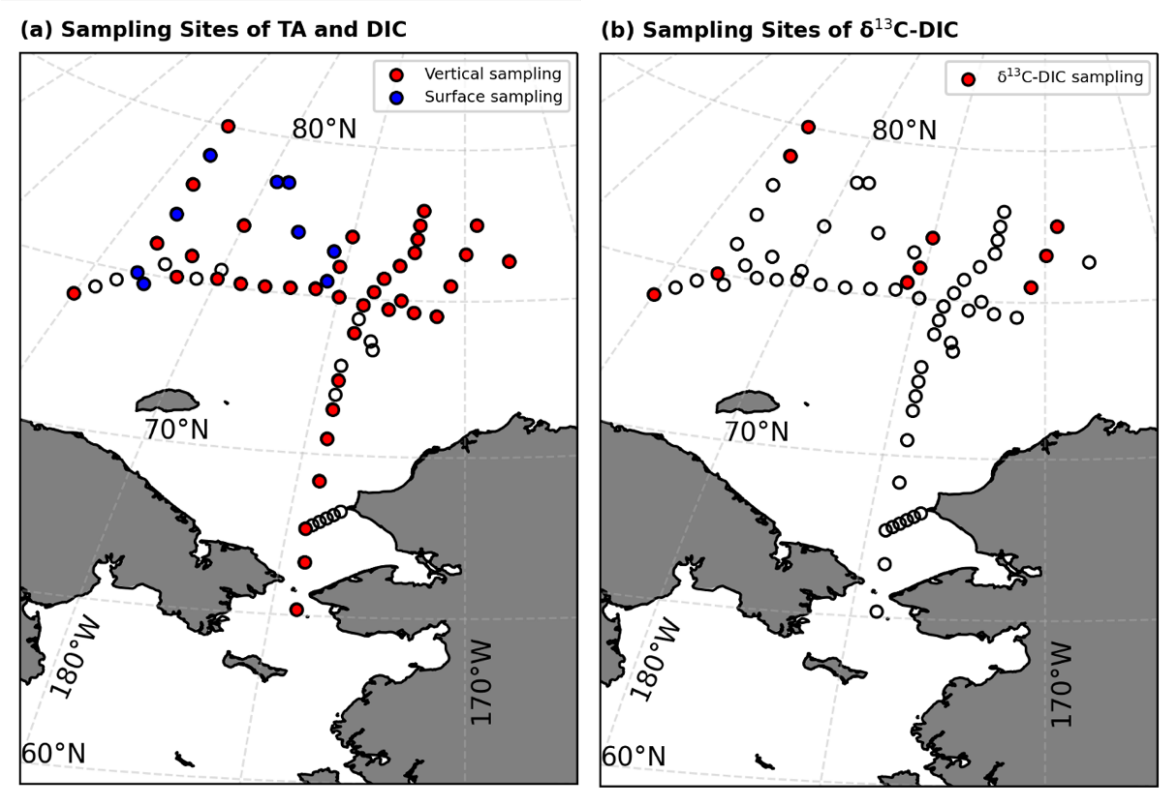

Figure 3.1.2.1 Sampling sites for (a) total alkalinity (TA) and dissolved inorganic carbon (DIC), and (b) stable isotope of DIC (δ^{13}C-DIC). Red and blue dots indicate the vertical and surface sampling, respectively.

To observe underway pCO2 during the cruise, the Contros HydroC pCO2 sensor was equipped with newly developed flow heads that used the platform movement to provide a constant and directed stream of water to the HydroC's membrane. Usually, a submersible pump is used to create this water flow required to speed up the partial pressure equilibration between dissolved gases in the water and the gaseous headspace behind the membrane. We collected 20 samples of underway seawater with the same DIC and TA sampling processes to calibrate the Contros HydroC pCO2 sensor (Figure 3.1.2.2) (Mo et al., 2023). After this cruise, these samples will be analyzed with the VINDTA system in the Marine Environment Research Lab of Korea University.

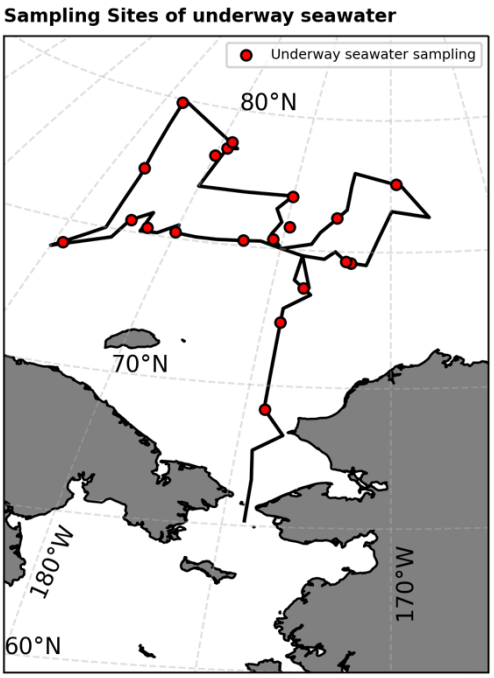

Figure 3.1.2.2. Sampling sites of underway seawater to calibrate the Contros HydroC pCO_2 sensor. Red dots and black line indicate the sampling sites and cruise track, respectively.

References

Fietzek, P., Steinhoff, T., Kortzinger, A. (2014) In situ quality assessment of a novel underwater pCO2 sensor based on membrane equilibration and NDIR spectrometry. Journal of Atmospheric and Oceanic Technology, 31, 181-196.

Mo, A., Park, K., Park, J., Hahm, D., Kim, K., Ko, Y. H., ... & Kim, T. W. (2023). Assessment of austral autumn air–sea CO2 exchange in the Pacific sector of the Southern Ocean and dominant controlling factors. Frontiers in Marine Science.

Pierrot, D., Neill, C., Sullivan, K., Castle, R., Wanninkhof, R., Lu¨ger, H., Johannessen, T., Olsen, A., Feely R.A., Cosca, C.E. (2008) Recommendations for Autonomous Underway pCO2 Measuring Systems and Data Reduction Routines. Deep-Sea Research Part II.

3.2. Nutrients and organic carbon

3.2.1. Nutrients

Jinyoung Jung[1] and Juyoung Son[1,2]

[1]Korea Polar Research Institute, Incheon 21990, Korea (jinyoungjung@kopri.re.kr)

[2]Pukyoung National University, Busan 48513, Korea (mh0980@kopri.re.kr)

1. Introduction

The Arctic Ocean undergoes rapid environmental changes, including accelerated warming (Ballinger et al., 2020) and a strongly declining summer sea ice extent that coincides with an intense loss of multi-year sea ice (Cavalieri & Parkinson, 2012; Perovich et al., 2020). Diminishing sea-ice cover has important consequences for ecosystem dynamics, associated biogeochemistry and the capacity of the Arctic Ocean to absorb atmospheric CO2, and will cause the Arctic marine system to receive more photosynthetically active radiation (PAR) suggesting that there will be significant increases in primary production. For example, Lewis et al. (2020) reported that annual net primary production (NPP) increased by 57% over the Arctic Ocean between 1998 and 2018.

The major controls on aquatic primary production are nutrient availability and radiation. These direct controls are modulated by stratification and circulation features that enhance or constrain the nutrient supply and/or influence the radiation exposure of phytoplankton. The largest nutrient inputs to the Arctic marine system are advective inputs via the Atlantic and Pacific entrances. The Pacific input is less saline and richer in nutrients than the Atlantic input. Although the total volume of Pacific Origin waters entering the Arctic is much less than the volume of the Atlantic inflow, the low salinity of the Pacific inflow concentrates its effect in the upper layers of the Pacific Arctic (Codispoti et al., 2005). As a consequence, the impact of the Pacific inflow exceeds the impact of the Atlantic inflow with respect to nutrient inputs to the photic zone.

Nutrient depletion, especially nitrogen, in Arctic surface waters during the summer is common due to biological uptake and intense stratification caused by sea ice melting and riverine water inputs, which restricts the upward mixing of nutrients into the euphotic zone.

However, the Arctic changes associated with the anomalous nutrient supply have already impacted biogeochemical components (e.g., Polyakov et al., 2020) and primary production (e.g., Lewis et al., 2020; Jung et al., 2021), suggesting that the changes in the circulation pathways of specific water masses can control the availability of nutrients in the Arctic Ocean (Polyakov et al., 2020). Thus, it is quite important to keep monitoring of nutrients in the Arctic Ocean and investigate their variation and impact on the Arctic carbon cycle.

2. Materials and methods

Seawater sampling for nutrients was carried out at 53 stations over the Chukchi and East Siberian seas using a CTD/rosette sampler holding 24-10 L Niskin bottles (SeaBird Electronics, SBE 911 plus) during Korea research ice breaker R/V Araon cruise (ARA14B, August 3−28, 2023) (Fig. 3.2.1.1). Samples for nutrients were collected from the Niskin bottles into 50 ml conical tubes and immediately stored in a refrigerator at 4°C prior to chemical analyses. Concentrations of nutrients were measured using standard colorimetric methods adapted for use on a 4-channel continuous Auto-Analyzer (QuAAtro, Seal Analytical, Germany). The channel configurations and reagents were prepared according to the ‘QuAAtro Applications’. Standard curves were run with each batch of samples using freshly prepared standards that spanned the range of concentrations in the samples. The r2 values of all the standard curves were greater than or equal to 0.99.

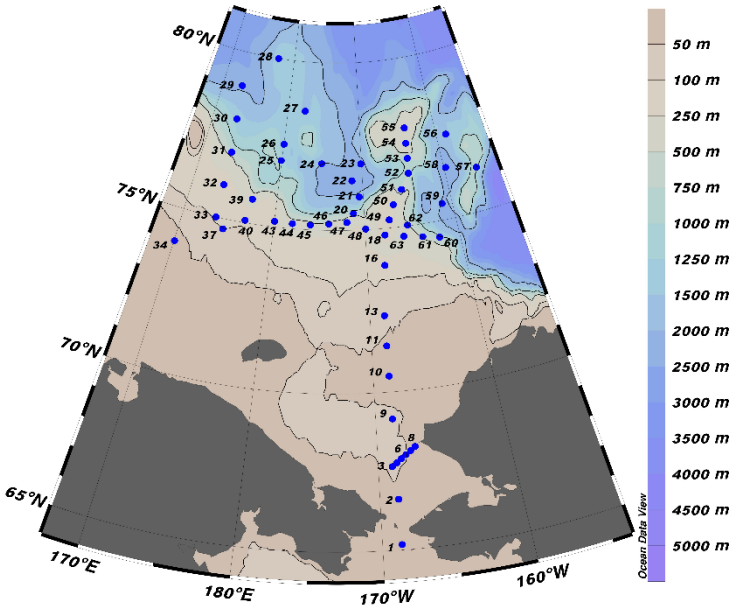

Fig. 3.2.1.1. Map of study area. Blue dots show the CTD stations during the expedition. The numbers indicate the station numbers.

References

Ballinger, T. J., Overland, J. E., Wang, M., Bhatt, U. S., Hanna, E., Hanssen-Bauer, I., et al. 2020. Surface air temperature. [in NOAA Arctic Report Card 2020]. Available at: https://www.arctic.noaa.gov/Report-Card.

Cavalieri, D.J., Parkinson, C.L., 2012. Arctic sea ice variability and trends, 1979–2010. Cryosphere 6, 881–889. https://doi.org/10.5194/tc-6-881-2012.

Codispoti, L. A., Flagg, C., Kelly, V., Swift, J. H., 2005. Hydrographic conditions during the 2002 SBI process experiments. Deep-Sea Research ‖ 52, 3199-3226.

Jung, J., Cho, K.-H., Park, T., Yoshizawa, E., Lee, Y., Yang, E. J., et al., 2021. Atlantic-origin cold saline water intrusion and shoaling of the nutricline in the Pacific Arctic. Geophysical Research Letters, 48, e2020GL090907. http://doi.org/10.1029/2020GL090907.

Lewis, K. M., van Dijken, G. L., Arrigo, K. R., 2020. Changes in phytoplankton concentration now drive increased Arctic Ocean primary production. Science, 369, 198–202. http://doi.org/10.1126/science.aay8380.

Perovich, D., Meier, W., Tschudi, M., Hendricks, S., Petty, A.A., Divine, D., et al., 2020. Sea ice. [in NOAA Arctic Report Card 2020]. Available at: https://www.arctic.noaa.gov/Report-

Card.

Polyakov, I. V., Alkire, M. B., Bluhm, B. A., Brown, K. A., Carmack, E. C., Chierici, M., et al., 2020. Borealization of the Arctic Ocean in response to anomalous advection from sub-Arctic seas. Frontiers in Marine Science, 7, 1–32. http://doi.org/10.3389/fmars.2020.00491.

3.2.2. Dissolved and particulate organic carbon

Jinyoung Jung[1] and Juyoung Son[1,2]

[1]Korea Polar Research Institute, Incheon 21990, Korea (jinyoungjung@kopri.re.kr)

[2]Pukyoung National University, Busan 48513, Korea (mh0980@kopri.re.kr)

1. Introduction

Massive inputs of river water make the influence of terrigenous dissolved organic matter (or carbon) (DOM or DOC) stronger in the Arctic Ocean than in other ocean basins (Goncalves-Araujo et al., 2016); the Arctic Ocean receives approximately 10% of the global river discharge while accounting for only ~1% of the global ocean volume (McClelland et al., 2012). Furthermore, increasing air temperatures in the Arctic lead to permafrost thaw (Turetsky et al., 2020), which in turn will likely result in increases in terrigenous DOM output to surface waters of the Arctic Ocean (Le Fouest et al., 2018). The pan-Arctic flux of riverine DOC to the Arctic Ocean is estimated to be 25–36 Tg C yr−1 (Holmes et al., 2012), suggesting a strong influence of riverine DOC supply on the Arctic Ocean. Understanding the fate of terrigenous DOC in the Arctic Ocean is a critical, as increased riverine DOC input could have profound impacts on the global carbon cycle as well as the marine carbon and biogeochemical cycles in the Arctic Ocean.

Given the strong seasonal signals (ice cover, light, biological production, etc.) and the impact of these on the carbon cycle, the Arctic Ocean remains under-sampled for DOC. The Chukchi Sea shelf waters are highly productive due to inflow of nutrient-rich Pacific water through Bering Strait and exchanges with the Canada Basin and adjacent Arctic shelves (via the East Siberian Current). The inflow of Pacific water to the Chukchi Sea is approximately 0.8 Sv,

primarily as the Anadyr Current and the Alaskan Coastal Current (Mathis et al., 2005). Along with the influx of Pacific water, the Alaskan Coastal Current brings a significant amount of terrigenous DOC from the Yukon River, which empties into the Bering Sea. In addition to transport of terrigenous DOC, autochthonous production of DOC by marine phytoplankton and bacterial degradation of particulate organic matter (POC) within the Chukchi Sea contribute to the DOC pool.

The fate of terrestrial DOC in the marine environment is still a matter of debate. Some have argued that riverine DOC in high-latitude areas is refractory and behaves conservatively in the estuaries and shelves of the Arctic Ocean based upon shelf DOC-salinity relationships, with little influence on biological cycles and the net ocean-atmosphere exchange of CO2. In contrast, others have argued that riverine DOC in high-latitude areas has a relatively large labile fraction and is broken down by microbial respiration or photochemical oxidation, either within the water column or in the sediments after burial (Cooper et al., 2005; Holmes et al., 2008). To improve our understanding of roles of nutrients, DOC and POC in biogeochemical processes, we investigated spatial and temporal variations of DOC and POC in seawater collected over the Chukchi and East Siberian seas. The results obtained from this cruise would be valuable for filling the data gap, and useful to understand biogeochemical cycles of C and its sequestration by biological carbon pump in the western Arctic Ocean.

2. Materials and methods

For DOC measurements, a pre-cleaned (soaked in 10% HCl and rinsed with ultrapure water) Teflon tube was used to connect between the Niskin bottles spigot and a pre-cleaned 47 mm filtration holder made of PP (PP-47, ADVANTEC). About 200 ml of seawater was filtered through a pre-combusted (at 550°C for 6 hours) Whatman GF/F filter (47 mm in diameter) under gravity. The filtered seawater samples were collected directly into pre-cleaned glass bottles. The filtrate was distributed into two pre-combusted 20 ml glass ampoules using a sterilized serological pipette. Each ampoule was sealed with a torch, quick-frozen, and preserved at approximately −20°C until the analysis in our land laboratory. DOC analysis will be basically made with a HTCO system consisting of a commercial unit, the Shimadzu TOC-L system (Shimadzu Co.).

Water column sample for analysis of POC was drained from the Niskin bottles into amber polyethylene bottle. POC samples were collected with pre-combusted (6 hrs. at 450°C) GF/F filters using a filtering system under low (<0.1 MPa) pressure. POC samples were stored frozen at −20oC until analysis in the home laboratory. POC samples will be determined with a CHN analyzer.

References

Cooper, L. W., Benner, R., McClelland, J. W., Peterson, B. J., Holmes, R. M., Raymond, P. A., Hansell, D. A., Grebmeier, J. M., Codispoti, L. A., 2005. Linkages among runoff, dissolved organic carbon, and the stable oxygen isotope composition of seawater and other water mass indicators in the Arctic Ocean, Journal of Geophysical Research 110, G02013, doi:10.1029/2005JG000031.

Goncalves-Araujo, R., Granskog, M.A., Bracher, A., Azetsu-Scott, K., Dodd, P.A., Stedmon, C.A., 2016. Using fluorescent dissolved organic matter to trace and distinguish the origin of Arctic surface waters. Scientific Reports 6, 1–12. https://doi.org/10.1038/srep33978.

Holmes, R.M., McClelland, J.W., Peterson, B.J., Tank, S.E., Bulygina, E., Eglinton, T.I., Gordeev, V.V., Gurtovaya, T.Y., Raymond, P.A., Repeta, D.J., Staples, R., Striegl, R.G., Zhulidov, A.V., Zimov, S.A., 2012. Seasonal and annual fluxes of nutrients and organic matter from large rivers to the Arctic Ocean and surrounding seas. Estuaries and Coasts 35, 369–382. https://doi.org/10.1007/s12237-011-9386-6.

Holmes, R.M., McClelland, J.W., Raymond, P.A., Frazer, B.B., Peterson, B.J., Stieglitz, M., 2008. Lability of DOC transported by Alaskan rivers to the Arctic Ocean. Geophysical Research Letters 35, L03402. https://doi.org/10.1029/2007GL032837.

Le Fouest, V., Matsuoka, A., Manizza, M., Shernetsky, M., Tremblay, B., Babin, M., 2018. Towards an assessment of riverine dissolved organic carbon in surface waters of the western Arctic Ocean based on remote sensing and biogeochemical modeling. Biogeosciences 15, 1335–1346. https://doi.org/10.5194/bg-15-1335-2018.

McClelland, J.W., Holmes, R.M., Dunton, K.H., Macdonald, R.W., 2012. The Arctic Ocean estuary. Estuaries and Coasts 35, 353–368. https://doi.org/10.1007/s12237-010-9357-3.

Turetsky, M.R., Abbott, B.W., Jones, M.C., Anthony, K.W., Olefeldt, D., Schuur, E.A.G., Grosse,

G., Kuhry, P., Hugelius, G., Koven, C., Lawrence, D.M., Gibson, C., Sannel, A.B.K., McGuire, A.D., 2020. Carbon release through abrupt permafrost thaw. Nature Geosciences 13, 138–143. https://doi.org/10.1038/s41561-019-0526-0.

Mathis, J.T., Hansell, D.A., Bates, N.R., 2005. Strong hydrographic controls on spatial and seasonal variability of dissolved organic carbon in the Chukchi Sea. Deep-Sea Research II 52, 3245–3258. https://doi.org/10.1016/j.dsr2.2005.10.002.

3.3. Oxygen isotope

Jinyoung Jung[1] and Juyoung Son[1,2]

[1]Korea Polar Research Institute, Incheon 21990, Korea (jinyoungjung@kopri.re.kr)

[2]Pukyoung National University, Busan 48513, Korea (mh0980@kopri.re.kr)

1. Introduction

Freshening of the Arctic Ocean has been attributed to increased sea ice melting and contributions from runoff. Sea ice has radically decreased in concentration, volume, and duration, with summer sea ice predicted to disappear completely by mid-century (Lewis et al., 2020). In addition, Arctic river discharge has substantially increased over the last century due to changes in atmospheric circulation modes and permafrost thaw (Bring et al., 2016). Since 1976, river discharge from North American and Eurasian rivers has increased by 2.0 ± 1.8 % and 3.3 ± 1.6 % per decade, respectively (Holmes et al., 2018); thus, the warming (solar insolation) and freshening (sea ice melting and riverine water inputs) of the Arctic Ocean during summer increase stratification and suppress the upward mixing of nutrients into the euphotic zone (Codispoti et al., 2013). Therefore, the objective of this study is to investigate distributions of freshwater in the Chukchi and East Siberian seas and examine the freshwater composition and sources using the oxygen isotope ratio (d18O) and salinity (S) of water.

2. Material and methods

For the determination of δ18O, seawater samples were collected using the same method as for DOC sampling (see Section 3.2.2). For each sample, the filtrate was placed in an acid-cleaned 20-mL glass vial, sealed with Parafilm, and stored at 4 °C until the analysis in our land laboratory analysis.

References

Bring, A., Fedorova, I., Dibike, Y., Hinzman, L., Mård, J., Mernild, S. H., et al., 2016. Arctic terrestrial hydrology: A synthesis of processes, regional effects, and research

challenges. Journal of Geophysical Research: Biogeosciences, 121, 621–649. http://doi.org/10.1002/2015JG003131.

Holmes, R. M., Shiklomanov, A. I., Suslova, A., Tretiakov, M., McClelland, J. W., Spencer, R. G. M., et al., 2018. River discharge [in NOAA Arctic Report Card 2018]. Available at: https://www.arctic.noaa.gov/Report-Card.

Lewis, K. M., van Dijken, G. L., Arrigo, K. R., 2020. Changes in phytoplankton concentration now drive increased Arctic Ocean primary production. Science, 369, 198–202. http://doi.org/10.1126/science.aay8380.

3.4. Amino acids and Black Carbon

Jun-Oh Min

Korea Polar Research Institute, Incheon, Republic of Korea

E-mail: jomin@kopri.re.kr

3.4.1 Introduction

The organic matter (OM) plays an important role in the biogeochemistry of the ocean's organic carbon cycle during its production, recycling in the water column, and export to deep water and to sediments. Heterotrophic bacteria (hereafter bacteria) are a significant biological component almost exclusively responsible for the mineralization of dissolved organic carbon (DOC), the largest organic carbon pool in the ocean. Besides selectively utilizing the bio-reactive dissolved organic matter (DOM) including amino acids (AA), bacteria contribute to the pool of living and non-living organic matter pool in the form of bacterial cell walls and other molecular bacteria. Bacteria synthesize a variety of unique organic compounds (e.g., D-enantiomers, muramic acid, peptidoglycan) that can be used as indicators of bacterial contributions to particulate organic matter (POM) and dissolved organic matter (DOM) in the oceans. Furthermore, particulate amino acid (PAA) and dissolved amino acid (DAA) have been used as qualitative and quantitative indicators of bioavailable organic matter over broad spatial and temporal scales in various aquatic systems. Certain amino acids, such as glycine and non-protein amino acids, increase relative abundance during DOM degradation, thereby providing additional insights into DOM alteration. In this study, we used a biomarker approach to provide quantitative estimates of the bacterial contributions to nonliving organic carbon and nitrogen pools in the Western Arctic Ocean.

The Dissolved black carbon (DBC) is by far the largest known refractory dissolved organic carbon pool in the ocean (Dittmar and Paeng, 2009). It can persist in the open ocean for tens of thousands of years, having a much slower average turnover rate than DBC in sediment (Ohlson et al., 2009). Therefore, the cycling of DBC in the ocean is a crucial component of the global carbon flux, and it is important to constrain the sources and sinks of oceanic DBC. Despite the importance of quantitative evaluation of black carbon to understanding the carbon cycle, limited studies have been conducted in the Western Arctic Ocean. Thus, the

purpose of this study is to understand the carbon cycle in the Western Arctic Ocean, where the increase in sea-ice meltwater due to climate change has recently become an issue.

3.4.2 Materials and Methods

Sample collection

Sampling for amino acid (AA), and black carbon (BC) was carried out in the Western Arctic Ocean aboard R/V ARAON in August 2023. We collected experimental samples from 46 stations in the Western Arctic Ocean (Chukchi Sea, East Siberian Sea) and 5 stations at the melt pond in the Ice Camp, respectively (Figure 3.4.1). Water samples were collected using a Sea Bird sampler (24 Niskin bottles, 10 L each) attached to a conductivity–temperature–depth (CTD) rossette system. Water samples were collected within 0.1 m depth using a transfer vacuum pump in a melt pond.

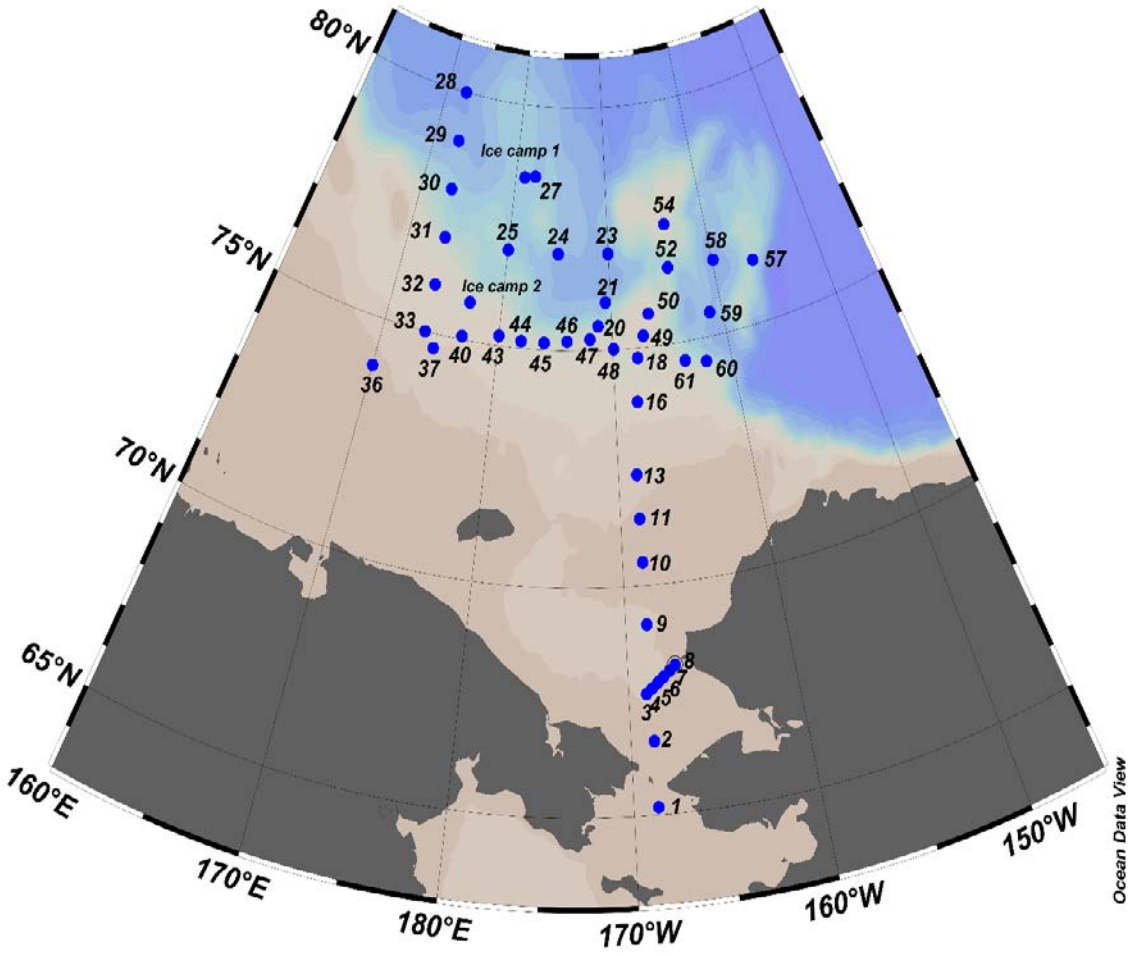

Figure 3.4.1. A map of the study area with the sampling locations in the Western Arctic Ocean.

Particulate Amino Acid and Dissolved Amino Acid

The particulate amino acid (PAA) was measured by filtering 4 ~ 8L of seawater on pre-combusted (4 h, 450 °C) 47mm glass fiber filters (GF/F, Whatman, nominal pore size 0.45 µm) (Figure 3.4.2). The filters were stored frozen (-80 °C) until processed. Hydrolysis and derivatization followed the procedures described by Kaiser and Benner (2005). Briefly, seawater samples 10 mL were dried and hydrolyzed using a vapor-phase technique with HCl at 170 °C for 30 min. Amino acid enantiomers were derivatized with OPA and IBLC and were separated on a EC-18 column (Shen et al., 2016).

Samples for quantitative evaluation of dissolved amino acid (DAA) were collected in a 50 mL amber glass vial pre-burned (450 °C, 6 hours) of filtered seawater samples, stored in a freezer (-24 °C) until analysis, and then analyzed using an HPLC-Evaporative Light Scattering Detector (HPLC-ELSD) system after this cruise.

Figure 3.4.2. The particulate amino acid and dissolved amino acid samples filtration system

Dissolved Black Carbon (DBC)

The remaining volume (4 ~ 20 L) of acidified seawater was then solid phase extraction following the method of Dittmar et al. (2008). The samples collected were loaded onto 1g styrene divinyl benzene polymer type sorbents PPL solid phase extraction columns at a low rate of about 2 mL per minute (Figure 3.4.3). The columns were rinsed with 20 mL of pH 2 pure water to wash off residual salts and dried pure Air-gas before being eluted HPLC grade

methanol. Dissolved black carbon was determined at the molecular level via a modified version of the benzene polycarboxylic acid (BPCA) method after Dittmar (2008).

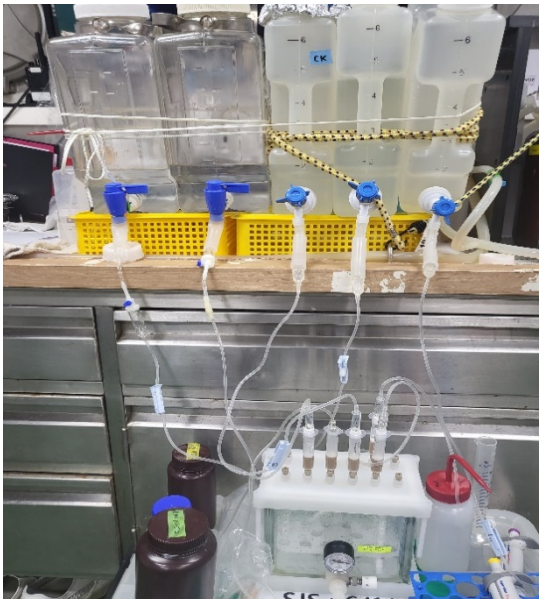

Figure 3.4.3. Dissolved black carbon adsorption system using benzene polymer type column.

3.4.3 References

Dittmar, T., Koch, B.P., Hertkorn., N., and Kattner, G. A simple and efficient method for the solid-phase extraction organic matter (SPE-DOM) from seawater, Limnol. Oceanogr., Methods, 6, 230-235 (2008).

Dittmar T. and Paeng J. A heat-induced molecular signature in marine dissolved organic matter. Nat. Geosci. 2, 175–179. 10.1038/ngeo440 (2009).

Kaiser, K. and Benner, R. Major bacterial contribution to the ocean reservoir of detrital organic carbon and nitrogen, Limnol. Oceanogr., 53 (1), 99–112 (2008).

Shen, Y., Benner, R., Murray, A.E., Gimpel, C., Mitchell, B. C., Weiss, E.L., and Reiss C. Bioavailable dissolved organic matter and biological hot spots during austral winter in Antarctic waters. J. Geophys. Res. Ocean, 122, 508-520, doi:10.1002/2016JC012301 (2016).

Ohlson, M., Dahberg, B., Okand, T., Brown, K. and Halvorsen, R. The charcoal carbon pool in boreal forest soils. Nat. Geosci. 2, 692-695 (2009).

3.5. Dissolved oxygen

Ahra Mo

Korea Polar Research Institute, Incheon, Republic of Korea

E-mail: ahramo@kopri.re.kr

3.5.1. Introduction

Due to its central role in biological redox reactions and the availability of reliable sensors, dissolved oxygen (DO) is one of the most commonly measured chemical parameters in sea-going observations. In the cruise, along with the oxygen sensor (SBE-43) attached to the CTD-rosette system, we determined oxygen concentration by the amperometric Winkler titration method (Figure 3.5.1.1) (Langdon, 2010). The method involves applying a potential to electrodes placed in a solution and adding thiosulfate to react with I2 to form 2I–. The gradual decrease of I2 during the reaction results in the decrease of the current measured at the electrodes. The endpoint is determined as the point at which the current does not decrease further. The bottle oxygen measurements will be used to check whether the SBE-43 oxygen sensor shows any drift or malfunctioning.

Figure 3.5.1.1 Automted amperometric titrator system

3.5.2. Material and methods

Water samples were collected from a selected number of CTD casts to calibrate the CTD oxygen sensor. A total of 8 CTD casts (Figure 3.5.2.1 and Table 3.5.2.1) were sampled for DO, which were the first samples to be drawn from the Niskin bottles. Seawater was collected directly into pre-calibrated glass bottles using a Tygon® tube. Before the sample was drawn, the bottles were flushed with seawater for several seconds (for about 3 times the volume of the bottle). The fixing reagents (i.e., manganese chloride and sodium hydroxide/sodium iodide solutions) were added. Care was taken to avoid bubbles inside the sampling tube and sampling bottle. Samples were thoroughly mixed following the addition of the fixing reagents and were then kept for 30-40 min to allow the precipitate to settle to <50% of the volume of the bottle. Once the precipitate had settled all samples were thoroughly mixed for a second time to maximize the efficiency of the reaction. Finally, results will be recalculated using salinity and temperature data from the CTD after the cruise.

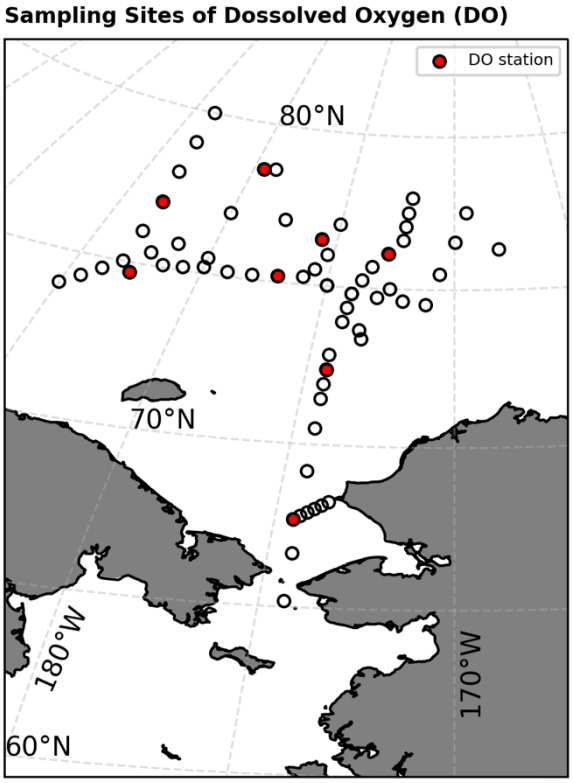

Figure 3.5.2.1 Map of sampling sites for dissolved oxygen.

Table 3.5.2.1 Depths of dissolved oxygen samples were taken at each station. All samples were collected in duplicate.

Station	Date	LAT	LONG	Depth (m)
3	2023.08.03	67°40.20002' N	168°57.59917' W	0, 10, 15, 20, 30, 40
13	2023.08.05	72°21.55355' N	168°39.76623' W	0, 10, 18, 25, 30, 45
22	2023.08.07	76°29.41094' N	171°16.16620' W	0, 15, 33, 50, 110, 150, 230, 400, 1000, 1600, 2200
26	2023.08.09	77°30.04515' N	179°59.87947' W	0, 10, 26, 50, 70, 100, 160, 300, 700, 1000, 1453
31	2023.08.15	77°0.0027' N	173°35.9893' E	0, 10, 20, 34, 50, 70, 100, 140, 280, 500, 729
37	2023.08.17	74°41.52354' N	174°37.44187' E	0, 10, 20, 30, 40, 50, 62
46	2023.08.22	75°11.71819' N	173°59.23582' W	0, 18, 30, 50, 80, 100, 120, 180 ,280, 353
51	2023.08.23	76°6.93814' N	165°28.63653' W	0, 10, 20, 40, 60, 100, 140, 200, 350, 500, 700

References

Dickson, A. G. (1995) Determination of dissolved oxygen in seawater by Winkler titration. WOCE Operations Manual. WHP Office Report WHPO 91–1, 1995.

Langdon, C. (2010) Determination of dissolved oxygen in seawater by Winkler titration using the amperometric technique. GO-SHIP Repeat Hydrography Manual. IOCCP Report No. 14, ICPO Publication Series No. 134.

3.6 Trace metal

Ijin Lim, Jiwoo Kim

Pukyong National University, Busan 48513, Korea

Email: ijinlim@pukyong.ac.kr; jiukim999@gmail.com

3.6.1. Introduction

Dissolved trace metals generally present in seawater at low concentrations (10-12 – 10-9 mol/L). Trace metals, such as iron (Fe), copper (Cu), nickel (Ni), zinc (Zn), cobalt (Co), are well known essential micro-nutrients for many marine microorganisms (Anderson, 2020). However, detailed distributions of trace metals have not been investigated well in the Arctic Ocean. Therefore, we will study the distributions of dissolved trace metals (Fe, Mn, Zn, Cu etc.) in the Arctic Ocean including the Bering Sea, the Chukchi Sea, and the East Siberian Sea.

Moreover, chemical speciation of trace metals is also considered to be an important factor of the biological availability of these trace metals. For example, organic complexed Zn, which is bound with organic ligands, reduces the fraction of free metal ion (Zn2+) to a level as 10-15M, which could limit the growth of some phytoplankton species (Sunda and Huntsman, 1992). On the other hand, dissolved Cu can be toxic to most microorganisms in the absence of Cu binding organic ligands. But in most ocean environments, Cu is not toxic to microorganisms because of Cu is bound with organic ligands (Sunda and Huntsman, 1998). For better understanding of biogeochemical cycles of trace elements in the ocean, it is the first step to clarify the speciation of these elements in seawater. However, little is known about the organic complexation of trace metals in open-ocean waters. In this study, therefore, we will investigate trace metal speciation in the Arctic Ocean using cathodic stripping voltammetry (CSV).

Iron has four stable isotopes, 54Fe, 56Fe, 57Fe, and 58Fe and fractionation is occurred by their mass differences. Iron stable isotopes (δ56Fe) are the new key to acquiring knowledge of iron cycling in the ocean such as sources and sinks (Fitzsimmons and Conway, 2023). However, a study of iron isotope in the Arctic Ocean is rarely proceeded. Therefore, we will study the iron stable isotopes in the Arctic Ocean.

Rare earth elements (REEs), comprising 15 lanthanide elements (La to Lu), are an extremely coherent group in terms of their chemical behavior. In the ocean, REEs have been used as

tracers of biogeochemical cycles and water mass mixing (Nozaki, 2001). Among the REEs, neodymium (Nd) isotopes have been used as a water mass tracer due to the shorter residence time of Nd (300-500 yr) (Amakawa et al., 2004), compared to the global ocean mixing time (1500 yr) (Broecker and Peng, 1982). However, REEs and Nd isotopes data in the Arctic Ocean are scarce. Therefore, we will investigate distributions of dissolved REEs and the water mass structure and ocean circulations using Nd isotopic composition in the Arctic Ocean.

3.6.2. Material and methods

3.6.2.1. Sampling location

Trace metal samples were collected at 30 stations (Fig. 3.6.1) during ice breaker R/V Araon research cruise (ARA14B) from August 1st to August 31th, 2023. Detailed information of stations is described in Table 3.6.1.

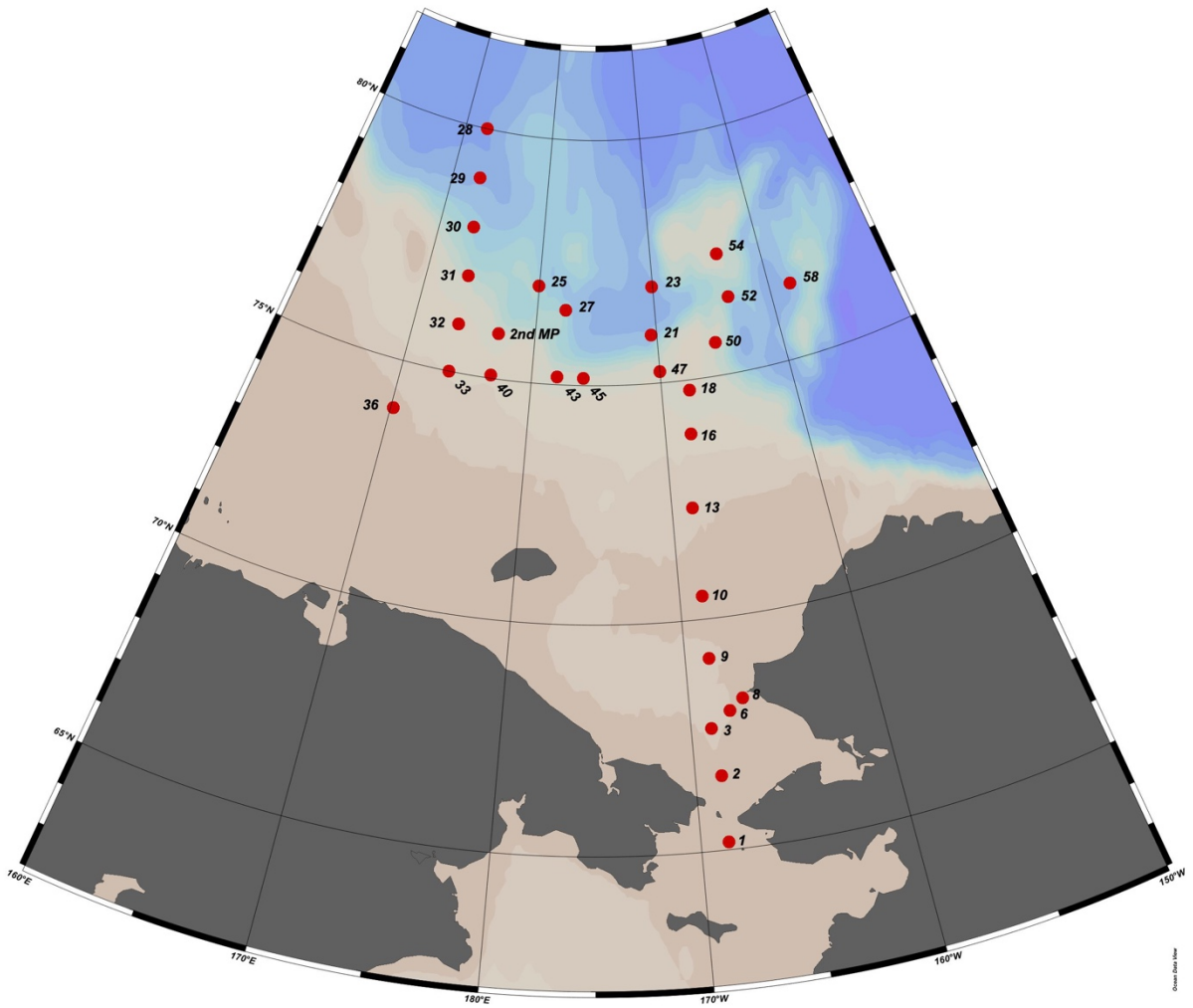

Figure 3.6.1. Map of sampling locations during ARA14B research cruise.

Table 3.6.1. Information of sampling locations and water samplings.

Station	Latitude	Longitude	Date (UTC) (YYYY. MM.DD)	Arrival Time (UTC)	Bottom Depth (m)	Trace Metal	Speciation	Fe isotopes	Nd isotopes
1	65°10.40850'N	168°41.44688'W	2023.08.03	03:02	48.7	O	O		O
2	66°37.8135'N	168°41.2446'W	2023.08.03	13:26	44	O	O	O	
3	67°40.2005'N	168°57.5984'W	2023.08.03	20:56	50	O	O		
6	68°0.7759'N	167°52.0140'W	2023.08.04	04:28	52	O	O	O	O
8	68°14.5179'N	167°7.3240'W	2023.08.04	09:19	43	O	O	O	
9	69°10.0090 'N	168°40.0010'W	2023.08.04	15:56	51	O	O	O	
10	70°29.9908'N	168°39.9645'W	2023.08.05	00:52	39.8	O	O		O
13	72°21.5537'N	168°39.7616'W	2023.08.05	14:21	55	O	O		O
16	73°53.3194'N	168°11.9870'W	2023.08.06	10:24	180	O	O	O	O
18	74°48.0340'N	167°53.9306'W	2023.08.06	19:47	194	O	O	O	O
21	75°59.9958'N	170°30.0070'W	2023.08.07	12:50	1313	O	O	O	O
23	76°59.4109'N	170°6.0654'W	2023.08.08	04:39	2212	O	O	O	O
25	77°0.2833'N	179°54.2579'E	2023.08.07	07:37	1079	O	O		O
27	76°32.4498'N	177°35.1547'W	2023.08.13	08.40	1008	O	O		
28	80°0.0059'N	172°24.0420'E	2023.08.13	17:04	2646	O	O		
29	79°0.0012'N	172°47.9844'E	2023.08.14	06:17	2560	O	O	O	O
30	78°0.0041'N	173°11.8546'E	2023.08.14	19:40	1131	O	O	O	
31	77°0.0029'N	173°35.9871'E	2023.08.15	15:34	739	O	O	O	O
32	75°59.9956'N	173°36.0256'E	2023.08.15	20:55	264	O	O	O	
33	75°0.0044'N	173°36.0436'E	2023.08.16	17:25	146	O	O	O	O
36	74°0.1454'N	170°9.8273'E	2023.08016	20:51	46	O	O	O	O
2nd MP	75°56.35100'N	176°57.25664'E	2023.08.19	17:10	551	O	O		
40	75°4.4956'N	176°48.0031'E	2023.08.20	12:49	194	O	O	O	
43	75°10.2099'N	179°57.9486'W	2023.08.21	02:16	534	O	O	O	
45	75°9.0191'N	176°0.0144'W	2023.08.21	18:08	326	O	O		O
47	75°14.4263'N	171°58.3546'W	2023.08.22	06:31	505	O	O	O	
50	75°41.4680'N	166°38.2773'W	2023.08.23	09:54	291	O	O		
52	76°34.0456'N	164°21.6868'W	2023.08.23	22:10	548	O	O		
54	77°28.0662'N	164°6.0906'W	2023.08.24	16:25	279	O	O		
58	76°31.06007'N	159°47.15828'W	2023.08.26	16:25	2076	O	O		
					Total Samples	241	235	85	70

2.2. Clean seawater sampling

The clean seawater sampling system for trace metal sample is consisted of a polyurethane coated Al frame holding acid-cleaned 12 L Teflon coated Niskin-X samplers (General Oceanics Inc., FL, USA) mounted on a Carousel array with auto firing module (Sea Bird Electronics Inc., USA), which attached to an Ultra High Molecular Weight Polyethylene (UHMWPE) rope (Kim et al., 2023; Fig. 3.6.2). After seawater collection, sampling system was moved into the trace metal clean van. Samples for trace metal concentration and Fe isotopes analysis were obtained through an acid-cleaned 0.2 μm filter cartridge (Acropak, Pall) connected to sampler directly with pressured air (Fig. 3.6.3). Filtered samples (125 mL LDPE bottle for trace metal concentration and 1 L LDPE bottle for Fe isotope analysis) were acidified to pH<1.8 by adding ultra-pure HCl (ODLAB, Korea) and stored. Samples for chemical speciation analysis were filtered in the same way with those of trace metal samples. Filtered samples (500 mL LDPE bottle) were then frozen at -18oC and stored until analysis. Samples for Nd isotopic composition analysis were collected in the same way with those of trace metal except for sampling volume (6 L in LDPE collapsible containers). Subsequently, 5 mg/L of Fe was added into each sample for iron coprecipitation. After 24 h equilibrium, ammonia solution (20–22%, OPTIMA, Fisher Chemical, USA) was added into each sample to increase the pH to 8.0. After 48 h, the supernatant was discarded. The collected iron hydroxide will be determined in the on-land laboratory.

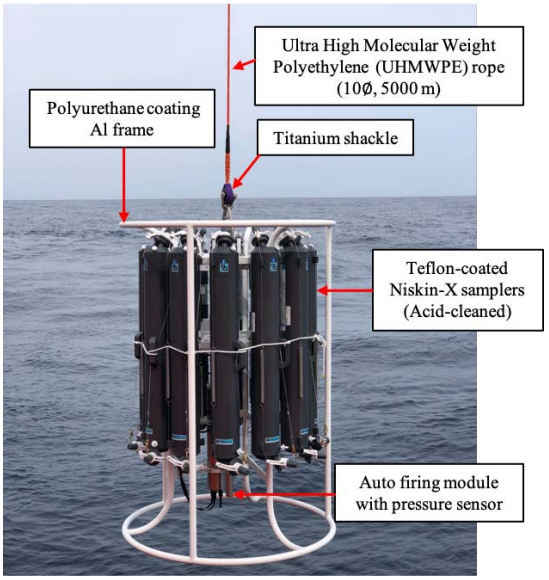

Figure 3.6.2. Clean seawater sampling system for trace metal samples.

Figure 3.6.3. Subsampling for clean seawater samples.

2.3. Analytical method

Concentrations of trace metals will be determined by an automated system (SC-DX seaFAST, ESI) with online pH buffering connected to a high-resolution inductively coupled plasma mass spectrometry (HR-ICP-MS) (Kim et al., 2020). Chemical speciation such as Cu or Fe will be determined by a titration method using cathodic stripping voltammetry (CSV) (Kim et al., 2015; Wong et al., 2018) in the on-land laboratory. Neodymium isotopic compositions and Fe isotopes will be determined using a multi-collector inductively coupled plasma mass spectrometer (MC-ICP-MS) (Amakawa et al., 2019; Conway et al., 2013).

References

Amakawa, H., Yu, T. L., Tazoe, H., Obata, H., Gamo, T., Sano, Y., Shen, C-C., Suzuki, K. (2019). Neodymium concentration and isotopic composition distributions in the southwestern Indian Ocean and the Indian sector of the Southern Ocean. Chemical Geology, 511, 190-203. https://doi.org/10.1016/j.chemgeo.2019.01.007

Amakawa, H., Alibo, D.S., Nozaki, Y., 2004. Nd abundance and isotopic composition distributions of surface seawaters of the Northwest Pacific Ocean and its adjacent seas. Geochem. J. 38, 493–504. https://doi.org/10.2343/geochemj.38.493.

Anderson, R.F., 2020. GEOTRACES: Accelerating Research on the Marine Biogeochemical Cycles of Trace Elements and Their Isotopes. Annual Review of Marine Science, 12(1):

49 - 85. doi:10.1146/annurev-marine-010318-095123

Broecker, W.S., Peng, T.-H., 1982. Tracers in the Sea. Eldigio Press, Palisades, New York (689 pp).

Conway, T.M., Rosenberg, A.D., Adkins, J.F. and John, S.G., 2013. A new method for precise determination of iron, zinc and cadmium stable isotope ratios in seawater by double-spike mass spectrometry. Analytica Chimica Acta, 793: 44 – 52. DOI: 10.1016/j.aca.2013.07.025

Fitzsimmons, J.N. and Conway, T.M., 2023. Novel Insights into Marine Iron Biogeochemistry from Iron Isotopes. Annual Review of Marine Science, 15(1): 383 – 406. Doi: 10.1146/annurev-marine-032822-103431

Kim, J., Sim, H., Lim, I., Kim, T., Jung, J., Cho, K.H., Kim, T.W., Park, J., Yang, E.J., Chen, X. and Seo, H., 2023. Trace-Metal-Clean Sampling System: Application to Ice-Breaking Research Vessel Araon. Ocean Science Journal, 58:23. https://doi.org/10.1007/s12601-023-00118-x

Kim, T., Kim, H. and Kim, G., 2020. Tracing river water versus wastewater sources of trace elements using rare earth elements in the Nakdong River estuarine waters. Marine Pollution Bulletin, 160: 111589. doi:10.1016/j.marpolbul.2020.111589

Kim, T., Obata, H., Kondo, Y., Ogawa, H. and Gamo, T., 2015. Distribution and speciation of dissolved zinc in the western North Pacific and its adjacent seas. Marine Chemistry, 173: 330 - 341. doi:10.1016/j.marchem.2014.10.016

Nozaki, Y., 2001. Rare earth elements and their isotopes in the ocean. Encyclopedia of Ocean Sciences, 4, 2354–2366.

Sunda, W.G. and Huntsman, S.A., 1992. Feedback interactions between zinc and phytoplankton in seawater. Limnology and oceanography, 37(1): 25 - 40. doi:10.4319/lo.1992.37.1.0025

Sunda, W.G. and Huntsman, S.A., 1998. Interactions among Cu2+, Zn2+, and Mn2+ in controlling cellular Mn, Zn, and growth rate in the coastal alga Chlamydomonas. Limnology and oceanography, 43(6): 1055 – 1064

Wong, K.H. et al., 2018. Organic complexation of copper in estuarine waters: An assessment of the multi-detection window approach. Marine Chemistry, 204: 144 - 151. doi:10.1016/j.marchem.2018.07.001

3.7. Stable isotope ecology

Jinsoo Son

Hanyang University, Ansan, 15588, Korea (tngur1107@hanyang.ac.kr)

3.7.1. Introduction

In recent decades, as global warming continues and the extent of Arctic sea ice decreases rapidly, the Arctic Ocean is experiencing dramatic environmental changes, affecting the biogeochemical flux, organism community composition and ecosystem structure. Given these significant changes in the Arctic Ocean, the input of nitrogen (N) derived from different water columns clearly has impact on the biological interaction between ecosystem structures.

N sources of organic matter or organisms have been assessed by stable isotope analysis of the particulate organic matter (POM). Moreover, size-fractionated POM gives detailed information on specific diet source for consumers.

Compound-specific isotope analysis of amino acid (CSIA-AA) is increasingly used as an improved analytical tool in marine ecology and biogeochemistry. The advantage of CSIA-AA is in accurate estimation of trophic position (TP) of organisms (Bowes and Thorp, 2015) and N baseline (Sherwood et al., 2014, Vokhshoori et al., 2014). However, there is little known as a spatial distribution of N source using POM samples, especially by detailed size-fractionated organic particles because POM samples have usually been covered in a couple of literatures to define microbial degradation of organic matter (McClelland and Montoya, 2002, McCarthy et al., 2007, Yamaguchi and McCarthy, 2018). In this study, N source of different size class of organic matter will be demonstrated in the Western Arctic, which contains various current and different N baseline.

3.7.2. Material and methods

Sample collection was carried out at 27 stations during the Korean research ice breaker R/V ARAON expedition (ARA14B; Aug 01 to 31 in 2023) in the Arctic Ocean (Figure 3.7.1). Sampling sites are covering Bering Strait, Northern Chukchi Sea, Southern Chukchi Sea and North Eastern Siberian Sea.

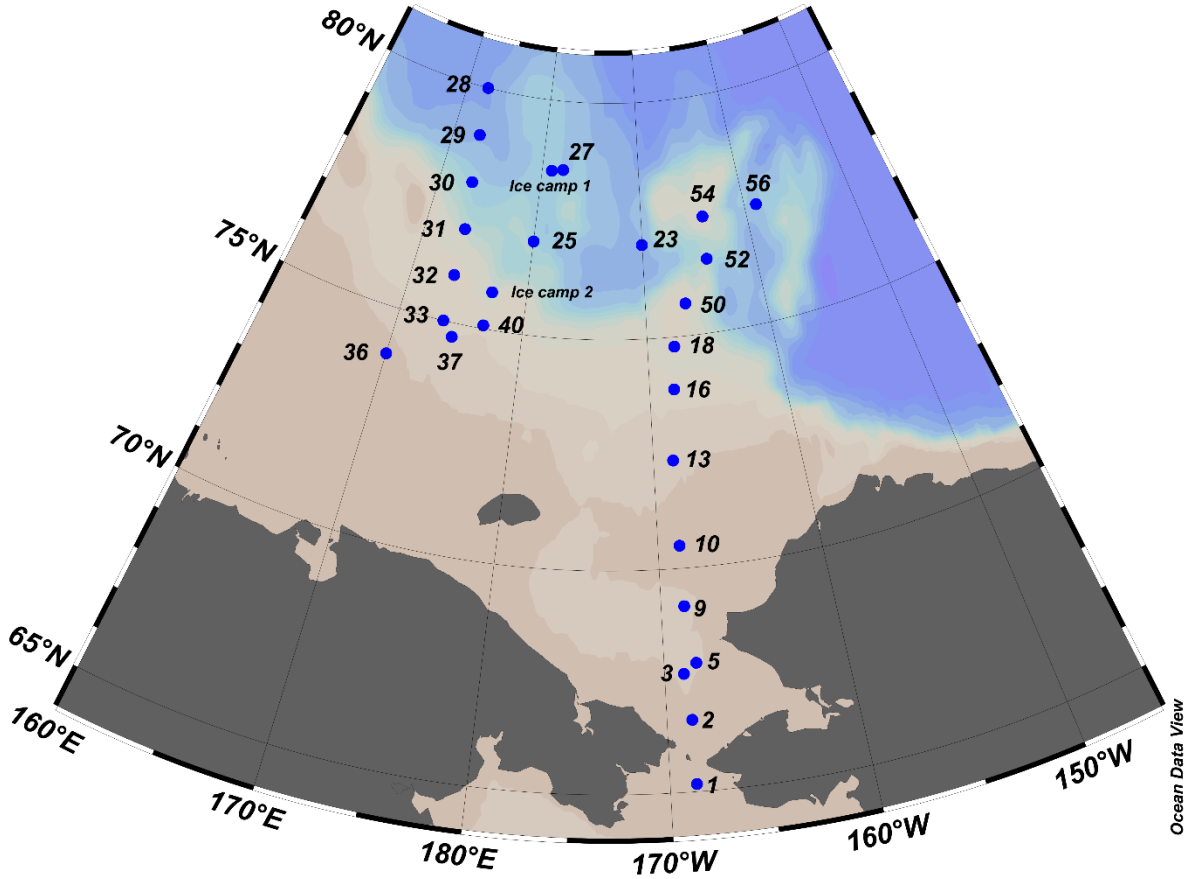

Figure 3.7.1 **Map of study area. The numbers indicate the station numbers.**

Seawater samples (CTD) were collected from bottom, surface chlorophyll maximum (SCM) and 0m depth using a CTD/rosette sampler holding 10 L Niskin bottles (OceanTest Equipment Inc., FL, USA). Approximately 2.1L~24.6L seawater in niskin bottles was filtered through GF/F filter (0.7µm pore size, 47 mm diameter, Whatman) to measure stable isotopic values of carbon and nitrogen in POM (Figure 3.7.2-A).

Underway seawater pumped from R/V ARAON is used for nitrogen isotope of amino acid analysis. 130~9453L of underway seawater is filtered to collect >100µm and 20~100µm size class POM (Figure 3.7.2-B). 4.3~41.7L of underway seawater is used to collect 0.7~20µm size class POM (Figure 3.7.2-C).

3.7.3. Expected results

The N baseline of POM sample would be different with both location and size class. In highly productive location, larger size class of POM would be more dominant and continuous N input

could be inferred. In this case, N baseline is depending on influents. In contrast, oligotrophic location would have less dominance of larger size class of POM. Due to the continuous recirculation of N sources, high N baseline would be observed. These spatial variations would easily affect smaller size class of POM which N utilization is mainly occur.

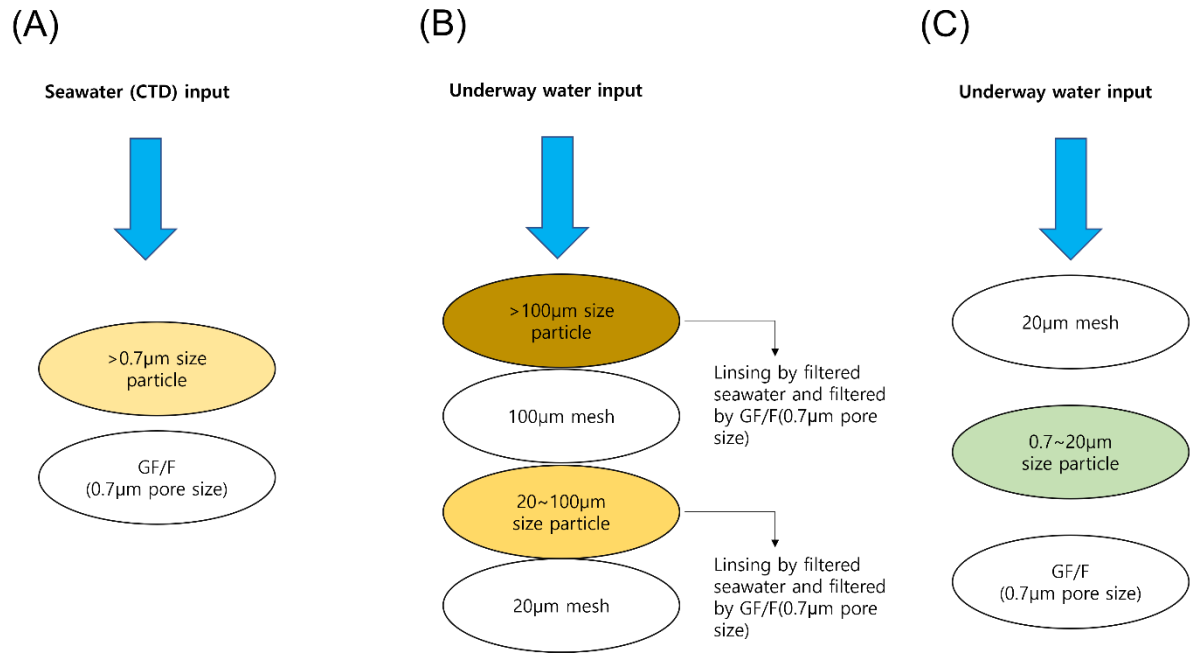

Figure 3.7.2 **Detailed filtration method of size-fractionated organic particle in underway water and seawater in niskin bottle.**

References

BOWES, R. E. & THORP, J. H. 2015. Consequences of employing amino acid vs. bulk-tissue, stable isotope analysis: a laboratory trophic position experiment. Ecosphere, 6, 1-12.

MCCARTHY, M. D., BENNER, R., LEE, C. & FOGEL, M. L. 2007. Amino acid nitrogen isotopic fractionation patterns as indicators of heterotrophy in plankton, particulate, and dissolved organic matter. Geochimica et Cosmochimica Acta, 71, 4727-4744

MCCLELLAND, J. W. & MONTOYA, J. P. 2002. Trophic relationships and the nitrogen isotopic composition of amino acids in plankton. Ecology, 83, 2173-2180.

SHERWOOD, O. A., GUILDERSON, T. P., BATISTA, F. C., SCHIFF, J. T. & MCCARTHY, M. D. 2014. Increasing subtropical North Pacific Ocean nitrogen fixation since the Little Ice Age. Nature, 505, 78

VOKHSHOORI, N. L. & MCCARTHY, M. D. 2014. Compound-specific δ15N amino acid measurements in littoral mussels in the California upwelling ecosystem: A new approach to generating baseline δ15N isoscapes for coastal ecosystems. PloS one, 9, e98087.

YAMAGUCHI, Y. T. & MCCARTHY, M. D. 2018. Sources and transformation of dissolved and particulate organic nitrogen in the North Pacific Subtropical Gyre indicated by compound-specific δ15N analysis of amino acids. Geochimica et Cosmochimica Acta, 220, 329-347

3.8 Transparent exopolymer particle

Sanghoon Park

Department of Oceanography, Pusan National University, Korea

Email: mossinp@pusan.ac.kr

3.8.1. Introduction

During the recent decades, increased temperatures in the Arctic Ocean have decreased the extent and thickness of perennial sea ice, allowing more light availability underwater. These recent changes in climate and ice conditions could alter the patterns of primary production of phytoplankton (Tremblay et al., 2015). Primary production is the main source of transparent exopolymer particles (TEP) in sea water. TEP are carbon-rich sticky organic particles, mostly formed by acidic polysaccharides, and stainable with Alcian Blue (Alldredge et al., 1993). TEP mainly originate from dissolved precursors, mostly dissolved polysaccharides released by phytoplankton (Passow, 2000). These precursors contribute to the dissolved organic matter (DOM) pool in the water column. Therefore, the formation of TEP is important as a major pathway in which the DOM is switched into the POM (Passow, 2000). In addition, TEP play a pivotal role in biogeochemical cycles. Because of their high stickiness, TEP enhance the formation of large aggregate, strengthening the vertical transport of particulate organic carbon (POC) to the deep ocean (Passow et al., 2001). Variations in carbon export fluxes affected by TEP are presumed to be significant for CO2 sequestration on global scale (Jokulsdottir & Archer, 2016). Arctic Ocean is known to have a large influence on the CO2 sequestration compared to other areas of the world's ocean (Anderson et al., 1990). Evaluating the importance of TEP for particle export in the arctic, however, is impeded by a lack of. investigation (Busch et al., 2017, Engel et al., 2017). Furthermore, our ability to accurately predict how TEP dynamics in the Arctic Ocean will respond to recent significant climate change is limited by an incomplete understanding of the Arctic carbon cycle. Our research conducted in this cruise would be helpful to estimate the significance of TEP to the vertical carbon flux and to understand the impact of climate change on carbon cycle in the Arctic Ocean.

3.8.2. Materials and methods

Seawater samples for TEP were obtained at 12 stations over the Chukchi Sea and East Siberian Sea (Fig 3.8.1) using CTD/rosette sampler equipped with 24-10L Niskin bottles. Water samples (0.1-0.3L) collected from different 8-10 depths were filtered through 0.4 µm pore sized polycarbonate membrane filters (ADVANTEC; 25mm, Toyo Roshi Kaisha, Tokyo, Japan) under low vacuum (<150 mm Hg). The filters were stained with 500 µL of Alcian Blue solution (8GX, Sigma), rinsed with distilled water, and immediately kept at -20 °C until further analyses. At the home laboratory, the stained TEP on the filters will be soaked in 6 mL of 80 % sulfuric acid for 3 hours. According to the spectrophotometric method of Passow and Alldredge (1995) with consideration of the updated method described in Bittar et al (2018), the absorbance for TEP concentration will be measured at 787nm with a spectrophotometer (Hitachi-UH 5300, Hitachi, Tokyo, Japan).

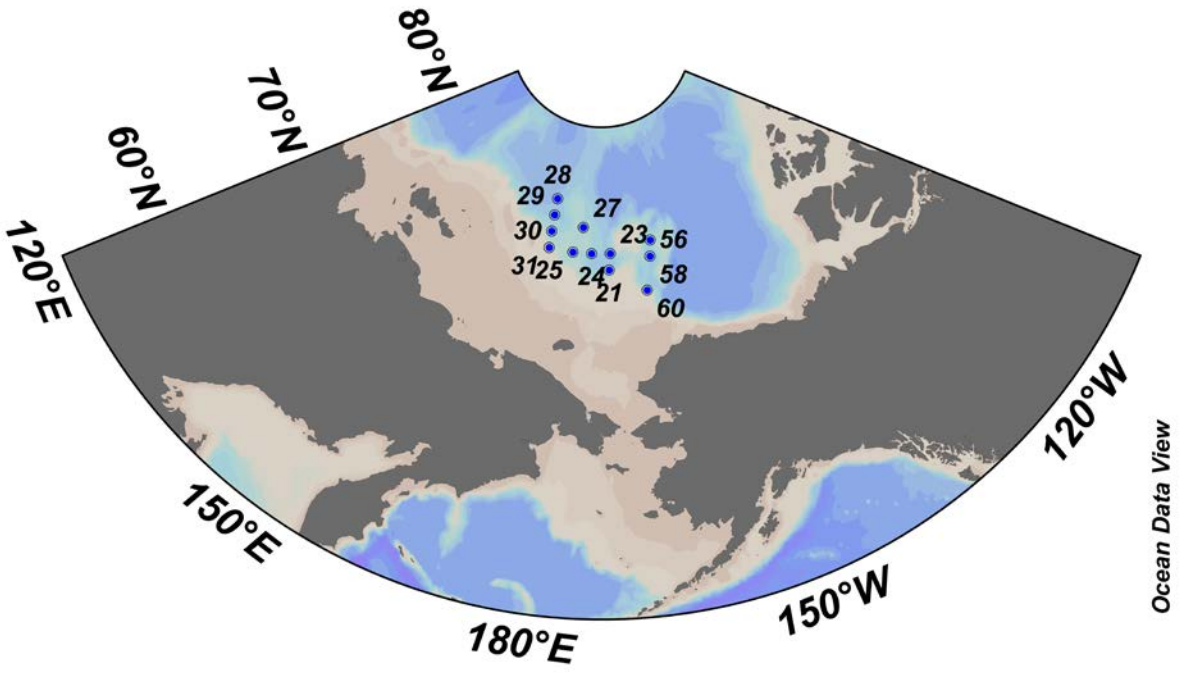

Figure 3.8.1. Sampling stations for TEP during the 2023 Arctic cruise.

References

Alldredge, A. L., Passow, U., & Logan, B. E. (1993). The abundance and significance of a class of large, transparent organic particles in the ocean. Deep Sea Research Part I: Oceanographic Research Papers, 40(6), 1131-1140.

Anderson, L. G., Dyrssen, D., & Jones, E. P. (1990). An assessment of the transport of atmospheric CO2 into the Arctic Ocean. Journal of Geophysical Research: Oceans, 95(C2), 1703-1711.

Busch, K., Endres, S., Iversen, M. H., Michels, J., Nöthig, E. M., & Engel, A. (2017). Bacterial colonization and vertical distribution of marine gel particles (TEP and CSP) in the Arctic Fram Strait. Frontiers in Marine Science, 4, 166.

Engel, A., Piontek, J., Metfies, K., Endres, S., Sprong, P., Peeken, I., ... & Nöthig, E. M. (2017). Inter-annual variability of transparent exopolymer particles in the Arctic Ocean reveals high sensitivity to ecosystem changes. Scientific reports, 7(1), 1-9.

Jokulsdottir, T., & Archer, D. (2016). A stochastic, Lagrangian model of sinking biogenic aggregates in the ocean (SLAMS 1.0): model formulation, validation and sensitivity. Geoscience Model. Development 9(4), 1455–1476.

Passow, U. (2000). Formation of transparent exopolymer particles, TEP, from dissolved precursor material. Marine Ecology Progress Series, 192, 1-11.

Passow, U., Shipe, R. F., Murray, A., Pak, D. K., Brzezinski, M. A., & Alldredge, A. L. (2001). The origin of transparent exopolymer particles (TEP) and their role in the sedimentation of particulate matter. Continental Shelf Research, 21(4), 327-346.

Passow, U.; Alldredge, A.L. (1995) Passow, U., & Alldredge, A. L. (1995). A dye-binding assay for the spectrophotometric measurement of transparent exopolymer particles (TEP). Limnology and Oceanography, 40(7), 1326-1335.

Tremblay, J. É., Anderson, L. G., Matrai, P., Coupel, P., Bélanger, S., Michel, C., & Reigstad, M. (2015). Global and regional drivers of nutrient supply, primary production and CO2 drawdown in the changing Arctic Ocean. Progress in Oceanography, 139, 171-196.

Chapter 4. Biological Oceanography

4.1. Phytoplankton Community

Jong Kuk Moon and Chorom Shim

Korea Polar Research Institute, Incheon 21990, Korea

Email: jkmoon@kopri.re.kr; *chorom@kopri.re.kr*

4.1.1. Introduction

As temperature has increased in recent decades, the Arctic Ocean has undergone the drastic changes, which are the accelerated retreat of seasonal sea ice, minimize of sea ice shrinking in summer (Perovich, 2011; Parkinson and Comiso, 2013), and increasing river discharge to the Arctic Ocean (Peterson et al., 2002). There are several studies about the sea ice retreat and the consequent effect on marine ecosystem, but conflicting results existed. The remote sensing data revealed that the loss of sea ice has resulted in a dramatic increase in Arctic productivity because reduced ice cover is expose more ocean surface to winds, thereby deepening surface mixed layer and bringing more nutrients to the surface from deeper waters (Arrigo et al., 2008;). The massive phytoplankton blooms were observed under arctic sea ice which is much thinner first-year ice with higher light transmission to waters than multiyear ice pack (Arrigo et al., 2012). By contrast, the surface freshening had a negative impact on primary producers as sea ice melt intensifies ocean stratification, which will make it more difficult for nutrients to supply into surface waters (Coupel et al., 2015). Rapid retreat and thinning of seasonal sea ice could influence not only primary production but also phytoplankton community structure. In the northern Chukchi Sea, haptophytes and prasinophytes dominated in melt and cold years, respectively (Fujiwara et al., 2014), while the timing of the sea ice retreat plays a crucial role in the phytoplankton size structure in the Chukchi and Bering shelves (Fujiwara et al., 2016) and Canada Basin (Coupel et al., 2012). The phytoplankton distributions in the Canada Basin east of the Chukchi Plateau have been well established, but the study on phytoplankton in the East Siberian Sea west of the Chukchi Plateau is rare (Okolodkov, 1993). The Chukchi and East Siberian Seas are one of the rapidly changing area, where the timing of the sec ice retreat getting earlier and primary production rapidly

increasing (Arrigo et al., 2011). In addition, this area has a complex system influenced by the Pacific Summer Water, Siberian Shelf Water, Atlantic Water, and Beaufort Gyre (Weingartner et al., 1999; Proshutinsky et al., 2002; Brugler et al., 2014). Our hypothesis is that phytoplankton community and primary production in the Chukchi and the East Siberian Seas could be affected by rapid sea ice change and water mass distribution. Therefore, we investigated the primary production and phytoplankton standing crops derived from photosynthetic pigments in the study area (Parkinson and Comiso, 2013). It will be important information to understand the effect of environmental change on primary production and phytoplankton community structure because phytoplankton dynamics play a crucial role in biogeochemistry and marine food web (Macdonald et al., 2005; Anderson et al., 2011).

4.1.2. Materials and methods

Field survey

Field survey was conducted onboard the Korean Research IBRV Araon in the Bering, the Chukchi and the East Siberian Seas during the summer from August, 2023 (Figure 4.1.1). Water samples for chlorophyll a (Chl-a) concentration, picophytoplankton, and pigments were collected from 2~6 depths in the whole water column using a 10-L PVC Niskin water sampler attached to a CTD rosette system (Table 4.1.1).

Size-fractionated Chl-a concentration

Subsamples from the Niskin bottles were filtered through a cascade connection of 20-µm nylon mesh, Nuclepore filter (Whatman International) with pore size of 2 µm, and a Whatman GF/F filter to determine size-fractionated Chl-a (Sieburth 1978; Takahashi and Bienfang, 1983). Thus, micro-Chl-a (>20 µm), nano-Chl-a (2-20 µm), and pico-Chl-a (<2 µm) could be measured directly. Subsamples for total Chl-a were filtered onto 47 mm GF/F Whatman filters. Each filter was extracted in 90% acetone, and Chl-a concentrations were measured with a fluorometer (Fig.4.1.2) (model Trilogy, Turner Designs, USA; method: Parson et al.,1984).

Picoplankton abundance

Water samples for picophytoplankton and heterotrophic bacteria were fixed for 15 min with

paraformaldehyde (final concentration: 1%) and stored at -80 ºC. Also samples were analyzed on an Accuri C6 flow cytometer (Fig.4.1.2) (Becton Dickinson) equipped with an air-cooled argon laser (488 nm, 15 mW) to enumerate picophytoplankton and heterotrophic bacteria. Picophytoplankton groups could be identified and enumerated using the characteristics of 90°-angle light scatter, orange fluorescence from phycoerythrin, and red fluorescence from chlorophyll (Marie et al., 1997). Bacteria could be identified for their side light scatter and green fluorescence signals. Raw data from the flow cytometer will be processed using the FlowJo program (Tree Star, www.flowjo.com).

Photosynthetic pigments

The CHEMTAX program based on photosynthetic pigments data has potential benefits for the estimation of phytoplankton composition, including small and fragile forms. For photosynthetic pigments analysis, 2-4 L water samples from the Niskin bottles were filtered onto 47 mm GF/F Whatman filters and stored at -80 ºC. The pigments will be analyzed with high performance liquid chromatography (HPLC) in the laboratory.

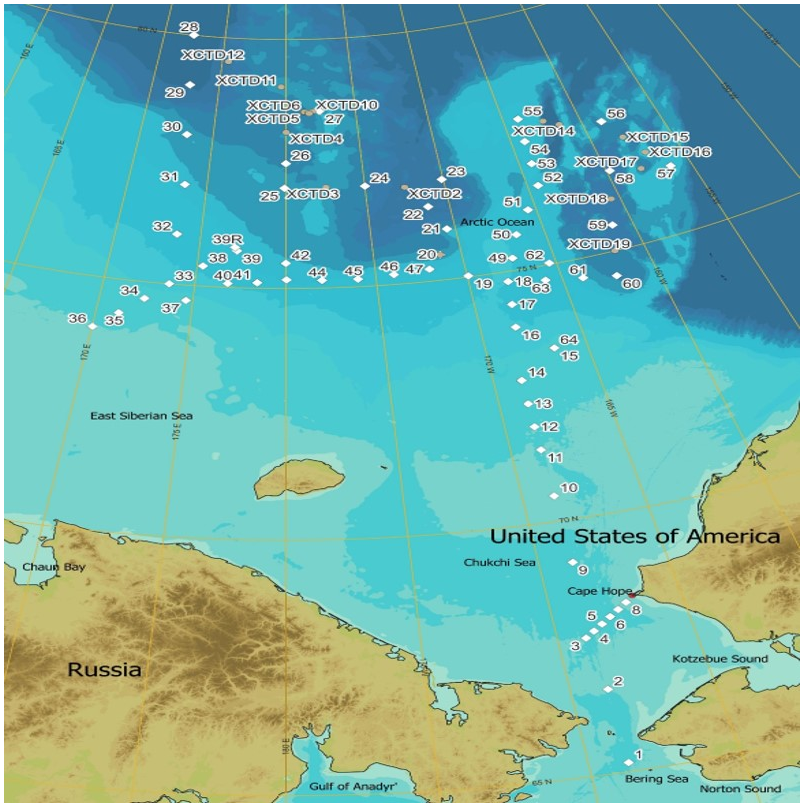

Figure 4.1.1. Sampling stations the Bering, the Chukchi and the East Siberian Seas during the

2023 Arctic cruise.

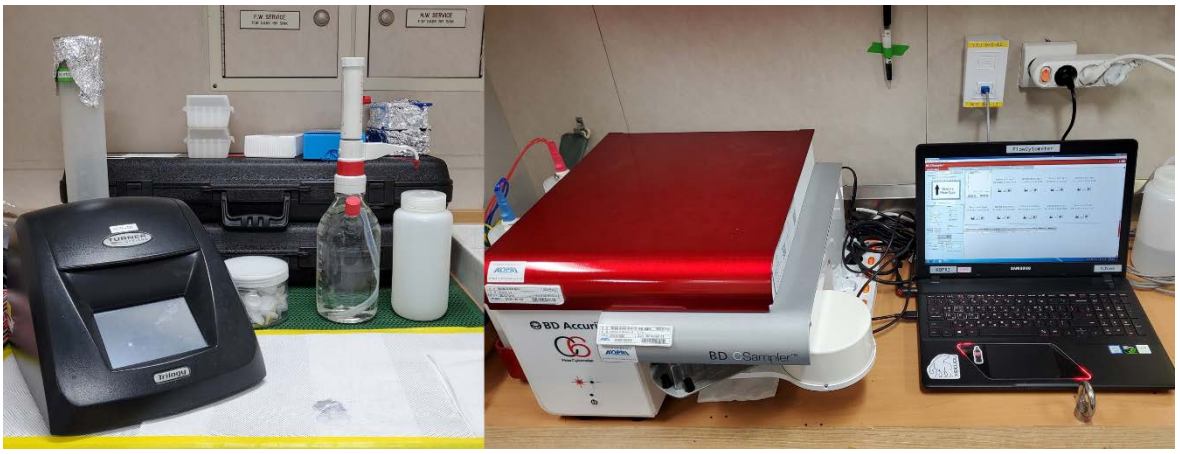

Figure 4.1.2. Fluorometer and Accuri C6 flow cytometer.

Table. 4.1.1. Stations for phytoplankton pigments during the 2023 Arctic cruise.

Cruise	St.	Latitude	Longitude	Depth	Total	Size	Picoplankton	Photosynthetic
ARA14B	1	65°10.40812' N	168°41.44416' W	-50	o	o	o	o
ARA14B	2	66°37.79674' N	168°41.25318' W	-44	o	o	o	o
ARA14B	3	67°40.20037' N	168°57.59685' W	-50	o	o	o	o
ARA14B	4	67°46.98000' N	168°36.13180' W	-50	o	o	o	o
ARA14B	5	67°53.88024' N	168°14.09833' W	-58	o	o	o	o
ARA14B	6	68°00.78004' N	167°52.08263' W	-52	o	o	o	o
ARA14B	7	68°07.68246' N	167°29.70120' W	-49	o	o	o	o
ARA14B	8	68°14.51996' N	167°07.32027' W	-43	o	o	o	o
ARA14B	9	69°10.00376' N	168°39.98665' W	-51	o	o	o	o
ARA14B	10	70°29.99991' N	168°40.00062' W	-39	o	o	o	o
ARA14B	11	71°25.80083' N	168°40.00826' W	-48	o	o	o	o
ARA14B	13	72°21.56909' N	168°39.70536' W	-54	o	o	o	o
ARA14B	16	73°53.09436' N	168°11.69237' W	-178	o	o	o	o
ARA14B	18	74°48.07461' N	167°53.96157' W	-195	o	o	o	o
ARA14B	21	76°00.15777' N	170°29.61209' W	-1313	o	o	o	o
ARA14B	23	76°59.77668' N	169°59.39867' W	-2212	o	o	o	o
ARA14B	24	76°59.75843' N	174°59.50080' W	-2010	o	o	o	o
ARA14B	25	76°59.72191' N	179°56.37066' E	-1979	o	o	o	o
ARA14B	27	78°32.71929' N	177°34.27956' W	-1008	o	o	o	o
ARA14B	28	80°00.00999' N	172°24.14447' E	-2700	o	o	o	o
ARA14B	29	79°00.00232' N	172°48.00830' E	-2511	o	o	o	o
ARA14B	30	78°00.00123' N	173°11.97534' E	-1132	o	o	o	o
ARA14B	31	76°59.99067' N	173°35.96399' E	-737	o	o	o	o
ARA14B	32	75°59.86984' N	173°36.62966' E	-264	o	o	o	o
ARA14B	33	75°00.00288' N	173°36.02031' E	-146	o	o	o	o
ARA14B	36	74°00.14793' N	170°09.82032' E	-47	o	o	o	o
ARA14B	37	74°41.62241' N	174°37.43723' E	-71	o	o	o	o
ARA14B	39	75°43.71751' N	177°10.57387' E	-483	o	o	o	o
ARA14B	40	75°04.42174' N	176°47.86464' E	-194	o	o	o	o
ARA14B	43	75°09.87831' N	179°58.11511' W	-538	o	o	o	o
ARA14B	45	75°08.99823' N	175°59.99945' W	-326	o	o	o	o

ARA14B	46	75°11.71825' N	173°59.23691' W	-363	o	o	o	o
ARA14B	47	75°14.42832' N	171°58.33430' W	-505	o	o	o	o
ARA14B	48	75°01.28263' N	169°56.14169' W	-256	o	o	o	o
ARA14B	50	75°41.46883' N	166°38.27955' W	-291	o	o	o	o
ARA14B	52	76°34.04476' N	164°21.73095' W	-549	o	o	o	o
ARA14B	54	77°28.04589' N	164°05.73205' W	-279	o	o	o	o
ARA14B	55	77°55.66502' N	163°58.03662' W	-270	o	o	o	o
ARA14B	56	77°28.92375' N	158°44.05107' W	-1323	o	o	o	o
ARA14B	57	76°18.23419' N	156°13.26701' W	-725	o	o	o	o
ARA14B	58	76°31.11499' N	159°47.35463' W	-2076	o	o	o	o
ARA14B	59	75°29.90637' N	161°08.82813' W	-2097	o	o	o	o
ARA14B	60	74°30.98022' N	162°09.11245' W	-1595	o	o	o	o
ARA14B	61	74°36.91356' N	163°55.01843' W	-833	o	o	o	o
ARA14B	62	75°01.51895' N	165°21.16946' W	-543	o	o	o	o
ARA14B	63	74°42.48257' N	165°54.45331' W	-406	o	o	o	o

References

Perovich, D. K. 2011. The changing arctic sea ice cover. Oceanography 24:162-173.

Parkinson, C. L. and J. C. Comiso. 2013. On the 2012 record low Arctic sea ice cover: Combined impact of preconditioning and an August storm. Geophysical Research Letters 40:1356-1361.

Peterson, B. J. R. M. Holmes, J. W. McClelland, C. J. Vörösmarty, R. B. Lammers, A. I. Shiklomanov, I. A. Shiklomanov, and S. Rahmstorf. 2002. Increasing river discharge to the Arctic Ocean. Science 298:2171-2173.

Arrigo, K. R., G. van Dijken, and S. Pabi. 2008. Impact of a shrinking Arctic ice cover on marine primary production. Geophysical Research Letters 35.

Arrigo, K. R., D. K. Perovich, R. S. Pickart, Z. W. Brown, G. L. Van Dijken, K. E. Lowry, M. M. Mills, M. A. Palmer, W. M. Balch, and F. Bahr. 2012. Massive phytoplankton blooms under Arctic sea ice. Science 336:1408-1408.

Coupel, P., A. Matsuoka, D. Ruiz-Pino, M. Gosselin, D. Marie, J.-É. Tremblay, and M. Babin. 2015.

Pigment signatures of phytoplankton communities in the Beaufort Sea. Biogeosciences 12: 991-1006.

Fujiwara, A., T. Hirawake, K. Suzuki, I. Imai, and S.-I. Saitoh. 2014. Timing of sea ice retreat can alter phytoplankton community structure in the western Arctic Ocean. Biogeosciences 11:1705-1716.

Coupel, P., H. Jin, M. Joo, R. Horner, H. Bouvet, M.-A. Sicre, J.-C. Gascard, J. Chen, V. Garçon,

and D. Ruiz-Pino. 2012. Phytoplankton distribution in unusually low sea ice cover over the Pacific Arctic. Biogeosciences 9:4835–4850.

Okolodkov, Y. B. 1993. A checklist of algal species found in the East Siberian Sea in May 1987. Polar Biology 13:7-11.

Arrigo, K. R. and G. L. van Dijken. 2011. Secular trends in Arctic Ocean net primary production. Journal of Geophysical Research: Oceans 116(C9).

Weingartner, T. J., S. Danielson, Y. Sasaki, V. Pavlov, and M. Kulakov. 1999. The Siberian Coastal Current: A wind-and buoyancy-forced Arctic coastal current. Journal of Geophysical Research: Oceans 104:29697-29713.

Proshutinsky, A., R. H. Bourke, and F. A. McLaughlin. 2002. The role of the Beaufort Gyre in Arctic climate variability: Seasonal to decadal climate scales. Geophysical Research Letters 29:15-11.

Brugler, E. T., R. S. Pickart, G. W. K. Moore, S. Roberts, T. J. Weingartner, and H. Statscewich. 2014. Seasonal to interannual variability of the Pacific water boundary current in the Beaufort Sea. Progress in Oceanography 127:1-20.

Macdonald, R., T. Harner, and J. Fyfe. 2005. Recent climate change in the Arctic and its impact on contaminant pathways and interpretation of temporal trend data. Science of the Total Environment 342:5-86.

Anderson, L. G., G. Björk, S. Jutterström, I. Pipko, N. Shakhova, I. Semiletov, and I. Wåhlström. 2011. East Siberian Sea, an Arctic region of very high biogeochemical activity. Biogeosciences 8:1745.

Marie D, Partensky F. Jacquet S, Vaulot D, 1997. Enumeration and cell-cycle analysis of natural populations of marine picoplankton by flow cytometry using the nucleic-acid stain SYBR Green I. Appl Environ Microb, 14: 113-118.

Sieburth JMcN, 1978. Pelagic ecosystem structure: Heterotrophic compartments of the plankton and their relationship to plankton size fractions. Limnol Oceanogr, 23: 1256-1263.

Takahashi M, Bienfang PK, 1983. Size structure of phytoplankton biomass and photosynthesis in subtrophical Hawaiian waters. Mar Biol, 76: 203-211.

Parsons TR, Maita Y, Lalli CM, 1984. A manual of chemical and biological methods for seawater analysis. Pergamon Press, Oxford, 173p.

4.2. Phytoplankton physiology (photochemistry)

CHOROM SHIM

Korea Polar Research Institute, Incheon 21990, Korea (chorom@kopri.re.kr)

4.2.1. Introduction/Objectives

Over the past few decades, the Arctic Ocean has been exposed to dramatic climate change, increasing river runoff and water temperatures, melting sea ice, and reduced amounts of permafrost (Wassmann et al. 2011). Recent changes in the marine environment have a profound impact on the biogeochemical cycle of the Arctic Ocean. In particular, the increase in fresh water caused by melting sea ice and river runoff has enhanced the stratification in the ocean's upper layer, impeding the supply of nutrients from the deeper layers to the surface (Timmermans et al. 2011; Carmack et al. 2016). Meanwhile, increased turbulence, generated by upwelling in the coastal waters due to climate changes, is likely to supply nutrients and trace metal through transport polar drift to the Arctic Ocean shelf and central basin (Kipp et al. 2018). Remote sensing data have shown a tendency of earlier phytoplankton blooms and increased primary production owing to continued decrease in sea ice in the Arctic Ocean over the past few decades (Arrigo and van Dijken, 2015). However, the physiological response of phytoplankton to specific environmental factors can only be inferred from in situ data. To forecast how phytoplankton productivity could change in the future, it is important to elucidate how environmental factors affect the growth and physiological state of phytoplankton in the Arctic Ocean.

Phytoplankton rapidly adapt their physiological status to the surrounding environment; hence, the physiological responses of organisms vary greatly in time and space (Cullen, 1982). Thus, measurements of an extensive suite of physiological characteristics are needed to quantify the impact of varied environmental conditions on phytoplankton photosynthesis. The photosynthetic characteristics of phytoplankton can be quantified in real time using variable fluorescence techniques, which have the advantage of being fast and sensitive (Falkowski and Kolber, 1995). In this field, we used a new miniaturized fluorescence induction and relaxation (a mini-FIRe) instrument to determine the variable fluorescence of phytoplankton at total 33 stations (Fig. 4.2.1; station map).

Here, the goals of this study were to evaluate the phytoplankton photophysiological

characteristics during summer in diverse environments of the western Arctic Ocean and quantify their photophysiological responses to nitrate availability.

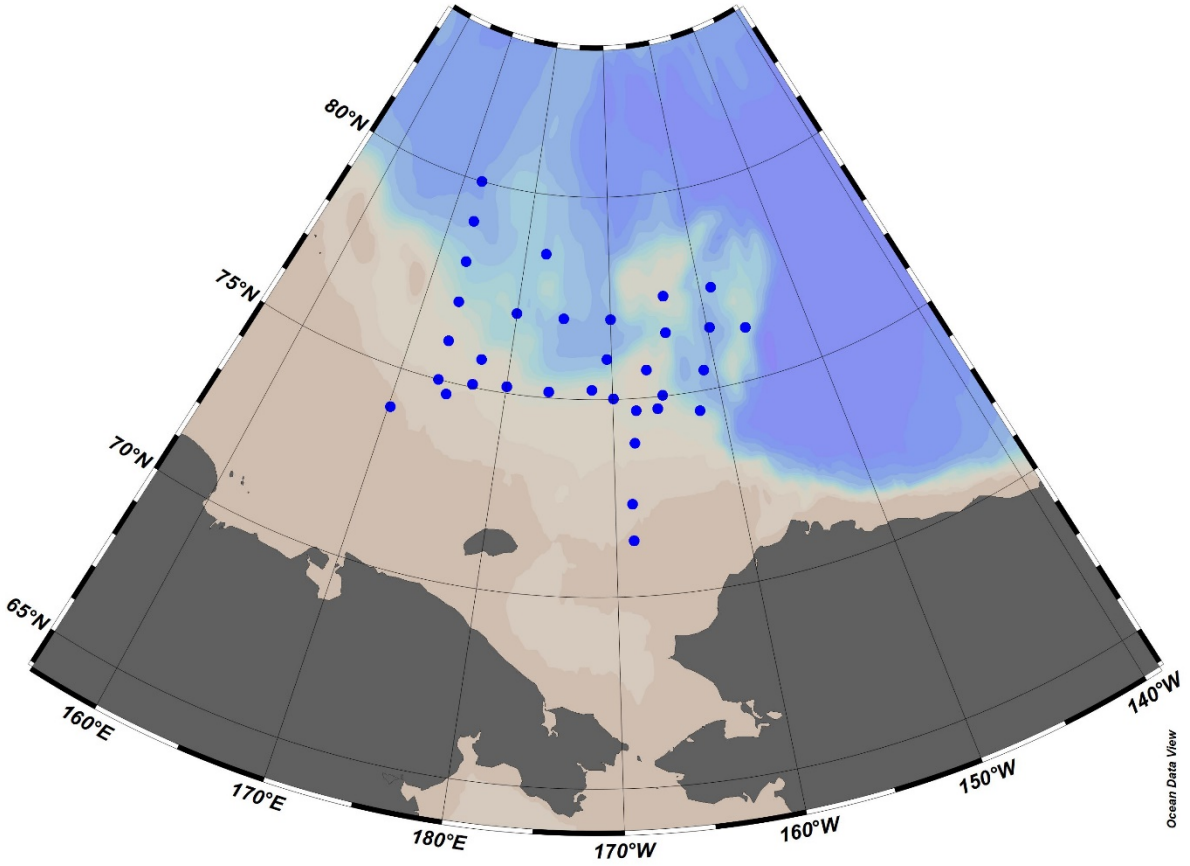

Figure 4.2.1. Station map in 2023 Arctic cruise for phytoplankton physiological study.

4.2.2. Work at sea

During this cruise, we observed phytoplankton physiological (photochemistry) parameters using a mini-FIRe (Fig. 4.2.2). Water samples were retrieved from 6 different depths ranging from the surface to 100 m below the surface using 10L Niskin bottles mounted on the conductivity, temperature, and depth rosette system (911 +, SeaBird Electronics). Samples were kept at in situ temperature and in low-light conditions (~10 µmol quanta m−2 s −1) for approximately 30 min, which was essential for the recovery from photoinhibition and nonphotochemical quenching. The photosystem II parameters, including the minimal fluorescence yield (Fo; when all reaction centers are open), maximal fluorescence yield (Fm; all reaction centers are closed), photochemical efficiency of PSII (Fv/Fm), and functional absorption cross-section (σPSII), were measured as described by Kolber et al. (1998). Fv/Fm was calculated using the ratio of variable fluorescence (Fv = Fm − Fo) for the maximum

fluorescence (Fm). The blank signals were estimated using surface samples after filtering the seawater with a syringe filter (0.2 µm). Near-surface water was collected ship's underway system which supply seawater from ca. 7 m depth and samples were directly measured through a flow system of mini-FIRe system in a constant temperature room maintained in situ sea surface temperature.

Figure 4.2.2. A custom built-Miniaturized Fluorescence Induction and Relaxation (mini-FIRe) System onboard Araon.

References

Arrigo, K. R., & van Dijken, G. L. (2015). Continued increases in Arctic Ocean primary production. Progress in Oceanography, 136, 60–70. https://doi.org/10.1016/j.pocean.2015.05.002

Carmack, E. C., Yamamoto-Kawai, M., Haine, T. W. N., Bacon, S., Bluhm, B. A., Lique, C., et al. (2016). Freshwater and its role in the Arctic marine system: Sources, disposition, storage, export, and physical and biogeochemical consequences in the Arctic and global oceans. Journal of Geophysical Research: Biogeosciences, 121, 675–717. https://doi.org/10.1002/2015JG003140

Cullen, J. J. (1982). The deep chlorophyll maximum: Comparing vertical profiles of chlorophyll a. Canadian Journal of Fisheries and Aquatic Sciences, 39(5), 791–803. https://doi.org/10.1139/f82-108

Falkowski, P. G., & Kolber, Z. (1995). Variations in chlorophyll fluorescence yields in phytoplankton in the world oceans. Australian Journal of Plant Physiology, 22(2), 341–355. https://doi.org/10.1071/Pp9950341

Kipp, L. E., Charette, M. A., Moore, W. S., Henderson, P. B., & Rigor, I. G. (2018). Increased fluxes of shelf-derived materials to the central Arctic Ocean. Science Advances, 4(1), eaao1302. https://doi.org/10.1126/sciadv.aao1302

Kolber, Z. S., Prasil, O., & Falkowski, P. G. (1998). Measurements of variable chlorophyll fluorescence using fast repetition rate techniques: Defining methodology and experimental protocols. Biochimica et Biophysica Acta-Bioenergetics, 1367(1–3), 88–106. https://doi.org/ 10.1016/S0005-2728(98)00135-2

Timmermans, M. L., Proshutinsky, A., Krishfield, R. A., Perovich, D. K., Richter-Menge, J. A., Stanton, T. P., & Toole, J. M. (2011). Surface freshening in the Arctic Ocean's Eurasian Basin: An apparent consequence of recent change in the wind-driven circulation. Journal of Geophysical Research, 116, C00D03. https://doi.org/10.1029/2011JC006975

Wassmann, P., Duarte, C. M., Agusti, S., & Sejr, M. K. (2011). Footprints of climate change in the Arctic marine ecosystem. Global Change Biology, 17(2), 1235–1249. https://doi.org/10.1111/j.1365-2486.2010.02311.x

4.3 Primary production and macromolecular composition of phytoplankton

Sanghoon Park

Department of Oceanography, Pusan National University, Korea

E-mail: mossinp@pusan.ac.kr

4.3.1. Introduction

Over the past several decades, higher temperatures have decreased the extent and thickness of perennial sea ice as well as increased the number of melting ponds in the Arctic Ocean (Perovich et al., 2009). The removal of permanent sea ice cover and increasing number of melting ponds altered several important processes, such as the depth of mixing, stratification, light penetration, nutrient supply, temperature-related processes, and possibly photochemical reactions (Tremblay et al., 2008; Codispoti et al., 2009; Lee et al., 2010). These recent changes in climate and ice conditions could change the patterns and the total amount of carbon production of phytoplankton and consequently the production at higher trophic levels (Tynan and DeMaster, 1997). However, whether these climate change conditions enhance or reduce the overall production in the Arctic Ocean is controversial. Arrigo et al. (2008) reported increases in annual net primary production (NPP) by phytoplankton based on a satellite ocean color data were particularly large on the continental shelves of the Chukchi Sea, whereas Lee et al. (2007) reported that the primary production rates from in situ measurement up to three times lower than those previously reported in the shelf of the Chukchi Sea. Therefore, in this study we measured in situ carbon and nitrogen uptake rates for primary and new productions of overall phytoplankton production and macromolecular composition to study the physiological status and nutritional composition of phytoplankton in the Chukchi Sea and East Siberian Sea.

4.3.2. Materials and methods

To estimate the carbon and nitrogen uptake rate of phytoplankton in the Chukchi Sea and East Siberian Sea, productivity experiments were executed by incubating phytoplankton in the incubators on the deck for 4-6 hours (Figure. 4.3.1) after stable isotopes (13C, 15NO3, and 15NH4) as tracers were inoculated into each bottle. Total 11 productivity experiments were completed at water column station during this cruise (Figure. 4.3.2), respectively. At primary

production stations, the seawater samples were collected by CTD rosette water samplers at 6 different light depths (100, 50, 30, 12, 5, and 1%). After the incubation, all sample waters for the total and small (<5μm) phytoplankton production were filtered on GF/F (ø = 25 mm) filters for laboratory isotope analysis at University of Alaska Fairbanks after this cruise. For the background data of the productivity stations, water samples were collected for alkalinity, total and size-fractionated chlorophyll-a concentration. In addition, water samples for macromolecular composition of phytoplankton obtained from 3 light depths (100, 30, and 1%). All sample waters for macromolecular composition of phytoplankton were filtered on GF/F (ø = 47 mm) filters and was then immediately stored at 80 °C until analysis. Samples for macromolecular compositional analysis of phytoplankton were obtained at selected 22 stations in the Chukchi Sea and East Siberian Sea (Figure 4.3.2).

Figure 4.3.1. In situ incubation on deck for 4-6 hours.

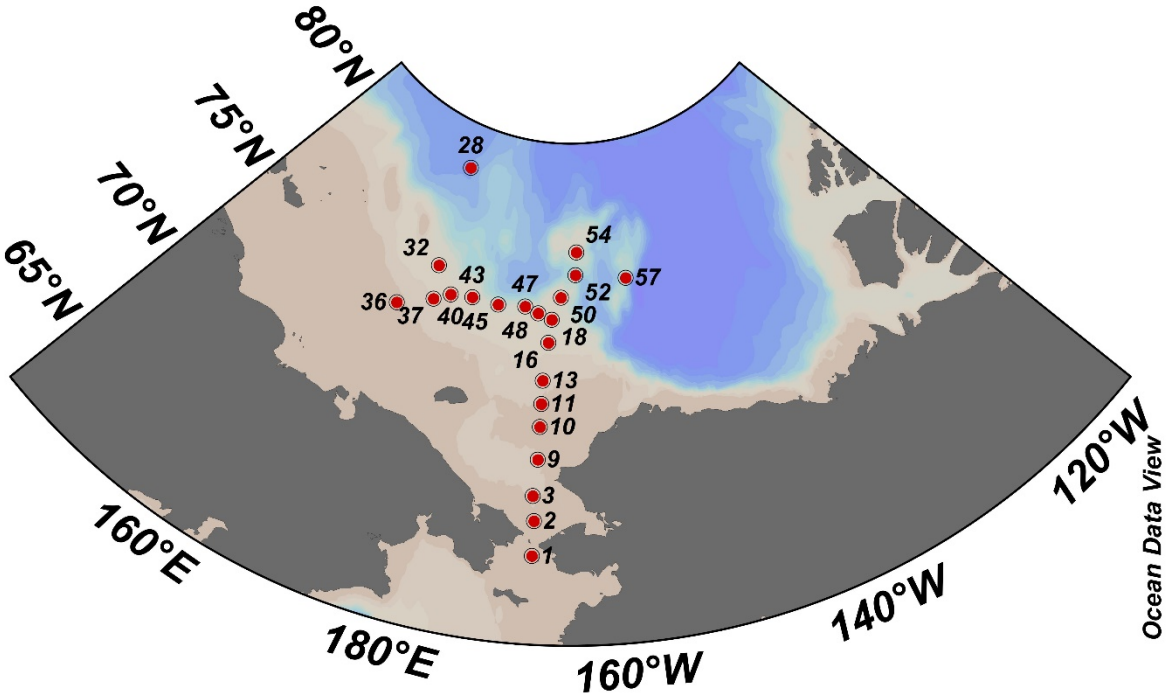

Figure 4.3.2. Stations for primary production and macromolecular compositions of phytoplankton during the 2023 Arctic cruise.

References

Arrigo, K.R., van Dijken, G., Pabi, S., 2008. Impact of a shrinking Arctic ice cover on marine primary production. Geophys. Res. Lett. 35, L19603. doi:10.1029/2008GL035028.

Codispoti LA, Flagg CN, Swift JH (2009) Hydrographic conditions during the 2004 SBI process experiments. Deep-Sea Research II 56:1144-1163.

Dowgiallo, A., 1975 Chemical composition of an animal's body and its food. In: Grodzinski, W., Klekowski, R.Z., Duncan, A. (Eds.), Methods for Ecological Bioenergetics. IBP Handbook No. 24. Blackwell, London, pp. 160-199.

Lee, S.H., Whitledge, T.E., Kang, S.H., 2007. Recent carbon and nitrogen uptake rates of phytoplankton in Bering Strait and the Chukchi Sea. Cont. Shelf Res. 27, 2231-2249.

Lee, S.H., Kim, H.J., Whitledge, T.E., 2009. High incorporation of carbon into proteins by the phytoplankton of the Bering Strait and Chukchi Sea. Cont. Shelf Res. 29, 1689-1696.

Lee SH, Stockwell D, Whitledge TE (2010). Uptake rates of dissolved inorganic carbon and nitrogen by under-ice phytoplankton in the Canada Basin in summer 2005. Polar

Biology.33:1027-1036

Lindqvist, K., Lignell, R., 1997. Intracellular partitioning of 14CO2 in phytoplankton during a growth season in the northern Baltic. Mar. Ecol. Prog. Ser. 152, 41-50.

Morris, M.J., Hopkins, T.L., 1983. Biochemical composition of crustacean zooplankton from the eastern Gulf of Mexico. J. Exp. Mar. Biol. Ecol. 69, 1–19.

Parrish, C.C., McKenizie, C.H., MacDonald, B.A., Hatfield, E.A., 1995. Seasonal studies of seston lipids in relation to microplankton species composition and scallop growth in South Broad Cove, Newfoundland. Mar. Ecol. Prog. Ser. 129, 151-164.

Perovich DK, Richter-Menge JA (2009) Loss of sea ice in the Arctic. Annual Review of Marine Science 1:417-441

Scott, C.L., Kwasniewski, S., Falk-Petersen, S., Sargent, J.R., 2000. Lipids and life strategies of Calanus finmarchicus, Calanus glacialis and Calanus hyperboreus in late autumn, Kongsfjorden, Svalbard. Polar Biol. 23, 510–516.

Smith, R.E.H., Gosselin, M., Kattner, G., Legendre, L., Pesant, S., 1997a. Biosynthesis of macromolecular and lipid classes by phytoplankton in the Northeast Water Polynya. Mar. Ecol. Prog. Ser. 147, 231–242.

Tremblay, J.-É., Simpson, K., Martin, J., Miller, L., Gratton, Y., Barber, D., Price, N.M., 2008. Vertical stability and the annual dynamics of nutrients and chlorophyll fluorescence in the coastal, southeast Beaufort Sea. Journal of Geophysical Research 114, C07S90, doi:10.1029/2007JCoo4547, 2008.

Tynan, C.T., DeMaster, D.P., 1997. Observations and predictions of Arctic climatic change: potential effects on marine mammals. Arctic 50, 308-322.

Winberg, G.G., 1971b. Methods for the estimation of production of aquatic animals. (Translated by Duncan, A.) Academic Press, London.

4.4. Microzooplankton community and grazing

Hyeju Yoo

Korea Polar Research Institute, Incheon 21990, Korea

Email: hjyoo@kopri.re.kr

4.4.1. Introduction

Heterotrophic protists ingest a broad size spectrum of prey, from bacteria to phytoplankton, and are themselves important prey items for mesozooplankton. Many researchers suggest that heterotrophic protists contribute to the trophic linkage between phytoplankton and mesozooplankton and are important in the pelagic food webs of many oceanic waters. The importance of heterotrophic protists in pelagic ecosystems has become increasingly evident in the past two decades, and trophic interaction between heterotrophic protists and phytoplankton has been reported in various marine. However, there is no information on the relative importance of heterotrophic protists in the pelagic ecosystem of the Western Arctic Sea. The Arctic Ocean is currently experiencing rapid environmental change due to natural and anthropogenic factor that includes warming, sea ice loss and other physical change as well as biology and ecosystem structure change. In this study area, we investigated the meso-scale variations and structure of heterotrophic protist communities and grazing rates on phytoplankton in the various environmental conditions such as open ocean. During this cruise, we investigated protozoa abundance, biomass and grazing rates in total 44 stations. (Table 4.1).

4.4.2. Materials and methods

▪ ***Abundance and community structure of heterotrophic protists***

To determine the abundance of heterotrophic protists, a CTD-Niskin rosette sampler was used to take water samples from the following 3 or 4 depths. For ciliates and sarcodina, 500 ml water from the vertical profiles was preserved with 1% acid Lugol's iodine solution these samples were then stored in darkness. For heterotrophic nanoflagellates and heterotrophic dinoflagellates smaller than 20 μm, 500 ml of water was preserved with glutaraldehyde (0.5% final concentration) and stored at 4° C.

▪ ***Grazing experiments***

Grazing rates of heterotrophic protists were determined by the dilution method (Landry and Hassett 1982). Water for grazing experiments was collected from 2 depth (surface, SCM) of each station. At each station, 20L seawater were collected in a Niskin bottle and transferred to a polycarbonate carboy. Part of this water was filtered through the 0.22-µm filtration system. Dilution series were set up in ten 1.3-l PC bottles. Nine bottles were used to establish a nutrient-enriched dilution series consisting of triplicate bottles with 20%, 100%, 100N(not add the nutrients) of natural seawater. The bottles were incubated on deck for 24 – 48 h at ambient sea surface temperatures and screened to the ambient light level with neutral density screening (Figure 4.?). Subsamples were collected from triplicate bottles at 0 and 24-48h to determine chlorophyll-a concentrations.

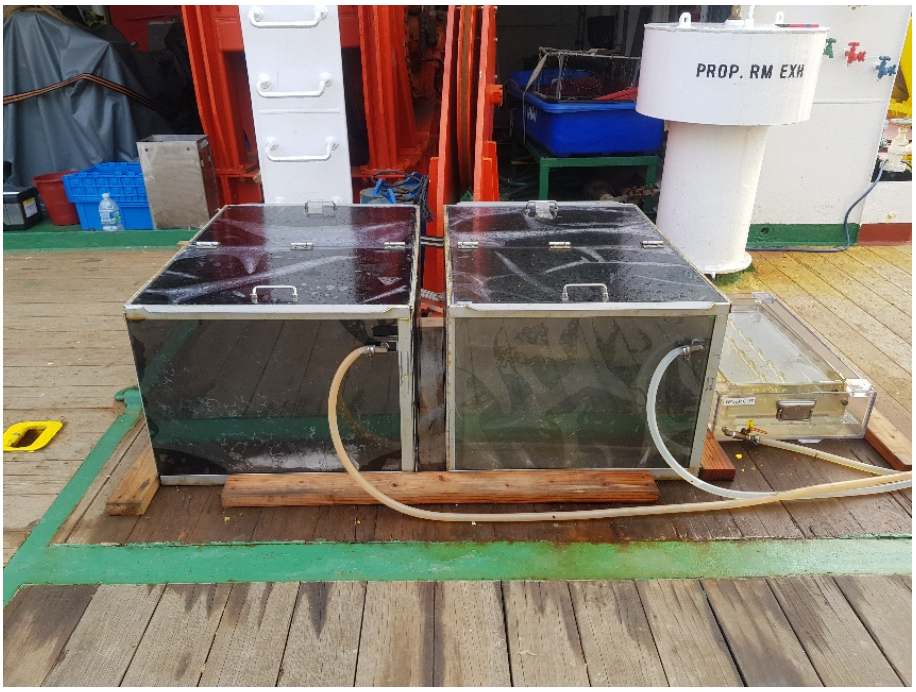

Figure 4.1. Incubation for grazing experiments.

Table 4.1. Sampling locations of heterotrophic protists community structure and grazing rates during the ARA14B 2023 cruise.

Cruise	St.	Lat_Deg10	Lon_Deg10	Depth (m)	Net (Depth)	Net (Volume)	Heterotrophic protists community	Grazing Exp. (Depth)
ARA14B	1	65.1735	-168.6907	-50	45	170	o	0m, 10m
ARA14B	2	66.6299	-168.6875	-44	35	290	o	-
ARA14B	3	67.6700	-168.9600	-50	45	245	o	0m, 24m
ARA14B	4	67.7830	-168.6020	-50	-	-	o	-
ARA14B	5	67.8980	-168.2350	-58	-	-	o	-
ARA14B	6	68.0130	-167.8670	-52	-	-	o	-
ARA14B	7	68.1280	-167.4950	-49	-	-	o	-
ARA14B	8	68.2420	-167.1220	-43	38	190	o	-
ARA14B	9	69.1667	-168.6667	-51	46	400	o	
ARA14B	10	70.5000	-168.6667	-39	35	190	o	0m, 22m
ARA14B	11	71.4300	-168.6667	-48	42	190	o	-
ARA14B	13	72.3600	-168.6667	-54	50	330	o	0m, 16m
ARA14B	16	73.8887	-168.2001	-178	100	230	o	-
ARA14B	18	74.8006	-167.8983	-195	100	220	o	0m, 22m
ARA14B	21	76.0000	-170.5000	-1313	100	300	o	-
ARA14B	23	77.0005	-170.0509	-2212	100	250	o	0m, 30m
ARA14B	24	77.0000	-175.0000	-2010	100	215	o	-
ARA14B	25	77.0000	-180.0000	-1979	100	210	o	0m, 24m
ARA14B	27	78.5609	-177.8475	-1008	100	200	o	0m, 25m
ARA14B	28	80.0000	172.4000	-2700	100	200	o	0m, 18m
ARA14B	29	79.0000	172.8000	-2511	100	180	o	-
ARA14B	30	78.0000	173.2000	-1132	100	200	o	-
ARA14B	31	77.0000	173.6000	-737	100	170	o	0m, 34m
ARA14B	32	76.0000	173.6000	-264	100	190	o	-
ARA14B	33	75.0000	173.6000	-146	100	140	o	0m, 30m
ARA14B	36	74.0000	170.0000	-47	40	210	o	0m
ARA14B	37	74.7005	174.5278	-71	60	150	o	-
ARA14B	39	75.8018	177.0548	-483	100	180	o	-
ARA14B	40	75.0750	176.8000	-194	100	220	o	-
ARA14B	43	75.2060	-179.9900	-538	100	330	o	0m, 35m
ARA14B	45	75.1500	-176.0000	-326	100	250	o	-
ARA14B	46	75.1950	-173.9870	-363	100	-	o	-
ARA14B	47	75.2404	-171.9725	-505	100	190	o	0m, 23m
ARA14B	50	75.6911	-166.6382	-283	100	200	o	0m, 35m
ARA14B	52	76.5775	-164.3325	-539	100	180	o	0m,38m
ARA14B	54	77.4722	-164.1180	-278	100	250	o	0m, 32m
ARA14B	56	77.5000	-158.8750	-1313	100	380	o	-
ARA14B	57	76.3039	-156.2212	-715	100	215	o	-
ARA14B	58	76.5389	-159.8910	-2076	100	175	o	-
ARA14B	59	75.4984	-161.1470	-2088	100	230	o	-
ARA14B	60	74.5163	-162.1520	-1595	100	250	o	-
ARA14B	62	75.0000	-165.0000	-539	100	-	o	-

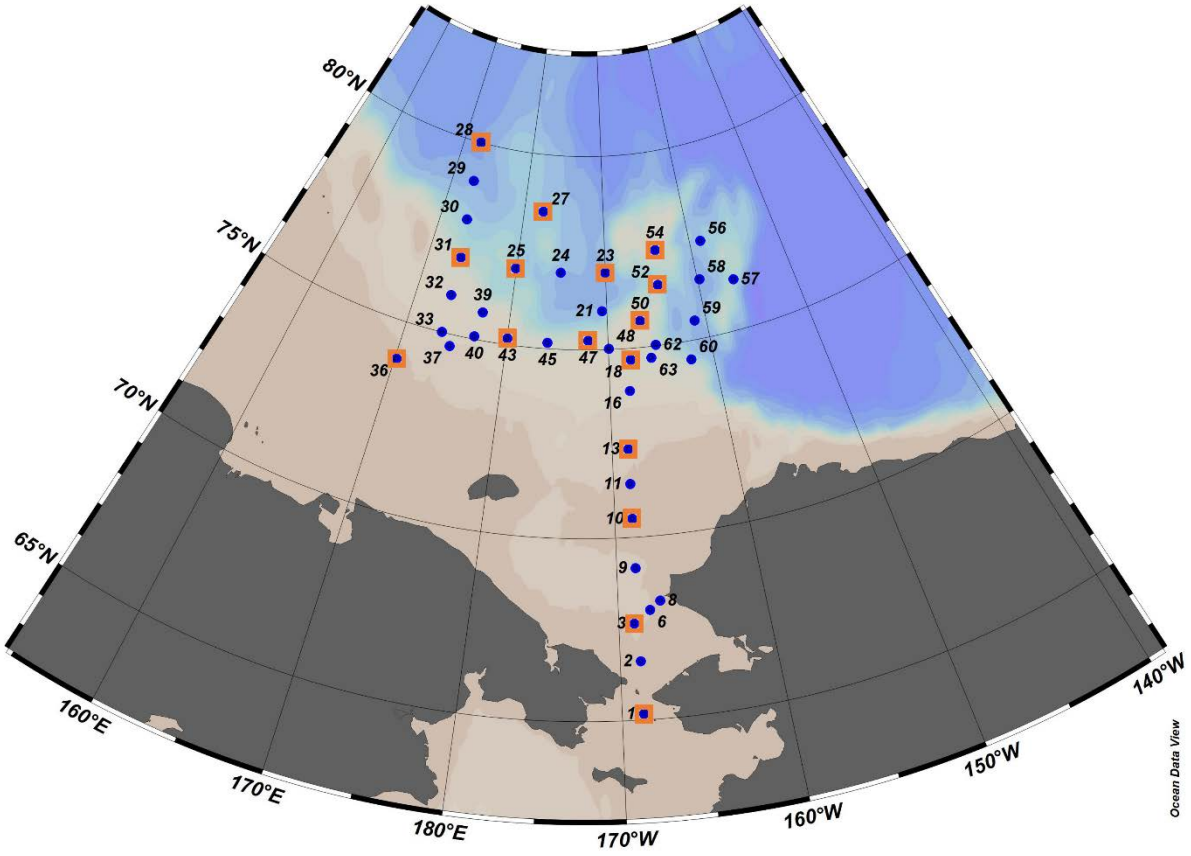

Figure 4.2. A map shows study area(Bering, the Chuckchi and the East Siberian Seas) and sampling stations during the 2023 Arctic cruise. Small orange squares represent the station conducting experiment for grazing rates of heterotrophic protists.

4.5. Mesozooplankton community and UVP

Jee-Hoon Kim and Jeong-Hyun Kim

Division of ocean science, Korea Polar Research Institute, Korea (Jeehoonkim@kopri.re.kr)

4.5.1. Introduction

Across the whole oceans, zooplankton communities are influenced by regional (large-scale: advection, upwelling), meso-scale (eddies, convergence/divergence), and local scale factors (stratification, light, species interactions), but polar zooplankton communities are uniquely influenced by additional features as well. Sea ice, inclusive of ice edges, melting, timing and extent of ice retreat, influences community composition, seasonality and timing of production, diel vertical migration, and trophic interactions. Approximately 300 species of holoplanktonic zooplankton have been recorded for the Arctic (Sirenko, 2001), excluding the wider variety of meroplanktonic larvae occurring particularly within the shallow waters of the marginal seas. In particular, copepods of the genus Calanus commonly dominate the biomass of zooplankton in temperate and polar seas and serve as a critical link between microbial primary/secondary production and higher trophic levels, such as fish, birds and marine mammals (Dahl et al., 2003; Falk-Petersen et al., 2009). Despite the great abundance and ecological significance of zooplankton in Arctic Ocean, their pathways and roles in the Arctic ecosystem are still not well known because of the logistical difficulty with access.

The type of zooplankton sampling gear used influences the abundance, biomass, and composition of the catch as a result of extrusion or avoidance (Skjoldal et al., 2013). When comparing zooplankton datasets, differences in sampling gear must be considered, especially the sizes of the mesh and net mouth. Traditionally, ring (or bongo, 500 µm, 0.5–1 m mouth diameter), Nansen (333 µm, 0.7 m mouth diameter), or Juday (~ 170 µm, 0.37 m mouth diameter) nets are used (Ershova et al., 2015b). Recently, 150 µm nets have been used to survey small species in Arctic research (Pinchuk and Eisner, 2017, Spear et al., 2019). Coarse mesh nets (e.g., 500 µm nets) can undersample small species, which commonly make up > 90% of the total abundance in this area, while fine mesh nets (<170 µm) may under-represent the larger, faster, and rarer species (Questel et al., 2013). Therefore, we used 330 µm and 150 µm nets (both 0.6 m mouth diameter) which are common enough to be well represented when collected with fine-mesh nets, but large enough to be captured by most coarse nets.

The aim of this research is to provide the zooplankton composition in the Bering Strait, the Chukchi Sea, and the East Siberian Sea as fundamental information of Arctic marine ecosystem and understand the ecological characteristics of zooplankton and changes in environmental conditions (water temperature, salinity, chlorophyll a, and sea ice concentration).

Underwater Vision Profiler 6 (UVP6)

The UVP6 is a high technology instrument used to understand the distribution and composition of large particulate matter in the ocean using images. These images include various particles such as phytodetritus, marine snow, and zooplankton ranging from 100 to 2000 µm. The UVP is installed on the rosette profiler with the CTD, therefore generating high spatial resolution data in conjunction with CTD measurements depending on the selected imaging frequency (Hz). UVP6 results will also be compared to net sampling results and analyzed, providing a better understanding of the vertical distribution of zooplankton in the Pacific Arctic region.

4.5.2. Material and methods

Sample collection and Processing

Zooplankton net hauls were carried out in the Bering strait, Chukchi sea and East Siberian sea in 2 August 2023 to 28 August 2023 (Table 4.5.1). In all cases a bongo net was used, hauled vertically between 200 m and the surface. The bongo net and 150 net had 330 & 500 µm mesh and 150 µm mesh, respectively (Figure 4.5.1). There were 88 net hauls at 45 stations (Table 4.5.1), and the volume of seawater filtered was estimated from flow meter measurements.

Samples were immediately fixed and preserved with 5% neutralized formaldehyde for quantitative analyses and were identified to the lowest taxonomic level using a microscope. Sub-samples from 500 µm net were transferred into 2 ml vial and 250 ml bottle with 99% ethanol, which were frozen at –20 °C for the post analysis.

Figure 4.5.1. Zooplankton Sampling with 150 µm mesh Net (Left), and Bongo net (Right, 330 and 500 µm mesh)

Table 4.5.1. Sampling locations of zooplankton composition during ARA14B.

항차	St.	Date (Local)	Bongo (150X2)			Bongo (330&500)		
			Time	Flow	Depth (m)	Time	Flow	Depth (m)
ARA14B	1	8.02	20:52-20:57	173	45	20:39-20:43	252	45m
ARA14B	2	8.03	06:51-06:55	26	20	06:36-06:41	130	35m
ARA14B	3	8.03	15:00-15:06	32	45	14:46-14:52	156	45m
ARA14B	4	8.03	17:23-1727	85	45	17:09-17:13	192	45m
ARA14B	5	8.03	19:14-19:19	99	50	19:05-19:10	114	50m
ARA14B	6	8.03	21:50-21:55	46	45	21:40-21:43	186	45m
ARA14B	7	8.03	00:04-00:09	171	40	23:51-23:56	226	40m
ARA14B	8	8.04	02:39-02:44	89	38	02:29-02:33	217	38m
ARA14B	9	8.04	09:53-09:58	77	45	09:43-09:47	105	45m
ARA14B	10	8.04	18:48-18:51	45	30	18:39-18:43	103	30m
ARA14B	11	8:05	00:33-00:37	51	40	00:23-00:28	178	40m
ARA14B	13	8.05	08:20-08:25	94	50	08:09-08:14	137	50m
ARA14B	16	8.06	05:02-05:12	320	165	04:47-04:57	431	165m
ARA14B	18	8.06	14:37-14:53	149	185	14:15-14:30	350	185m
ARA14B	21	8.07	08:48-09:00	595	200	08:30-08:43	587	200m
ARA14B	23	8.08	01:23-01:35	478	200	01:23-01:35	584	200m
ARA14B	24	8.08	14:17-14:29	497	200	14:36-14:47	830	200m
ARA14B	25	8.09	03:05-03:17	572	200	03:24-03:35	929	200m
ARA14B	27	8.12	N/A	N/A	N/A	17:50-18:02	549	200m
ARA14B	28	8.13	14:11-14:23	527	200	14:30-14:43	649	200m
ARA14B	29	8.14	02:43-02:55	547	200	03:00-03:13	646	200m
ARA14B	30	8.14	14:38-14:52	772	200	15:58-16:11	861	200m
ARA14B	31	8.15	01:30-01:44	701	200	01:50-02:03	840	200m
ARA14B	32	8.15	15:34-15:46	784	200	15:51-16:03	834	200m
ARA14B	33	8.16	01:17-01:27	349	140	01:32-01:43	328	140m
ARA14B	36	8.16	14:41-14:46	143	40	14:46-14:55	173	40m
ARA14B	37	8.17	11:04-11:09	189	60	11:15-11:21	261	60m
ARA14B	39	8.18	03:17-03:30	504	200	03:37-3:49	511	200m
ARA14B	39-1.	8.19	N/A	N/A	N/A	17:19-17:22	113	25m
ARA14B	40	8.20	06:10-06:20	624	185	06:26-06:36	646	185m
ARA14B	43	8.20	20:56-21:08	470	200	21:13-21:26	629	200m
ARA14B	45	8.21	12:30-12:43	491	200	12:48-13:01	344	200m
ARA14B	47	8.22	01:04-01:17	456	200	01:22-01:34	350	200m
ARA14B	48	8.22	14:04-14:16	423	200	14:21-14:33	548	200m
ARA14B	50	8.23	03:30-03:43	397	200	03:47-04:00	598	200m
ARA14B	52	8.23	16:51-17:03	533	200	17:09-17:20	294	200m
ARA14B	54	8.24	10:47-10:59	476	200	11:04-11:18	515	200m
ARA14B	55	8.24	18:08-18:20	420	200	18:29-18:40	393	200m
ARA14B	56	8.25	04:05-04:17	533	200	04:22-04:34	246	200m
ARA14B	57	8.25	21:10-21:22	548	200	21:27-21:39	281	200m
ARA14B	58	8.26	13:47-13:58	558	200	14:03-14:15	532	200m
ARA14B	59	8.27	01:42-01:54	600	200	01:59-02:11	237	200m
ARA14B	60	8.27	10:23-10:35	677	200	10:40-10:52	494	200m
ARA14B	62	8.28	02:56-03:08	795	200	03:13-03:25	466	200m
ARA14B	63	8.28	06:31-06:44	764	200	06:49-07:01	615	200m

UVP operating

The observation of zooplankton images using UVP6-HF(High Frequency) was conducted at 43 stations in the East Siberian and Chukchi Seas. The UVP was installed on the rosette frame, and programmed to automatically start acquisition (25 Hz image frequency) below 1 m water depth during CTD casts. The instrument is also set up to autonomously stop when reaching an estimated 50 m depth difference during the upward casts to collect as many plankton and particle vignettes as possible.

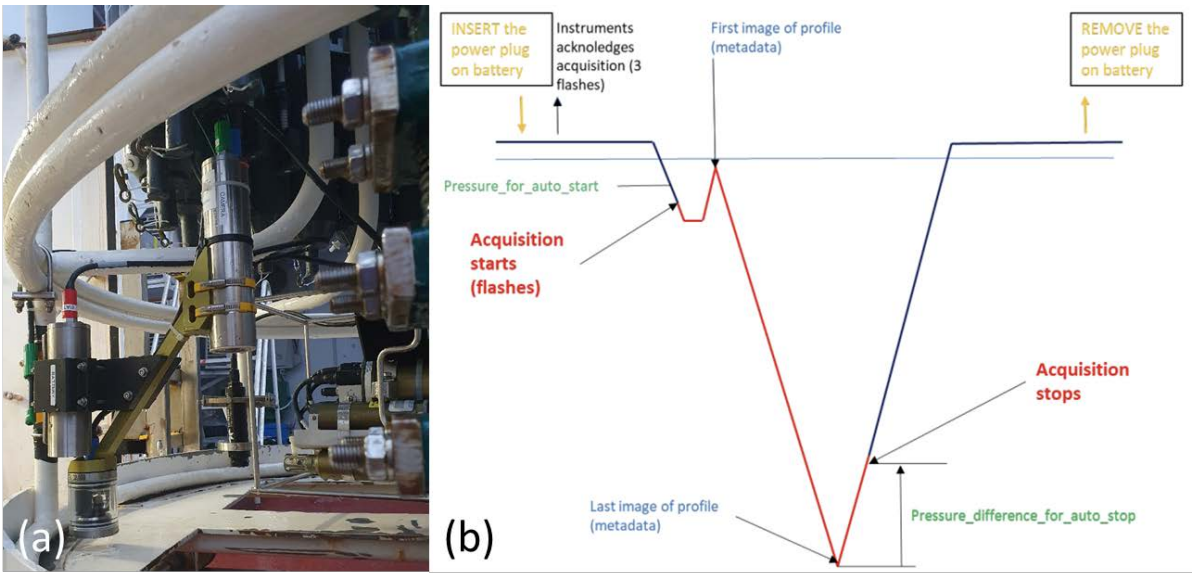

Figure 4.5.3. (a) UVP6-HF installation on the rosette frame and (b) Deployment scheme (Marc and Camille, 2022)

Table 4.5.2. Deployment locations of UVP6-HF during ARA14B

Station	Sampling time (Local)	Water depth (m)	Casting depth (m)
1	2023.08.02 19:09	50	41
2	2023.08.03 05:33	44	35
3	2023.08.03 13:04	49	40
9	2023.08.04 07:58	50	40
10	2023.08.04 17:00	39	30
11	2023.08.04 23:56	47	40.3
13	2023.08.05 06:30	55	45
16	2023.08.06 02:32	181	172
18	2023.08.06 11:50	194	184
21	2023.08.07 04:57	1313	1304
23	2023.08.07 20:37	2212	2203

24	2023.08.08 12:21	2010	2002
25	2023.08.08 23:37	1079	1069
28	2023.08.13 09:05	2700	2692
28	2023.08.13 14:55	2700	1500
29	2023.08.13 22:18	2560	2551
30	2023.08.14 11:18	1132	1122
30	2023.08.14 15:22	1132	1122
31	2023.08.14 22:33	737	727
32	2023.08.15 12:55	264	255
33	2023.08.15 23:50	146	135
36	2023.08.16 12:22	47	42.5
38	2023.08.17 21:47	230	220
39	2023.08.18 02:16	499.5	490.3
40	2023.08.20 04:10	194.6	185.8
42	2023.08.20 15:24	937	928.5
43	2023.08.20 18:16	538	529
46	2023.08.21 17:12	363	353
47	2023.08.21 22:34	505	495
50	2023.08.23 01:53	291.8	282.3
51	2023.08.23 08:58	709	700
52	2023.08.23 14:10	549	539
53	2023.08.24 04:22	418	409
54	2023.08.24 08:25	279.3	269.8
55	2023.08.24 17:27	270	260
56	2023.08.25 02:35	1323	1313
57	2023.08.25 19:53	725	715
58	2023.08.26 08:26	2112	2102
59	2023.08.26 23:44	2097	2088
60	2023.08.27 08:46	1595	1585
62	2023.08.27 21:52	544	529
62	2023.08.28 02:01	543	534
63	2023.08.28 05:37	406	400

4.5.3. Preliminary results and discussion

A total 12 taxonomic communities of zooplankton, Copepoda (Over 10 Species), Chaetognatha, Cladocera, Euphausiacea, Ostracoda, Amphipoda, Fish (larvae), Cirriped (larvae), Decapoda (larvae), Gastropoda (larvae), Ophioplutes (larvae), Polychaeta (larvae), were identified at 43 stations.

Calanoid copepods were dominant species with more than 60% of total meso-zooplankton communities at all stations. They are the most important biomass species and the prime omnivores in the Arctic Ocean. Oithona similis and Microcalanus spp. are also dominant

species in abundance (ind. / m-3) but not in biomass cause small body size. The greatest diversity of Arctic holo-zooplankton occurs within the copepods (~150 species), which dominate the zooplankton community in both abundance and biomass (Kosobokova and Hopcraft, 2010). Copepods constitute over 80% of the total mesozooplankton community in Arctic Ocean, which they play a major role in energy flow and biogeochemical cycles. Some of the ingested organic carbon of zooplankton is used for metabolic activities, so quantifying this carbon is of prime importance to better understand energy transfer and elemental cycling via zooplankton in Arctic ecosystems. Calanus glacialis and C. hyperboreus (Figure 4.5.3) are regarded as biological indicators of Arctic water mass.

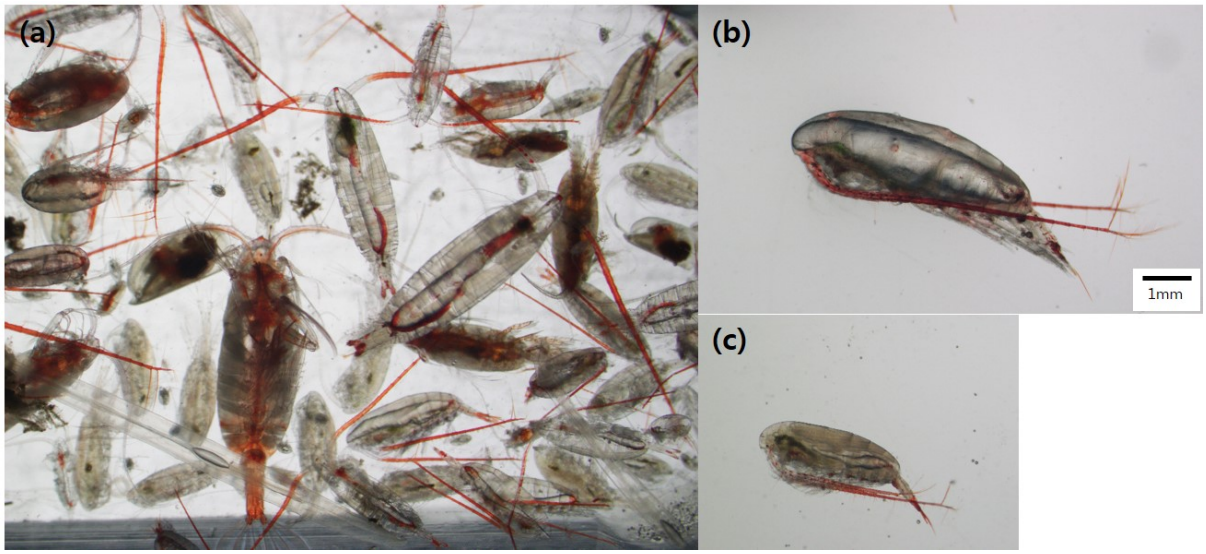

Figure 4.5.4. (a) Zooplankton assemblage by 330 µm bongo net, (b) *Calanus hyperboreus*, (c) *Calanus glacialis*.

4.6. Zooplankton Respiration

Jeong-Hyun Kim

Division of ocean science, Korea Polar Research Institute, Korea (jeonghkim@kopri.re.kr)

4.6.1. Introduction

As heterotrophs, zooplankton graze on primary producers and transfer energy to the higher trophic level of the ocean food web (Campbell et al., 2009). In this process, they use the ingested organic matter for respiration, growth, and reproduction or release some into the water column without assimilation (Del Giorgio and Williams, 2005). Particularly, the respiration of zooplankton is known to be a major physiological process balancing the production and loss of organic carbon in the pelagic ecosystem (Steinberg and Landry, 2017). The respiratory flux from vertical migration also transfers carbon from the surface to depth as active transport, which could potentially affect the biological pump. Therefore, the respiration rate of zooplankton is considered an important factor to understand the mechanisms of the ocean carbon cycle.

Zooplankton respiration has been reported to correspond to about 50 % of the carbon they absorbed, but the specific proportion is affected by various factors, especially, temperature and body mass (Steinberg and Landry, 2017, Ikeda, 2014). The effect of habitat temperature on respiration rate typically has a positive correlation and represents a Q10 value of 1.9 on average for metazooplankton, which is the ratio at which metabolic rate increases when the temperature rises by 10 ℃ (Ikeda, 2014). Furthermore, a large body mass commonly results in high respiration rates but leads to low weight-specific respiration rates (Del Giorgio and Williams, 2005). Other components such as pressure and salinity may also complicate the metabolism of zooplankton, so these environmental factors should be considered.

Respiration is a useful parameter to understand the fate of carbon in the ocean and the response of pelagic ecosystem structure to climate change. During the present cruise, incubation experiments were conducted to measure the respiration rate of the main zooplankton species in the Pacific Arctic region.

4.6.2. Material and methods

Zooplankton for incubation were collected using a bongo net (505 µm mesh size) during the R/V ARAON Arctic survey (ARA14B, from 1 to 31 August 2023) at 13 stations in the Chukchi and East Siberian Seas (Figure 4.6.1., Table 4.6.1.). Samples were immediately transferred into a 3 L bucket filled with seawater to dilute the high density and sorted to the lowest taxonomic level as possible using a dissecting microscope within 1 hour after collection (Figure 4.6.2a.). Each species was gently placed into 0.2 µm filtered seawater and acclimatized at 0 ± 1 ℃ for at least 5 hours.

After acclimatization, 2-5 individuals were transferred into 60 ml biological oxygen demand (BOD) bottles. Respiration rates were obtained by measuring the decrease in dissolved oxygen concentrations over time. Oxygen concentration in the respiration experiments was measured with an optode sensor (FireStingO2, Pyroscience, Germany; Figure 4.6.2b.) at 0 ± 1 ℃ in the dark during at least 10 hours. A two-point calibration of the optode was performed using an air-saturated 0.2 µm filtered seawater and a oxygen-depleted solution that was obtained by mixing Na2SO3 into distilled water. The net respiration rate was determined by subtracting the zooplankton-free respiration rates (controls) from the zooplankton respiration rates (experiments). Experimental zooplankton were preserved with a borate-neutralized formalin solution added to 0.2 µm filtered seawater (10 % concentration) to determine weight-specific respiration rates in the laboratory.

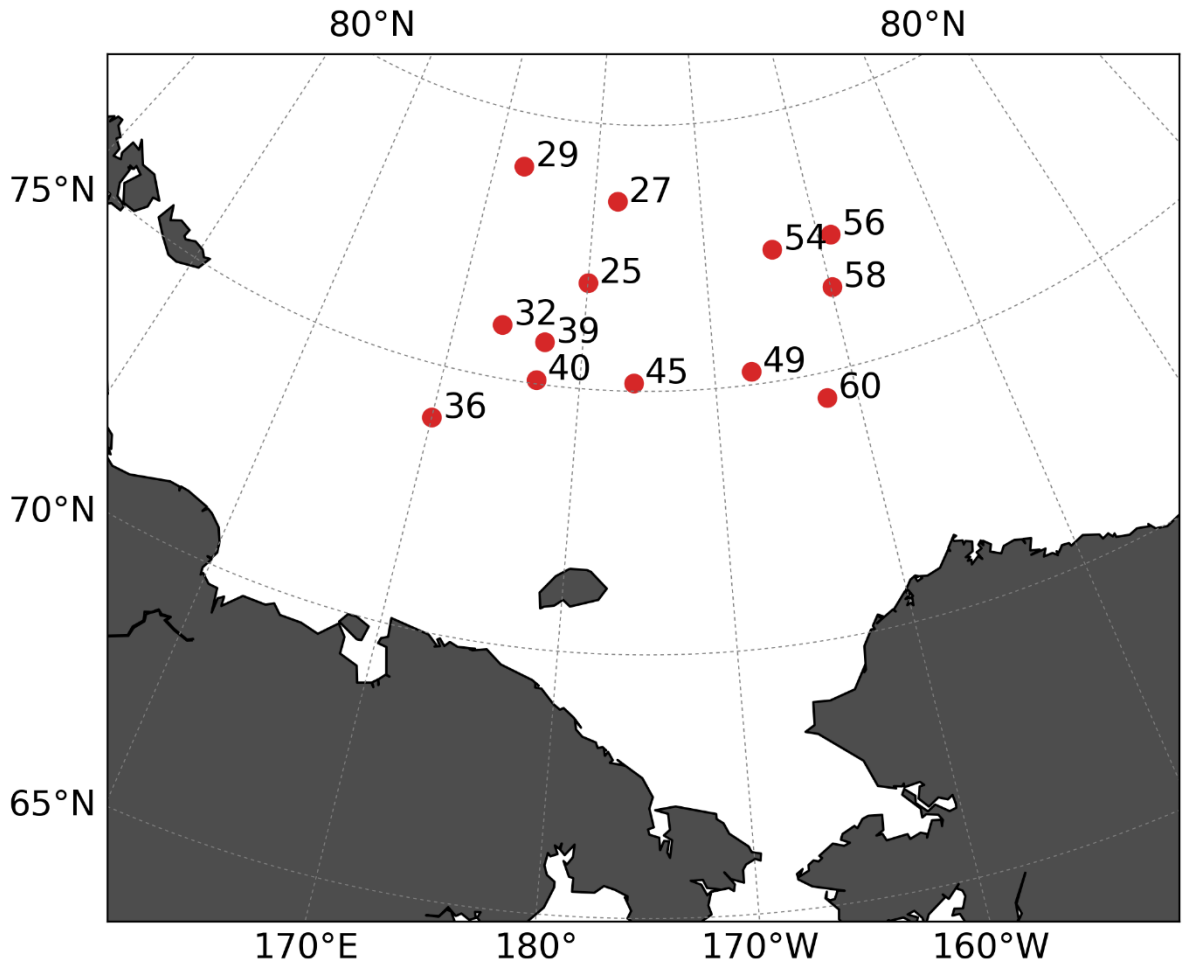

Figure 4.6.1. Zooplankton sampling stations for incubation

Table 4.6.1. General information about zooplankton sampling and incubation

Station	Sampling time (Local)	Duration	Species	Zooplankton per bottle
25	2023.08.09 03:35	10 hrs 12 min	*Calanus glacialis* F	5
27	2023.08.12 18:02	13 hrs 20 min	*Calanus hyperboreus* F	3
		13 hrs 18 min	*Calanus glacialis* F	5
29	2023.08.14 03:13	11 hrs 47 min	*Calanus hyperboreus* F	3
		11 hrs 47 min	*Scaphocalanus magnus* F	3
32	2023.08.15 16:03	11 hrs 12 min	*Calanus hyperboreus* F	3
		11 hrs 11 min	*Metridia longa* C5-F	5
36	2023.08.16 14:55	11 hrs 48 min	*Calanus glacialis* C4	5
39	2023.08.18 03:49	10 hrs 31 min	*Calanus glacialis* F	3
		10 hrs 32 min	Chaetognaths	5
40	2023.08.20 06:36	10 hrs 58 min	*Metridia longa* C5-F	5
		10 hrs 57 min	*Paraeuchaeta glacialis* F	2
45	2023.08.21 13:01	10 hrs 29 min	*Metridia longa* C5	5
49	2023.08.22 14:33	13 hrs 57 min	Chaetognaths	3
		13 hrs 56 min	*Metridia longa* F/M	5
54	2023.08.24 11:18	10 hrs 43 min	*Themisto* spp.	3

		10 hrs 42 min	*Calanus glacialis* F	5
56	2023.08.25 04:34	10 hrs 55 min	*Calanus hyperboreus* F	3
58	2023.08.26 14:15	12 hrs 21 min	Chaetognaths	3
60	2023.08.27 10:52	11 hrs 50 min	*Calanus hyperboreus* F	3

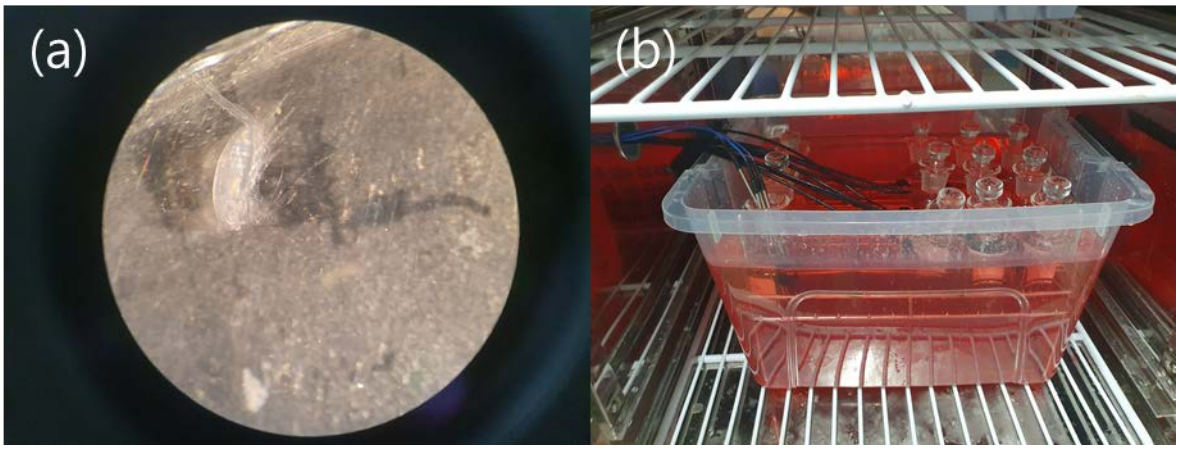

Figure 4.6.2. (a) *Metridia longa* F and (b) Respiration rate measurements in the incubator (Red fluid is eco-friendly antifreeze.)

4.6.3. References

CAMPBELL, R. G., SHERR, E. B., ASHJIAN, C. J., PLOURDE, S., SHERR, B. F., HILL, V. & STOCKWELL, D. A. 2009. Mesozooplankton prey preference and grazing impact in the western Arctic Ocean. Deep-Sea Research Part Ii-Topical Studies in Oceanography, 56, 1274-1289.

DEL GIORGIO, P. & WILLIAMS, P. 2005. Respiration in aquatic ecosystems, OUP Oxford.

IKEDA, T. 2014. Respiration and ammonia excretion by marine metazooplankton taxa: synthesis toward a global-bathymetric model. Marine Biology, 161, 2753-2766.

STEINBERG, D. K. & LANDRY, M. R. 2017. Zooplankton and the Ocean Carbon Cycle. Ann Rev Mar Sci, 9, 413-444.

4.7. Fisheries and Ichthyoplankton

Jee-Hoon Kim and Jeong-Hyun Kim

Division of ocean science, Korea Polar Research Institute, Korea (jeehoonkim@kopri.re.kr)

4.7.1. Introduction

Arctic ecosystems are changing rapidly, with potential consequences for northern species (Reist et al., 2006; Wassman et al., 2011) and human communities that rely on hunting and fishing (Ford et al.,2010; Rosol et al., 2016). Large-scale commercial harvesting of mammals (Christensen et al., 1992; Allen and Keay, 2006) and fish (Iversen, 1934) already occurs adjacent to the Arctic Ocean. The harvesting potential of marine sub-Arctic regions is predicted to increase with global warming (Cheung et al., 2011). Some species currently targeted in fisheries in these regions may expand into the Arctic Ocean (Hollowed et al., 2013). In addition, currently unexploited species may become harvestable, either in conventional fisheries or in new fisheries, as technology develops (e.g. zooplankton harvest; Grimaldo et al., 2010; Nicol et al., 2012) or because of marine bioprospecting (Svenson, 2012). Also, new species are emerging in these areas, either as a result of artificial introduction or bio-invasion.

Despite the ecological significance of harvestable marine resources, our knowledge on Arctic ichthyoplankton, and fish are still insufficient in the high-latitude Arctic Ocean because of the harsh sea ice conditions that limit access. In particular, few studies have been conducted around the East Siberian Sea in the Pacific sector of Arctic Ocean while most of studies were focused on the sub-Arctic waters of the northern Bering, Chukchi and Beaufort Seas (Falardeau et al., 2014; De Robertis et al., 2017; Randall et al., 2019). The aim of this study was to describe the communities of harvestable marine resources such as ichthyoplankton and fish in the northern Bering Strait, Chukchi Sea, and East Siberian Sea in summer. This result can provide the further knowledge to understand the variation in the species of fishes, as well as the ecology of Ichthyoplankton in the Arctic Ocean.

4.7.2. Material and methods

All samples were collected during an oceanographic cruise on-board during the Korean research ice breaker R/V ARAON expedition (ARA14B; August 1th to 31th in 2023).

Ichthyoplankton samplings were carried out going to the Central Arctic Ocean across the Bering strait, Chukchi Sea, and East Siberian Sea (Figure 4.7.1).

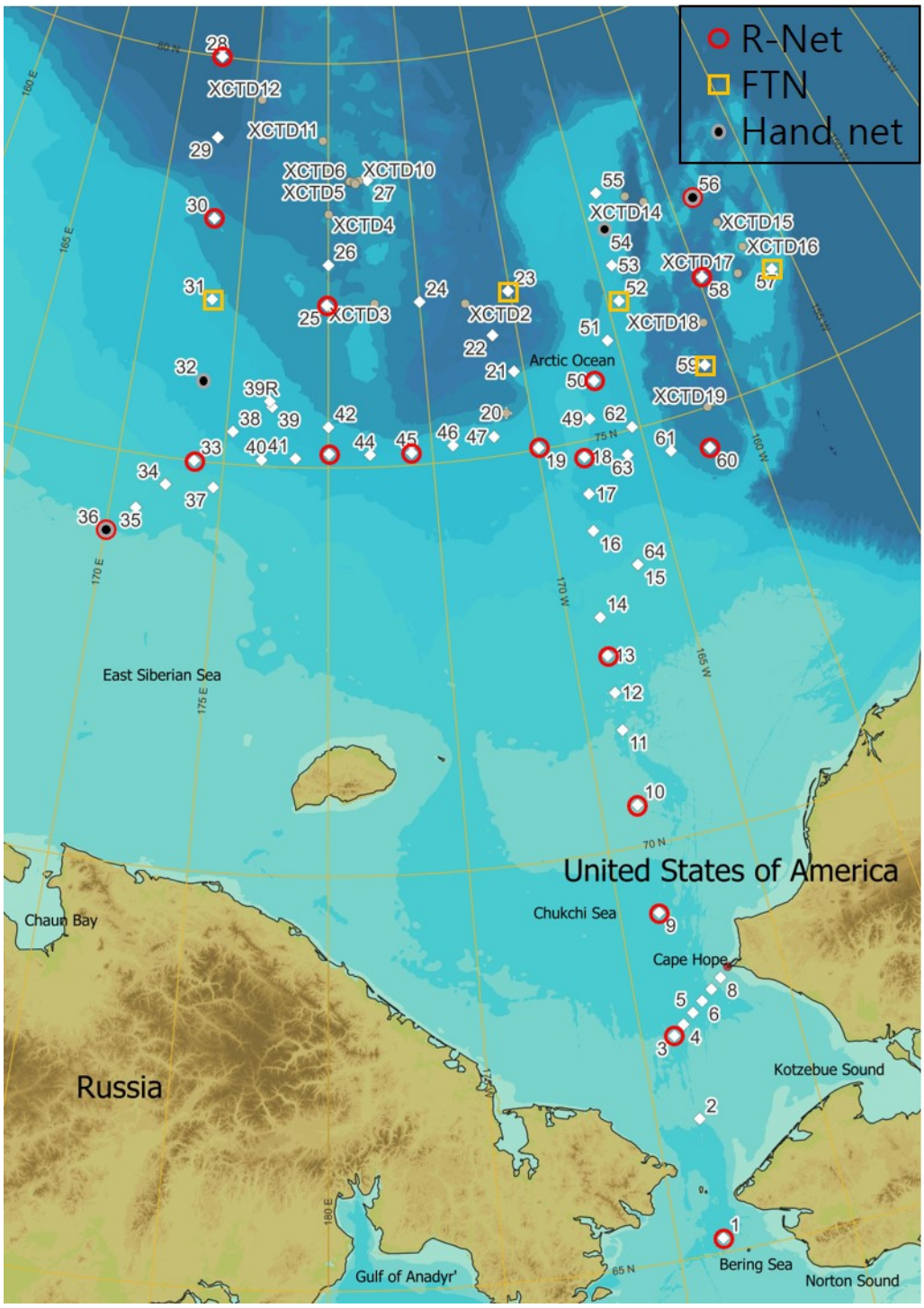

Figure 4.7.1. Study area and sampling stations on the bathymetry in the Arctic Ocean (See Table 4.7.1 ~ 4.7.3 for details).

Ichthyoplankton were collected using a R net (Rectangular net, 505 μm mesh) and frame trawl net (1 mm mesh) at all stations (Figures 4.7.1 and 4.7.2). Fish was collected using a hand net (Figure 4.7.3) and Fish pot. The nets were obliquely hauled with a speed of 60 m min^{-1} within the 500 m of water column. In the shallow stations below 200 m depth, the net was towed from 10 m above bottom to the surface. Tow speed and duration were about 2 – 3 knots and 20 – 30 min, respectively. The net depth was decided associated with the depth of sound scattering layers collected by scientific echosounder (EK80). The number of R net hauls was 18 and frame trawl net was 5 in this year (Tables 4.7.1; 4.7.2). The volume of seawater filtered was estimated from flow meter measurements. Ichthyoplankton from both ring net and frame trawl net was immediately sorted on the eyes and transferred into 20 ml vial and preserved in 95% ethyl alcohol. And then left samples were split from ½ with a Folsom plankton splitter (Van Guelpen et al., 1982) into sub-samples. Half of samples were fixed and preserved with 95% ethyl alcohol for quantitative analyses and the other half samples were stored with -20℃ refrigerator for the post analysis. The number of hand net survey was 4, and one fish sample were obtained from Fish pot survey in St. 36 (Tables 4.7.3). Fish samples were fixed and preserved with 95% ethyl alcohol and the sub-samples were stored with -20℃ refrigerator for the post analysis.

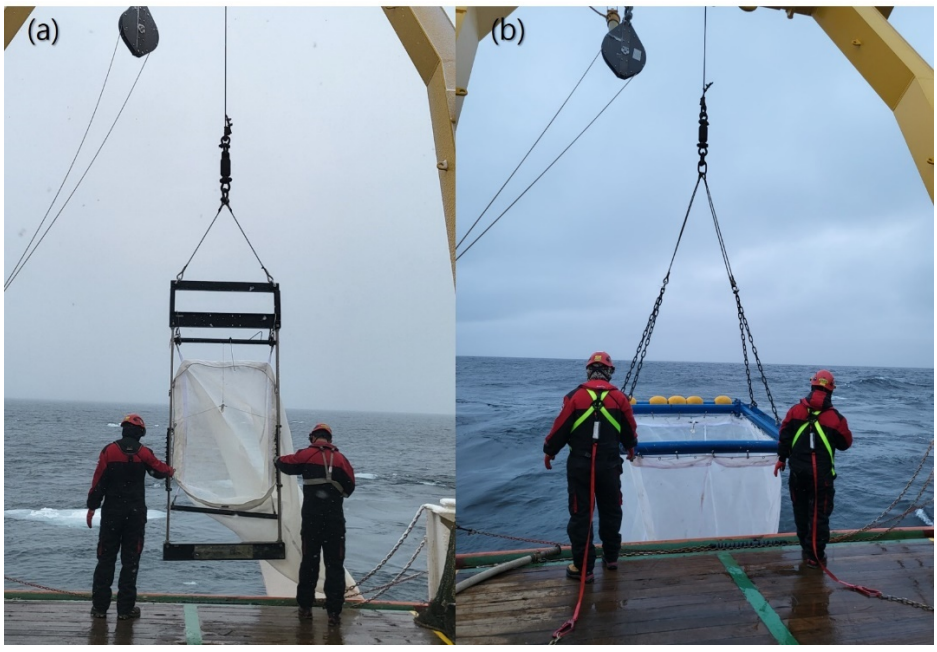

Figure 4.7.2. Ichthyoplankton sampling with Rectangular net (a) and Frame Trawl net (b)

Figure 4.7.3. Fish sampling with hand net on the Araon

Table 4.7.1. Information of Rectangular Net survey during ARA14B

St. No.	Date (UTC)	Time (UTC)	Start Lat.	Start Lon.	Depth	Cast Depth	Angle
1	03-Aug-23	5:49 - 5:58	65° 10.40770' N	168° 41.44783' W	50	65	45°
3	03-Aug-23	23:31 - 23:38	67° 40.20837' N	168° 57.60016' W	50	65	45°
9	04-Aug-23	18:10 - 18:15	69° 10.04935' N	168° 39.99080' W	50	65	45°
10	05-Aug-23	2:59 - 3:06	70° 30.00088' N	168° 39.99625' W	30	50	45°
13	05-Aug-23	16:39 - 16:42	72° 21.69642' N	168° 39.54263' W	54	60	45°
18	06-Aug-23	23:05 - 23:17	74° 48.08870' N	167° 53.96924' W	193	240	45°
25	09-Aug-23	11:47 - 12:00	77° 00.19333' N	179° 55.21326' E	1979	200	45°
28	14-Aug-23	0:17 - 0:57	79° 59.93739' N	172° 24.00506' E	2700	1000	45°
30	15-Aug-23	0:29-1:22	77° 59.93968' N	173° 11.83116' E	1132	1300	45°
33	16-Aug-23	9:53 - 10:32	75° 00.00771' N	173° 36.00935' E	146	180	45°
36	16-Aug-23	23:14 - 23: 25	73° 59.55852' N	170° 12.17432' E	47	50	45°
43	21-Aug-23	5:38 - 6:52	75° 09.85097' N	179° 58.05071' W	538	600	45°
45	21-Aug-23	21:22 - 22:06	75° 08.99858' N	175° 59.99999' W	323.6	360	45°
48	22-Aug-23	23:46 - 0:27	75° 00.34148' N	169° 45.43210' W	243	300	45°
50	23-Aug-23	13:02 - 13:38	75° 39.88330' N	166° 39.19778' W	282	250	45°
56	25-Aug-23	14:54 - 15:25	77° 28.43412' N	158° 45.50170' W	1311	500	45°
58	27-Aug-23	1:26 - 2:01	76° 29.64613' N	159° 51.53142' W	2070	800	45°
60	27-Aug-23	21:40 - 22:22	74° 30.98885' N	162° 09.39286' W	1595	1000	45°

Table 4.7.2. Information of Frame trawl Net survey during ARA14B

St. No.	UTC Date	UTC Time	Start Lat.	Start Lon.	Depth	Cast Depth	Angle
23	08-Aug-23	10:56 - 11:09	76° 57.75555' N	169° 52.30132' W	2212	187	50°
31	15-Aug-23	10:12 - 11:44	76° 59.99145' N	173° 35.96283' E	737	1000	50°
52	24-Aug-23	2:18 - 3:12	76° 35.00128' N	164° 30.31234' W	558	1100	50°
57	26-Aug-23	6:54 - 7:51	76° 18.18866' N	156° 13.43792' W	717	1150	50°
59	27-Aug-23	10:58 - 11:41	75° 29.39063' N	161° 08.26267' W	2063	500	50°

Table 4.7.3. Information of Hand Net survey during ARA14B

St. No.	UTC Date	UTC Time	Start Lat.	Start Lon.	Sampling depth (m)
32	16-Aug-23	0:42 - 2:00	76° 01.18834' N	173° 40.21147' E	0
36	17-Aug-23	7:47 - 9:50	73° 59.14530' N	170° 21.13269' E	0
54	24-Aug-23	20:06 - 22:14	77° 27.81381' N	164° 00.85417' W	0
56	25-Aug-23	16:18 - 17:42	77° 29.98545' N	158° 50.88318' W	0

4.7.3. Preliminary results and discussion

The samples from net catches were immediately preserved in frozen at –20 °C for the post analysis. 43 fish samples were collected using hand nets (Figure 4.7.4), one fish sample was collected by fish pot (Figure 4.7.5). Identification is important for the ecological monitoring of Arctic marine populations whether commercially exploited or not, as well as it is fundamental as it integrates ontogeny in phylogenetic studies. Identification of ichthyoplankton and fish will be processed in the laboratory. In addition, Arctic cod was observed in the both northern Chukchi Shelf and East Siberian Sea. During this year cruise (ARA14B), we have sampled ichthyoplankton and fish in the spatially wider regions than those in the last year. We expect these sampled could support to give a better knowledge to understand the spatial distribution of ichthyoplankton community in the Arctic Ocean.

Figure 4.7.4. Fish sample by hand net

Figure 4.7.5. Fish sample by fish pot

4.8. Benthic organism

Jee-Hoon Kim

Division of ocean science, Korea Polar Research Institute, Korea (jeehoonkim@kopri.re.kr)

4.8.1. Introduction

The western Arctic shelf is characterized by high productivity, rich benthic communities, and tight benthic-pelagic coupling when compared on a pan-Arctic scale (Grebmeier et al., 2006). This is particularly true for the Chukchi Sea shelf, where macroinfaunal biomass can accumulate up to 50–100 gCm-2 (Feder et al., 2007). In the western Arctic shelf regions where these benthic communities are particularly rich, they provide important feeding grounds for bottom-feeding marine mammals. This high biomass is the consequence of tight pelagic–benthic coupling, specifically because of a lack of significant grazing of the primary production in the water column, resulting in large amounts of organic material settling onto the seafloor.

Despite the ecological significance of benthic faunal communities, our knowledge on Arctic benthos are still insufficient in the high-latitude Arctic. In particular, few studies have been conducted around the East Siberian Sea in the Pacific sector of Arctic Ocean while most of studies were focused on the sub-Arctic waters of the northern Bering, Chukchi and Beaufort Seas (De Robertis et al., 2017; Randall et al., 2019). The aim of this study was to describe the communities of harvestable marine benthos in the northern Bering Strait, Chukchi Sea, and East Siberian Sea in summer. This result can provide the further knowledge to understand the variation in the species of fishes, as well as the ecology of benthos in the Arctic Ocean.

4.8.2. Material and methods

All samples were collected during an oceanographic cruise on-board during the Korean research ice breaker R/V ARAON expedition (ARA13B; Auguest 1th to 31th in 2023). Benthos samplings were carried out using a dredge going to the Central Arctic Ocean across the Chukchi Sea and the East Siberian Sea (Figure 4.8.1).

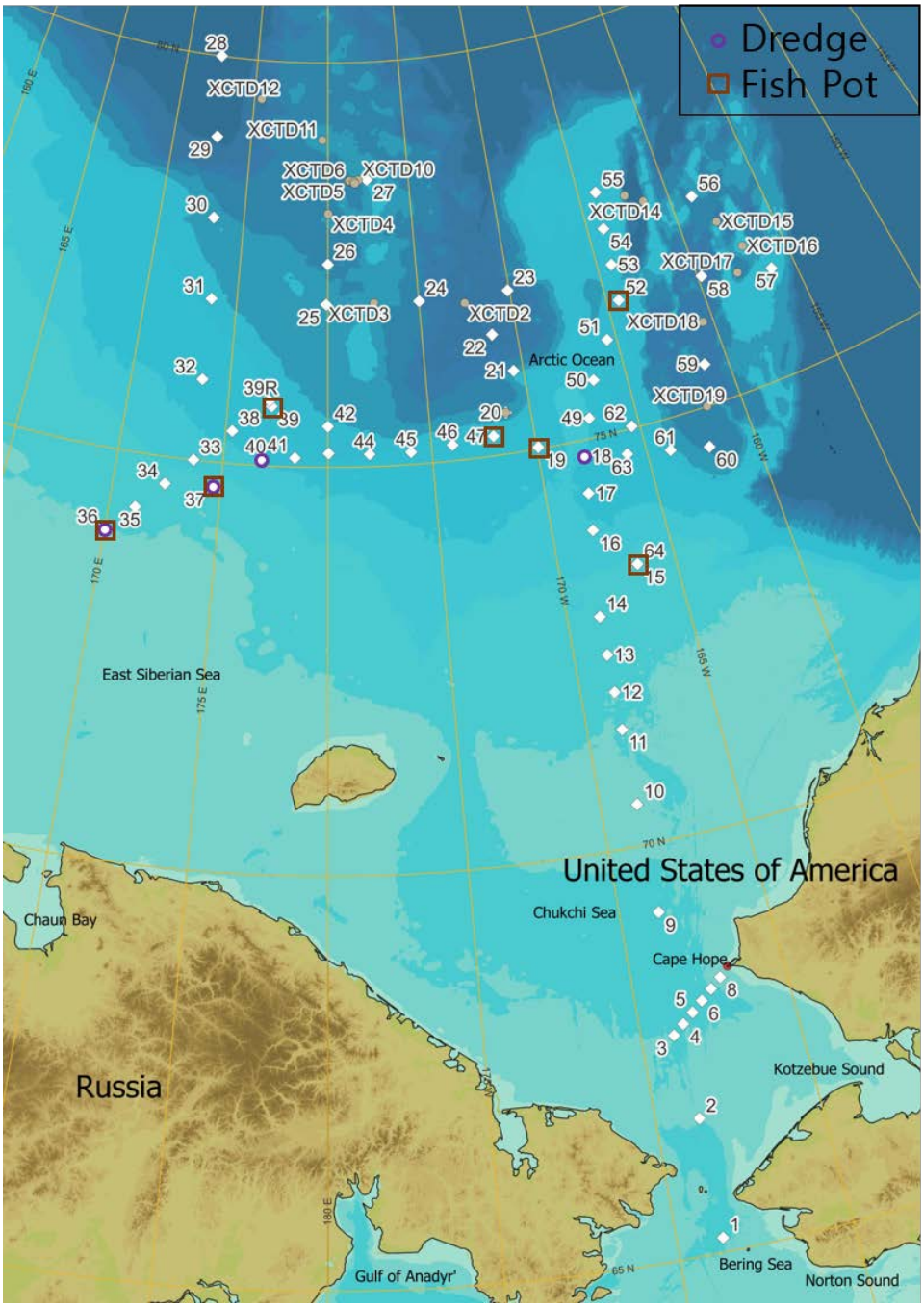

Figure 4.8.1. Study area and Benthos sampling stations in the Arctic Ocean (See Table 4.8.1 - 4.8.2 for details).

Benthos samples were collected using a Dredge (3 cm mesh) and Bite trap (2 cm mesh) at all stations (Figures 4.8.1). The dredge was hauled with a speed of 60 m min-1 with 2 knots on the sea floor. Tow speed and duration were about 2 – 3 knots and 30 – 60 min, respectively. The number of dredge survey was 4 and Fish pot survey was 7 in this year (Tables 4.8.1 and 4.8.2). Benthos samples from both dredge and bite trap were immediately sorted on the eyes

and transferred into 100 ml or 500ml vial and preserved in 95% ethyl alcohol. And then sub-samples were stored with -20oC refrigerator for the post analysis.

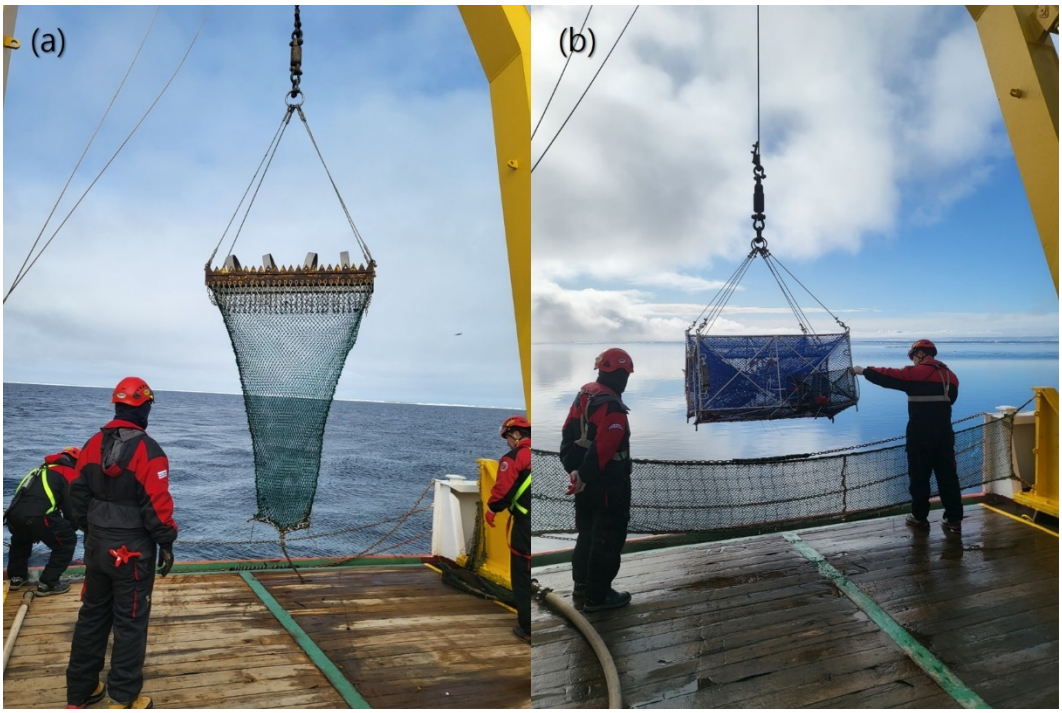

Figure 4.8.2. Benthos sampling with Dredge (a) and Fish pot (b)

Table 4.8.1. Sampling locations of Dredge during ARA14B

St. No.	UTC Date	UTC Time	Start Lat.	Start Lon.	Sampling depth (m)
18	07-Aug-23	0:53 - 1:35	74° 51.94472' N	168° 33.15705' W	168m
36	17-Aug-23	0:20 - 0:42	73° 59.45654' N	170° 12.59105' E	46m
37	17-Aug-23	20:27 - 20:50	74° 41.60378' N	174° 36.92950' E	70m
40	20-Aug-23	14:54 - 15:37	75° 03.69430' N	176° 45.17727' E	206m

Table 4.8.2. Information of Fish pot during ARA14B

St. No.	UTC Date	UTC Time	Start Lat.	Start Lon.	Sampling depth (m)
36	17-Aug-23	4:40 - 6:56	74° 00.23999' N	170° 09.83219' E	46m
37	17-Aug-23	21:44 - 23:52	74° 41.51082' N	174° 37.45688' E	70m
39	20-Aug-23	1:36 - 3:57	75° 48.19663' N	177° 03.96697' E	520m
47	22-Aug-23	15:29 - 17:58	75° 14.09979' N	172° 00.50877' W	490m
48	23-Aug-23	0:46 - 3:08	74° 58.78849' N	169° 49.50694' W	242m
52	24-Aug-23	6:49 - 9:16	76° 34.26769' N	164° 26.96722' W	553m
64	29-Aug-23	9:59 - 18:05	73° 24.45275' N	166° 29.67693' W	72m

4.8.3. Preliminary results and discussion

Benthic macrofaunal communities in the Chukchi Sea exhibit high density and biomass in the shallow waters of the region. Figure 4.8.3 – 4.8.4 show the benthos sampled by dredge and bite trap. Various benthos such as red crab, conch, and shellfish were collected. Identification is important for the ecological monitoring of Arctic marine populations whether commercially exploited or not, as well as it is fundamental as it integrates ontogeny in phylogenetic studies. Identification of benthos will be processed in the laboratory. In addition, we have sampled red crabs in the spatially wider regions than those in the last year. We expect these data could support give a better knowledge understanding of the spatial distribution of the benthic faunal community in the Arctic Ocean.

Figure 4.8.3. Benthos samples by Fish pot in the St. 39 (a), and St. 64 (b)

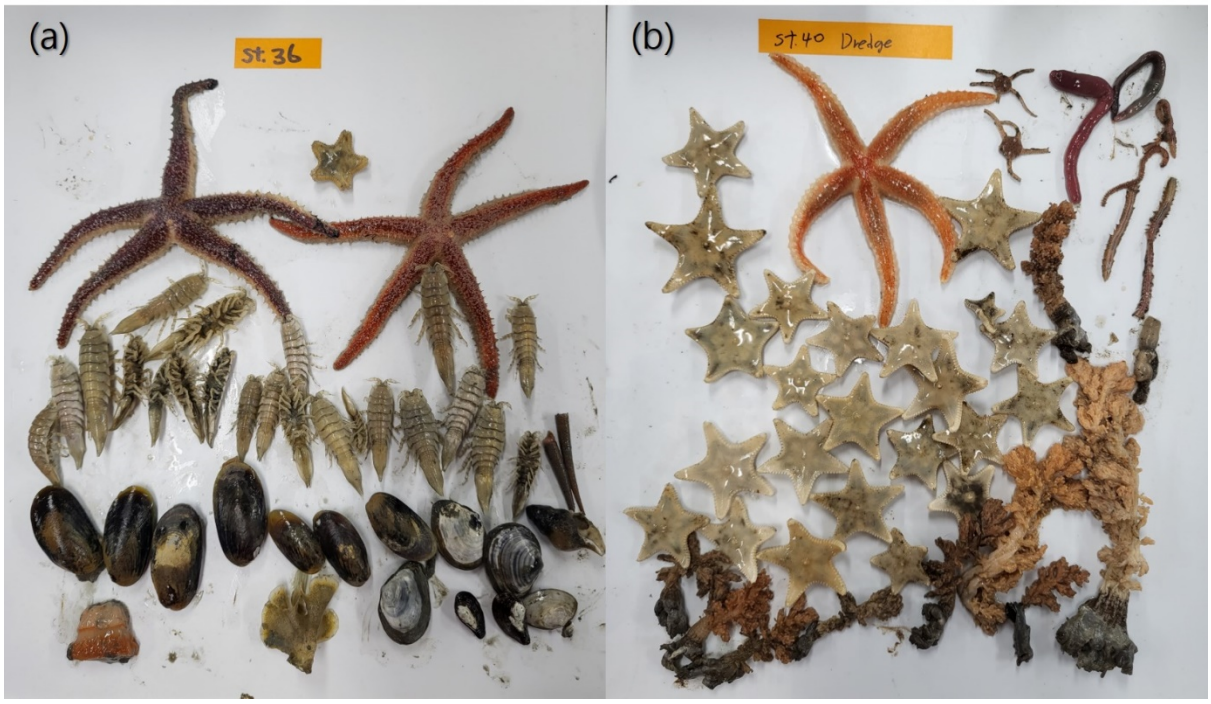

Figure 4.8.4. Benthos sample by Dredge in the St. 36 (a), and St. 40 (b)

4.9. Deep Sea Camera

Hyunggyu Choi & Eun-Jin Yang

Korea Polar Research Institute, Incheon, Republic of Korea

Email: langyu7@kopri.re.kr; ejyang@kopri.re.rk

4.9.1. Material and methods

To observe seabead environment, we operated Deep Sea Camera recording video, pictures and lighting in deep sea. And also Deep Sea Camera can mount any sensors monitor ocean data.

Fig 4.9.1. Deep Cam Survey

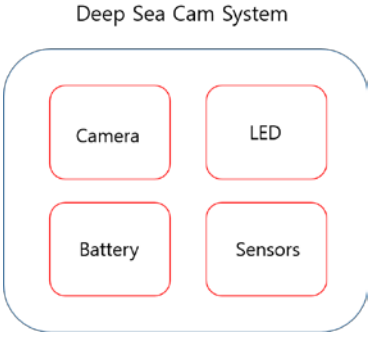

Fig 4.9.2. Deep Cam Diagram

Table 4.9.1 Deep Sea Camera information

Station	Start location		Date (UTC)		Cast depth
	Lon (Deg)	Lat (Deg)	Start	Stop	(m)
31	173.23.284E	76.57.922N	2023/08/15 12:36	2023/08/15 15:15	607
36	170.09.786E	74.00.228N	2023/08/17 02:09	2023/08/17 03:59	47
39R	177.03.296E	75.48.106N	2023/08/19 22:19	2023/08/20 00:47	518
47	171.58.257W	75.14.453N	2023/08/22 10:06	2023/08/22 12:30	505
52	164.26.768W	76.34.226N	2023/08/24 04:03	2023/08/24 06:36	553
57	156.21.428W	76.15.935N	2023/08/26 08.16	2023/08/26 10:48	695

4.9.2. Specification

Deep Sea Cam consists of housings and a frame. Camera module and LED module are able to use in housing. Deep Sea Cam collects data that kinds of video, picture, timelapse etc in ocean. We developed new version components like Camera module, LED module and housing since ARA13B. Components specification is below like this.

1) Camera module

Fig 4.9.3. Camera module in Deep Sea Cam

Table 4.9.2. Camera module Specifiaction

Model	Gopro 8 Hero Black
Battery Run-time	Max about 6H (10,000 mah Battery)
Function	Video, Picture, Timelapse

2) New version Camera module

Fig 4.9.4. New Camera module in Deep Sea Cam

Table 4.9.3. New version Camera module Specifiaction

Model	Transcend DP20(DrivePro20)
Battery Run-time	Max about 8H (with 5,000 mah Battery)
Function	Video

3) LED module

Fig 4.9.5. LED module in Deep Sea Cam

Table 4.9.4. LED module Specifiaction

Model	Cutomize development
Battery Run-time	Max about 4H (8,000 mah Battery)

4) New version LED module

Fig 4.9.6. New version LED module in Deep Sea Cam

Table 4.9.5. New versionLED module Specifiaction

Model	FALCONLIGHT LZ-01 PLUS
Battery Run-time	Max about 4.5H (4,500 mah Battery)

5) Housing

Fig 4.9.7. Housing in Deep Sea Cam

Table 4.9.6. Housing Specifiaction

Dimension (D X L) (mm)	125 X 330
Weight	About 20kg
Depth	Max about 5,000m

6) New version Housing

Fig 4.9.8. New version Housing in Deep Sea Cam

Table 4.9.7. Housing Specifiaction

Dimension (D X L) (mm)	75 X 216
Weight	About 7kg
Depth	Max about 3,000m (concluded from 2023 Test Cruise)

7) Frame

Fig 4.10.6. Frame in Deep Sea Cam

Table 4.10.5. Frame Specifiaction

Dimension (W X D*L) (mm)	1,400 X 1,400 X 1,800
Weight	About 400kg
Depth	Max about 5,000m
Max Quantity of Housing mounted (EA)	8EA (recommended : Old ver housing) *6EA(Old ver)+2EA(New ver) during ARA14B

4.9.3. Preliminary results

St. 31

St. 52

St. 52

St. 57

St. 57

St. 47

Chapter 5. Biological Acoustics(EK80)

Dong Ha Kang

Gyeongsang National University, Tongyeong, Republic of Korea

E-mail: rkdehdgk789@naver.com

Arctic warming has profoundly affected marine ecosystems in the Arctic Ocean from plankton to predators. Understanding the mechanisms by which climate variability impacts multiple trophic levels is critical for determining the Arctic marine ecosystems response to climate change. However, most of long-term studies in the polar marine ecosystems are limited to observing lower trophic levels (i.e. phytoplankton) by satellite remote. Studies are scarce and sporadic on the spatio-temporal variability of mid- to high-trophic levels, which form important links in the food web. It is still unclear, how climate change affects mid- to high-tropic levels in the Arctic Ocean and trophic coupling. Thus, the new strategies are required to develop further insights into how multiple trophic levels have responded to rapid environmental change.

The aim of this research is to observe the long-term variability of mid- to high-trophic levels from zooplankton to cetacean in the Arctic Ocean through the simultaneous observation using the fisheries and bioacoustic systems. The systems will enable us to acquire the essential data on monitoring the Arctic marine ecosystems and sustained observations would be key to the understanding of the causes and consequences of Arctic marine ecosystems changes related to climate change.

To improve our knowledge of this biological hotspot in the Arctic Ocean, the multidisciplinary expeditions were conducted by the icebreaker Araon in August 2023. In the current work, we characterize the acoustic scattering layers for pelagic marine organism using the various acoustic systems (EK 80) in the various habitats in the western Arctic Ocean, verify the essential environmental variables that can be responsible for zooplankton and fish spatial distribution, and linkages between the major zooplankton and fish abundance and environmental conditions in the different regions.

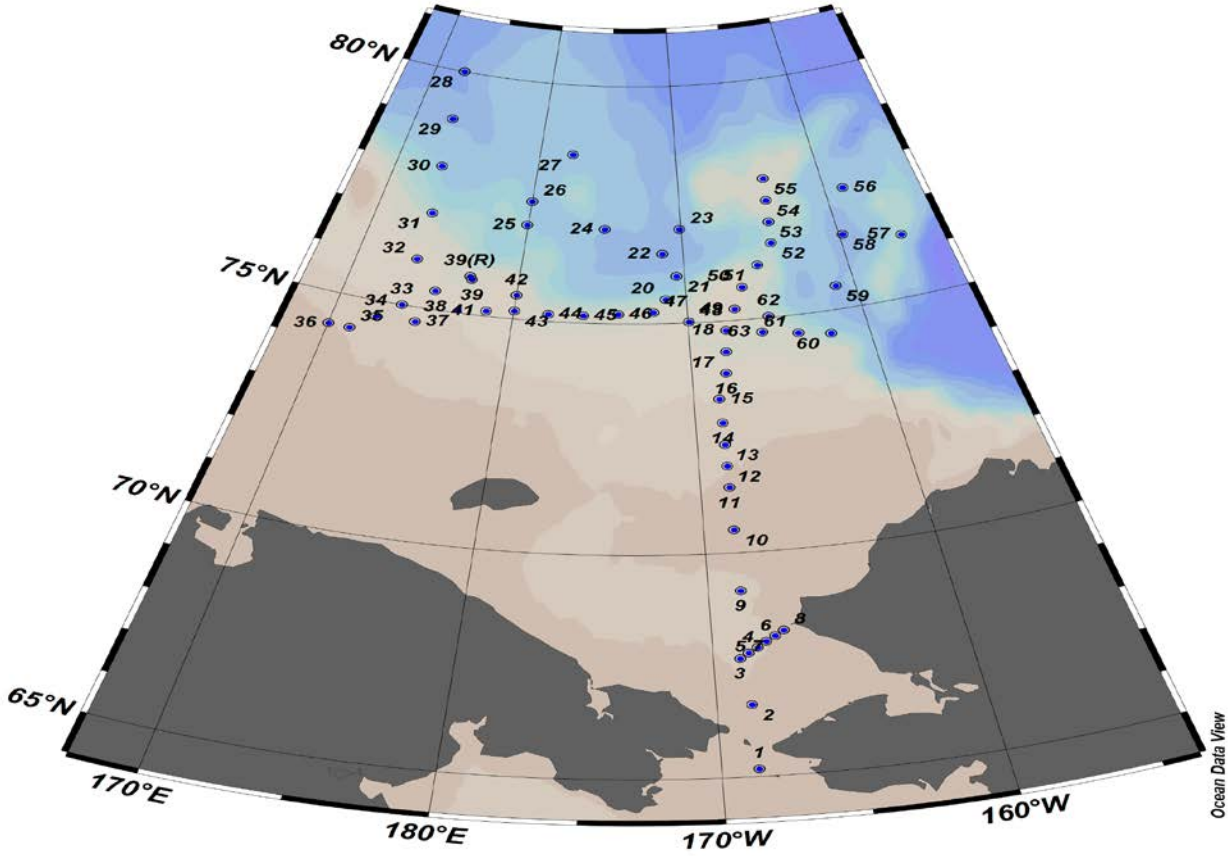

Figure 5.1.1. Study area showing the stations with processed EK80 data during the ARA14B cruise.

5.1. Ship-based acoustic system

Dong Ha Kang (rkdehdgk789@naver.com)

5.1.1. Introduction

Ship-based acoustic system and net samplings are useful complementary methods to observe spatial and temporal distribution of mid-trophic level in the water column. They make up for their own weak points each other and known as the best way to observe the pelagic marine organisms in the existing observation methods. Acoustic surveys have been widely conducted to determine the spatial distribution of zooplankton and fish abundance and their ecology in the Arctic Ocean since the early 1970's. Target identification methods using multi-frequency echo sounders are often used for identifying zooplankton and fish in biomass surveys and in zooplankton ecology studies and also to observe the spatial and temporal

distribution and abundance variation of zooplankton and fish.

Acoustic and biological samplings were undertaken to understand the ecology of key zooplankton and fish how the environmental changes affect their behavior and distribution in the Arctic Ocean during the summer. The overall purposes of acoustic observation are:

To collect acoustic data to accompany all stations, transects, and net tows during the survey

To determine the horizontal and vertical distribution of relative abundance of zooplankton and fish

To understand the essential environmental factors controlling the distribution of zooplankton and fish

5.1.2. Materials and methods

5.1.2.1. Acoustic data collection and processing

The EK80 was run throughout ARA14B to collect information on the horizontal and vertical distribution of zooplankton and to derive estimates of zooplankton and fish biomass in the Arctic Ocean and to contribute data from transects around the western Arctic Ocean (Fig. 5.1). Acoustic data (EK80.raw) was collected during the whole survey period when the ship was run along the transect periods between stations, as well as she was stopped at each station for the biological, chemical, and physical observations.

EK80.raw data files were logged to the workstation (192.168.0.120), which is backed up at the extra hard drives. All raw data were collected to 1000 m. The echosounder PC and the EK80 workstation are integrated into the ship's LAN with Seatex Seapath 200 (KONGSBERG) for the ship motion and GPS information. All raw data were saved in a general folder D:/ARA14B_EK80/raw, all echolog data were also saved in the extra hard drives. All files were prefixed with ara13b. Calibration for the echosounders (38, 120, and 200 kHz) was not available during the cruise, thus the recent calibration variables were applied to echo sounder (C:/Users/Public/Documents/Simrad/EK80/Calibration). The EK80 system was calibrated on June before cruise near Pohang harbor in the East Sea of Korea.

Table 5.1.1. EK80 system variables

Category	Parameters		
Frequency [kHz]	38	120	200
Beam type	Split		
Electric Power [w]	2000	250	150
Beamwidth Along ship [deg]	6.93	5.66	6.79
Beamwidth Athwart ship [deg]	6.78	5.72	6.80
Transmitted Pulse duration [ms]	1.024	1.024	1.024
Sa correction [dB]	-0.45	-0.14	-0.19
Transducer gain [dB]	26.28	26.07	25.47
Gain adjusts (dB)	0.08	0.92	-0.13
RMS error (dB)	0.1	0.26	0.37
Ramping	fast	fast	Fast
Recording range (m)	1000	1000	1000
Environmental variables (before St.13)	8.0 oC / 29.5 psu/ 8.0 pH/ 1476.0 m/s		
Environmental variables (from St. 13)	0.0 oC / 28.5 psu/ 8.0 pH/ 1440.8 m/s		

Table 5.1.2. EK80 recording information at stations

Station	Start location		Date (UTC)		Water
	Lon	Lat	Start	Stop	depth (m)
1	-168.691	65.17357	2023-08-03 3:00	2023-08-03 6:09	50
2	-168.688	66.62999	2023-08-03 13:28	2023-08-03 15:46	44
3	-168.96	67.67043	2023-08-03 20:51	2023-08-03 23:47	50
4	-168.602	67.78281	2023-08-04 0:44	2023-08-04 1:51	50
5	-168.236	67.89798	2023-08-04 2:36	2023-08-04 3:25	58
6	-167.867	68.01308	2023-08-04 4:34	2023-08-04 6:15	52
7	-167.495	68.12825	2023-08-04 7:16	2023-08-04 8:16	49
8	-167.122	68.24208	2023-08-04 9:19	2023-08-04 10:53	43
9	-168.667	69.16675	2023-08-04 15:50	2023-08-04 18:20	50
10	-168.667	70.5	2023-08-05 0:55	2023-08-05 3:15	39

11	-168.667	71.43015	2023-08-05 7:47	2023-08-05 9:12	49
12	-168.669	71.89511	2023-08-05 11:26	2023-08-05 11:48	50
13	-168.663	72.35925	2023-08-05 14:20	2023-08-05 16:49	55
14	-168.658	72.83374	2023-08-05 20:20	2023-08-05 20:45	57
15	-168.695	73.34675	2023-08-06 3:16	2023-08-06 5:37	70
16	-168.2	73.88856	2023-08-06 10:23	2023-08-06 13:21	181
17	-168.05	74.34502	2023-08-06 16:18	2023-08-06 16:52	253
18	-167.898	74.80054	2023-08-06 19:35	2023-08-06 23:31	193
19	-169.937	75.02066	2023-08-07 4:24	2023-08-07 4:52	255
20	-171.215	75.50696	2023-08-07 8:11	2023-08-07 9:47	1285
21	-170.5	76.00007	2023-08-07 12:52	2023-08-07 17:07	1313
22	-171.302	76.48104	2023-08-07 20:46	2023-08-08 0:30	2213
23	-170.101	76.99015	2023-08-08 4:33	2023-08-08 11:18	2212
24	-174.996	76.99992	2023-08-08 19:50	2023-08-08 23:43	2010
25	179.9051	77.00459	2023-08-09 7:31	2023-08-09 12:07	1079
26	-179.995	77.5019	2023-08-09 14:58	2023-08-09 21:40	1463
27	-177.586	78.54082	2023-08-12 22:26	2023-08-13 2:09	1008
28	172.4018	80.00019	2023-08-13 16:55	2023-08-14 1:06	2700
29	172.8003	79.00001	2023-08-14 6:13	2023-08-14 13:19	2561
30	173.1977	77.99708	2023-08-14 18:45	2023-08-15 1:27	1132
31	173.6025	76.99978	2023-08-15 6:22	2023-08-05 15:33	739
32	173.6	75.99982	2023-08-15 20:45	2023-08-16 2:00	264
33	173.6026	75	2023-08-16 7:20	2023-08-16 10:43	147
34	172.4006	74.66677	2023-08-16 13:10	2023-08-16 13:48	63
35	171.1999	74.33315	2023-08-16 16:51	2023-08-16 17:38	54
36	170.0237	74.34136	2023-08-16 20:15	2023-08-17 9:50	47
37	174.598	74.69532	2023-08-17 17:50	2023-08-18 1:59	70
38	175.2394	75.39991	2023-08-18 5:40	2023-08-18 6:06	230
39	177.1899	75.73423	2023-08-18 10:10	2023-08-18 12:29	499
39R	177.0451	75.79935	2023-08-19 18:38	2023-08-20 7:04	518

40	176.7993	75.0748	2023-08-20 12:02	2023-08-20 16:01	194
41	178.4203	75.10786	2023-08-20 18:27	2023-08-20 18:58	311
42	179.9936	75.50068	2023-08-20 22:58	2023-08-21 0:11	937
43	-179.966	75.17017	2023-08-21 2:11	2023-08-21 9:14	538
44	-178	75.15074	2023-08-21 14:11	2023-08-21 15:16	540
45	-176	75.1515	2023-08-21 17:57	2023-08-21 22:17	326
46	-173.988	75.19508	2023-08-22 1:04	2023-08-22 2:00	363
47	-171.972	75.24046	2023-08-22 6:34	2023-08-22 18:08	505
48	-169.94	75.02094	2023-08-22 20:58	2023-08-23 3:16	256
49	-167.269	75.24587	2023-08-23 6:45	2023-08-23 7:21	186
50	-166.638	75.69102	2023-08-23 9:50	2023-08-23 13:46	291
51	-165.486	76.13266	2023-08-23 16:49	2023-08-23 19:12	709
52	-164.362	76.56744	2023-08-23 22:02	2023-08-24 9:39	549
53	-164.223	77.015	2023-08-24 12:14	2023-08-24 13:01	419
54	-164.116	77.46671	2023-08-24 16:07	2023-08-24 22:14	279
55	-163.971	77.92738	2023-08-25 1:09	2023-08-25 3:16	270
56	-158.741	77.49972	2023-08-25 10:32	2023-08-25 17:43	1323
57	-156.2075	76.30289	2023-08-26 1:37	2023-08-26 11:15	725
58	-159.7926	76.53554	2023-08-26 16:16	2023-08-27 2:10	2112
59	-161.1466	75.49831	2023-08-27 7:34	2023-08-27 11:46	2097
60	-162.1534	74.5158	2023-08-27 16:40	2023-08-27 22:37	1595
61	-163.918	74.61514	2023-08-28 0:47	2023-08-28 01:47	833
62	-165.3827	75.026	2023-08-28 5:45	2023-08-28 11:31	544
63	-165.91	74.7	2023-08-28 13:34	2023-08-28 13:34	406

The acoustic data was processed to validate the zooplankton distribution and biomass of predominant species using the Myriax Echoview software (Echoview 12.1)to remove the non-biological signals from surface bubbles, ice fragments, bottom, and false bottom echoes. Matlab was used to analyze the further data processes with noise-removed acoustic data to classify the acoustic signals for fish, microzooplankton, and mesozooplankton (Fig. 5.1.2). Acoustic signals were extracted within the range of 4 < Sv120-38 kHz < 20 dB corresponding

to zooplankton. The extracted acoustic signals were identified to microzooplankton and mesozooplankton with dB difference between two frequencies, Sv200-120kHz. We have checked the depth distribution of acoustic backscatter from the identified acoustic signals for fish, microzooplankton, and mesozooplankton.

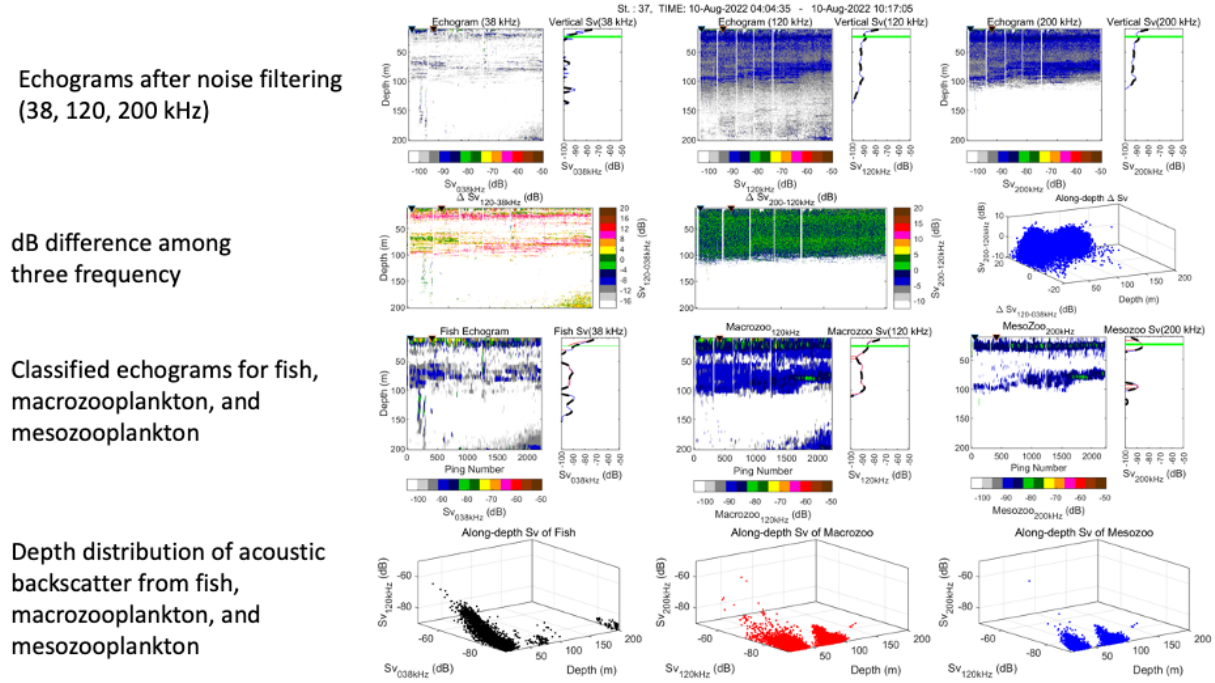

Figure. 5.1.2. Acoustic identification processes to classify the acoustic signals from fish, microzooplankton, and mesozooplankton with three frequencies (38, 120, and 200 kHz)

The nautical area scattering coefficient (NASC, m2 nmi-2) is calculated as the integral of the volume backscattering strength from 20 m to 200 m for the horizontal distribution of zooplankton and fish.

5.2. Passive acoustic monitoring

Dong Ha Kang (rkdehdgk789@naver.com)

5.2.1. Introduction

Arctic Ocean is an exclusive and remote environment, facing radical changes with sea ice reduction and sea level rise related to the ice bergs melting in the last four decades. A renewed

emphasis on its study in the Arctic Ocean has been driven in part of the basic concern with anthropogenic noise and the ecology of marine mammals because of the dramatic decline of sea ice extent in recent decades.

Passive acoustic system is widely used to observe and assess the contributions of sound sources to the ocean sound filed for marine animal conservation. It is essential to monitor ambient sound on a broad scale as well as on the local areas because many species travel long distances or maintain a wide range of seasonal habitats. Observing the ocean sound with passive acoustic system is a non-invasive and economic strategy that can identify a comprehensive assessment of ecosystem dynamics and human impact. Despite the significant amount of attention and ecological significance of underwater ambient noise, Arctic Ocean have a relatively shorter history with little attention because of the heavy sea ice conditions that limit access. The most of studies were focused in the Beaufort Sea, the Fram Strait in the Greenland Sea, northern Barents Sea, while the underwater ambient noise around the East Siberian Shelf remains poorly understood. Here, we established a mooring system to assess the underwater ambient noise in the East Siberian Shelf for the long-term observation purpose. It is convinced that the sustainable long-term observation could provide implications for the seasonal variability of underwater ambient noise as the soundscape from one of the most largely unidentified places in the Arctic Ocean.

5.2.2. Materials and methods

A passive acoustic system (MTE instruments, AURAL-M3) was recovered (ESS_I2022), and new system (MTE instruments, AURAL-M3) was deployed (ESS_I2023) on the similar location on the East Siberian Shelf (74 o 41.684’N, 174o 36.258’E) (Table 5.4.1, Figure 5.4.1). A hydrophone of passive acoustic system was programmed to record acoustic data for 10 min/0.5 h with 16-bit resolution and 32,768 Hz sampling rate. HTI-96-MIN hydrophone (High Tech Inc.) was used with gain of 18 dB and receiving voltage sensitivity of that was -165 dB re 1V/uPa with pre-amplifier. The receiving voltage sensitivity is almost flat with +- 2dB error in a frequency range of 10 Hz to 10 kHz.

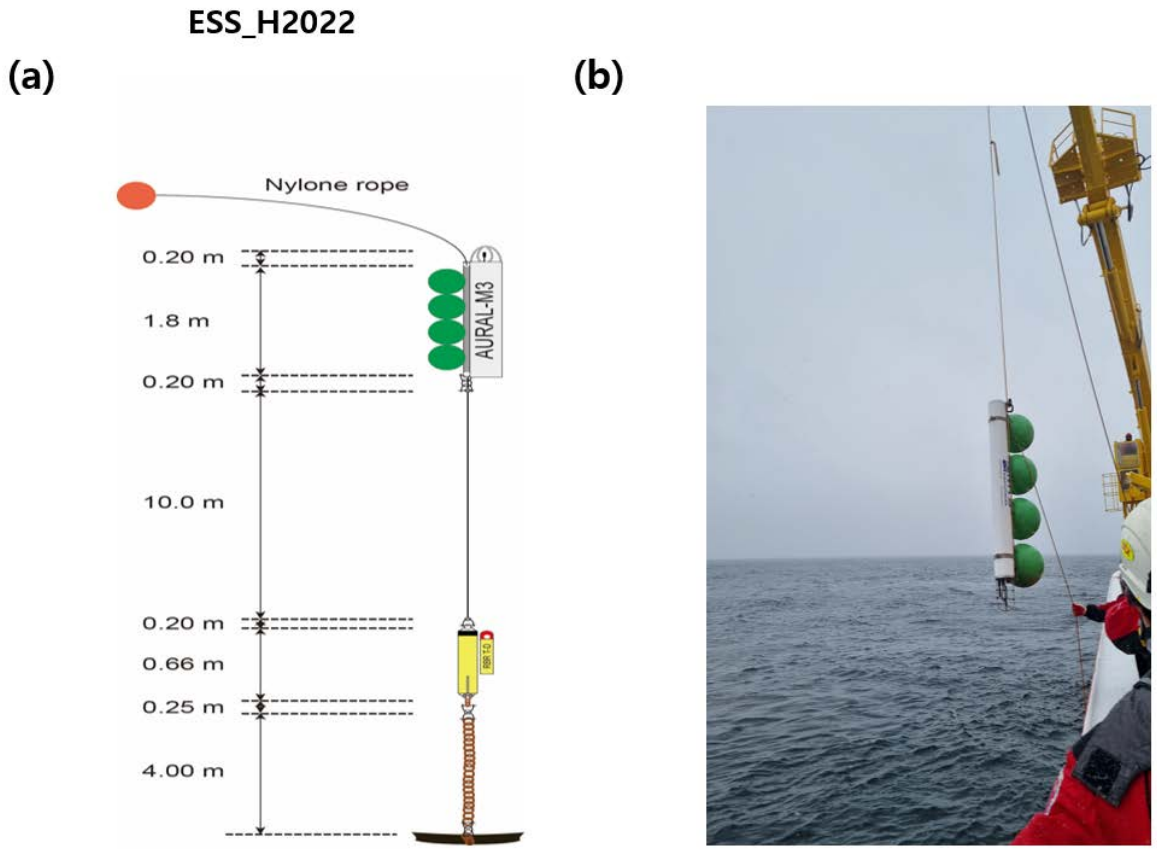

Figure 5.2.1. Mooring design and the recovery picture of ESS_H2022 during ARA14B cruise

Table 5.2.1. Recovery and deployment information of ESS_H. Recovery date and time represent the time of acoustic release on the deck after release the anchor. Deployment date and location represent the anchor drop time and position.

	Date and time (UTC)	Longitude (DM)	Latitude (DM)	Depth (m)	Equipment
Recovery	2023. 08. 17 18:15	174o 35.861'E	74o 41.693'N	69	-AURALM3 (SN:MTEAU000310LF)
Deployment	2023. 08. 18 00:41	174o 41.684'E	74 o 41.684'N	70	-AURALM3 (SN:MTEAU000300LF)

To visualize the long-observation recordings, we measured the mean power spectrum of each 10-minute audio clip with a long-term spectrogram (LTS). LTS can be used investigate

biological sounds and transient calls for separating different soundscape components. For the further process, LTS can be a input data for separating components using a periodicity-coded nonnegative matrix factorization algorithm, which is a self-learning algorithm.

Chapter 6. Particle Flux

Catherine Lalande[1], Jong Kuk Moon[1], Jeong-Hyun Kim[1,2]

1Korea Polar Research Institute, Incheon, Republic of Korea

[2]University of Science and Technology, Daejeon, Republic of Korea

Email: catherine.lalande@kopri.re.kr; jkmoon@kopri.re.kr; jeonghkim@kopri.re.kr

6.1. Mooring sediment traps

6.1.1. Objectives

Sediment traps collect particles sinking from the upper waters towards the seafloor. The sequential sediment traps deployed at the four KAMS mooring sites (KAMS1, KAMS2, KAMS4, and KAMS5) have 21 sample cups (McLane) or 26 sample cups (Nichiyu Giken Kogyo, Japan) attached on a carrousel that is programmed to rotate every 7 to 90 days, depending on the season. Sample cups are filled with seawater containing a 10% formalin solution buffered with sodium borate to preserve samples and prevent microbial remineralization of organic matter. Particles collected into the sample cups consist of algae, fecal pellets produced by copepods, and aggregates of material called marine snow. The continuous collection of these sinking particles over an annual cycle allows us to quantify the spatial and temporal variations in the export of total particulate matter, organic carbon, calcium carbonate, and biogenic silica, therefore providing a better understanding of the biological pump in the Pacific Arctic region. In addition, these time-series measurements allow us to track the timing, magnitude, and composition of the spring bloom, and to monitor the composition of the zooplankton community at the trap depth through the collection of zooplankton actively entering the sediment traps (swimmers).

6.1.2. Work at sea

Sequential sediment traps deployed in 2021 in the East Siberian Sea (KAMS 1; 100m and 320m) and at the Northwind Ridge (KAMS 4; 100m and 500m) that had not been recovered in 2022 due to heavy ice were recovered during the ARA14B cruise. Both sediment traps deployed at KAMS1 collected 26 samples, while at KAMS4 the 100 m sediment trap collected 9 samples and the 500 m sediment trap did not rotate and therefore did not collect samples.

Two sediment traps that were deployed in the Chukchi Sea (KAMS 2; 100 m and 320m) in 2022 were recovered; the 100 m sediment trap did not rotate and did not collect samples, while the 320 m sediment trap collected 4 samples. The KAMS5 mooring deployed in 2022 was not recovered due to heavy ice. However, an additional line with a sediment trap at 320 m was deployed at KAMS5. Sediment traps were also redeployed at KAMS1, KAMS2 and KAMS4. The KAMS4 mooring sites changed location to the Northwind Ridge, and only one sediment trap was deployed at 329 m instead of the two previous depths (100 m and 500 m). The sediment traps were programmed to collect particles during one (KAMS4) or two annual cycles (KAMS1, KAMS2, and KAMS5; Table 6.1.1).

Table 6.1.1. Sediment trap deployment programs at the KAMS sites.

Bottle number	KAMS1 100 m + 320 m Japan	KAMS2 100 m McLane	KAMS2 320 m Japan	KAMS4 329 m McLane	KAMS5 320 m McLane
1	2023-08-20	2023-08-23	2023-08-23	2023-08-30	2023-08-22
2	2023-09-01	2023-09-01	2023-09-01	2023-09-16	2023-09-01
3	2023-10-01	2023-10-01	2023-10-01	2023-10-01	2023-10-01
4	2023-11-01	2023-11-01	2023-11-01	2023-10-16	2023-11-01
5	2024-01-01	2024-02-01	2024-01-01	2023-11-01	2024-02-01
6	2024-03-01	2024-05-01	2024-03-01	2023-11-16	2024-05-01
7	2024-04-01	2024-06-01	2024-04-01	2023-12-01	2024-06-01
8	2024-05-01	2024-07-01	2024-05-01	2023-12-16	2024-07-01
9	2024-06-01	2024-07-16	2024-06-01	2024-01-01	2024-07-16
10	2024-06-16	2024-08-01	2024-06-16	2024-02-01	2024-08-01
11	2024-07-01	2024-08-16	2024-07-01	2024-03-01	2024-08-16
12	2024-07-16	2024-09-01	2024-07-16	2024-04-01	2024-09-01
13	2024-08-01	2024-10-01	2024-08-01	2024-05-01	2024-10-01
14	2024-08-16	2024-11-01	2024-08-16	2024-06-01	2024-11-01
15	2024-09-01	2024-12-01	2024-09-01	2024-06-16	2024-12-01
16	2024-10-01	2025-03-01	2024-10-01	2024-07-01	2025-03-01
17	2024-11-01	2025-06-01	2024-11-01	2024-07-16	2025-06-01
18	2025-01-01	2025-06-16	2025-01-01	2024-08-01	2025-06-16
19	2025-03-01	2025-07-01	2025-03-01	2024-08-08	2025-07-01
20	2025-04-01	2025-07-16	2025-04-01	2024-08-16	2025-07-16
21	2025-05-01	2025-08-01	2025-05-01	2024-08-23	2025-08-01
22	2025-06-01	2025-08-16	2025-06-01	2024-08-30	2025-08-16
23	2025-06-16		2025-06-16		
24	2025-07-01		2025-07-01		
25	2025-07-16		2025-07-16		
26	2025-08-01		2025-08-01		
27	2025-08-08		2025-08-08		

The collected samples were sealed with tape and stored at 4°C in the refrigerator until analyses at KIOST and KOPRI (example: Fig. 6.1.1).

Figure 6.1.1. Sediment trap samples collected at KAMS1-320 m

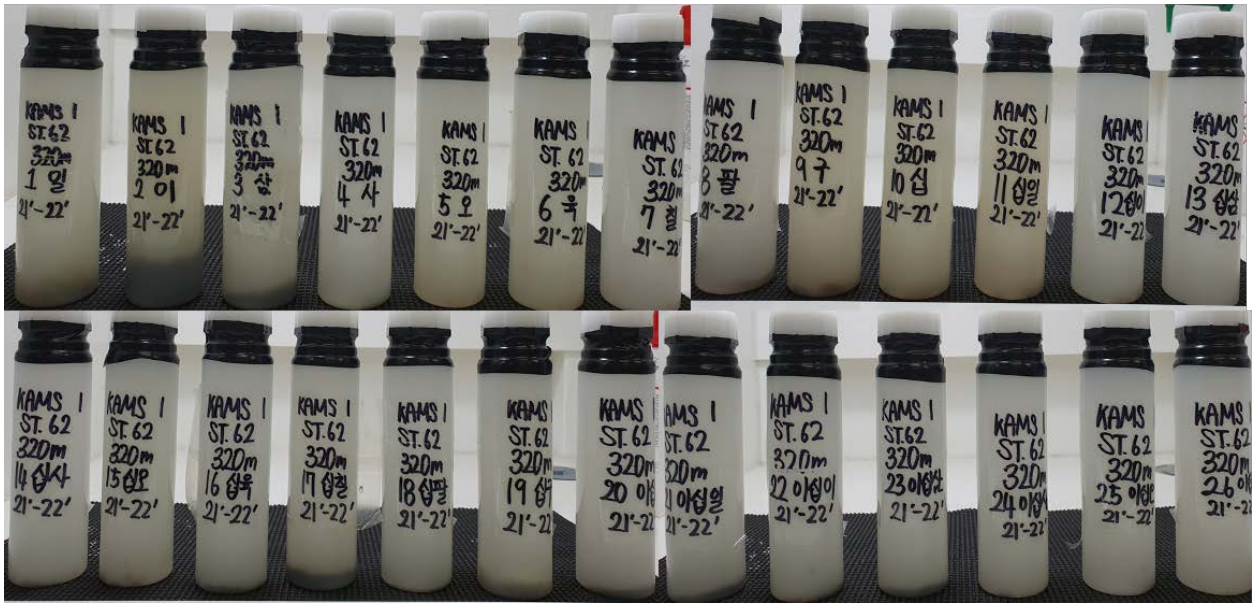

6.2. Ice camp sediment traps

6.2.1. Introduction

The ongoing decline in sea ice extent and thickness and the associated increase in sunlight transmission due to larger meltpond coverage are causing unprecedented changes in the biogeochemistry of the Arctic Ocean. These physical changes are expected to affect export fluxes differently on Arctic shelves and over the deep Arctic basins. Indeed, while a general increase in primary production and particulate organic carbon (POC) export is expected on Arctic shelves, POC export is likely to remain low above the central basins unless additional nutrients are supplied to surface waters. As export flux measurements remain very limited in the East Siberian Sea and Chukchi Borderland regions, it is unclear how the reduction in sea ice cover and increase in sunlight transmission will affect POC export in this section of the Arctic Ocean. In this context, the objectives of this project are to assess spatial variability in under-ice export fluxes of biogenic matter using short-term sediment traps deployed at the ice camp during the 2022 expedition, and to compare these results with previous flux measurements obtained at ice camps visited during the 2018, 2019, and 2022 expeditions.

6.2.2. Work at ice camp

Ten short-term cylindrical sediment traps were deployed at the ice camp from August 10 to August 12, 2023 (Fig. 1). Sediment traps were deployed under the ice at 5 m (3 traps), 10 m (3 traps), 25 m (2 traps) and 50 m (2 traps) for approximately 48 hours. Traps were filled with a formalin solution to preserve the samples during deployment. Upon recovery, subsamples (200-300 ml) were used to measure total and size-fractionated chlorophyll a (chl a) fluxes. In addition to chl a fluxes, total particulate matter, particulate organic carbon and nitrogen, phytoplankton, and zooplankton fecal pellet fluxes will be measured to evaluate the amount and composition of the material exported from the ice. Swimmers collected in the sediment traps will also be identified and quantified.

Figure 6.2.1. Sediment trap deployments at the ice camp

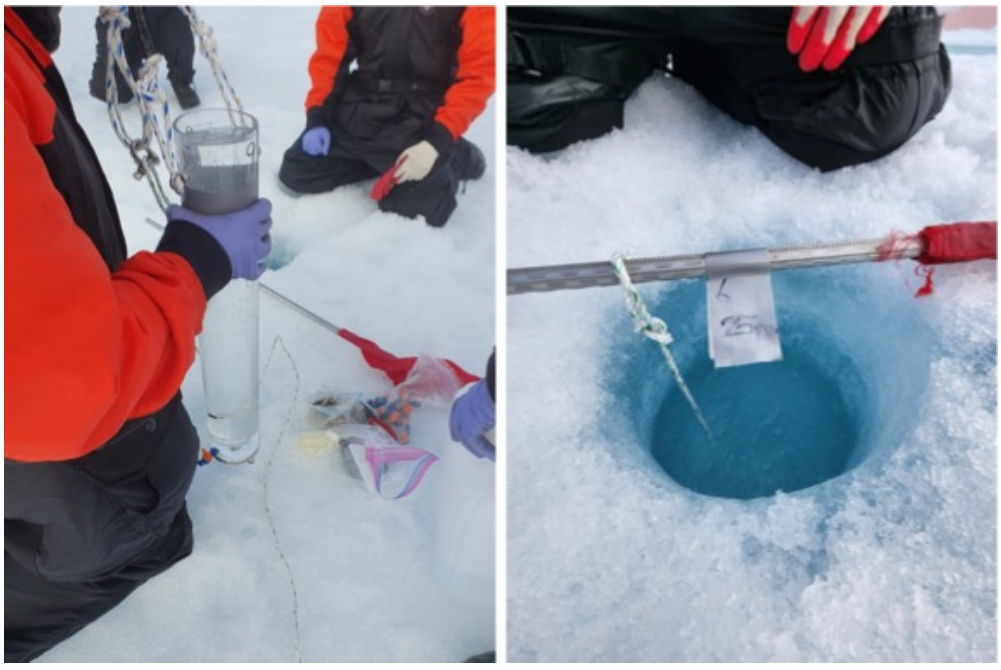

Chapter 7. Remote Sensing

Jeong-Won Park[1], Sungjae Lee[1], and Seong Yong Lee[2]

[1]Korea Polar Research Institute, Incheon, Republic of Korea

[2]Sejong University, Seoul, Republic of Korea

Email: jeong-won.park@kopri.re.kr; sungjae@kopri.re.kr; apex01@sejong.ac.kr

The team of Remote Sensing (RS) has participated the ARA14B cruise to collect various in-situ data that will be used for calibrating and validating results from satellite observation. The 31-day long itinerary of the field work includes i) ocean optics measurement for identifying optical properties of seawater along depths, ii) drone observation for areal mapping and spectral measurement of sea ice and melt pond, and iii) ice-wave motion measurement for developing and verifying satellite- and model-based wave-induced ice breaking. Figure 7.0.1 shows the locations of research stations, underway seawater sampling, and ice camp.

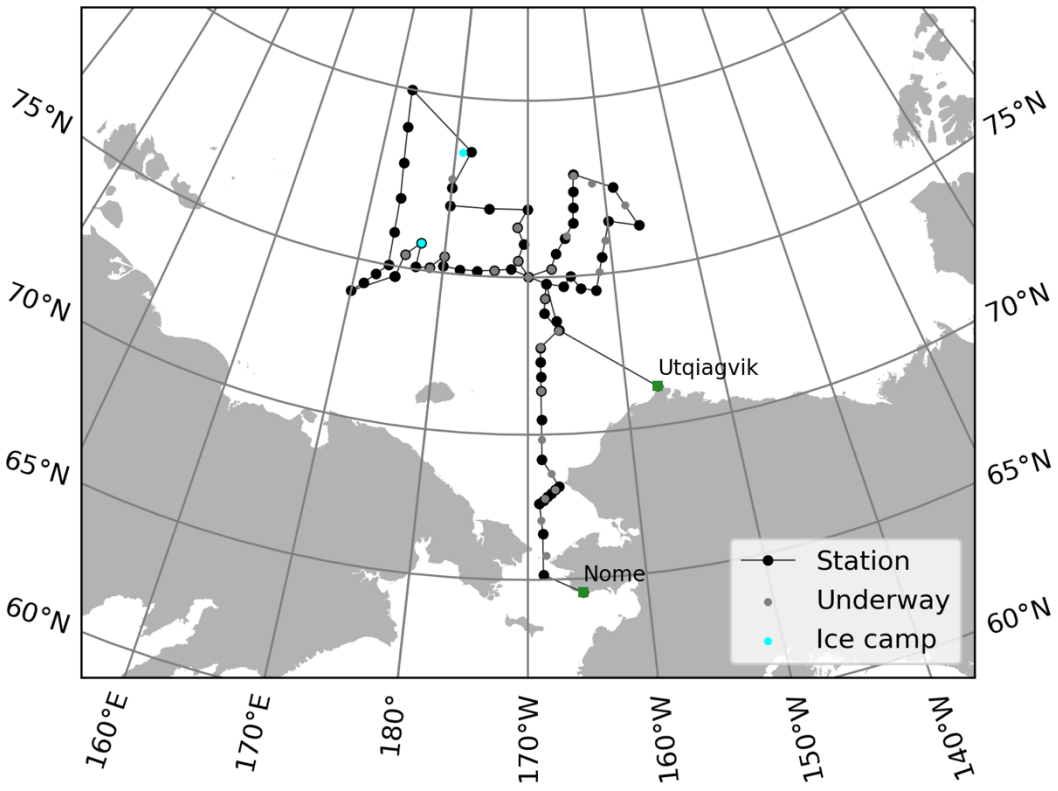

Figure 7.0.1. Location map of entire field work

7.1. Ocean Optics and measurement

7.1.1. Introduction

Optical properties are important factors to reflect physical processes related to solar energy absorption and distribution in ocean and sea ice. They could be used to analyze the influence from biomasses, including phytoplankton and algae on the light field. Also, the light absorption and scattering will influence heat transportation and dispersion in the ocean. On the other hand, the optical data, together with the analysis for the inherent optical property of particles in the water, could be used for calibration and validation of visible remote sensing.

In this cruise, we tried to get bio-optical relationships to improve ocean color data quality by observing inherent optical properties (IOPs) of water such as absorptions by phytoplankton, suspended sediment (SS), and colored dissolved organic matters (CDOM), and apparent optical properties (AOPs) of water such as downward irradiances (Ed) and upwelling radiance (Lu).

Our major goal in this study was to collect bio-optical data in conjunction with measurements of CDOM, phytoplankton and detrital absorption in support of NASA's efforts to develop robust empirical and semi-analytic algorithms for ocean color products in high latitude regions. This effort is a part of longer strategic objective of understanding the impacts of changing climate on biological oceanographic processes in the Arctic Ocean using ocean color satellite data.

For this purpose, we prepared instruments to measure apparent optical properties, inherent properties, and reflectivity during the cruise. In this chapter, we will introduce our observations and their preliminary results.

The optical properties of the ocean and sea ice are linked with the water structure that might be related to the Arctic surface water, Pacific water, shelf water, and the river water. The optical properties might describe the details of the waters from variety of spectral data.

The optical observations were performed at about 60 sites as shown in Figure 7.1.1. The specifications of the observations at stations are listed in Table 7.1.1.

Table 7.1.1. Specifications of optical observation stations

No.	Site ID	Date(UTC)	latitute	longitute	CTD	Underway water sampling	Trios Ramses
1	Station-001	2023/08/03 05:26	65.173467	-168.690753	O		
2	Underway-001	2023/08/03 09:24	65.860450	-168.418312		O	
3	Station-002	2023/08/03 15:17	66.629952	-168.687517	O		O
4	Underway-002	2023/08/03 18:01	67.083320	-168.805237		O	
5	Station-003	2023/08/03 22:13	67.669982	-168.960015	O		O
6	Underway-003	2023/08/04 02:01	67.837385	-168.427695		O	
7	Station-006	2023/08/04 04:34	68.012977	-167.866922	O		O
8	Underway-004	2023/08/04 07:36	68.128038	-167.495025		O	
9	Station-008	2023/08/04 09:30	68.241987	-167.122028	O		
10	Underway-005	2023/08/04 13:07	68.679138	-167.843193		O	
11	Station-009	2023/08/04 16:55	69.166732	-168.666590	O		O
12	Underway-006	2023/08/04 21:33	69.831868	-168.665922		O	
13	Station-010	2023/08/05 01:56	70.499995	-168.666665	O		O
14	Underway-007	2023/08/05 08:10	71.430020	-168.666835		O	
15	Station-013	2023/08/05 15:26	72.359490	-168.661818	O		O
16	Underway-008	2023/08/05 20:25	72.833823	-168.658178		O	
17	Underway-009	2023/08/06 03:31	73.346635	-166.695455		O	
18	Station-016	2023/08/06 12:03	73.886210	-168.187718	O		O
19	Underway-010	2023/08/06 16:35	74.344872	-168.050033		O	
20	Station-018	2023/08/06 21:10	74.800837	-167.899875	O		O

21	Underway-011	2023/08/07 04:32	75.020565	-169.936542		O	
22	Underway-012	2023/08/07 08:14	75.507107	-171.213798		O	
23	Station-021	2023/08/07 15:27	76.001243	-170.499308	O		O
24	Underway-013	2023/08/07 20:58	76.481348	-171.305905		O	
25	Station-023	2023/08/08 08:32	76.994902	-170.011843	O		O
26	Station-024	2023/08/08 23:11	76.992550	-175.003028	O		O
27	Station-025	2023/08/09 10:04	76.997993	179.942367	O		O
28	Underway-014	2023/08/09 22:55	77.759655	179.888703		O	
29	Ice camp-1	2023/08/10 18:20	78.521967	-179.021967			
30	Station-027	2023/08/13 01:06	78.541098	-177.586268	O		O
31	Station-028	2023/08/13 21:17	80.000172	172.402253	O		O
32	Station-029	2023/08/14 11:26	79.000018	172.800112	O		O
33	Station-030	2023/08/14 21:48	78.000058	173.199613	O		O
34	Station-031	2023/08/15 08:28	76.999892	173.599302	O		O
35	Station-032	2023/08/15 22:30	75.999258	173.608743	O		O
36	Station-033	2023/08/16 08:32	75.000058	173.600407	O		O
37	Station-036	2023/08/16 22:04	74.002477	170.163735	O		O
38	Station-037	2023/08/17 19:39	74.693680	174.623927	O		O
39	Underway-015	2023/08/18 05:41	75.399913	175.330313		O	
40	Station-039	2023/08/18 12:12	75.726657	177.171437	O		O
41	Ice camp-2	2023/08/19 16:37	75.934504	176.972873			
42	Station-040	2023/08/20 13:25	75.074973	176.800047	O		

43	Underway-016	2023/08/20 18:42	75.108072	178.420268		O	
44	Underway-017	2023/08/20 23:06	75.500647	179.999882		O	
45	Station-043	2023/08/21 04:06	75.165175	-179.968172	O		O
46	Station-045	2023/08/21 19:34	75.149948	-176.000247	O		O
47	Underway-018	2023/08/22 01:07	75.195067	-173.987940		O	
48	Station-047	2023/08/22 08:12	75.240485	-171.972460	O		O
49	Station-048	2023/08/22 22:54	75.020603	-169.936122	O		
50	Underway-019	2023/08/23 06:50	75.245870	-167.268087		O	
51	Station-050	2023/08/23 12:14	75.691155	-166.637978	O		
52	Underway-020	2023/08/23 19:51	76.216440	-165.229903		O	
53	Station-052	2023/08/23 23:58	76.567402	-164.362157	O		O
54	Station-054	2023/08/24 17:53	77.467402	-164.097640	O		O
55	Underway-021	2023/08/25 01:23	77.927757	-163.967242		O	
56	Underway-022	2023/08/25 06:33	77.673090	-161.527552		O	
57	Station-056	2023/08/25 12:57	77.482062	-158.734110	O		O
58	Underway-023	2023/08/25 21:31	76.935878	-157.583233		O	
59	Station-057	2023/08/26 06:05	76.303905	-156.221120	O		O
60	Station-058	2023/08/26 20:59	76.518868	-159.789037	O		O
61	Underway-024	2023/08/27 05:00	75.986750	-160.528070		O	
62	Station-059	2023/08/27 10:30	75.498445	-161.147115	O		
63	Underway-025	2023/08/27 13:46	75.072990	-161.590292		O	
64	Station-060	2023/08/27 19:27	74.516337	-162.151895	O		O

7.1.2. Materials and methods

Ocean optical observation: IOPs

We collected 162 water samples from 60 stations (with three depths of surface, subsurface chlorophyll maximum (SCM), and bottom within euphotic depth) and intermediate sites between stations in underway route (Table 7.1.2). To measure inherent optical properties (IOPs) of water, seawater volumes of 1,000 ml were filtered on 25 mm glass-fiber filters (Whatman GF/F). For absorption by CDOM, seawater volumes of 50 ml were filtered onto disposable syringe filter unit of Advantec (cellulose acetate, 0.45 μm).

Optical densities of total particulate matters were measured directly on the wet filters by methods of Truper and Yentch (1967) with a double-beam recording spectrophotometer (Cary100, Agilent Technologies) in a spectral range 250–800 nm (spectrum resolution is 1 nm). The filter was placed in front of diffusing windows adjacent to an end-on photomultiplier of large surface area. For a reference blank and baseline variations, an unused wetted filter was taken as were automatically corrected. After the measurement of optical density of total pigments, the spectral absorption by nonalgal material was measured separately with method of Kishino et al., 1985. The filter was placed in absolute methyl-alcohol in order to extract pigments.

Table 7.1.2. Observation list: IOPs

Station ID	Depth of CTD seawater sampling (m)	Underway ID	Depth of underway seawater sampling (m)
Station-01	0, 10, 15, 30	Underway-01	0
Station-02	0, 27, 36	Underway-02	0
Station-03	0, 24, 30	Underway-03	0
Station-06	0, 18, 30, 40	Underway-04	0
Station-08	0, 12, 20, 25	Underway-05	0
Station-09	0, 13, 30, 40	Underway-06	0
Station-10	0, 22, 30	Underway-07	0
Station-13	0, 16, 30, 45	Underway-08	0
Station-16	0, 35, 50, 70	Underway-09	0
Station-18	0, 22, 70, 100	Underway-10	0
Station-21	0, 18, 50, 100	Underway-11	0
Station-23	0, 30, 50, 100	Underway-12	0

Station-24	0, 28, 50, 100	Underway-13	0
Station-25	0, 22, 60, 100	Underway-14	0
Station-27	0, 25, 60, 100	Underway-15	0
Station-28	0, 18, 50, 70	Underway-16	0
Station-29	0, 16, 60, 80	Underway-17	0
Station-30	0, 24, 45, 70	Underway-18	0
Station-31	0, 34, 50, 70	Underway-19	0
Station-32	0, 35, 50, 100	Underway-20	0
Station-33	0, 30, 55, 70	Underway-21	0
Station-36	0, 10, 40	Underway-22	0
Station-37	0, 30, 50	Underway-23	0
Station-39	0, 24, 40, 70	Underway-24	0
Station-40	0, 44, 70, 100	Underway-25	0
Station-43	0, 35, 60, 100		
Station-45	0, 26, 50, 70		
Station-47	0, 23, 50, 70		
Station-48	0, 38, 50		
Station-50	0, 35, 50		
Station-52	0, 38, 70		
Station-54	0, 32, 70		
Station-56	0, 45, 80		
Station-57	0, 48, 100		
Station-58	0, 37, 80		
Station-59	0, 40, 70		
Station-60	0, 50, 70		

Ocean optical observation: AOPs

For the measuring of apparent optical properties (AOPs) of water, we deployed TriOS, an inwater-spectroradiometer (Figure 7.1.2), with a spectral range of 320–950 nm of downward irradiance, downward radiance and upwelling radiance. For the reference as ambient irradiance variation, downward irradiance was measured on deck, where was not a shaded place of ARAON. The integrated instruments deployed through the A-frame at the stern of the Vessel. The deploying speed was 30 meters per minute. This data listed in Table 7.1.3 will be able to be used for calibrations and validations of currently operating ocean color remote sensing data.

Table 7.1.1. Observation list: TriOS

Station	Date(UTC, YYYY/MM/DD hh:mm)	Deployed Depth(m)
Station-02	2023/08/03 15:17	35
Station-03	2023/08/03 22:13	40
Station-06	2023/08/04 04:34	35
Station-09	2023/08/04 16:55	40
Station-10	2023/08/05 01:56	30
Station-13	2023/08/05 15:26	30
Station-16	2023/08/06 12:03	20
Station-18	2023/08/06 21:10	70
Station-21	2023/08/07 15:27	30
Station-23	2023/08/08 08:32	50
Station-24	2023/08/08 23:11	70
Station-25	2023/08/09 10:04	40
Station-27	2023/08/13 01:06	40
Station-28	2023/08/13 21:17	40
Station-29	2023/08/14 11:26	40
Station-30	2023/08/14 21:48	40
Station-31	2023/08/15 08:28	40
Station-32	2023/08/15 22:30	60
Station-33	2023/08/16 08:32	30
Station-36	2023/08/16 22:04	40
Station-37	2023/08/17 19:39	40
Station-39	2023/08/18 12:12	20
Station-43	2023/08/21 04:06	50
Station-45	2023/08/21 19:34	40
Station-47	2023/08/22 08:12	20
Station-52	2023/08/23 23:58	60
Station-54	2023/08/24 17:53	60
Station-56	2023/08/25 12:57	30
Station-57	2023/08/26 06:05	70
Station-58	2023/08/26 20:59	70
Station-60	2023/08/27 19:27	60

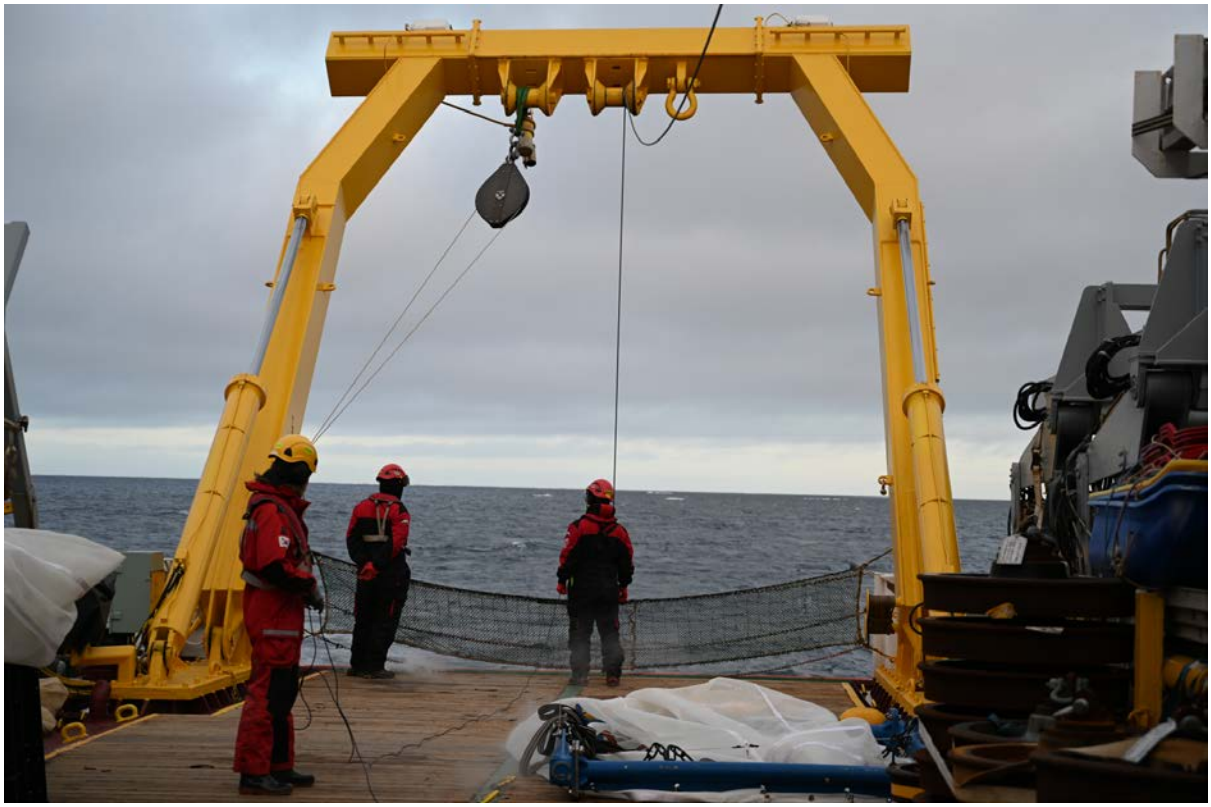

Figure 7.1.2. Deployment of inwater-spectroradiometer (TriOS)

7.1.3. Preliminary results

Ocean Optical observation: IOPs

The results from the IOPs will be able to show the bio-optical characteristics in water at each station and at each depth of the water sample (Figure 7.1.3).

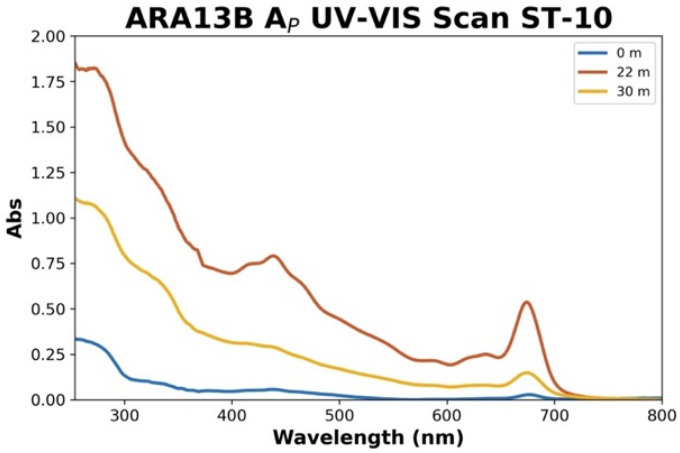

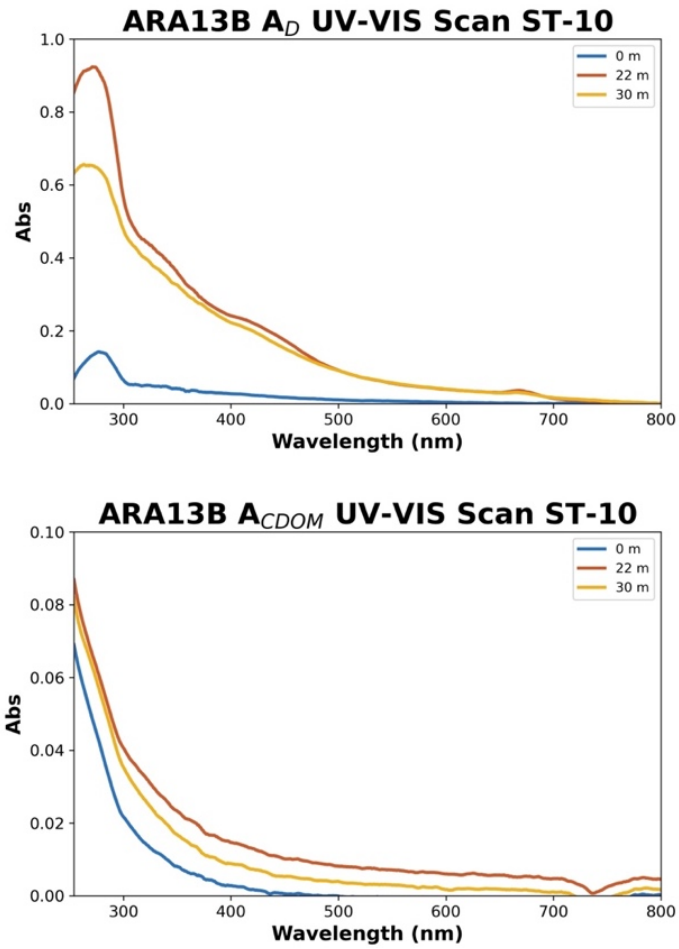

Figure 7.1.3. An example of absorptions by particle (top), detritus (middle), and CDOM (bottom) at the ARA13B station 10.

Ocean Optical observation: AOPs

The results from the AOPs, i.e. data from TriOS will be able to reflect the continuous bio-optical characteristics of water surface and the bio-optical profiles at the operated stations (Figure 7.1.4).

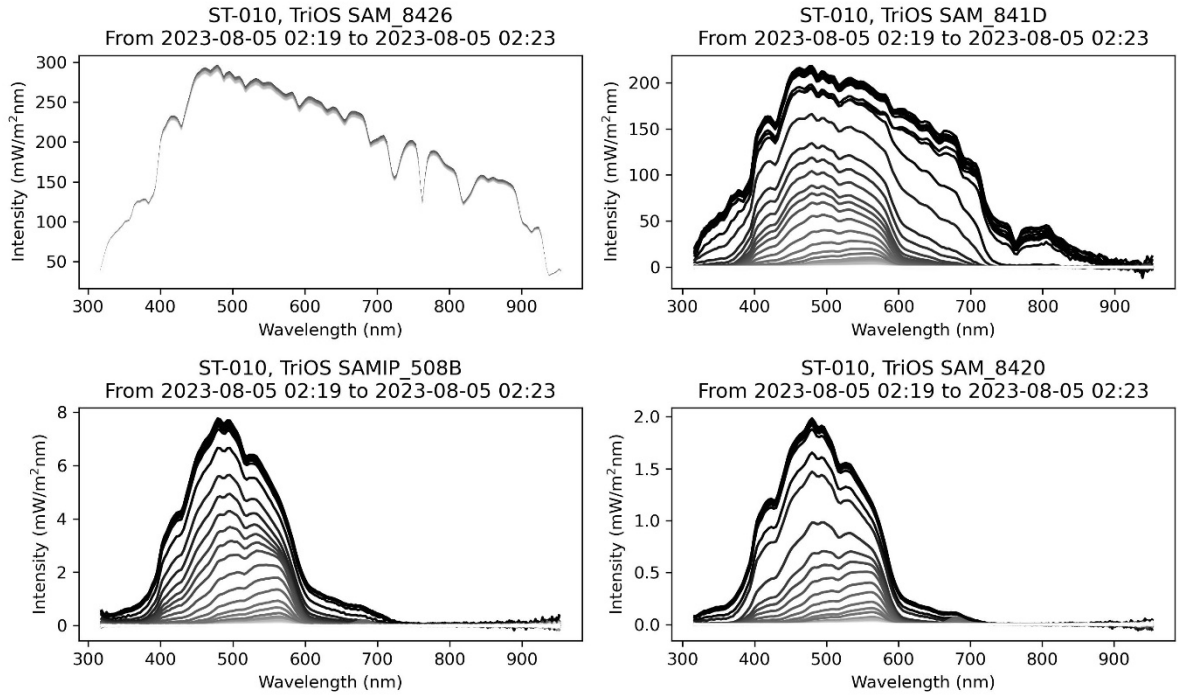

Figure 7.1.4. TriOS observation results recorded at the station 10.

7.1.4. Summary and conclusions

During this Arctic cruise, calibration/validation of satellite remote sensing ocean color data were collected. The IOPs reflected the bio-optical characteristics in water at the selected depths. The results from the AOPs such as data from TriOS showed continuous bio-optical characteristics of water surface and the bio-optical profiles at the operated stations. We are going to use these filed data for further detailed examination and correction of satellite data.

7.2. Airborne ice observation

7.2.1. Introduction

Airborne platforms have been used to acquire on-site very-high-resolution (VHR) data from lower flight height compared with remote sensing techniques using spaceborne platform. Various kinds of VHR data can be obtained depending on onboard sensors, e.g., RGB digital camera, multispectral imaging sensor, and thermal infrared imaging sensor. The VHR data of the spatial resolutions from few centimeters to tens of centimeters can be acquired in unfavorable cloudy conditions for optical satellite imagery acquisition with better spatial resolution. The mosaicked scene composed of each VHR image can be used for calibration and validation of satellite remote sensing data covering large area, high-resolution spatial analyses in various research fields, and recording field conditions during conducting research activities. Helicopter-based observation enables high-resolution data acquisition over enlarged area compared with the recent Unmanned Areal Vehicle (UAV)-based observation. Multiple imaging sensors can be equipped on the helicopter due to higher payload than UAV. However, a few studies using helicopter carried by icebreaker have been conducted (Hyun et al., 2019).

The purpose of this study is to demonstrate a feasibility of areal imaging technique on continuously drifting sea ice floe showing low contrast in brightness between surface features such as snow and ice. The results can be applicable to validation of lower resolution satellite data, satellite data-based products regarding sea ice, and more detailed morphological study about sea ice.

7.2.2. Helicopter-borne image acquisition

Sea ice camp was conducted at one site in the Arctic Ocean during the periods in August 10-12, 2023. A digital RGB camera (DJI Phantom4 RTK) and hyperspectral camera (Headwall VNIR SHARK 415) were attached Small UAVs. Coordinates of image acquisition positions were simultaneously recorded using integrated GPS receiver for georeferencing acquired images. Helicopter-borne images were acquired with enough amount of overlaps between images as forward overlap of more than 60% and side overlap more than 30% for reconstruction of three-dimentional imaging geometry, considering intrinsic low brightness contrast of sea ice

surface. Multiple survey flights had been planned initially, however, the weather condition did not allow except one-time short flight on the second day during the ice camp (Table 7.2.1). Nevertheless, a complete mapping over the study area was done successfully. The ice floes drift continuously, and their drifting hampers precise image matching based on the geographic coordinates of helicoptoer as of image acquisition.

Table 7.2.1. Specifications of Helicopter-borne image acquisition during sea ice camp

Image acquisition site		Date (UTC)	Number of acquired images
Sea ice camp	RGB	Aug 11, 2023	295
Sea ice camp	VNIR	Aug 11, 2023	64,000 (line scan)

7.2.3. Image processing

The images were processed using structure-from-motion (SfM) technique implemented software by following a series of processing chain; image alignment, dense point cloud extraction, digital elevation model (DEM) generation, image orthorectification, and mosaicking (Figure 7.2.1).

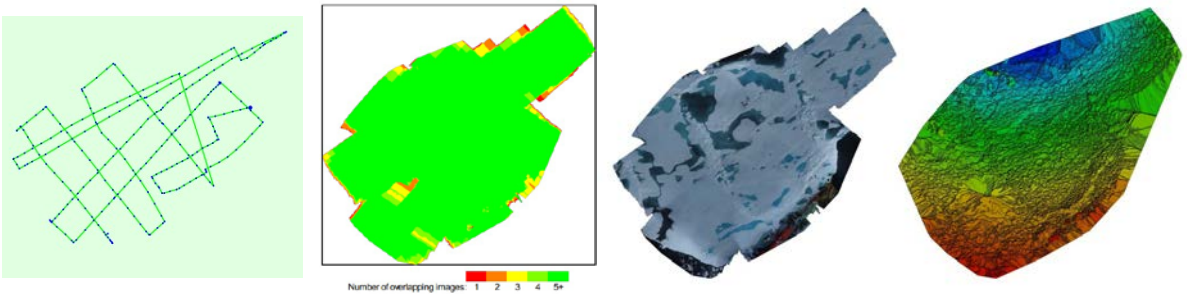

Figure 7.2.1. Processing steps for generating ortho-mosaic image

7.2.4. Preliminary results

The resulting ortho-mosaic image shows complete coverage over the ice camp site with high spatial resolution of 4 cm per pixel (Figure 7.2.2). The image will be shared primarily among the cruise members to help characterizing their sites where individual in-situ works were carried out.

The DEM and mosaicked image can be used for further analyses, e.g., sea ice surface roughness measurement, melt pond distribution analysis, and validation of satellite data-derived sea ice product. The mosaicked image can also support various field investigations conducted on sea ice by supplying detailed spatial information of study area.

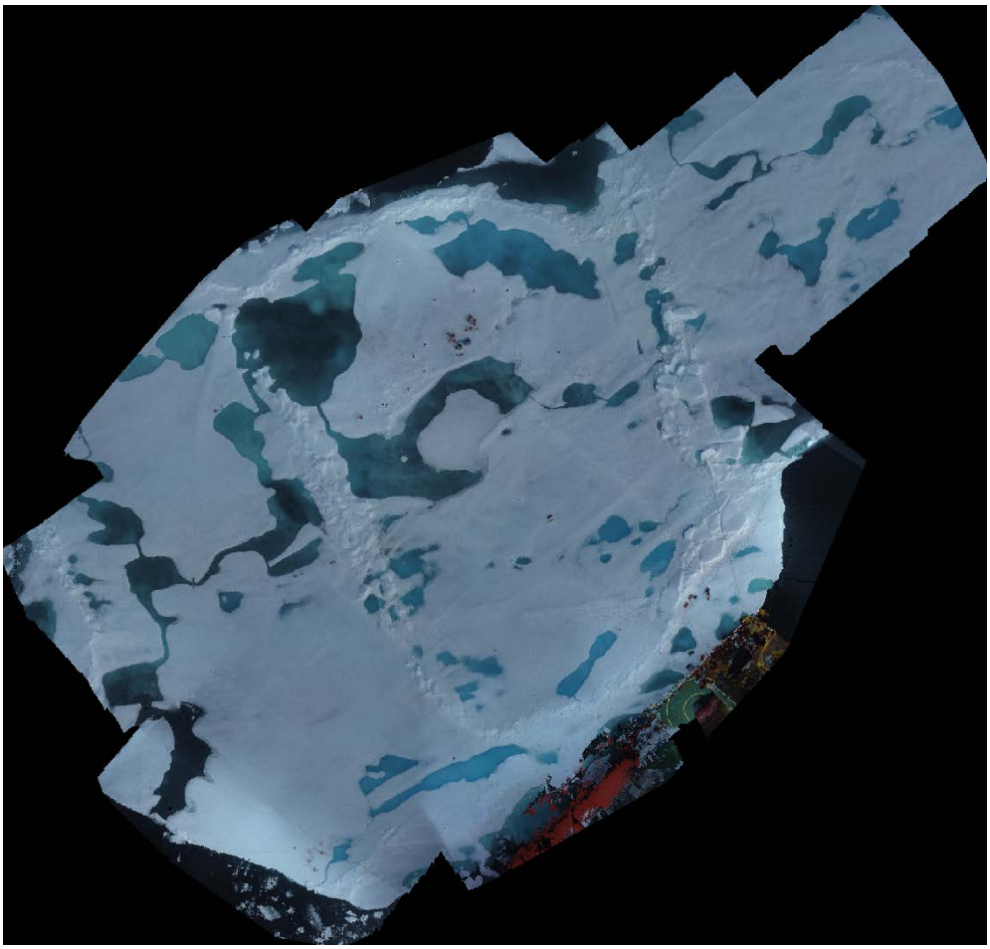

Figure 7.2.2. Preliminary results of UAV image processing

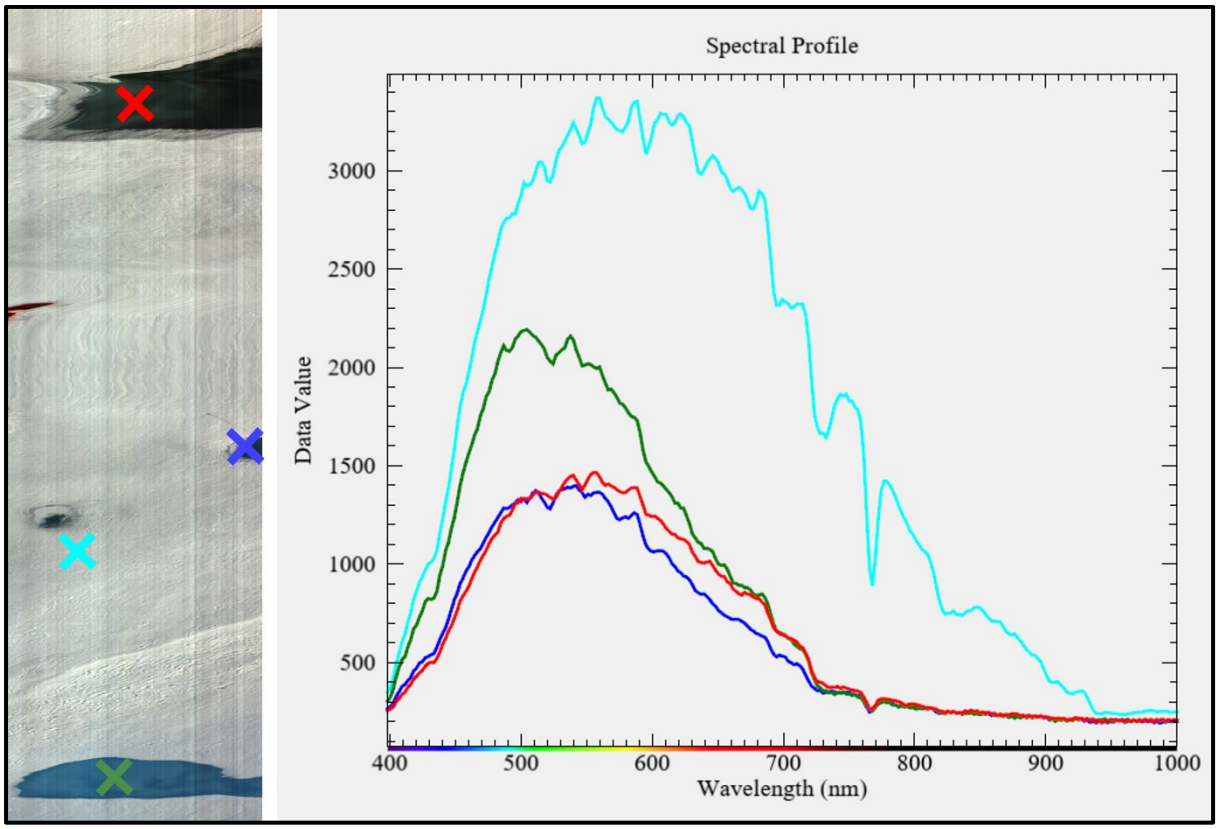

Figure 7.2.3 Preliminary result of Hyperspectral VNIR radiance spectral profile

7.3. Sea ice drift and wave measurement

In situ measurements of sea ice drift and waves are crucial for validation of the numerical modeling and satellite observations of waves in sea ice and for understanding the processes of ice break-up and wave attenuation. The Korea Polar Research Institute (KOPRI) and the Nansen Environmental and Remote Sensing Centre (NERSC) cooperated on a project for deploying 13 ice-wave buoys during the ARA14B cruise. Figure 7.3.1 shows the locations of wave buoys overlaid on the ice concentration map (U.S. National Ice Center) on August 25, 2023.

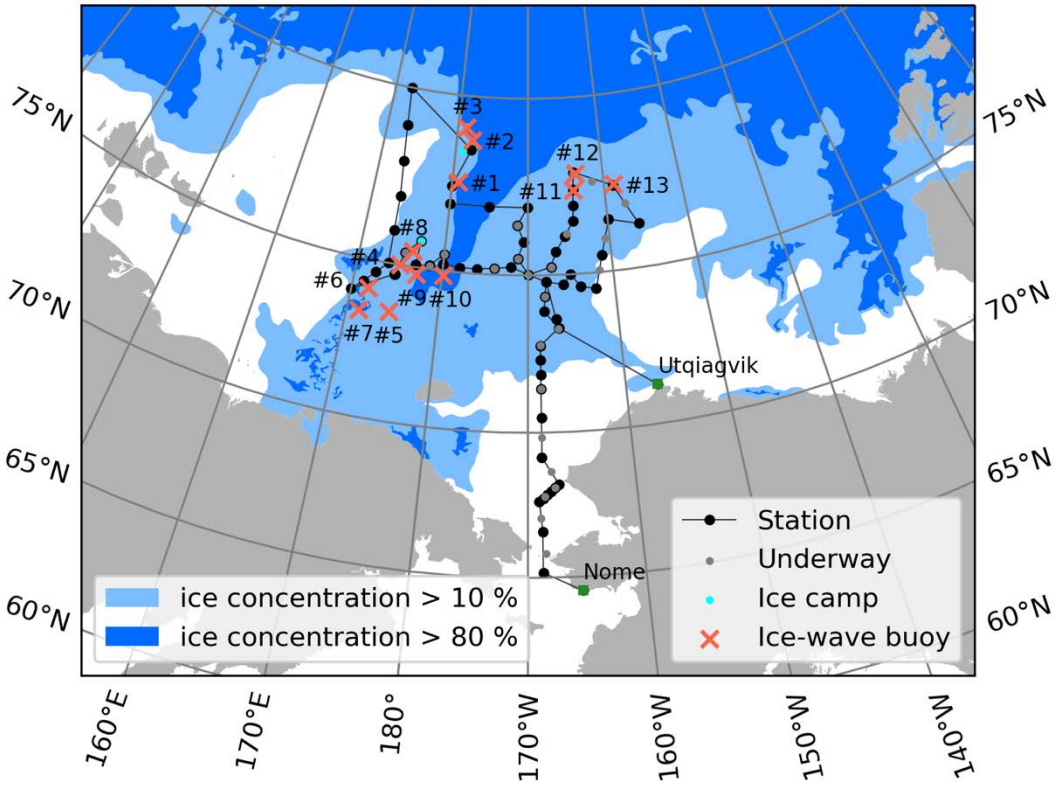

Figure 7.3.1. Location map of the deployed wave buoys

7.3.1. Background and Goal

Marginal ice zone (MIZ) is the region where ocean waves interact with sea ice. The waves bend and break the ice into floes and are attenuated by the ice. With the decrease in sea ice extent, impact of waves on sea ice is expected to grow in the 21st century (Boutin et al., 2020).

The wave model WaveWatch-III was coupled with the sea ice model neXtSIM developed at NERSC for improving accuracy of sea ice edge forecasting (Boutin et al., 2021). The coupled model was partly validated against observations of wave affected ice fraction (WAF) derived from satellite laser altimeter observations (Boutin et al., 2022), although both the model simulations and the satellite estimates don't represent the truth about the waves in sea ice. They both require thorough validation by in situ observations. However, the existing in situ data (e.g., Cooper et al., 2022) is quite sparse in space and time.

The goal of this project is to build and simultaneously deploy a large amount of wave and ice drift buoys for collecting substantial data on ice drift and wave spectrum in the Pacific sector of the Arctic Ocean that can be used for model and satellite data validation in a wide range of ice and wave conditions.

7.3.2. Ice-wave buoy

The OpenMetBuoy is an ice-wave buoy designed by (Rabault et al., 2022). It is easy-to-build, affordable, customizable, open-source instrument for oceanographic measurements of drift and waves in sea ice. The main component is the SparkFun Artemis Global Tracker transceiver. It combines the Artemis micro-computer board, Iridium 9603N Short Burst Data modem and u-blox ZOE-M8Q GNSS receiver. Other components include an inertial measurement unit (IMU, for example, LIS3MDL FeatherWing); GPS cable and antenna, two lithium D-cells, a breadboard for easier connection of components and a water-resistant box. A detailed assembly instructions are given on the OpenMetBuoys GitHub page (Rabault, 2021).

The buoys measure acceleration on 6 axis every minute and compute a wave power spectrum. The buoys send their position and wave spectrum via the Iridium modem every 120 minutes to spare the battery. The data is sent as a POST request to a dedicated webserver that accumulates data from all the buoys and saves in a database. The data can later be downloaded in a JSON format.

The buoy equipments were further processed to ensure safe operation by putting desiccant bags into the enclosure, securing batteries with nylon straps, and wrapping with silicon and vulcanizing tapes. A plastic hook was attached on top so that the buoy can be released by a fishing line. Figure 7.3.2 shows an exemplary ready for deployment.

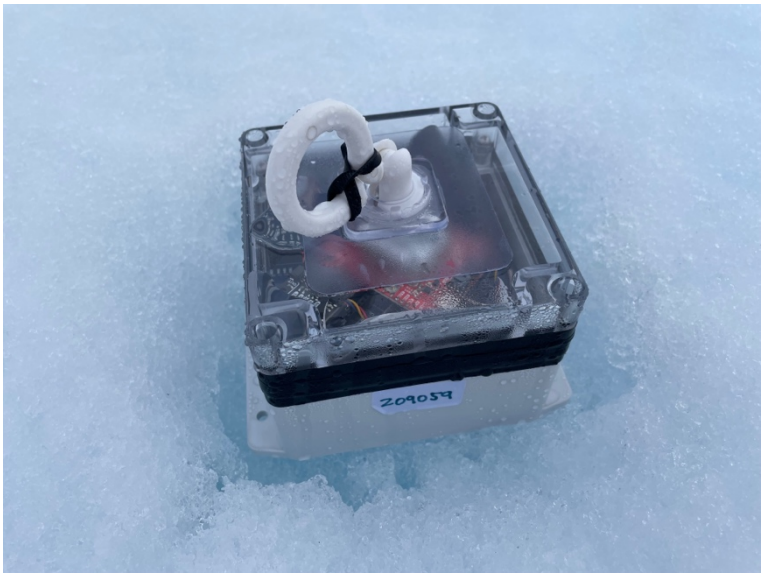

Figure 7.3.2. A photo of wave buoy ready for deployment

7.3.3. Deployment of buoys

The buoys were deployed during the passage of the ship through sea ice and the ice camp. The advantage of the OpenMetBuoy is that it is quite small and light, so deployment during stations or the passage can be done without leaving the deck. The drifters were deployed from the lowest (main) aft deck on starboard side. The 16.5 meters long crain was used to reach unbroken ice surface and release the buoy (Figure 7.3.3).

Figure 7.3.3. Wave buoy deployment using a crain

The buoy deployment positions were planned along the route of the cruise, and it depend on ice conditions. The optimal criteria for deployment position are as follows: ice thickness is between 0.8 and 2 meters, ice concentration is above 80 %, distance from ice edge is more than 50 nm. In these conditions most of the buoys will survive more than 3 weeks. During this period the ice will continue thinning and ice edge will continue propagating northwards, thus buoys will have the possibility to measure a wide range of conditions for wave propagation: thickness: 0–2 m, concentration: 0–100 %, distance to ice edge 0–100 nm.

However, the ice condition over the cruise route changed fast and it was not easy to get deep into the ice zone. We deployed 13 buoys on ices with less optimal conditions: ice concentration was mostly below 80 %, distance to ice edge was 10–50 nm. Figure 7.3.4 shows the ice conditions for the deployment locations: #7, #9, #12, and #13. Table 7.3.1 lists the time and locations of the buoys deployed.

Figure 7.3.4. Ice conditions over the locations of wave buoy deployment

Table 7.3.1. List of the deployed wave buoys

Number	Date(UTC)	Latitude	Longitude
1	2023-08-09 17:23:14	77.5189011	179.9438896
2	2023-08-10 18:11:57	78.5290417	-178.7350981
3	2023-08-13 04:53:09	78.8139298	-178.810946
4	2023-08-16 00:23:49	76.0086431	173.6362158
5	2023-08-16 13:38:40	74.6727012	172.3754097
6	2023-08-16 17:27:19	74.3417704	171.1401405
7	2023-08-17 07:38:00	73.9852902	170.3467959
8	2023-08-19 04:16:37	76.0310886	176.9437964
9	2023-08-20 09:02:01	75.4946354	176.6971877
10	2023-08-21 11:56:53	75.1868323	-179.2033823
11	2023-08-24 19:48:20	77.4530331	-164.0478244
12	2023-08-25 03:08:50	77.9286313	-163.8830252
13	2023-08-25 16:05:50	77.4998852	-158.8560396

7.3.4. Preliminary results

The Iridium short burst datasets from the 13 buoys deployed contain measurement of the buoy coordinates and wave spectrum performed every 30 minutes. Figure 7.3.5 shows the locations of wave buoy #2 tracked from the time of deployment (August 10, 2023). The buoy was installed during the first ice camp, which makes it possible to deploy it well inside of the ice floe, ensuring more favorable ice condition for longer survival of the buoy. According to the recored drift trajectory, the ice floe drifted fast during the early days, then it became rather stable after that. The trajectory also shows a clear influence of the inertial motion, which is a clockwise rotation with 12-hour cycle approximately.

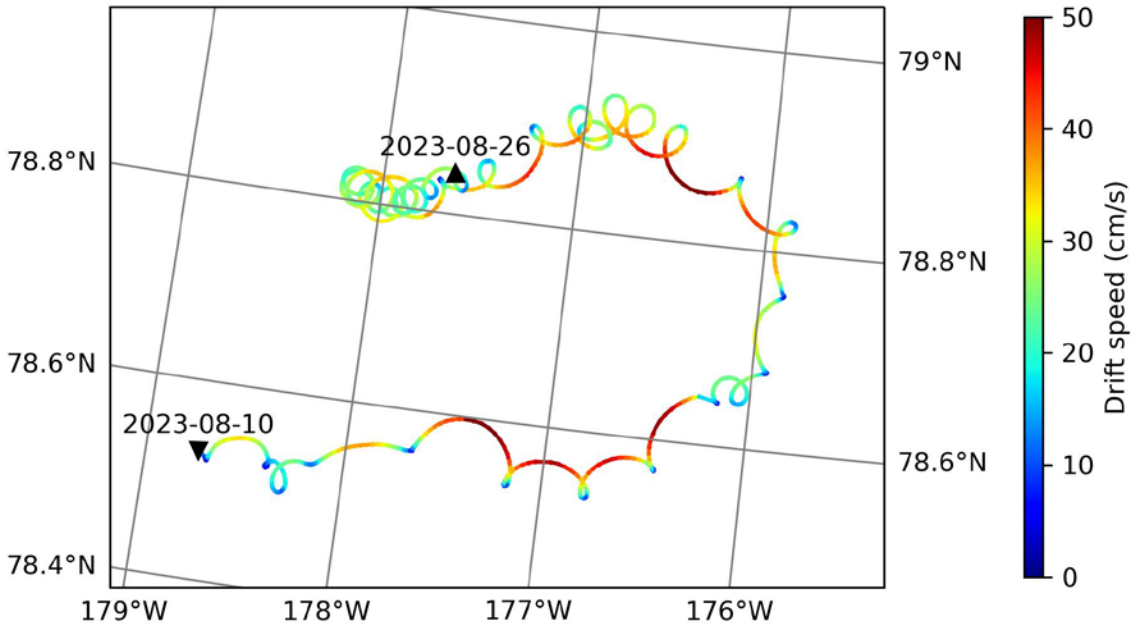

Figure 7.3.5. Drift trajectory of the wave buoy #2

Figure 7.3.6 shows the significant wave height and wave period recorded by the same buoy. From the recorded data, it is noticeable that there were several events over the study area, such as the one on 15 August. This coincides with the record of other buoy, #3 located nearby (Figure 7.3.7).

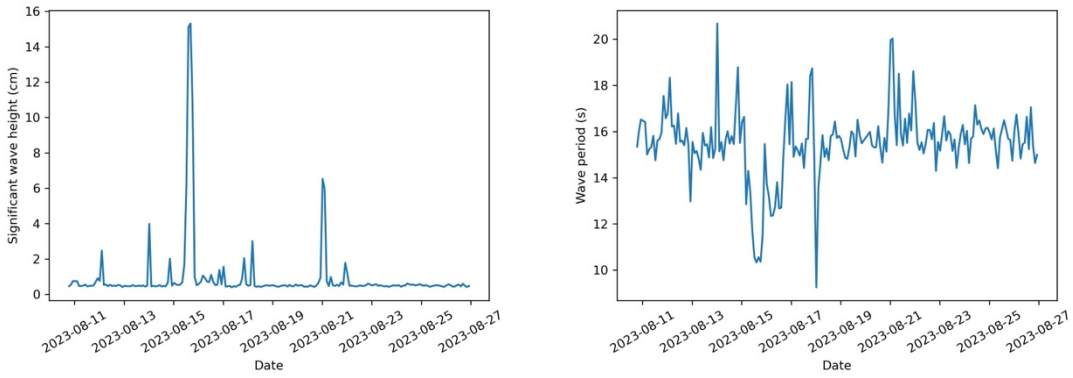

Figure 7.3.6. Significant wave height and wave period of the wave buoy #2

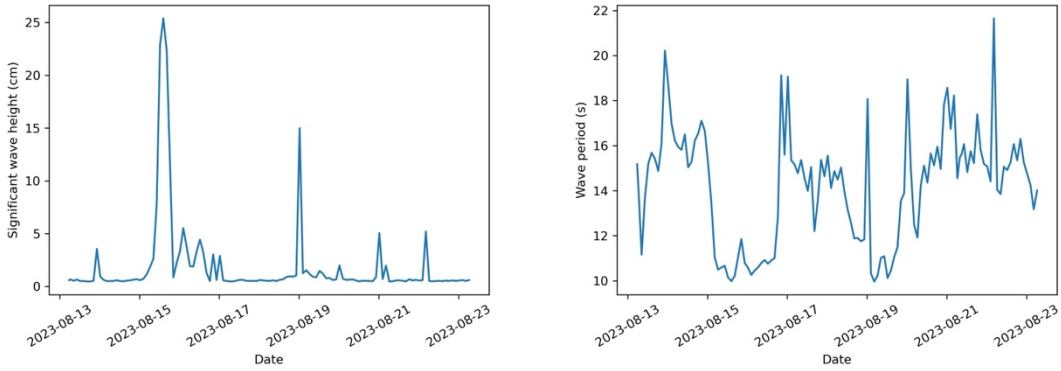

Figure 7.3.7. Significant wave height and wave period of the wave buoy #3

References

Boutin, G., Lique, C., Ardhuin, F., Rousset, C., Talandier, C., Accensi, M., and Girard-Ardhuin, F., 2020. Towards a coupled model to investigate wave–sea ice interactions in the Arctic marginal ice zone, The Cryosphere, 14:709–735.

Boutin, G., Williams, T., Rampal, P., Olason, E., and Lique, C., 2021. Wave–sea-ice interactions in a brittle rheological framework, The Cryosphere, 15:431–457.

Boutin, G., Williams, T., Horvat, C., and Brodeau, L., 2022. Modelling the Arctic wave-affected marginal ice zone: a comparison with ICESat-2 observations. Philosophical Transactions of the Royal Society A, 380: 20210262.

Cooper, V.T., Roach, L.A., Thomson, J., Brenner, S.D., Smith, M.M., Meylan, M.H. and Bitz,

C.M., 2022. Wind waves in sea ice of the western Arctic and a global coupled wave-ice model, Philosophical Transactions of the Royal Society A, 380:20210258.

Frankenstein, G. and Garner, R., 1967. Equations for Determining the Brine Volume of Sea Ice from −0.5° to −22.9°C, Journal of Glaciology, 6(48):943-944.

Han, H., Hong, S.-H., Kim, H.-c., Chae, T.-B., and Choi, H.-J., 2017. A study of the feasibility of using KOMPSAT-5 SAR data to map sea ice in the Chukchi Sea in late summer, Remote Sensing Letters, 8(5):468-477.

Hyun, C.U. and Kim, H.C., 2017. A Feasibility Study of Sea Ice Motion and Deformation Measurements Using Multi-Sensor High-Resolution Optical Satellite Images, Remote Sensing, 9:930.

Hyun, C.U., Kim, J.H., Han, H. and Kim, H.C., 2019. Mosaicking Opportunistically Acquired Very High-Resolution Helicopter-Borne Images over Drifting Sea Ice Using COTS Sensors, Sensors, 19:1251.

Rabault, J., 2021. OpenMetBuoy-v2021a (OMB / OMB-v21a): an easy to build, affordable, customizable, open source instrument for oceanographic measurements - that you can build yourself of buy commercially, GitHub repository, https://github.com/jerabaul29/OpenMetBuoy-v2021a

Rabault, J., Nosem T., Hope, G., Müller, M., Breivikm Ø., Voermans, J., Holem L.R., Bohlinger, P., Waseda, T., Kodaira, T. et al., 2021. OpenMetBuoy-v2021: An Easy-to-Build, Affordable, Customizable, Open-Source Instrument for Oceanographic Measurements of Drift and Waves in Sea Ice and the Open Ocean, Geosciences, 12(3):110.

Chapter 8. Sea Ice Camp

8.1. Buoy deployment and in-situ measurement

Joo-Hong Kim[1], Jung Hyun Park[1,2], Dong-Geon Lee[3], and Eun-Hye Park[4]

[1]*Korea Polar Research Institute, Incheon, Republic of Korea*

[2]*Pukyong National University, Busan, Republic of Korea*

[3]*Pohang University of Science and Technology, Pohang, Republic of Korea*

[4]*Navy, Republic of Korea*

Email: joo-hong.kim@kopri.re.kr; james70712@kopri.re.kr; donggeon0103@postech.ac.kr; eunhye1@navy.mil.kr

8.1.1. Buoy deployment

The sea ice mass balance buoy (IMB) is a novel equipment which takes in-situ measurement of changes in sea ice thickness, air-ice-ocean temperature profile and surface weather (air temperature and pressure). It autonomously operates and regularly transmits the observed data via satellite communication. Based on the signed letter of understanding between the K-AWARE project of the KOPRI and the 'Ice Mass Balance Buoys: A Contribution to the Arctic Observing Network (IMB-COAN)' project of the Dartmouth College, USA in 2022, two seasonal IMB version 3 (SIMB3) were deployed on sea ice in the ARA14B cruise. SIMB3 is an IMB model developed by Cryosphere Innovation (Planck et al., 2019). It is floatable and accurately measures sea ice thickness as it has both an underwater up-looking ice sounder and in-air down-looking snow sounder (Fig. 8.1.1). The specification of SIMB3 instruments is summarized in Table 8.1.1.

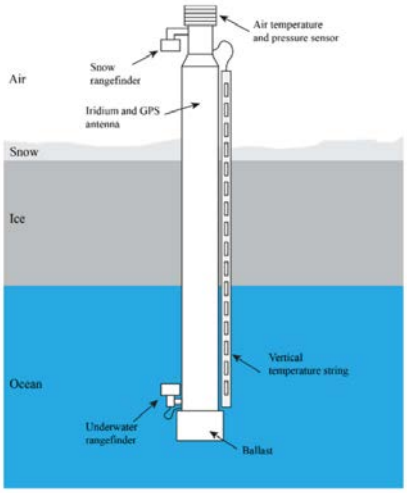

Fig 8.1.1. Schematic of the seasonal ice mass balance buoy (Planck et al., 2019)

Table 8.1.1. SIMB3 instruments, descriptions, accuracies, and reported precisions (Planck et al., 2019)

Instrument	Description	Accuracy	Reported Precision
Maxbotix MB7374	Downward looking snow rangefinder	±0.001 m	0.001 m
Airmar EchoRange+	Upward looking underwater rangefinder	±0.01 m	0.01 m
Bruncin 3.85m DTC	High resolution digital temperature chain	±0.25 ℃	0.125 ℃
DS18B20	Air temperature sensor	±0.5 ℃	0.0625 ℃
Bosch BME280	Barometric pressure sensor	±0.01 mbar	0.1 mbar
MTK3339 GPS	GPS module for position tracking	3 m	~0.1 m

Two ice camps were conducted - one during 10-12 August 2023, the other during 18-19 August 2023. The first ice camp site(IC1) was found around 22 UTC 10 August at (78.30°N, 178.19°E). The floe was a multi-year ice covered by frozen snow and some melt ponds (Fig. 8.1.2). The overall thickness measured was thicker than 2 m in general, but the flat surface with thickness around 1.3~1.5m.

Fig 8.1.2. Compass deck view of the ice camp site on 9 August. The dotted oval indicates the place of the first SIMB3 deployment

On the second day of the IC1 (11 August), we surveyed the floe on foot to find a suitable place to deploy the SIMB3. Following the guideline of site selection, we selected a adequate level place away from ridges with ice thickness around 1.44 m. On the selected site, the SIMB3

was activated and deployed in the local afternoon (around 22 UTC 11 August) through a drilled 10-inch hole (Fig. 8.1.3). The information on buoy and measurements are listed as follows:

Fig 8.1.3. (Left) Taking measurements after deployment, (Middle) Deploy completed, (Right) Close-up picture

- Activated on 22:35 UTC 11 August
- Buoy ID: Dartmouth 2023 #2
- S/N (IMEI): 300434066157890
- Ice thickness: 144 cm
- Snow thickness: 0 cm (frozen sfc)
- Freeboard: 12 cm
- Distance from ice to top sounder housing: 91 cm
- Distance from top of temperature string to ice: 98 cm

After the deployment, a datasheet including the deployment information was sent to Chris Polashenski at Dartmouth College and Cameron Planck at Cryosphere Innovation. Then we got a response of the registration of the buoy's modem on 12 August and some initial data.

The second ice camp site(IC2) was found around 00 UTC 19 August at (76.1°N, 177.11°E). The floe was huge multi-year ice in a square of 18 km length (Fig. 8.1.4) and had a large ridge running east-west through the center, creating areas with a thickness of more than 3 meters

along this ridge. The ice floe had numerous small-scale ridges, resulting in widespread areas with a thickness of over 2 meters.

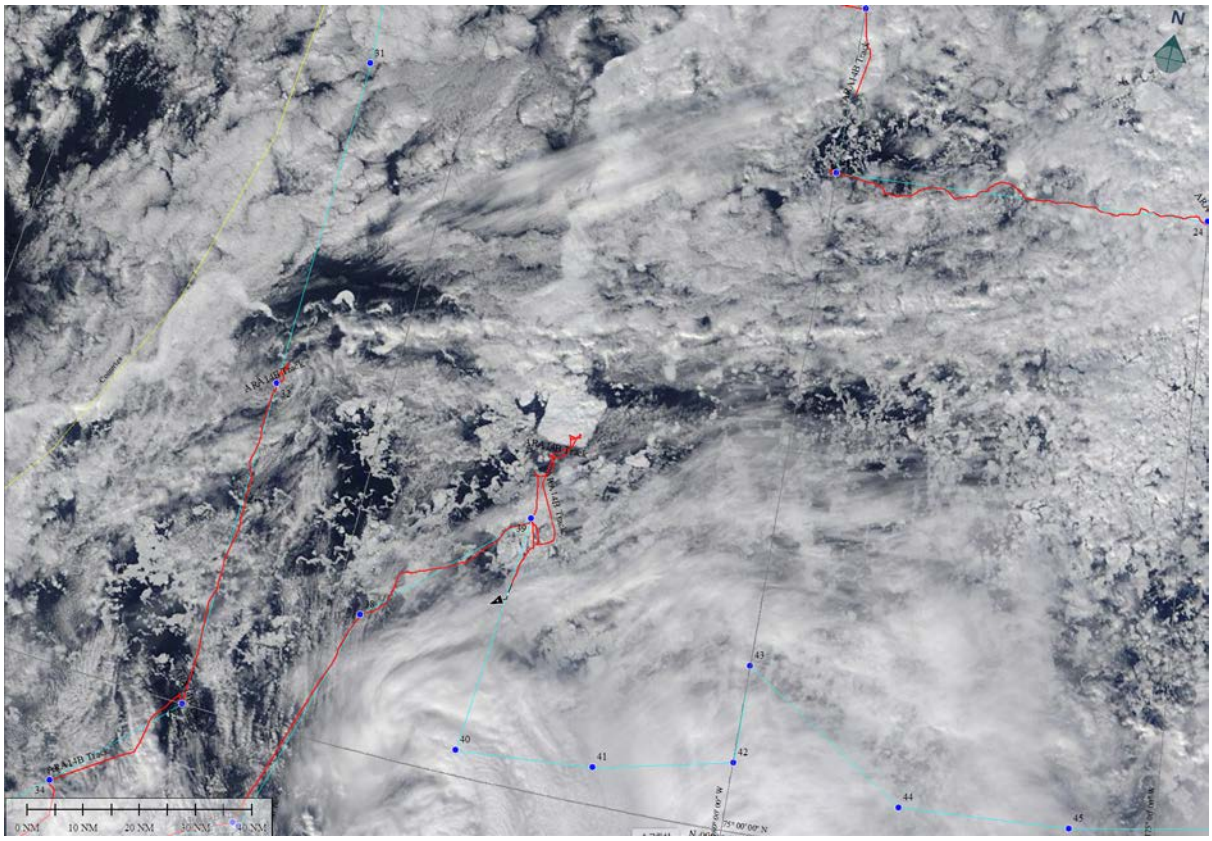

Fig. 8.1.4. Satellite image of the huge ice floe (MODIS Terra on 18 Aug)

On the first day of the IC2 (18 August), we attempted several explorations by helicopter to install the buoy inside the ice floe. However, most of the locations had a thickness of over 2.5 meters, making it difficult to find a suitable spot. Eventually, we found a spot with a thickness of 1.77 meters and attempted to install the buoy. Unfortunately, we discovered an underlying layer of ice beneath the water's surface, causing the attempt to fail as we couldn't create a hole. We had to retrieve everything back onto the ship.

We ran out of time to find a better location, so we decided to deploy it near the ship next day. On the second day of the IC2 (19 August), we surveyed the floe on foot to find a suitable place again. Following the guideline of site selection, we selected a adequate level place away from ridges with ice thickness around 1.48 m. Though the place was near the edge of a detached ice floe, the place meets the requirement, so we completed the installation.

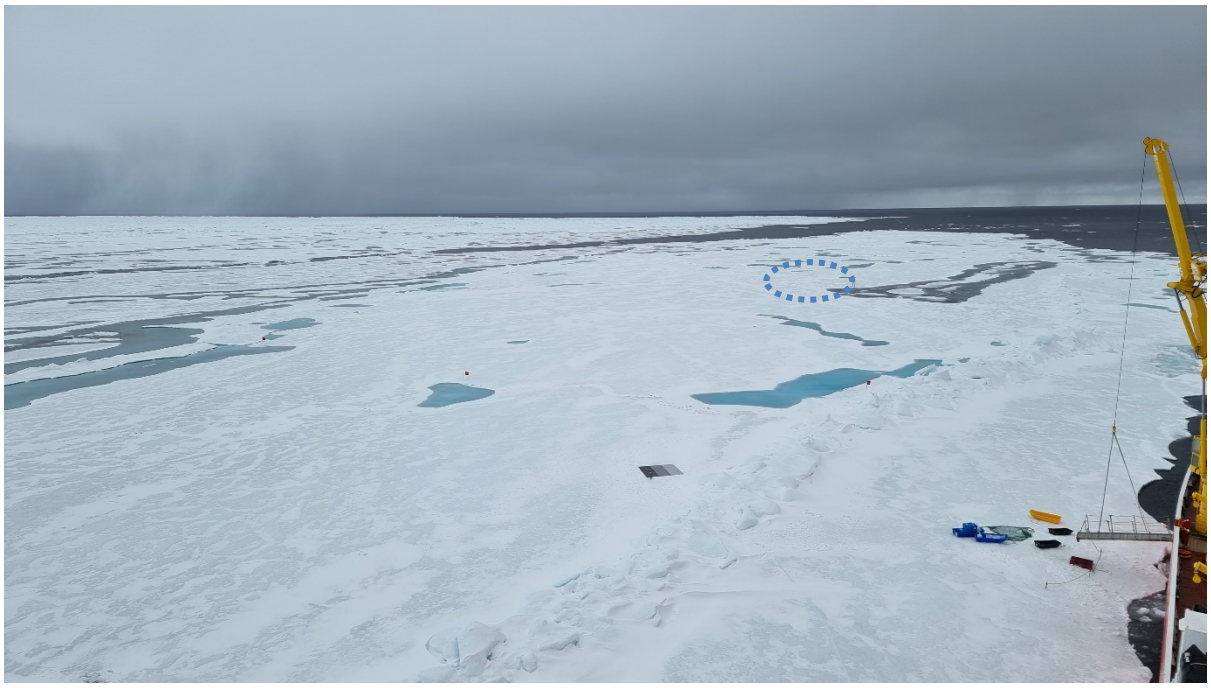

Fig 8.1.5. Compass deck view of the ice camp site on 18 August. The dotted oval is the place of the second SIMB3 deployment

On the selected site, the SIMB3 was activated and deployed in the local morning (around 06 UTC 19 August), through a drilled 10-inch hole (Fig. 8.1.6). The information on buoy and measurements are listed as follows:

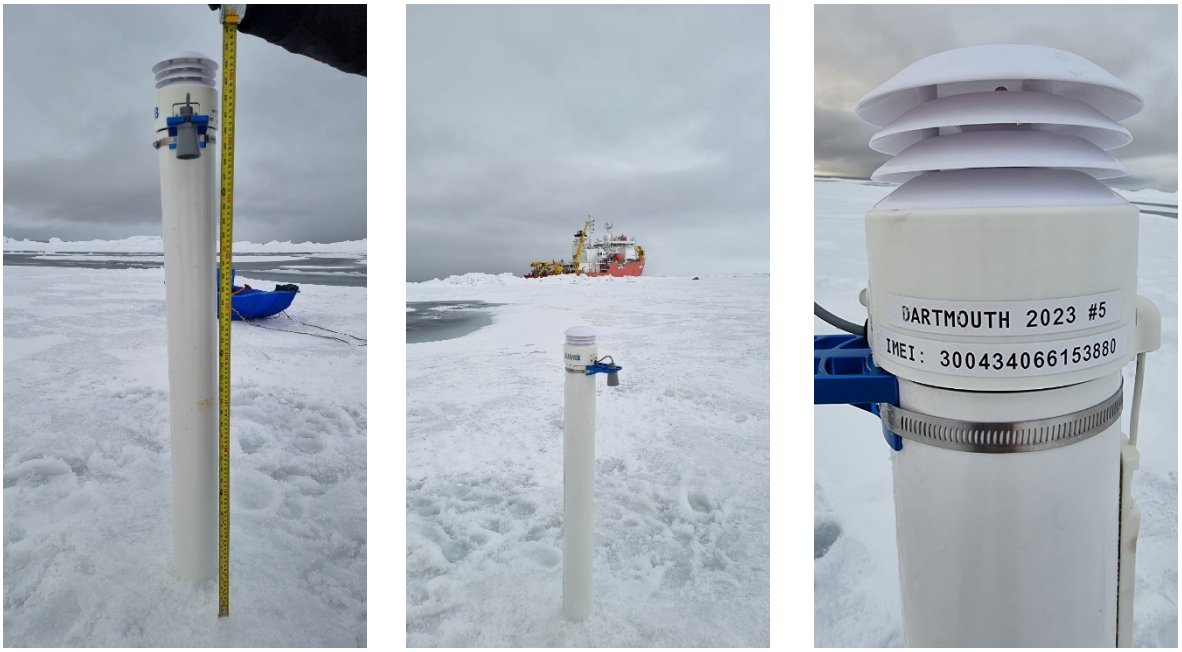

Fig 8.1.6. (Left) Taking measurements after deployment, (Middle) Deploy completed, (Right)

Close-up picture

- Activated on 06:05 UTC 19 August
- Buoy ID: Dartmouth 2023 #5
- S/N (IMEI): 300434066153880
- Ice thickness: 148 cm
- Frozen snow above freeboad: 13 cm (note: fresh snow layer of about 4 cm was scrapped away and, after deployment, we cover with scrapped snow and ice to make the surface flat)
- Freeboard: 5 cm
- Distance from ice to top sounder housing: 98 cm
- Distance from top of temperature string to ice: 117 cm

After the deployment, a datasheet including the deployment information was again sent to Chris Polashenski at Dartmouth College and Cameron Planck at Cryosphere Innovation. Then we got a response of the registration of the buoy's modem on 20 August and some initial data.

8.1.2. In-situ measurement

A melt pond observing system (MPOS) was designed to measure the 4 components of radiative fluxes (shortwave up/down & longwave up/down) on different surface conditions: ice/snow versus melt pond. It also measures air temperature and relative humidity (HMP155, Vaisala), wind speed and direction (WXT532, Vaisala), and water temperature and conductivity (HOBO U24, Onset). The water temperature and conductivity can be measured at multiple depth levels of melt pond depending on its depth. Figure 8.1.7 depicts the schematic diagram of the MPOS when deployed.

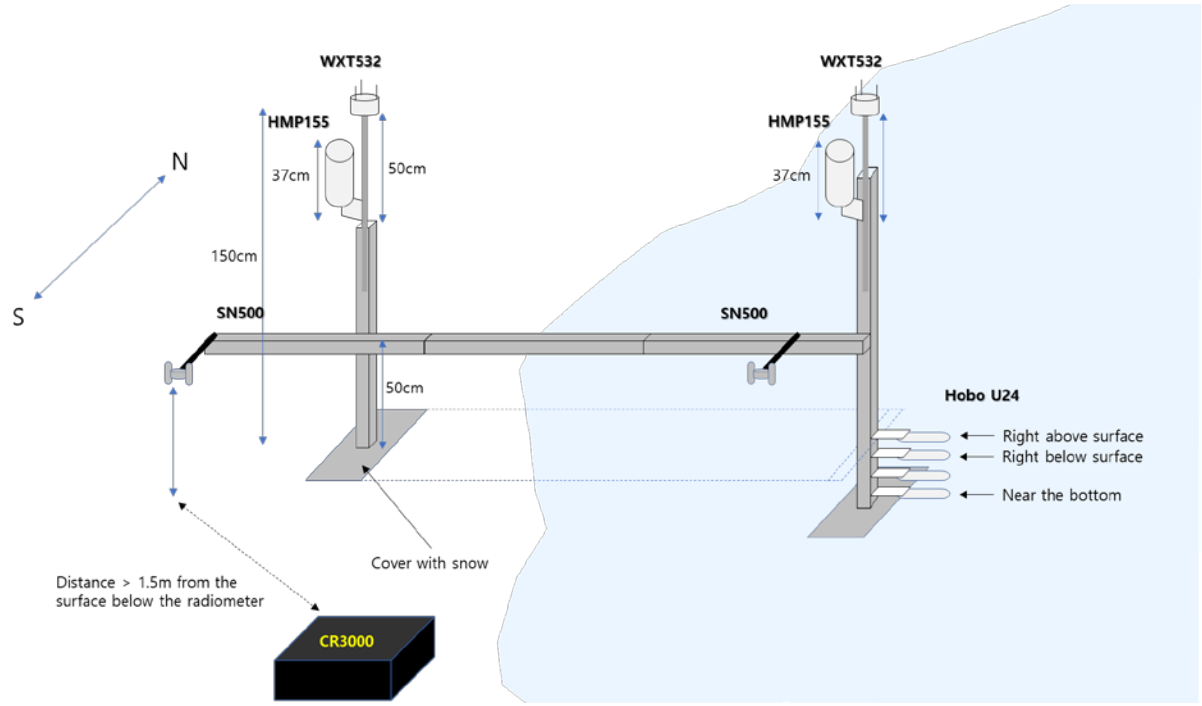

Fig 8.1.7. Schematic diagram of the melt pond observing system in 2023

We took the indoor test of differences of their measurements under same environment for several days (Fig. 8.1.8). For the downward (upward) longwave radiation, the mean and standard deviation of the differences were 0.269 (1.99) and 0.871 (0.964), respectively. Based on this test value, we supposed the observed differences between the two radiometers larger than 1 W m^{-2} to be signals.

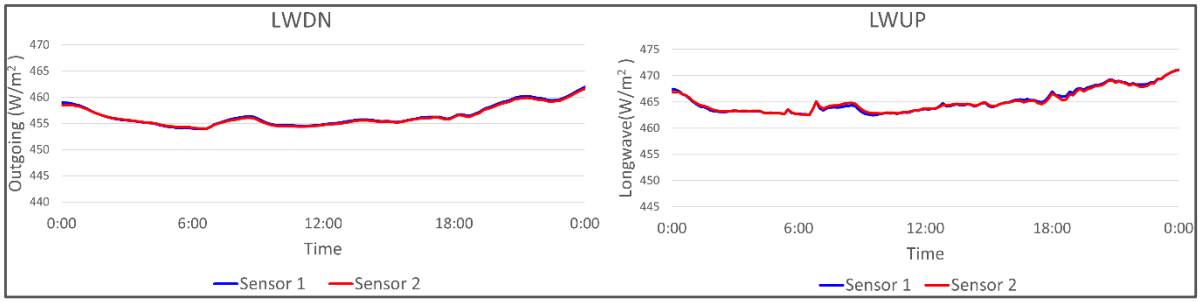

Fig 8.1.8. Indoor test of the difference of longwave radiative fluxes between two radiometers

We deployed the system on the first day of the ice camp (10 August) on one saline melt pond with a salinity of ~20 psu and a depth of 20 cm, located about 200 m away from the ship (Fig. 8.1.9). The system recorded the basic meteorological parameters and radiative fluxes over the ice and melt pond surfaces at 10-min intervals and logged pond's physical properties (temperature, salinity, and depth) at 10-sec intervals during the ice camp period (10-12 August).

Fig 8.1.9. The melt pond observing system deployed on a saline melt pond with ~ 20 cm depth

The air-side observations were made for about 42 hours from local 6pm (UTC-11) 10 August until 12am 12 August (Fig. 8.1.11). An expectable result is the notable difference in the upward shortwave radiation due to the surface color, which is a primary factor of positive ice-albedo feedback accelerating sea ice melt. The results are Interesting in terms of the air temperature and upward longwave radiative fluxes. The temperature over the pond was warmer than that over the ice and the more longwave radiative fluxes were emitted from the water during the daytime. The surface temperature of melt pond was over 1°C during the daytime of the second day indicating that the heat was used to warm the water surface, not melting the ice. Understanding this situation is not easy, but a clue to conjecture this problematic situation is a continuous intrusion of sea water at the bottom of the pond. Intrusion of heavier salty water at the bottom could make the pond much stable, so that most of the heat input from the atmosphere converged at the surface and warmed the surface water without melting sea ice. Higher water surface temperature led to more longwave emission over there. The significant difference in longwave radiative fluxes recalls that it would have a climatologically significant impact on sea ice evolution if the difference in outgoing fluxes (longwave + turbulent) is

persistent over the melt season (Kim et al., 2018).

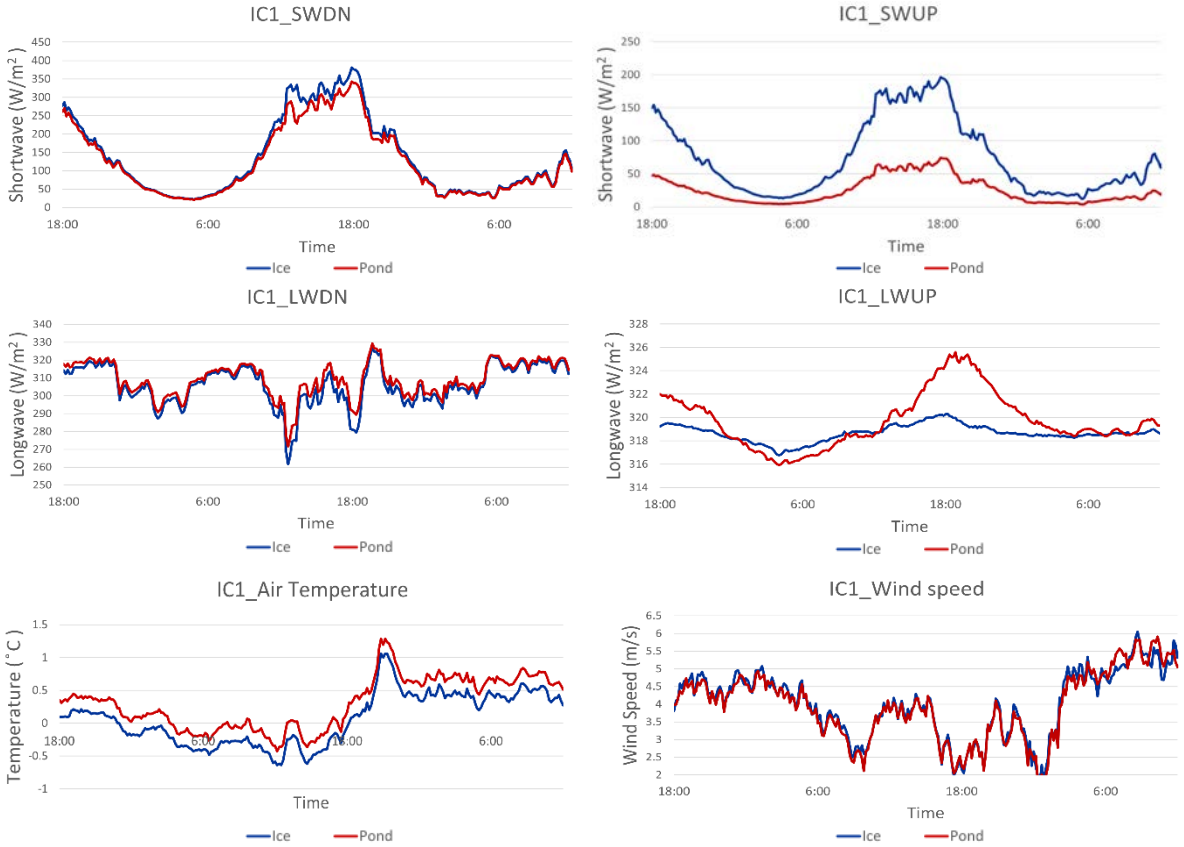

Fig 8.1.10. Time series of downward and upward shortwave (SWDN & SWUP) and downward and upward longwave (LWDN & LWUP) measured over two different surfaces (ice versus pond) , air temperature and wind speed

The temporal change of conductivity at three levels in the melt pond is shown in Fig. 8.1.11 This observation persisted during the entire sea ice camp period. The values for bottom three sensors (S4, S5 and S6) are presented after taking the correction of sensor discrepancies at laboratory (not shown), although there are still uncertainties in the corrected values. During the first half of the observed period, the conductivity was kept around 14,000~22,000 μS/cm for all levels until local 6am 11 August. However, it began to decrease sharply after local 8am, 11 August, indicating freshwater input increased possibly by sea ice melt. The conductivity decline was sharper at the top level, while it didn't change at the bottom.

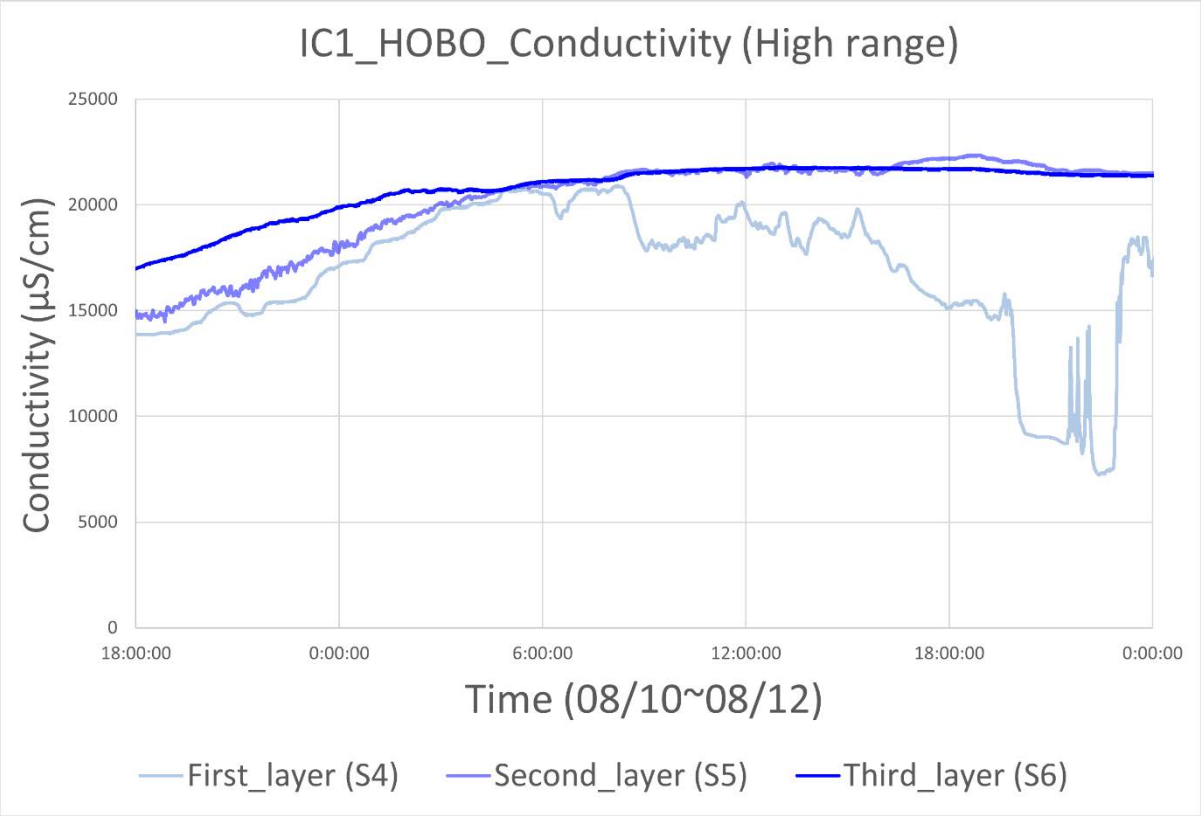

Fig 8.1.11. Time series of conductivity at three levels (S4: 4 cm below the surface (16 cm above the bottom), S5: 11 cm below the surface (9 cm above the bottom), S4: 18 cm below the surface (2 cm above the bottom)) in the melt pond with a depth of 25 cm

Another in-situ observation activity is the measurement of the melt pond's physical properties (temperature, salinity, and depth) for multiple melt ponds at the ice camp site (Fig. 8.1.12). The observation presents the control of pond temperature by the salinity-dependent melting temperature depression (Table 8.1.2). The existence of saline ponds makes the surface temperature lower, which might lead more energy can penetrate downward and be used to melt sea ice. This assumption will be proved by the sea ice model experiment by implementing melt water salinity impact on sea ice surface energy balance.

Fig 8.1.12. Compass deck view of the sea ice camp site with the deployed location of the melt pond observing system and the in-situ measured melt ponds

Table 8.1.2. Pond temperature, salinity and depth measured at the ice camp of ARA14B

No.	T (°C)	S (psu)	D (cm)	Remarks
1	1.2	0.961		MP01
2	-0.5	24.83	20	MP02, Meltpond observation
3	-0.3	25.49		MP03
4	-0.8	26.24	16	MP04
5	-0.9	26.22	13,5	MP05
6	0.3	0.566	8.3	MP06
7	0.4	0.1		MP07
8	-0.1	17.28	12.5	MP09
9	0.5	0.826	7.8	MP10
10	-0.8	27.57		MP11
11	-0.6	17.36	14.8	MP12
12	0.4	0.727	16.8	MP13
13	-1.1	27.72	22.9	MP14
14	1.2	11.21		Top level in #2
15	1.4	11.6		Top level in #4
16	1.1	11.79		Top level in #5
17	0.9	4.69~5.21		Top level in #8
18	-0.3	14.46		Top level in #10
19	0.7	2.147		Top level in #11
20	-0.4	4.832		Top level in #13

References

Kim, J. H., Moon, W., Wells, A. J., Wilkinson, J. P., Langton, T., Hwang, B., Granskog, M. A., Rees Jones, D. W. 2018. Salinity control of thermal evolution of late summer melt ponds on Arctic sea ice. Geophysical Research Letters, 45, 8304-8113.

Planck, C. J., Whitlock, J., Polashenski, C., Perovich, D. 2019. The evolution of the seasonal ice mass balance buoy. Cold Regions Science and Technology 165, 102792.

8.2. Under Sea Ice Mooring

Taewook Park[1], Jaeill Yoo[1], Myung Suk Kim[1]

[1]*Korea Polar Research Institute, Incheon, Republic of Korea*

E-mail: twpark@kopri.re.kr; jiyoo@kopri.re.kr; kmspban@kopri.re.kr

8.2.1 Motivation and Objective

Recent rapid sea ice reduction is associated with the underlying ocean stratification and upward heat flux from warm water such as PSW and NSTM. The heat flux is not constant but is affected by the small scale fluctuations of sea ice motions. To understand the condition for substantial heat release from the ocean, variations of vertical mixing in surface layers dominated by oscillatory Ekman spiral. The structure of the spiral is strongly controlled by the vertical eddy viscosity arising from internal wave breaking. The scientific goal is to investigate the heat and momentum transfers in the upper halocline layer by measuring current and water column structure under sea ice. Using the sea ice tethered mooring and ADCP, a part of the upper halocline layer measurement was performed. Based on density stratification and vertical shear of horizontal velocities, we will calculate variation of vertical eddy viscosity dependent on sea ice velocity including inertial motion.

8.2.2 Material and Methods

During the ice camp (August 10 to 12, 2023), we monitored temperatures using ice-tethered mooring systems. The ice-tethered was composed of 1 RBR T24 themistor cable with RBRconcerto data logger, one SBE 56 temperature-logger, and three SBE37SM microCAT CTD (Fig. 8.2.1). Icebreaker R/V Araon anchored at the marginal ice floe and the experimental site (179° 01.367' W, 78° 31.318' N) was on a drifting multi-year ice floe (Figure 8.2.2).

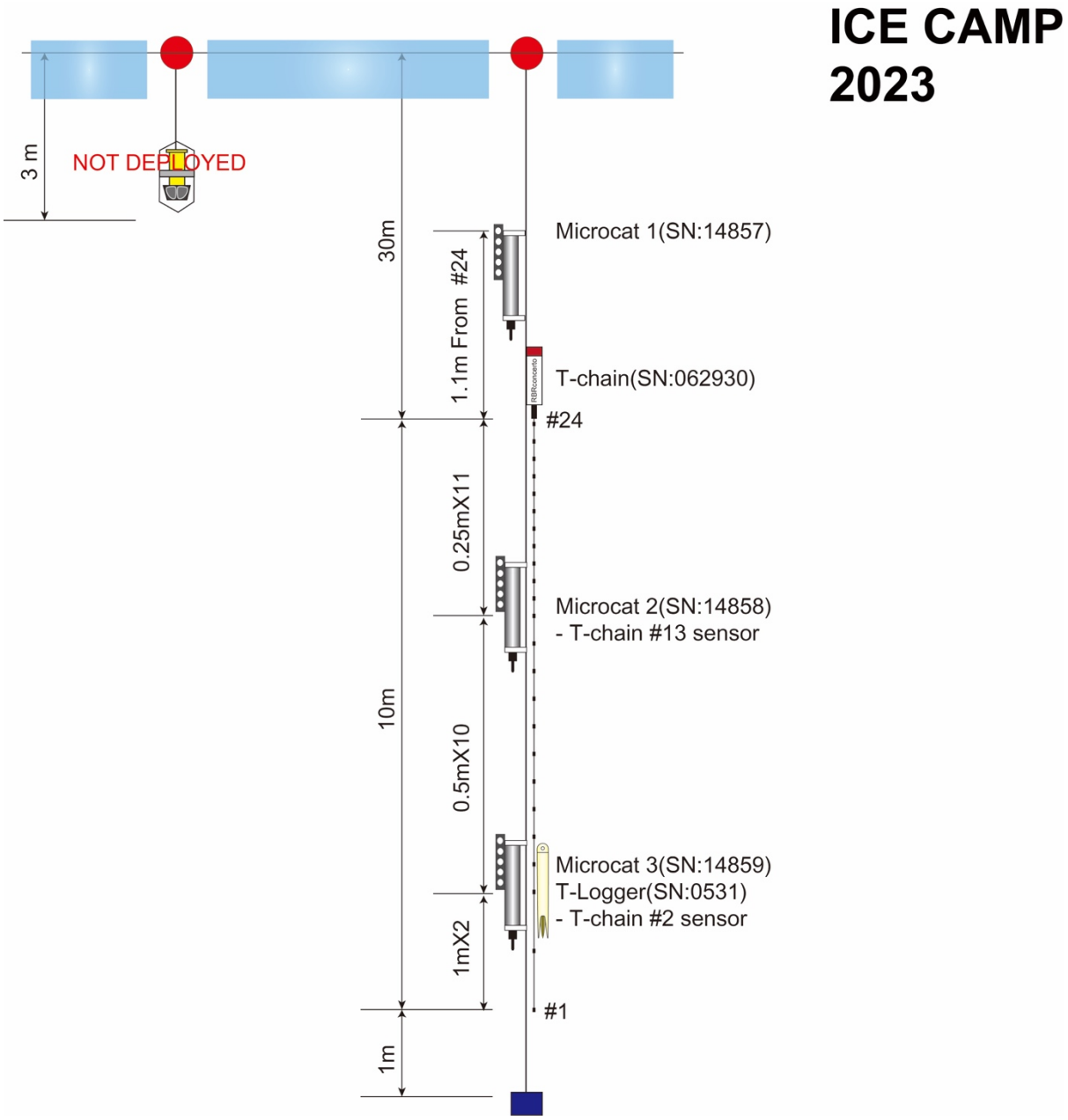

Figure 8.2.1 Schematic of ice-tethered mooring systems: thermistor mooring line.

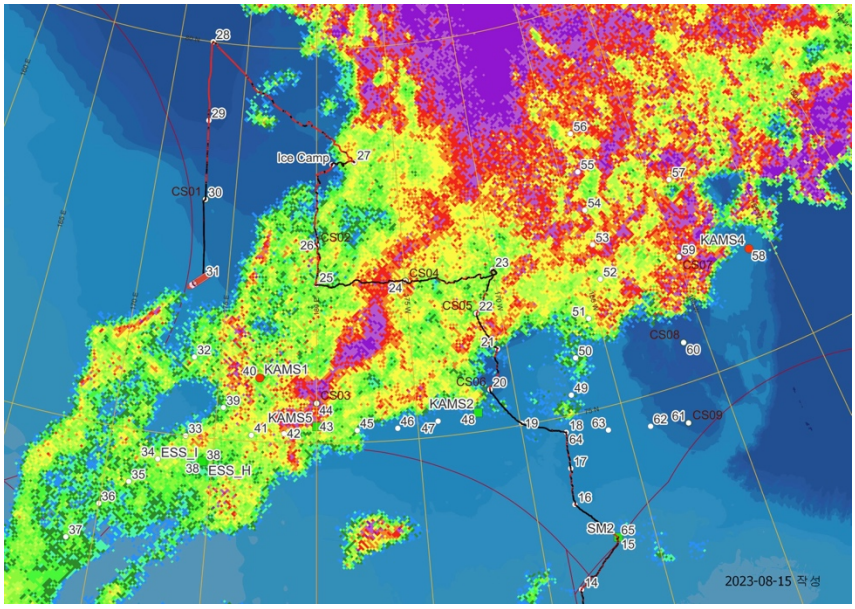

Figure 8.2.2. A map of the ice camp station on the sea ice concentration (color-shaded) with the location of ice camp and CTD locations.

8.3 Melt Pond

Jinyoung Jung[1], Jun-Oh Min[1], Ahra Mo[1], Jong KuK Moon[1], Chorom Shim[1], Jeong-Hyun Kim[1], Hyeju Yoo[1], Juyoung Son[1], Sanghoon Park[2], Ijin Lim[3], Jin Soo Son[4], and Jiwoo Kim[3]

[1]*Korea Polar Research Institute, Incheon, Republic of Korea*

[2]*Pusan National University, Busan, Republic of Korea*

[3]*Pukyong National University, Busan, Republic of Korea*

[4]*Hanyang University, Ansan, Republic of Korea*

E-mail: jinyoungjung@kopri.re.kr; jomin@kopri.re.kr; ahramo@kopri.re.kr;

jkmoon@kopri.re.kr, *chorom@kopri.re.kr;* jeonghkim@kopri.re.kr; *hjyoo@kopri.re.kr;*

mh0980@kopri.re.kr; mossinp@pusan.ac.kr; ijinlim@pukyong.ac.kr;

tngur1107@hanyang.ac.kr; jiukim999@gmail.com

8.3.1. Introduction

The oceanic cycles In the Arctic, meltwater can be partitioned within different habitats in the sea ice environment (Mundy et al. 2011). In the most recent spring and summer, the sea ice in the Arctic experienced a transformation associated with the increased air temperature, leading to the formation of surface melt ponds (MPs) and a strong reduction of the salinity of multiyear ice (Eicken et al. 2002). The resultant meltwater can be discharged through highly permeable ice or structural flaws and freshwater pooling in surface melt ponds, which are formed in the Arctic summer by melting snow; surface sea ice is an important feature of summer Arctic sea ice (Lüthje et al. 2006).

The melt pond is a distinct feature which is formed by the liquid water collecting in depressions on the surface and deepening them on the summer Arctic sea ice. The increase of melt pond area in the Arctic has been documented over the past decade, but plankton community structure and ecology have rarely been studied in the melt pond. In this study, we investigated the environmental factors (nutrient, POC, DOC, DIC, and δ13C-DIC) and the structure of microbial communities, including phytoplankton and heterotrophic protists.

8.3.2. Materials and methods

During the cruise, ice camps were conducted twice, from August 10 to 12 and August 19 to 20, 2023 (Figures 8.3.2.1 & 8.3.2.2). A total of 10 and 5 MPs were chosen during the first and second ice camps, respectively, with varying salinity levels (Tables 8.3.2.1 & 8.3.2.2). The melt water samples were collected from the surface of the MPs using silicon tubing connected to a peristaltic pump.

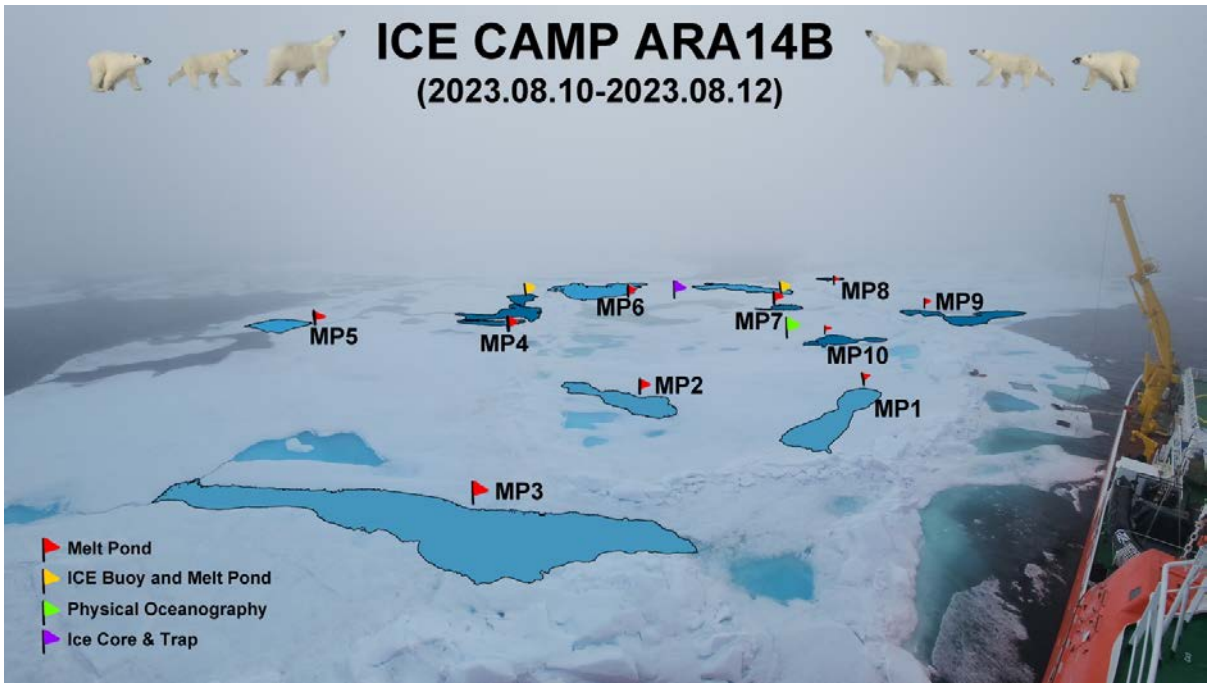

Figure 8.3.2.1 Photograph was taken of the melting ponds during the first sea ice camp of the ARA14B cruise. The red flags indicate the sampling location during the ice camp.

Table 8.3.2.1. Information on melt ponds during the first ice camp of the ARA14B cruise.

Melt pond	Latitude (N)	Longitude (W)	Salinity	Temperature
MP1	78° 31.972′	178° 46.508′	0.7	0.9

MP2	78° 31.945′	178° 46.352′	0.2	0.2
MP3	78° 31.926′	178° 46.213′	1.3	0.2
MP4	78° 31.913′	178° 46.256′	11.8	–0.4
MP5	78° 31.874′	178° 46.030′	6.5	–0.1
MP6	78° 31.891′	178° 45.858′	5.0	0.2
MP7	78° 32.878′	178° 33.978′	11.4	–0.6
MP8	78° 31.971	178° 32.533′	23.6	–1.0
MP9	78° 32.946	178° 31.891′	15.6	–1.4
MP10	78° 32.948	178° 30.667′	13.0	–0.6

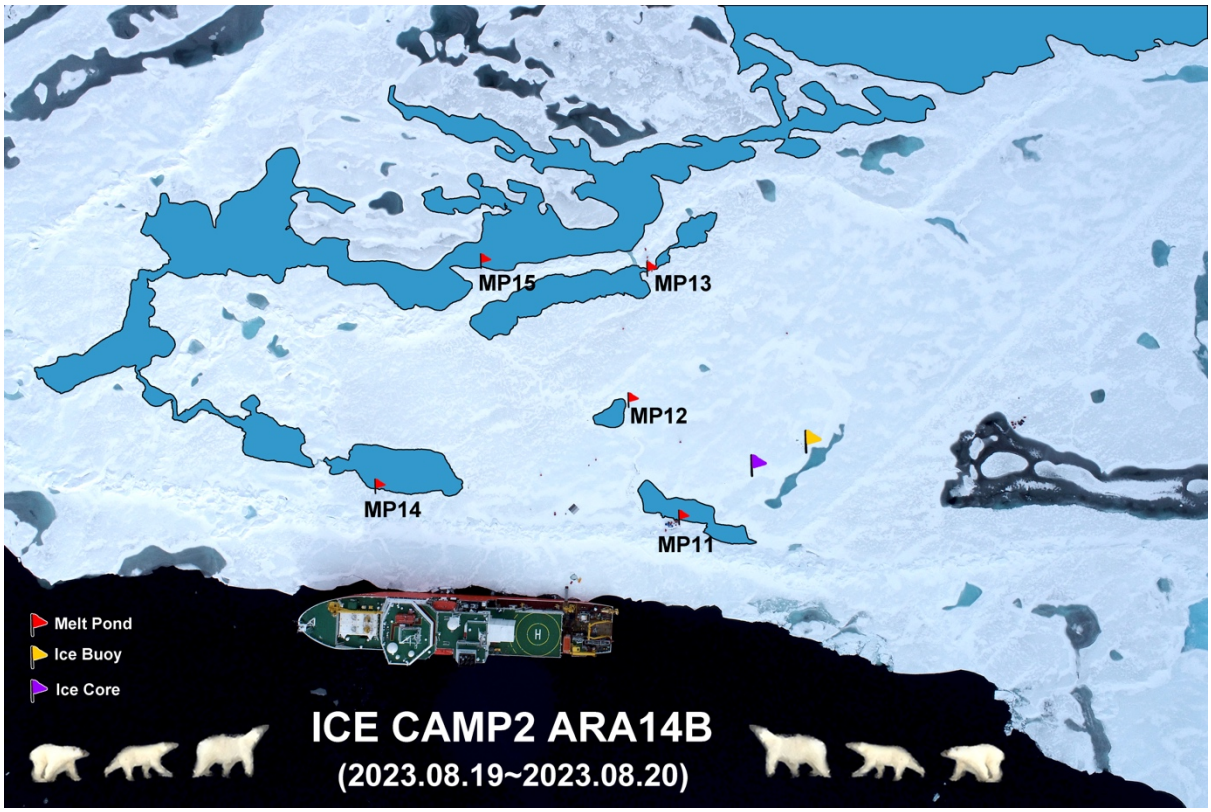

Figure 8.3.2.2. Photograph was taken of the melting ponds during the second sea ice camp of the ARA14B cruise. The red flags indicate the sampling location during the ice camp.

Table 8.3.2.2. Information of melt ponds during the second ice camp of the ARA14B cruise.

Melt pond	Latitude (N)	Longitude (W)	Salinity	Temperature
MP11	76° 01.208′	177° 18.305′	1.5	1.3
MP12	76° 01.117′	177° 18.138′	4.2	0.4
MP13	76° 01.009′	177° 17.957′	7.5	–0.2
MP14	76° 00.705′	177° 16.801′	7.4	–0.1
MP15	76° 00.538′	177° 16.198′	8.3	–0.5

Nutrients

Concentrations of nutrients were measured using standard colorimetric methods adapted for use on a 4-channel continuous Auto-Analyzer (QuAAtro, Seal Analytical). The channel configurations and reagents were prepared according to the 'QuAAtro Applications'. Standard curves were run with each batch of samples using freshly prepared standards that spanned the range of concentrations in the samples. The r^2 values of all the standard curves were greater than or equal to 0.99. In addition, reference materials for nutrients in seawater (RMNS) provided by 'KANSO Technos' (Lot. No. 'BV') were used along with standards at every batch of run in order to ensure accurate and inter-comparable measurements.

Dissolved organic carbon (DOC) and fluorescent dissolved organic matter (FDOM)

Water samples for analysis of dissolved organic carbon (DOC) and fluorescent dissolved organic matter (FDOM) were collected into a pre-cleaned (in 10% HCl) 4 L carboy. The filter holder was attached directly to the 4 L carboy. About 200 ml of seawater was filtered through a pre-combusted (at 550 °C for 6 hours) Whatman GF/F filter (47 mm in diameter) into pre-cleaned glass bottles under gravity. The filtrate was distributed into two pre-combusted 20 ml glass ampoules using a sterilized serological pipette. Each ampoule was sealed with a torch, quick-frozen, and stored at –24°C until the analysis in our land laboratory. DOC samples will be analyzed with high-temperature oxidation (HTCO) method (Sugimura & Suzuki, 1988) using a Shimadzu TOC-V system. To maintain quality control of sample analysis, 3–4 point calibration

curve of seawater DOC reference standards will be made. FDOM samples will be analyzed using a fluorescence spectrophotometer (F-7100, Hitachi Inc.).

Particulate organic carbon (POC)

Water samples for analysis of particulate organic carbon (POC) were drained into amber polyethylene bottle. POC samples were collected with same procedure as DOC sample by filtration of known seawater volume. POC samples were stored frozen at –20 °C until analysis in the home laboratory. POC samples will be determined with a CHN analyzer according to JGOFS protocol (JGOFS, 1996).

Inorganic carbon parameters and stable isotope of dissolved inorganic carbon (δ^{13}C-DIC)

Surface melt waters were sampled using the peristaltic pump to obtain values of stable isotope of DIC (δ^{13}C-DIC) and inorganic carbon parameters, such as dissolved inorganic carbon (DIC) and total alkalinity (TA). The sample bottles were flushed 3 times before starting collection in 500 mL borosilicate glass bottles. Making small headspace and injecting 200 µL of saturated $HgCl_2$ solution to prevent biological activities. Further, the vacuum grease was used to prevent contaminations and gas exchange between the sample and the atmosphere. After sampling, the bottles were tightened with rubber bands and stored in a dark place before analysis. After this cruise, the samples for TA and DIC will be analyzed using the VINDTA system in Korea University, and the samples for δ^{13}C-DIC will be analyzed using an Apollo DIC analyzer coupled to a carbon dioxide Picarro cavity ring-down spectrometer (CRDS) in KOPRI.

Abundance and community structure of heterotrophic protists

We measured abundance and community structure of heterotrophic protists at the melting ponds. In the melting pond, water samples were collected from the surface of the pond using silicon tubing connected to peristaltic pump.

For ciliates and sarcodina, 500 ml water from the surface was preserved with 1% acid Lugol´s iodine solution these samples were then stored in darkness. For heterotrophic nanoflagellates and heterotrophic dinoflagellates smaller than 20 µm, 250 ml of water was preserved with glutaraldehyde (0.5% final concentration) and stored at 4 °C.

Total and size-fractionated Chl a concentration

Subsamples from the melting ponds were filtered through a cascade connection of 20-µm nylon mesh, Nuclepore filter (Whatman International) with pore size of 2 µm, and a Whatman GF/F filter to determine size-fractionated Chl a (Sieburth 1978). Thus, micro-Chl a (>20 µm), nano-Chl a (2-20 µm), and pico-Chl a (<2 µm) could be measured directly. Subsamples for total Chl a in the melting ponds were filtered onto 47 mm GF/F Whatman filters and stored at –80 °C. Each filter was extracted in 90% acetone, and Chl a concentrations were measured with a fluorometer (model Trilogy, Turner Designs, USA; method: Parson et al., 1984).

Picoplankton abundance

Water samples for flow cytometry analysis were fixed for 15 min with paraformaldehyde (final concentration: 1%) and stored at –80 °C. Since fixation with added chemical reagents may result in loss of cells, natural samples were also analyzed on a Accuri C6 flow cytometer (Becton Dickinson) equipped with an air-cooled argon laser (488 nm, 15 mW), placed on-board so that after sample collection the analyses could immediately be performed. Picophytoplankton groups were identified and their abundance enumerated using the characteristics of 90°-angle light scatter, orange fluorescence from phycoerythrin, and red fluorescence from chlorophyll (Marie et al. 1997). For the enumeration of heterotrophic bacteria, seawater samples were stained with SYBR green I (Molecular Probes), and incubated in the dark at room temperature for 30 min before analysis. Bacteria were identified for their side light scatter and green fluorescence signals. Raw data from the flow cytometer will be processed using the FlowJo program (Tree Star, www.flowjo.com).

Photosynthetic pigments

The CHEMTAX program based on photosynthetic pigments data has potential benefits for the estimation of phytoplankton composition, including small and fragile forms. For photosynthetic pigment analysis, 4 L subsamples from the melting ponds were filtered onto 47 mm GF/F Whatman filters and stored at –80 °C. The pigments will be analyzed with high performance liquid chromatography (HPLC) in the laboratory.

Amino acid and Black Carbon

Amino acid (AA) and dissolved black carbon (DBC) sample were collected within 0.1 m depth using a transfer vacuum pump in a melt pond. The AA was measured by filtering 4 - 8L of seawater on pre-combusted (4 h, 450 °C) 47mm glass fiber filters (GF/F, Whatman, nominal pore size 0.45 μm). The filters were stored frozen (–80 °C) until processed. The remaining volume (4 - 20 L) of acidified sea water was then solid phase extraction following the method of Dittmar et al. (2008). Sample collected were loaded onto 1 g PPL (Agilent, USA) solid phase extraction columns at a low rate of about 2 mL per minute.

Transparent exopolymer particle and Biochemical composition of POM

Water samples for TEP and biochemical composition of particulate organic matter (Carbohydrates, Proteins, and Lipids) obtained from 0.1 m depth using a transfer vacuum pump at melt ponds. Seawater samples for TEP (0.1 L) were filtered through 0.4 μm pore sized polycarbonate membrane filters (ø = 25 mm) under low vacuum (<150 mm Hg). The filters were stained with 500 μL of Alcian Blue solution (8GX, Sigma), rinsed with distilled water, and immediately kept at –20 °C until further analyses. All sample waters for biochemical composition of particulate organic matter (1 L) were filtered on GF/F (ø = 47 mm) filters and were then immediately stored at –20°C until analysis

Trace metal

Water samples for trace metal concentrations and chemical speciation analysis were obtained using a peristaltic pump with pre-cleaned tubing connected to an acid-cleaned 0.2 μm filter cartridge (Acropak, Pall) from melt ponds. After water collection, filtered samples (125 mL LDPE bottle) were acidified to pH<1.8 by adding ultra-pure HCl (ODLAB, Korea) in the trace metal clean van and stored. For chemical analysis samples (500 mL LDPE bottle) were then frozen at –18 ^{o}C and stored until analysis.

Water samples for Fe stable isotopes analysis were collected directly using acid-cleaned bottles (500 mL LDPE bottle). Filtration was conducted within 3h in the clean bench in the onboard clean van. Seawater samples were filtrated through acid-cleaned 0.2 μm pore-size membrane filters and stored 1 L acid-cleaned LDPE bottles. Filtered samples were acidified to pH<1.8 by adding ultra-pure HCl (ODLAB, Korea) in the trace metal clean van and stored.

Carbon and nitrogen stable isotope ($\delta^{13}C$ and $\delta^{15}N$) in particulate organic matter

We collected experimental samples from 3 station at melt pond in the Ice Camp Ⅰ. The $\delta^{13}C$ and $\delta^{15}N$ in particulate organic matter (POM) were measured by filtering 50 L of seawater on pre-combusted (4 h, 450 °C) 47mm glass fiber filters (GF/F, Whatman, nominal pore size 0.7 μm). $\delta^{13}C$ and $\delta^{15}N$ values were measured using a stable isotope ratio mass spectrometer (isoprime vision; Elementar UK Ltd., Manchester, UK) with an elemental analyzer (EA, Vario EA Cube; Elementa GmbH). The $\delta^{13}C$ and $\delta^{15}N$ values (‰) were calculated using the following equation:

$$\delta X = [(R_{sample}/R_{standard})-1] \times 1000$$

where X indicates $\delta^{13}C$ or $\delta^{15}N$ and R is the corresponding ratio of $^{13}C/^{12}C$ or $^{15}N/^{14}N$. To determine the precision of isotope analysis, international standards (IAEA CH-3 and N-1) were used for $\delta^{13}C$ and $\delta^{15}N$ analysis, respectively.

References

Bowman, J.S., Rasmussen, S., Blom, N., Deming, J.W., Rysgaard, S., Sicheritz-Ponten, T. 2012. Microbial community structure of Arctic multiyear sea ice and surface seawater by 454 sequencing of the 16S RNA gene, The ISME Journal 6, 11-20.

Dittmar, T., Koch, B.P., Hertkorn., N., and Kattner, G. 2008. A simple and efficient method for the solid-phase extraction organic matter (SPE-DOM) from seawater, Limnol. Oceanogr., Methods, 6, 230-235.

Eicken, H., Krouse, H.R., Kadko, D., Perovich, D.K. 2002. Tracer studies of pathways and rates of meltwater transport through Arctic summer sea ice. J. Geophys. Res. 107: C108046. doi:10.1029/2000JC000583.

Lüthje, M., Feltham, D.L., Taylor, P.D., Worster, M.G. 2006. Modeling the summertime evolution of sea-ice melt ponds. J. Geophys. Res. 111: C020001.

doi:10.29/2004JC002818.

Marie D, Partensky F. Jacquet S, Vaulot D. 1997. Enumeration and cell-cycle analysis of natural populations of marine picoplankton by flow cytometry using the nucleic-acid stain SYBR Green I. Appl Environ Microb. 14: 113-118.

Mundy, C.J., Gosselin, M., Ehn, J.K., Belzile, C., Poulin, M., Alou, E., Roy, Su., Hop, H., Lessard, S., Papakyriakou, T. N., Barber, D. G., Stewart, J. 2011. Characteristics of two distinct high-light acclimated algal communities during advanced stages of sea ice melt. Polar Biol. 34:1869-1886.

Sieburth, JMcN. 1978. Pelagic ecosystem structure: Heterotrophic compartments of the plankton and their relationship to plankton size fractions. Limnol Oceanogr. 23: 1256-1263.

Parsons, T.R., Maita, Y., Lalli, C.M. 1984. A manual of chemical and biological methods for seawater analysis. Pergamon Press, Oxford, 173p.

8.4. Sea ice core

Jong KuK Moon, Chorom Shim, Jung-hyun Kim

Korea Polar Research Institute, Incheon, Republic of Korea

Email: jkmoon@kopri.re.kr; chorom@kopri.re.kr

8.4.1. Introduction

Sea ice extent at the end of the summer melt season has been used as a measure of the state of the Arctic Ocean sea ice field since the beginning of the satellite record in 1979. Since then satellite observation showed the decline of sea ice extent by 12% per decade, with the minimum to date occurring in 2007. The second lowest minimum sea ice extent to date was observed in 2011, when the ice extent was slightly (ca. 7%) higher than the 2007 minimum. During that period, the Chukchi Borderland (CBL), in particular, experienced a massive decline in sea ice concentration (NSIDC 2011). Number of feedbacks and factors discussed for such variability include solar heating, advection of warm current (Pacific), warm air advection, preconditioning of thin ice and simply advection of sea ice away from the region.

The aim of this research is to investigate the sea ice characteristics on the East Siberian Seas as fundamental information of Arctic marine ecosystem.

8.4.2. Material and methods

Study area

The study stations were located in the eastern Arctic Ocean (East Siberian Sea) in August 2023, during the cruise of R/V ARAON (Fig. 8.4.1). The sea ice cores were sampled from ice corer (Mark II). Several Ice cores (9.5 cm diameter) were collected from Sea ice camps.

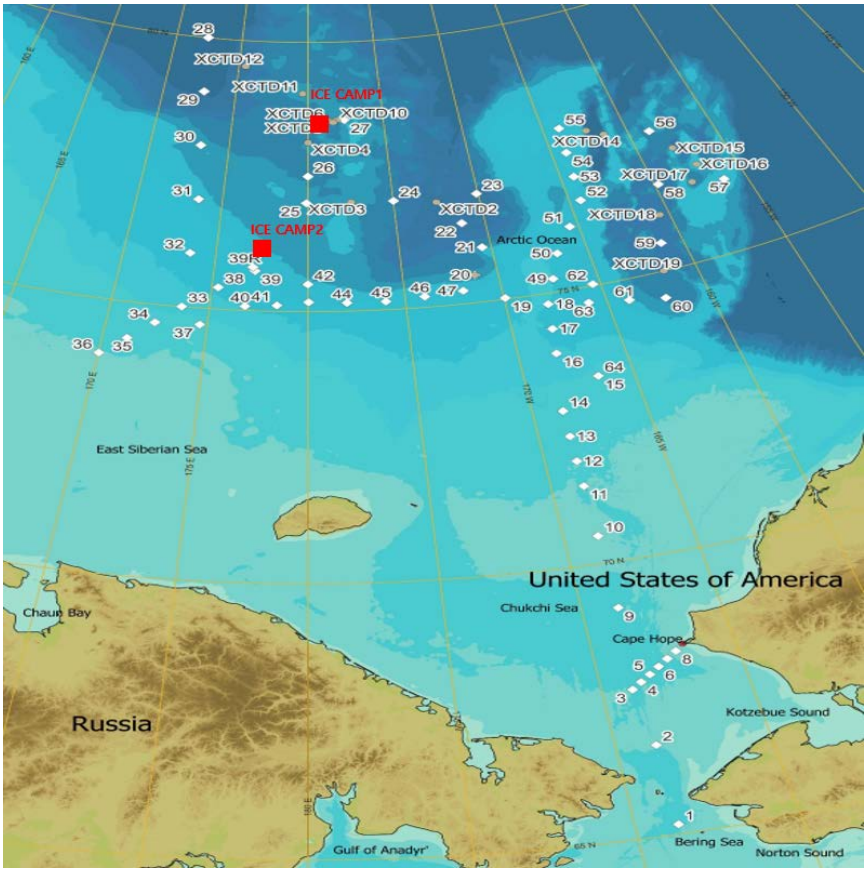

Fig. 8.4.1. Sea ice camp sites during the 2023 Arctic cruise.

Analysis Items of ice core

- Sea ice algae composition
- Chl-a concentration
- Nutrients
- POC, DOC and DON
- Temperature and salinity

ARA14B Sea ice camp Ice Core Sample

	JJY1	T (℃)	S (ppt)	length (cm)		JJY2	T (℃)	S (ppt)	length (cm)		JJY3	T (℃)	S (ppt)	length (cm)
Bot	1	-1.7	2.8	30	Bot	1	-2.7	2.7	30	Bot	1	-2.2	**3.0**	30
	2	-1.8				2	-2.6				2	-2.3		
	3	-2.2	3.1	20		3	-2.5	3.3	20		3	-2.4	3.1	20
	4	-2.3				4	-2.6				4	-2.4		
	5	-2.4	3.1	20		5	-2.5	3.6	20		5	-2.7	3.4	20
	6	-2				6	-2.6				6	-2.4		
	7	-1.6	2.7	20		7	-2.5	3.4	20		7	-2.5	3.4	20
	8	-1.6				8	-2.4				8	-2.1		
	9	-1.6	2.5	20		9	-2	3.2	20		9	-2.3	3.5	20
	10	-1.8				10	-1.9				10	-2.2		
	11	-1.5	1.7	20		11	-1.8	3.3	20		11	-2.1	3	20
	12	-1.6				12	-1.8				12	-2.1		
	13	-1.6	1.7	20		13	-1.7	2.4	20		13	-2.1	2.9	20
	14	-1.3				14	-1.3				14	-2		
	15	-1.2	1.2	20		15	-1.5	1.9	20		15	-1.8	**2.0**	20
	16	-1.2				16	-1				16	-1.1		
	17	0	0.2	20		17	-1.2	0.9	20		17	-1.1	**1.0**	20
Top	18	0.5				18	0.1				18	-1.2		
						19	0.2	0.1	20		19	0.3	0.1	20
					Top	20	0.7			Top	20	0.4		

Table 8.4.1. Temperature and salinity of the sea ice cores.

Chapter 9 Sea Ice Mechanics

Huichan Kim

Korea Maritime & Ocean University, Busan, KOREA

(khc1996@g.kmou.ac.kr)

Jeonguk Lee

Korea Maritime & Ocean University, Busan, KOREA

(wjddnr7078@g.kmou.ac.kr)

9.1. Introduction

Vessels operating in the ice-covered waters should satisfy the ice class rules for safe navigation; thus, shipyards should determine the most effective propulsion capacity and hull form during the design stage of a vessel. This can be done using a model test in an ice model basin and/or ice trials in the Arctic Ocean. In this research, ice trials of the IBRV ARAON were conducted during her Arctic cruise in the East Siberian Seas and the Chukchi Seas. Main objective of the full-scale trials is to investigate the performance of a ship moving in ice, i.e., to characterize icebreaking capability and ice-strengthening of the ship's hull. Ship performance in ice can be evaluated by means of three interrelated parameters such as ship speed, propulsion power and sea ice conditions. For investigating the ice-strengthening of ship's hull, it is necessary to understand the hull's capability to take ice loads preserving the strength of hull structural elements. The magnitude of ice load on the hull structure from the ship–ice interaction is determined by analysis of ship motion using a motion sensor to collect 6-DOF responses of a ship. The result can provide important information for the development of new design codes for ice-going vessels. In addition, the local ice load and hull strength is investigated by internal optical gauge measurements. The collected data can be used for calculating the response of the structural elements to ice impacts.

9.2. Research activity during the 2023 Arctic cruise

In particular, the ice load measurements were conducted during the cruise. To measure the global ice load on the ship's hull, a motion sensor was installed at the center of gravity of IBRV ARAON. This method assumes the ship is a rigid body and uses its whole-ship motions to determine external ice forces. The motion sensor measures the total ship acceleration and the rate sensors measure the three-dimensional angular rotational rate of the ship, along a fixed coordinate system. Figure 9.1 shows the installed motion and rate sensors.

The ice load exerted on the front port and starboard side's hull was also measured by the optical gauge modules and the rosette gauge sensors (total 21 F/O sensors, 21 R/G sensors, 126 channels) for stress monitoring system and these results will be analyzed later. Figure 9.2 shows the optical gauge sensors and the rosette gauge sensors installed on the inside surface of ARAON's hull plates. Figure 9.3 shows the real-time AXIS cameras installed 6 different places to record the sea-ice pattern while breaking ice.

Figure 9.4 shows several ice cores (9.0cm diameter) sampled from the sea ice camp. The weight, temperature, salinity, compression load analysis were performed to collect ice core data.

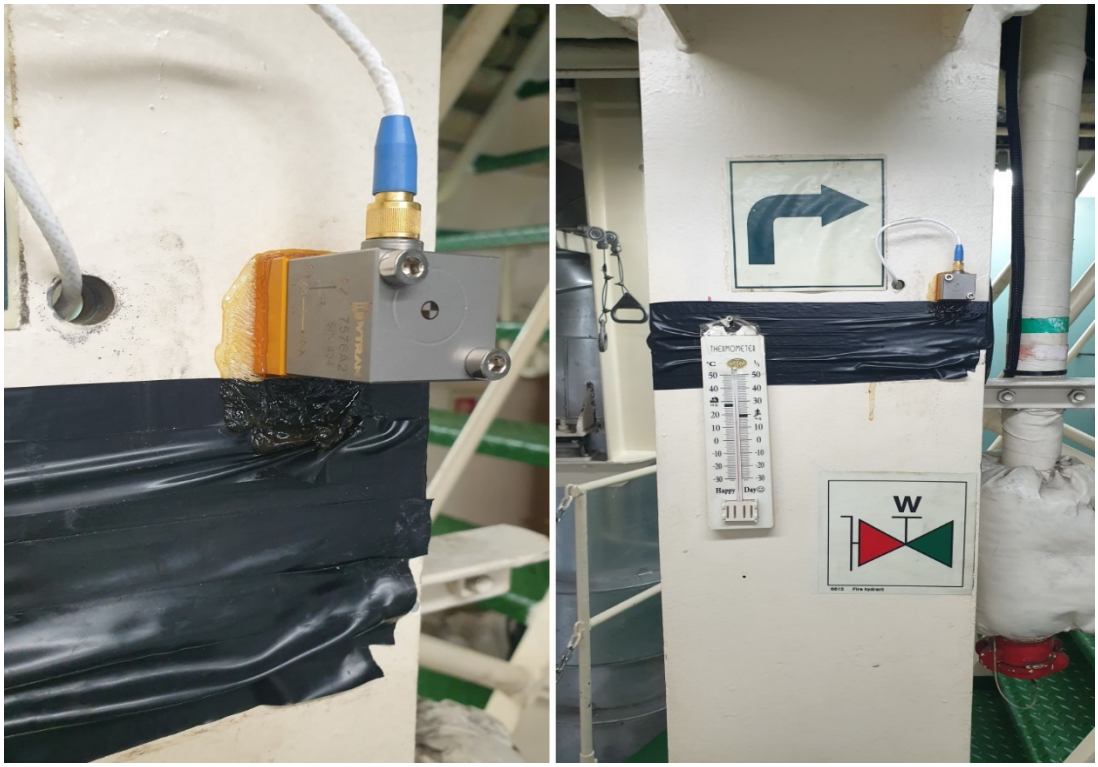

Fig 9.1. Installed motion sensor at the center of gravity of IBRV ARAON

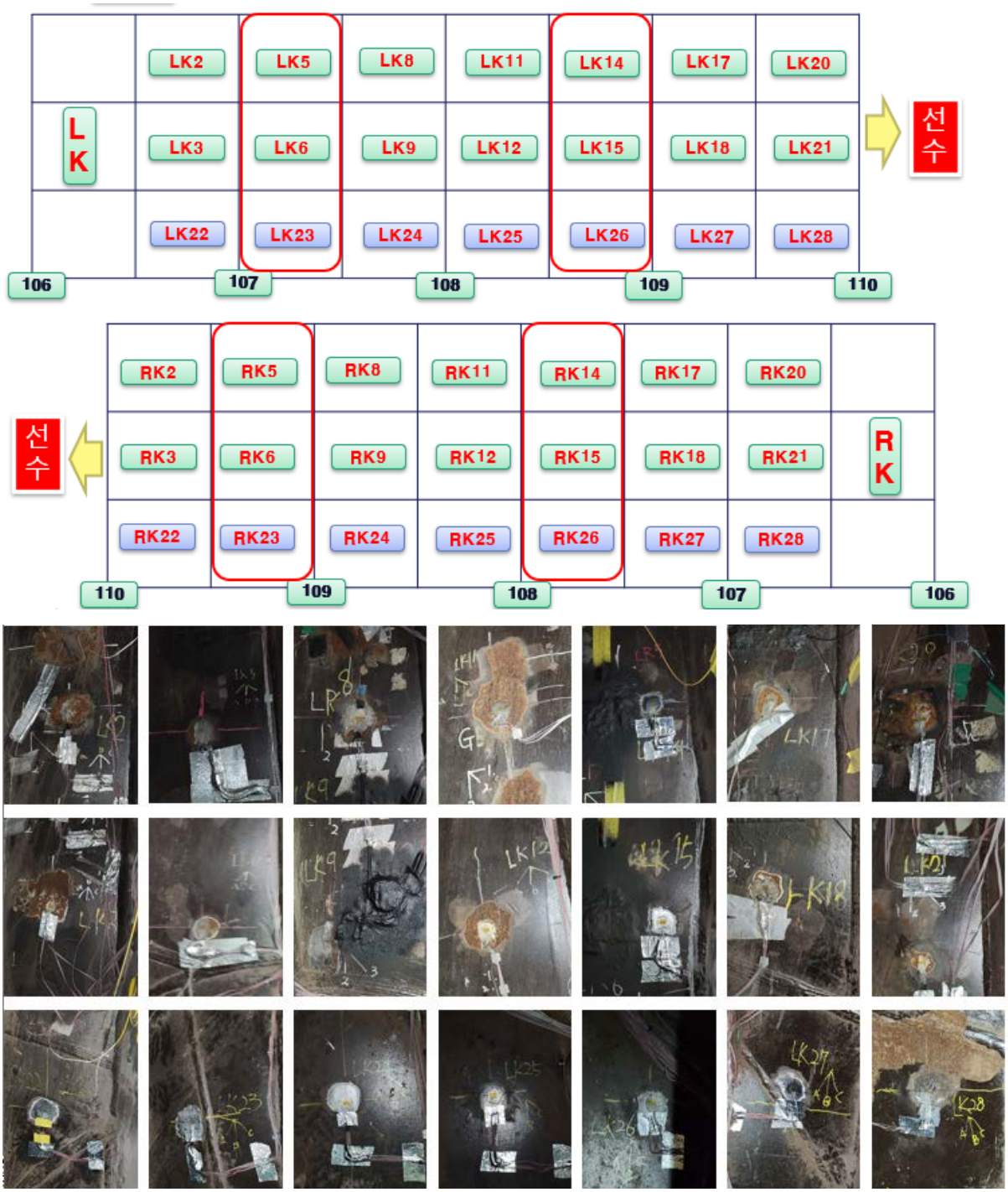

Fig 9.2. Installed gauge sensors

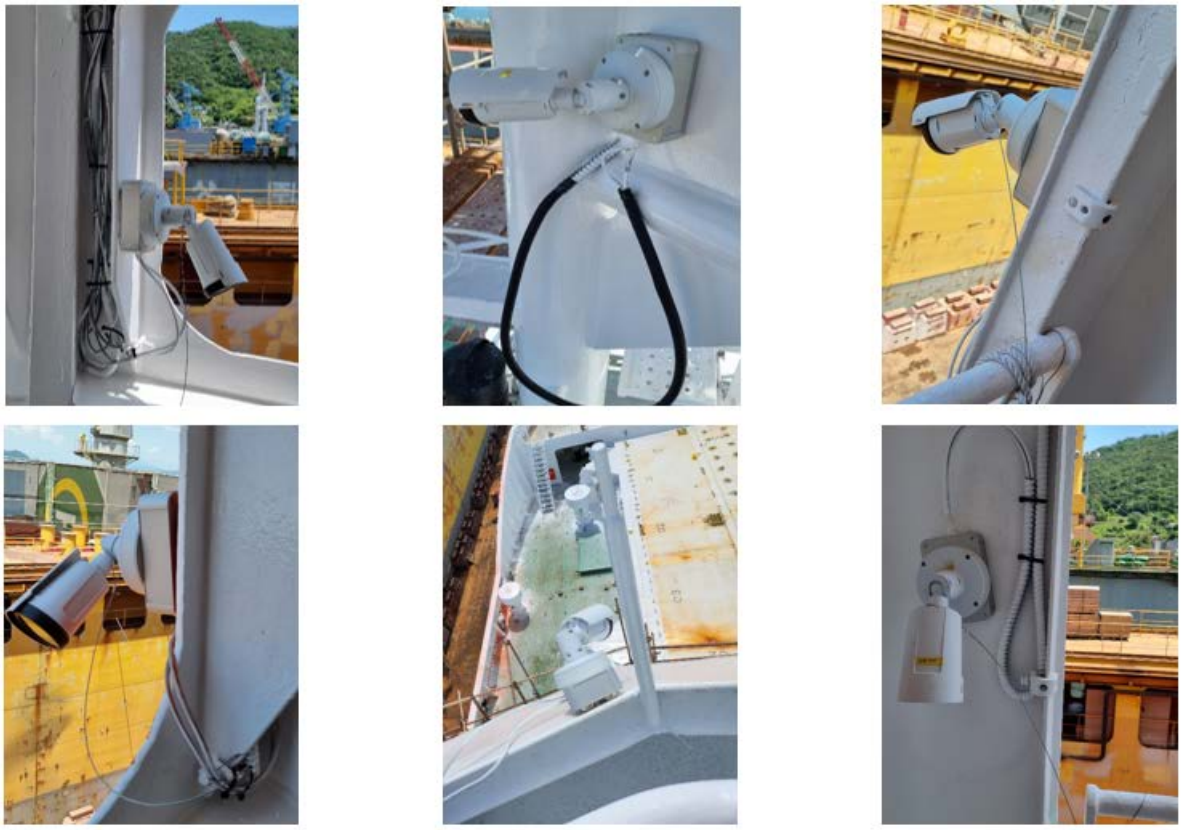

Fig 9.3. Installed AXIS real-time recording cameras

Fig 9.4. Ice core sampling at the sea ice camp

Summary and Discussions

The ARA14B Arctic cruise was undertaken in the East Siberian Seas and the Chukchi Seas during August 2023 to investigate the physical properties of the sea ice and ship performance in ice.

To estimate the global ice load on the ship's hull, a motion sensor was installed on IBRV ARAON and along a fixed coordinate system, the surge, sway and heave linear accelerations and the roll, pitch and yaw angular rotational rates of the ship were recorded during ship-ice interaction,. During the 2023 Arctic cruise, more than 3600 minutes data (sampling rate 50Hz) were collected form the ARAON's ice transit. In addition, the local ice pressures exerted on the port and starboard sides of ARAON's bow hull was also measured by the optical gauge modules and the rosette gauge sensors (total 126 channels as shown in Figure 9.2). The data obtained during the cruise will be analyzed later (Boersheim, 2007; Daley et al., 1984, 1990; Frederking, 2003; Freeman et al., 2003, Holm, 2012; Iyerusalimskiy et al., 2011). Figure 9.5 shows the real-time strain gauge data on the hull plates. The weight, temperature, salinity, compression load data were collected from ice camp (Table 9.1).

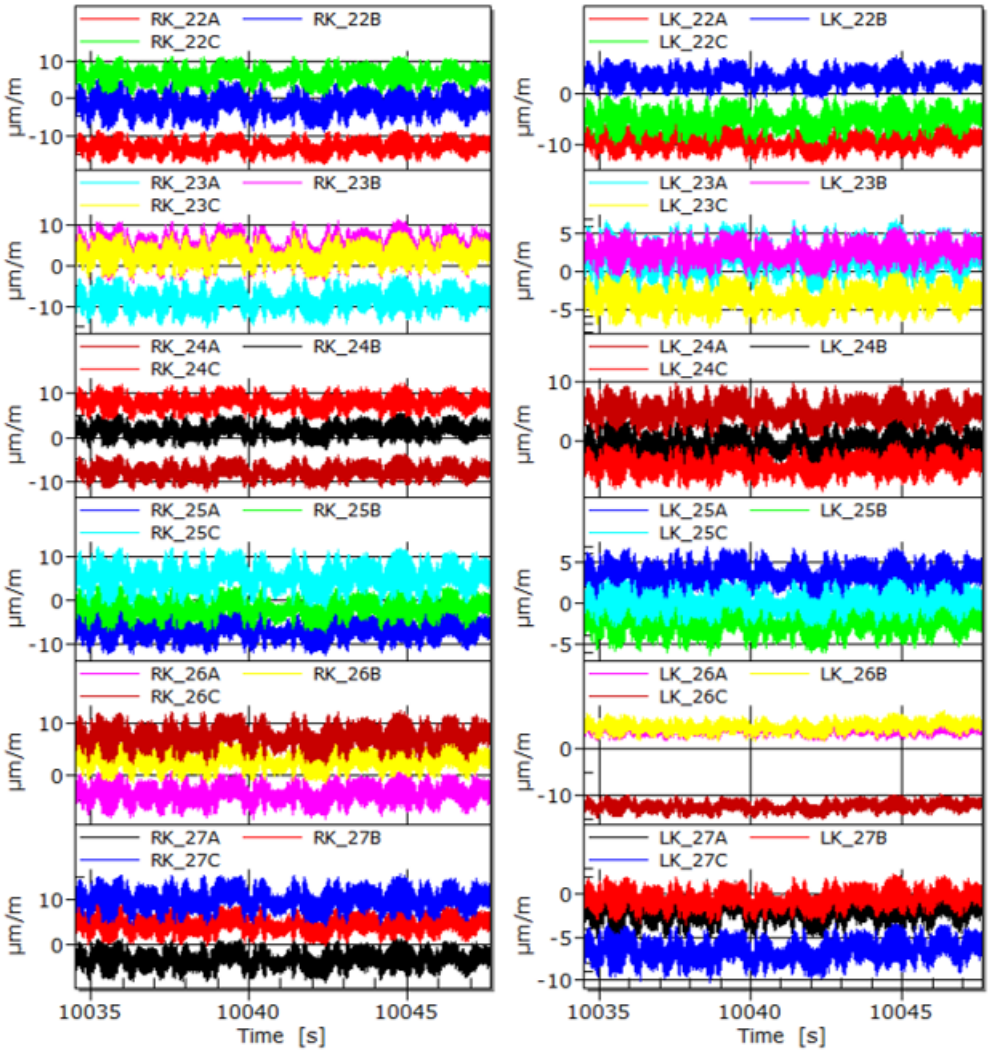

Fig 9.5. Real-time strain gauge data

References

Boersheim, L., 2007. Ship hull monitoring of ice-induced stresses, Master Thesis, NTNU, Norway.

Cox, G.F.N., Weeks, W.F., 1974. Salinity variations in sea ice. J. Glaciology. 13, pp. 109-120.

Daley, C.G., St. John, J.W., Seibold, F., Bayly, I., 1984. Analysis of extreme ice loads measured on USCGC Polar Sea, SNAME Trans., 92, pp.241-252.

Daley, C.G., St. John, J.W., Brown, R., Glen, L.F., 1990. Ice loads and ship response to ice, Consolidation Report SSC-340, SNAME Ship Structural Committee.

Frederking, R.M.W., 2003. Determination of local ice pressures from ship transits in ice, Proc.

13th ISOPE Conf., Honolulu, Hawaii, USA, pp.484-488.

Freeman, R., Ritch, R., Daley, C., Browne, R., 2003. Use of finite element methods to determine iceberg impact pressure based on internal strain gauge measurements, Proc. 17th POAC Symp., Tronheim, Norway, pp.699-708.

Haas, C., 1998. Evaluation of ship-based electromagnetic-inductive thickness measurements of summer sea-ice in the Bellingshausen and Amundsen Seas, Antarctica. Cold Reg. Sci. and Tech. 27, pp.1-16.

Holm, H., 2012, Ice-induced Loads on Ship Hulls, Master Thesis, Norwegian University of Science and Technology(NTNU), Trondheim, Norway.

Iyerusalimskiy, A. et al., 2011. The interim results of the long-term ice loads monitoring on the large Arctic tanker, Proc. 21st POAC Symp., Montreal, Canada, Paper No.088.

Nakawo, M., Sinha, N.K., 1981. Growth rate and salinity profile of first-year sea ice in the high Arctic. J. Glaciol. 27(96), pp. 315-330.

Shirasawa, K., Tateyama, K., Takatsuka, T., Kawamura, T., Uot. S., 2006. Ship-borne electromagnetic induction sounding of sea ice thickness in the Arctic during summer 2003. Polar Meteorol. Glaciol. 20, pp. 53-61.

Tateyama. K., Shirasawa. K., Uto, S., Kawamura, T., Toyota, T., Enomoto, H., 2006. Standardization of electromagnetic–induction measurements of sea-ice thickness in polar and subpolar seas. Annals-for Glaciology. 44, pp. 240-246.

Timco, G.W., Frederking, R.M.W., 1996. A review of sea ice density. Cold Reg. Sci. and Tech. 24(1), pp. 1-6.

Timco, G.W. and Weeks, W.F., 2010. A review of the engineering properties of sea ice. Cold Reg. Sci. and Tech. 60, pp. 107-129.

Tonboe, R.T., Pedersen, L.T., Haas, C., 2009. Simulation of the satellite radar altimeter sea ice thickness retrieval uncertainty. The Cryosphere Discuss. 3, pp. 513-559.

Weeks, W.F., Lee, O.S., 1958. Observations on the physical properties of sea-ice at Hopedale Labrador. Arctic, pp. 134-155.

References

Andres, M., Wimbush, M., Park, J.-H., Chang, K.-I., Lim, B.-H., Watts, D. R., Ichikawa, H. and

Teague, W. J. Observations of Kuroshio flow variations in the East China Sea. J. Geophys. Res., 113, C05013 (2008).

Book, J., Wimbush, M., Imawaki, S., Ichikawa, H., Uchida, H. and Kinoshita, H. Kuroshio temporal and spatial variations south of Japan, determined from inverted-echo-sounder measurements, J. Geophys. Res. 107 (2002).

Donohue, K.A., Watts, D.R., Tracey, K.L., Greene, A.D. and Kennelly, M. Mapping circulation in the Kuroshio extension with an array of current and pressure recording inverted echo sounders, Journal of Atmospheric and Oceanic Technology, 27 (3), 507–527 (2010).

Garrett, C. Topographic Rossby waves off east Australia: Identification and role in shelf circulation, J. Phys. Oceanogr., 9, 244–253. (1978)

Ghaemsaidi, S.J., Dosser, H., Rainville, L. and Peacock, T. The impact of layering on internal wave transmission, J. Fluid Mech. (2016).

Kim, S.Y., Lee, H.J., Park, J.-H., and Kim, Y.H. Effects of reduced vertical mixing under sea ice on Atlantic meridional overturning circulation (AMOC) in a global ice ocean model. Ocean Sci. J., 50, 155–161 (2015).

Kwok, R., Spreen, G., & Pang, S. (2013). Arctic sea ice circulation and drift speed: Decadal trends and ocean currents. Journal of Geophysical Research: Oceans, 118, 2408–2425. https://doi.org/10.1002/jgrc.20191

Ku, A., Seung, Y.H., Jeon, C., Choi, Y., Yoshizawa, E., Shimada, K., Cho, K. and Park, J. Observation of Bottom-Trapped Topographic Rossby Waves on the Shelf Break of the Chukchi Sea, J. Geophys. Res., 125(7) C015436 (2020).

Nilsen, F. Gjevik, B. and Schauer, U. Cooling of the West Spitsbergen Current: Isopycnal diffusion by topographic vorticity waves, J. Geophys. Res., 111, C08012 (2006).

Park, J.-H. and Watts, D. R. Near-inertial oscillations interacting with mesoscale circulation in the southwestern Japan/East Sea, Geophys. Res. Lett., 32, L10611 (2005).

Pickart, R.S., Moore, G.W.K., Mao, C., Bahr, F., Nobre, C., and Weingartner, T.J. Circulation of winter water on the Chukchi shelf in early summer. Deep-Sea Research II, 130, 56-75 (2016).

Polyakov, I. V., Pnyushkov, A. V., Alkire, M. B., Ashik, I. M., Baumann, T. M., Carmack, E. C., et al. (2017). Greater role for Atlantic inflows on sea-ice loss in the Eurasian Basin of the

Arctic Ocean. Science, 356, 285–291. https://doi.org/10.1126/science.aai8204

Rainville, L. and Woodgate, R.A. Observations of internal wave generation in the seasonally ice-free Arctic. Geophys. Res. Lett. 36, L23604 (2009).

Rippeth, T. P., Lincoln, B. J., Lenn, Y. D., Green, J. A. M., Sundfjord, A., & Bacon, S. (2015). Tide-mediated warming of Arctic halocline by Atlantic heat fluxes over rough topography. Nature Geoscience, 8(3), 191–194. https://doi.org/10.1038/ngeo2350

Shimada, K., Carmack, E.C., Hatakeyama, K., and Takizawa, T. Varieties of shallow temperature maximum waters in the western Canadian Basin of the Arctic Ocean. Geophysical Research Letters, 28(18), 3441-3444 (2001).

Steele, M., Morison, J., Ermold, W., Rigor, I., Ortmeyer, M., and Shimada, K. Circulation of summer Pacific halocline water in the Arctic Ocean. Journal of Geophysical Research, 109, C02027, doi:10.1029/2003JC002009 (2004).

Steele, M., Zhang, J., and Ermold, W. Mechanisms of summertime upper Arctic Ocean warming and the effect on sea ice melt. Journal of Geophysical Research, 115, C11004, doi:10.1029/2009JC005849 (2010).

Sun, C. and Watts, D.R. A circumpolar gravest empirical mode for the Southern Ocean hydrography. J. Geophys. Res., 106, 2833–2855 (2001).

Watts, D.R., Sun, C. and Rintoul, S. A two-dimensional gravest empirical mode determined from hydrographic observations in the subantarctic front. J. Phys. Oceanogr., 31, 2186–2209 (2001).

Zhang, J. and Steele, M. Effect of vertical mixing on the Atlantic Water layer circulation in the Arctic Ocean, J. Geophys. Res., 112, C04S04 (2007).

Zhao, B. and Timmermans, M. Topographic Rossby Waves in the Arctic Ocean's Beaufort Gyre, J. Geophys. Res., 123(9), 6521–6530 (2018).

Zhu, X.-H., Han, I.-S., Park, J.-H., Ichikawa, H., Murakami, K. Kaneko, A. and Ostrovskii, A. The northeastward current southeast of Okinawa Island observed during November 2000 to August 2001. Geophys. Res. Lett., 30, 1071 (2003).